UNIVERSITÀ POLITECNICA DELLE MARCHE

DEPARTMENT OF LIFE AND ENVIRONMENTAL SCIENCES (DISVA)

Research Doctorate in Life and Environmental Sciences

Curriculum Biomolecular Sciences

Cycle XXXIV°

EFFECTS OF PROBIOTICS AND MICRONUTRIENTS ON ZEBRAFISH SKELETAL DEVELOPMENT AND *IN VITRO* CELL CULTURE

Supervisor:
Prof. Oliana Carnevali

PhD candidate:
Jerry Maria Sojan

Co-supervisor:
Dr. Francesca Maradonna

2019-2022

This project has received funding from the European Union's Horizon 2020 research and innovation programme under the Marie Skłodowska-Curie grant agreement No. 766347

Aquaculture meets biomedicine: innovation in skeletal health research

"Life is not easy for any of us. But what of that? We must have perseverance and above all confidence in ourselves. We must believe that we are gifted for something and that this thing must be attained" ~ Marie Curie

Declaration

I hereby certify that this PhD dissertation, which is approximately 220 pages and 49,000 words in length, has been composed by me and this project was conducted by me from January 2019 to January 2022 towards the fulfilment of the requirements of the Università Politecnica delle Marche, Ancona, Italy for obtaining a research doctorate degree in Biomolecular Sciences under the supervision of Prof. Oliana Carnevali and the co-supervision of Dr. Francesca Maradonna.

13-05-2022

Ancona, Italy

Jerry Maria Sojan

TABLE OF CONTENTS

GENERAL INTRODUCTION

Importance of bones and maintenance of bone health

Bones are the main components in the skeletal system and it forms a rigid skeleton that has several important functions like providing support and structural framework, protection of soft internal organs, maintaining homeostasis of calcium, phosphate, sodium and magnesium, production of blood cells in the marrow (in case of mammals) and being the points of attachment for muscles in the skeletal system (Jerome et al. 2018) (Fig.1).

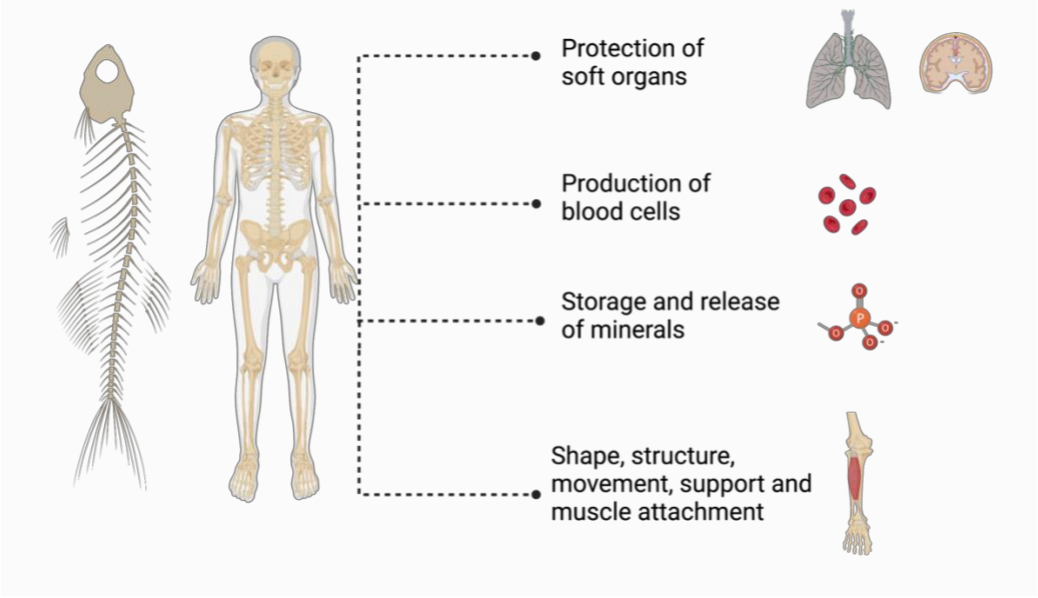

Fig.1. Some of the major functions of bones. Production of blood cells in bones are present only in the case of humans and other mammals, and not in fish (Created with BioRender.com).

Bone loss, which ultimately lead to osteoporosis, is a major concern of the global population nowadays (Ayub et al. 2021). It is most seen in women after menopause and in older population but can be even found in young adults with predisposing factors such as genetics, family history or lifestyle. Osteoporosis remain silent until it gets evident by fractures, particularly of vertebrae and hip, which lead to suffering of the individuals (Cosman et al. 2014). Some medical conditions like eating disorders or renal diseases can be a cause of secondary bone loss, which also can eventually lead to osteoporosis (Holroyd et al. 2008). Some drugs like oral glucocorticoids can lead to secondary bone loss and later cause osteoporosis as evidenced from a recent study in Europe (Nguyen et al. 2018). Therefore, poor bone health affecting people worldwide can be attributed to a broad spectrum of diseases but can be summarized as osteoporosis and related fractures (Bussell 2021). Osteoporosis also take a huge economic toll on the nations as it is reported that 1 out of every 3 women and 1 out of every 5 men of 50 years and older can experience osteoporotic fracture which result in high health care cost (Melton III et al. 1992, 1998). Around €56 billion are costing the health care in Europe each year from osteoporosis and associated 4.3 million fractures, based on the data from 2019 and it is estimated that 23 million people are categorized as high risk of osteoporotic fractures in EU alone (Kanis et al. 2021). Osteoporosis treatment and prevention is an important research area due to these reasons.

Bone development in vertebrates

The skeleton, along with its associated cartilage and connective tissues, originate from the mesenchymal stem cells (MSCs) and hematopoietic stem cells during vertebrate embryonic development (Kangari et al. 2020). Various areas of skeleton are formed from cells, which are originated from distinct embryonic cell lineages (Hall and Miyake 1992). These stem cells initially migrate to the correct zones inside the embryo during development where they aggregate, multiply and differentiate to chondrocyte or osteoblast. There could be three mechanisms of bone formation from the newly differentiated osteoblasts and chondrocytes: intramembranous ossification, endochondral and perichondral ossification. During intramembranous ossification, osteoblasts form bone directly through secretions. In endochondral ossification, a cartilaginous template is formed first by the chondrocytes which later gets replaced by bone. Perichondral ossification, defined as bone production in the perichondrium, is more prevalent in teleost skeletons than in the mammalian skeleton. In mammals, it has been classified as a kind of intramembranous ossification where osteoblasts gather on the surface of the cartilaginous template and deposit bone material into the perichondrium (Hall 2005; Tonelli et al. 2020). Even after the formation, bones undergo modelling during development and remodeling when bone loss or fractures happen, throughout the life.

The three main groups of bone cells, osteoblasts, osteocytes, and osteoclasts, mediate the constant modelling and remodeling of the bone

(Ansari et al. 2021) (Fig.2). Osteoblasts are the lining cells on the bone surface, and they are accountable for the secretion and mineralization of bone matrix. Osteocytes are formed by the differentiation of trapped osteoblasts in the bone, and they have a role in directing osteoblasts and osteoclasts to the respective bone areas through a mechano-sensing network (Ansari et al. 2021). Sclerostin is secreted by mature osteocytes present in the bone matrix and it is a known inhibitor of bone formation. The third group of bone cells, osteoclast, form directly by differentiation from the hematopoietic precursors and have a role in bone matrix resorption during bone remodeling (Crockett et al. 2011). For bone homeostasis, a coordinated activity of all the three bone cells is necessary and any perturbances in this balance can negatively affect the bone health.

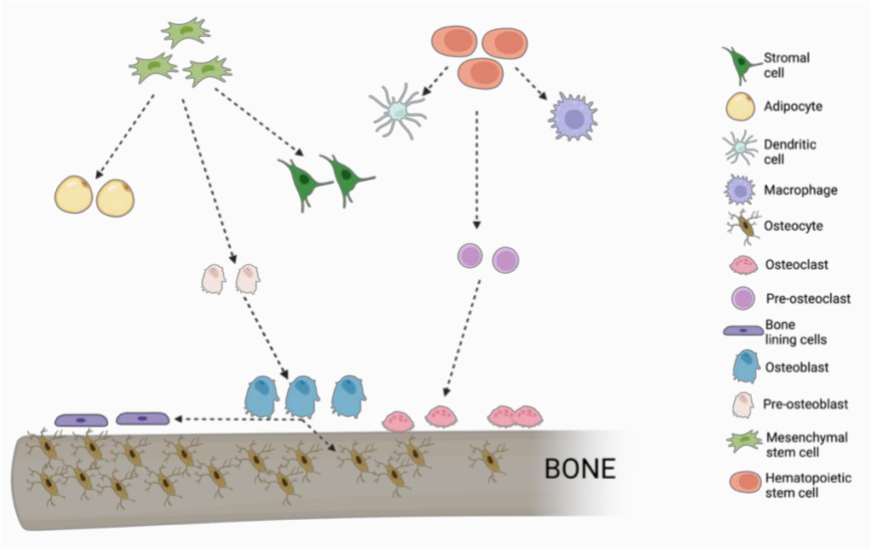

Fig.2. Mesenchymal and hematopoietic stem cells differentiate and form the three main category of bone cells- osteoblasts, osteocytes, and osteoclast which are involved in the formation and modelling of bone (Ansari et al. 2021). (Created with BioRender.com)

Key signaling pathways involved in the osteoblast differentiation and mineralization

Mitogen-activated protein kinase (MAPK)

The MAPK subfamily includes p38 MAPK, extracellular signal-regulated kinases (ERK), ERK5 and Jun N-terminal kinases (JNK). The p38 MAPK group consists of four members, each encoded by a different gene: p38α (*mapk14*), p38β (*mapk11*), p38γ (*mapk12*) and p38δ (*mapk13*) (Cuadrado and Nebreda 2010; Thouverey and Caverzasio 2015). Prior studies have demonstrated that p38 MAPK regulates osteoblast differentiation, extracellular matrix deposition, and mineralization in response to various osteogenic ligands such as Wnt proteins (Chang et al. 2007; Caverzasio and Manen 2007), TGF- β (Lai and Cheng 2002) and BMP2 (Guicheux et al. 2003; Nöth et al. 2003).

Retinoic acid (RA)

RA, which is the main active vitamin A derivative, is crucial for various biological functions including osteogenesis in living organisms. The action of RA is dependent on a variety of cross-talk with other signaling pathways like Wnt signaling and necessitates a coordinated control of its level and activity. The receptor protein that was found to be capable of binding all-trans-RA is termed as retinoic acid receptor (RAR), and it is a member of a subfamily of the nuclear receptor superfamily comprised of three members: RARα, RARβ and RARγ (Samarut et al. 2015). RA signaling

is found to play a key role in bone development as confirmed by previous studies (Cohen-Tanugi and Forest 1998; Iba et al. 2001; Skillington et al. 2002; Song et al. 2005). After osteoblasts have developed, RA can boost osteoblast activity and enhance bone mineralization. This postulated dual function for RA in bone growth might explain why *in vitro* investigations have shown contradictory findings (Samarut et al. 2015).

Transforming growth factor-beta/bone morphogenetic protein (TGF-β/BMP)

TGF-β/BMPs are well-known for their involvement in bone formation throughout mammalian development and for their many regulatory actions throughout the body. TGF-β/BMP signalling occurs through canonical Smad-dependent pathways (TGF-β/BMP ligands, receptors, and Smads) and non-canonical Smad-independent signalling pathways (e.g., p38 MAPK). Both the Smad and p38 MAPK pathways converge on the *runx2* gene response to TGF-β/BMP activation to regulate mesenchymal precursor cell development. Coordination of *runx2* and TGF-β/BMP-activated Smads is required for skeleton development (Chen et al. 2012). By the activation of receptor serine/threonine kinases, TGF-β/BMP plays a critical function in the control of bone organogenesis. Numerous proteins and pathways, including the transcription factor Runx2, influence this signalling. The signalling network involved in skeletal growth and bone production is enormously complex and time- and space-dependent. Also, TGF-β/BMP interacts with other key pathways which are involved in bone formation such as MAPK and Wnt (Rahman et al. 2015).

Wnt/β-catenin

The Wnt signaling pathway is one of the critical biochemical cascades that regulates bone formation. The Wnt signaling pathway is further divided into canonical pathways that are reliant on β-catenin function (Wnt/β-catenin pathway) and non-canonical pathways that are not dependent on β-catenin (planar cell polarity pathway and Wnt/Ca2+ pathway) (Duan and Bonewald 2016). The Wnt/β-catenin signaling pathway is intricate and involves a large number of receptors, inhibitors, activators, modulators, phosphatases, kinases, and other components. However, this process is dependent on one key molecule: β-catenin (Duan and Bonewald 2016). The Wnt/β-catenin signaling pathway regulates the differentiation of progenitor cells into osteoblasts or chondrocytes in the bone marrow (Day and Yang 2008). This signaling pathways further regulate osteoblast and chondrocyte differentiation at various phases of development as reported by multiple studies previously (Hu et al. 2005; Glass et al. 2005; Holmen et al. 2005; Rodda and McMahon 2006; Mak et al. 2006).

Zebrafish (*Danio rerio*) as a model organism to study bone formation, mineralization, or regeneration

The extensive use of zebrafish, a freshwater teleost fish, as a model to study skeleton have a wide range of advantages over classical models like rodents (Fernández et al. 2018). Zebrafish is a robust model organism due to many reasons including the possibility to easily generate large number of larvae which allows rapid, cheap, large-scale screening for novel compounds in pharmacological studies (Lieschke and Currie 2007). In order to deliver compounds to the zebrafish under study, water administration is a very efficient and convenient method (Wilkinson and Pritchard 2015). It can also be used in small scale screenings as zebrafish larvae can be studied in small volume of media in replicates. For studying bone development, it has the additional advantage of good visibility of developing bone or cartilage structures through various staining techniques such as Alizarin red (AR) or Calcein for bone minerals and Alcian blue for cartilaginous structures, due to its translucent body (Walker and Kimmel 2007).

Numerous traits separate teleost bone from that of mammals, including the absence of haematopoietic bone marrow tissue and the absence of osteocytes in the majority of species (Witten and Huysseune 2009; Spoorendonk et al. 2010), but still there are a great amount of morpho-physiological resemblances between zebrafish and mammal skeleton making it a very efficient model to study human skeleton (Tonelli et al. 2020). There exists a lot of similarities between zebrafish and human

bones from organ level to nano levels. At the organ level, the number of bones in adult zebrafish is much larger than an adult mammal but the number of vertebrae is around 31, similar to mammals (Cubbage and Mabee 1996; Bird and Mabee 2003). At macro level, both zebrafish and mammals possess cortical and cancellous bones even though the zebrafish cortical bone do not encapsulate a hematopoietic bone marrow cavity as cortical bones do in mammals (Weigele and Franz-Odendaal 2016). At a micro level, osteoblasts appear as a single monolayer in both mammals and zebrafish. Osteoclasts are both mono- and multi-nucleated in zebrafish whereas in mammals, mono-nucleated ones are just considered as a precursor to multi-nucleated ones. Osteocytes are found in both zebrafish and mammals; however, in zebrafish, osteocytes are not present in all bones resulting in two types of bones: cellular and acellular bones. At nano level, the organic matrix of the bone which is composed mainly of type 1 collagen with a triple helix structure composed of two alpha chains (encoded by *col1a1* and *col1a2* genes) in humans and three in zebrafish (encoded by *col1a1a, col1a1b* and *col1a2* genes) (Gistelinck et al. 2016). The alignment of these collagen fibrils, revealed by transmission electron microscopy (TEM) (Mahamid et al. 2008), are similar between mammals and zebrafish. Regarding the inorganic phase, both zebrafish and mammals got carbonated hydroxyapatite (HA) and other minerals as revealed by Fourier-transform infrared (FTIR) and Raman spectroscopy (Mahamid et al. 2008).

Furthermore, there is a notable resemblance between mammals and zebrafish for molecular pathways involved in skeleton development and

both having endochondral ossification as a mechanism of bone formation whereas differences such are also present (Laizé et al. 2014). Most of the key regulatory genes involved in osteogenesis, such as *runx2* and *sp7,* are conserved among both mammals and zebrafish (Valenti et al. 2020; Spoorendonk et al. 2010). The 71% of human genes has got a minimum of one orthologue in zebrafish and 47% of these human genes were found to map specifically and uniquely to their zebrafish orthologues, as revealed from investigating a high-quality reference genome (Howe et al. 2017). Zebrafish genome is continuously explored for superior knowledge and it keep leading to novel technologies for targeted genome editing (Varshney and Burgess 2014) to use as a support to personalized medicine. All these reasons along with their similar response to external stimulus as mammals, make zebrafish a very efficient model organism to study skeletal development (Apschner et al. 2011; Laizé et al. 2014).

Ossification of bony structures in zebrafish start around 4 to 5 days post fertilization (dpf) and it can happen by three possible ways: Intramembranous, endochondral or perichondral ossification. Intramembranous ossification occur in the operculum, cranial roof, maxillaries, premaxillaries, suboperculum, interoperculum, branchiostegal rays, vertebrae, scales, fin rays, etc. in zebrafish whereas in mammals it occurs in dentary and cranial vault (Hall 2005; Hirasawa and Kuratani 2015). Endochondral ossification, which is characterized by a cartilaginous template formed first by the chondrocytes which gets replaced by bone later, is how ceratohyals, epurals, pleural ribs, pterygiophores and hypurals are formed in zebrafish. However, it is the

main type of ossification in most of the human bones (Bird and Mabee 2003; Weigele and Franz-Odendaal 2016). The third type, perichondral ossification, is considered as the most common type of ossification in teleost, mainly seen in Meckel's cartilage and hyomandibula (Hall 2005).

Fig.3 summarises some of the reasons why zebrafish is considered as an excellent tool for studying bones. One of them is the possibility of analysing cell signaling during bone formation in zebrafish larval stages since it has an osteogenesis process that closely resembles the molecular pattern of mammals and involves orthologous genes and downstream genes coding for bone matrix proteins. Another reason is its capacity to regrow fully functioning appendages following damage, through the de-differentiation of mature osteoblasts into blastema and resetting the bone formation signaling pathway consisting of successive expression of genes involved in regeneration (Gemberling et al. 2013). Additionally, zebrafish transgenic lines expressing fluroscence reporters for specific bone related genes, such as *sp7* and *bglap*, make them very suitable to screen osteogenic compounds *in vivo* (Sojan et al. 2022). Exercise trials in adult zebrafish can provide in-depth information into the development of bone problems associated with aging (Suniaga et al. 2018; Printzi et al. 2021).

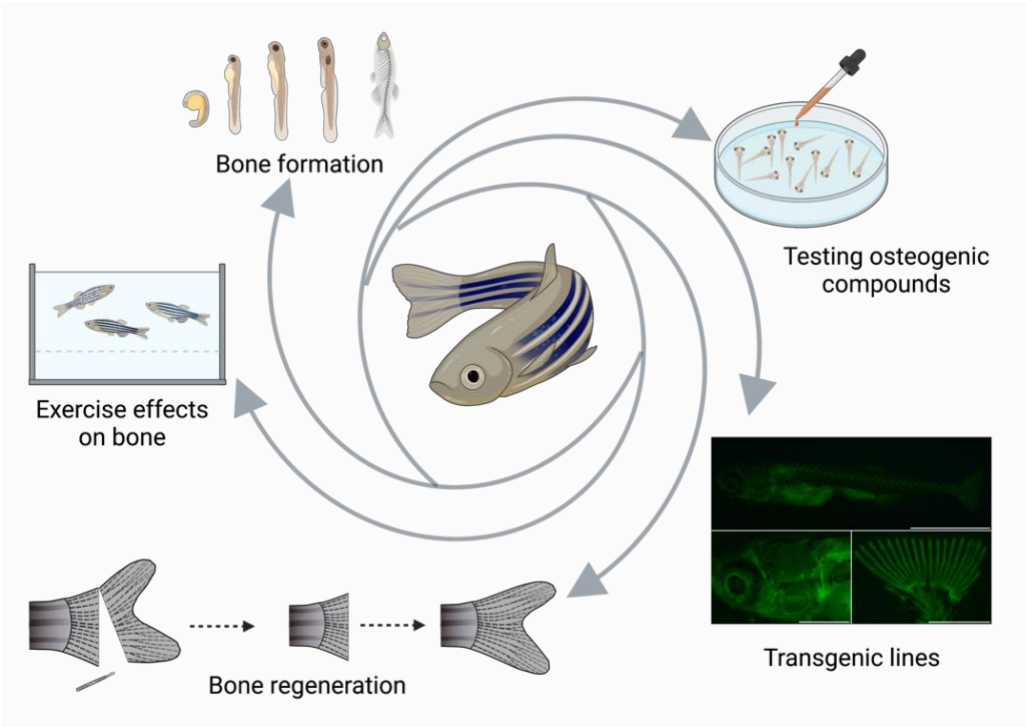

Fig.3. Zebrafish as a tool for studying bone formation, bone regeneration, exercise effects on bones, testing the potency of osteogenic compounds and transgenic lines for tracking the gene expression at cellular or tissue level (Created with BioRender.com).

Zebrafish caudal fin as a tool to study bone regeneration

The zebrafish is one of the most widely used tool to investigate regeneration since it has the ability to regenerate many of its organs including fins, heart, spinal cord, and brain (Gemberling et al. 2013). Regarding the usage of fins for regeneration studies, it has the additional advantages such as easy accessibility, fast regeneration within few weeks, live trackability of the course of regeneration and no detrimental effect on the animal after amputation (Xu et al. 2015). The zebrafish adult fin is also having a good optical accessibility throughout its life span. Moreover, the availability of large number of mutants and transgenic lines also make it a very useful model to study regeneration. One fish can regenerate the fin many times during its lifespan which gives the additional advantage to repeatedly use the same fish for follow-up studies (Azevedo et al. 2011). The regenerated fin not only reaches the original size but can also maintains the pattern and organization of the tissue (Pfefferli and Jaźwińska 2015).

The zebrafish caudal fin consists of several bifurcated and non-bifurcated fin rays (or otherwise called lepidotrichia) which are attached to the endochondral bones and muscles at the proximal end. To the most distal end, non-mineralized elements called actinotrichia are also present (König et al. 2018). Each fin ray is made of two concave hemi-rays with repetitive bony segments connected by collagenous ligaments and are formed by intramembranous ossification without cartilaginous template and osteocytes (Apschner et al. 2011). The pattern of segmentation in the

caudal fin of the zebrafish is also influenced by temperature (Christou et al. 2018). The hemi-rays have a single line of bone matrix depositing osteoblasts on both outer and inner sides and in addition to nerves, fibroblast connective tissues and capillaries seen in between the two hemi-rays (Johnson and Bennett 1998). Osteoclasts are known to have a role during fin regeneration since osteoclast marker tartrate-resistant acid phosphatase (TRAP) positive cells are found in the regenerating fin and not in un-amputated fin (Blum and Begemann 2015).

Zebrafish craniofacial bones as a screening tool for novel osteogenic compounds

Head skeletal development in zebrafish has a lot of resemblances to that of mammals and the mechanisms involved have been previously well described (Machado and Eames 2017). Zebrafish head skeleton functionally develop within 5 days post fertilization (dpf) and exhibit continuous growth throughout the life and is more complex in structure than other vertebrates, with 73 bones, which is at least 3-fold more than the mammalian skull (Cubbage and Mabee 1996; Bruneel and Witten 2015). The cartilaginous structures found in the early stages of the larval skeletal development are later replaced by bony structures through endochondral ossification (Bruneel and Witten 2015; Weigele and Franz-Odendaal 2016). Initially formed cartilaginous structures are visible from nearly 3 dpf whereas some of the bony structures start forming around 4 to 5 dpf (Bruneel and Witten 2015; Aceto et al. 2015). Some of the first bony structures developed by around 4 dpf are cleithrum and pharyngeal

teeth (Gavaia et al. 2006). In Fig.4, the flat mount of a 6.5 dpf larvae double stained with Alcian blue and Alizarin red (AR) shows cartilaginous and bony structures in lateral (Fig.4A), dorsal (Fig.4B), and ventral views (Fig.4C).

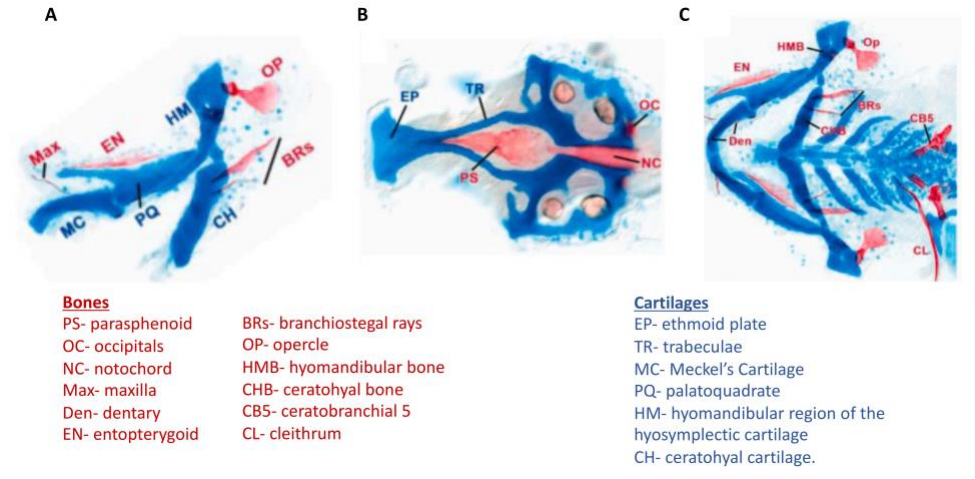

Fig.4. Flat mounts of 6.5 dpf larvae stained by acid-free double stain, Figure adapted and modified from Walker and Kimmel 2007. A) Lateral view of the jaw; B) Dorsal view of the neurocranium and C) Ventral view of the pharyngeal skeleton.

For screening compounds with osteogenic effects on zebrafish larvae, operculum is a very suitable option among the cranio-facial bones (Tarasco et al. 2017). The zebrafish operculum is one of the first bone to mineralise and the extend of mineralisation can be easily tracked *in vivo* by AR staining from as early as 3 dpf (Kimmel et al. 2010). It is also a good model to assess the bone morphogenetic variations (Huycke et al. 2012). The opercular bone is flat and it is located close to surface of the fish head, thus making its imaging and morphometric analysis very easy and

convenient. A representative image is given below showing the image analysis of the lateral and ventral views of a 7 dpf *Tg(col10a1a:col10a1a-GFP)* zebrafish head with opercular bone, eye and total head area marked in the lateral view, and total area of bony structures marked in the ventral view (Fig.5).

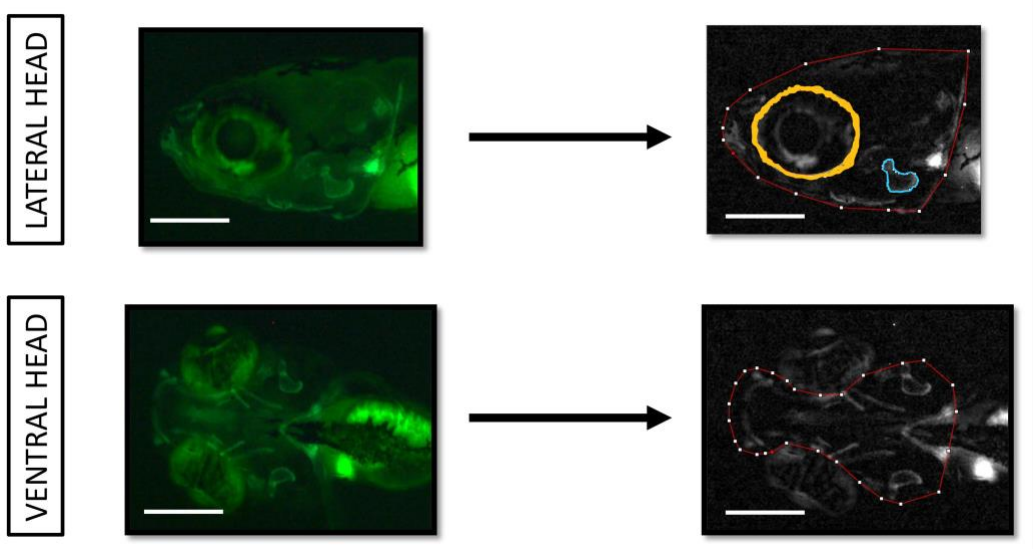

Fig.5. Image analysis of 7 dpf *Tg(col10a1a:col10a1a-GFP)* zebrafish larvae. Lateral head is measured for signal positive area in total head (red tracing) after subtracting the signal from eye (yellow tracing) and also area of operculum (blue tracing) is separately measured. Ventral head is measured for signal positive area of bony elements excluding eye (red tracing); scale bar= 200 μm

Zebrafish transgenic lines to test the effects of compounds on osteogenesis

Various zebrafish transgenic lines are available with cell or tissue specific promoters controlling the expression of fluorescent chromophores like green (GFP)/red fluorescent protein (RFP) and this is useful to analyze the specific gene expression of cells *in vivo.* Many zebrafish lines using this strategy are available for bone studies and these make zebrafish a valuable tool in also understanding the effects of various compounds on bone development. Some of the zebrafish transgenic lines are generated by injecting medaka promoter constructs into zebrafish embryos at one-cell stage because zebrafish and medaka are highly similar and conserved genetically in terms of ossification (Inohaya et al. 2007). For instance, in both zebrafish and medaka, *bglap* expression is downstream to *sp7* and later both are expressed in all the mineralized bones. *Sp7* is the key regulator of the differentiation of mesenchymal cells to osteoblasts and *bglap* is a marker of the bone matrix-producing osteoblasts which are already differentiated (Nakashima et al. 2002; Gavaia et al. 2006). Some of the available and studied zebrafish transgenic lines for osteoblasts include *sp7 (Tg(sp7:EGFP)b1212), runx2 (Tg(runx2:GFP)), col10a1a (TgBAC(col10a1a:Citrine)), entpd5a (TgBAC(entpd5a:Citrine)), bglap (Tg(ocn:GFP))* and for osteoclasts *ctsk (Tg(ctsk:YFP))* (DeLaurier et al. 2010; Knopf et al. 2011; Bussmann and Schulte-Merker 2011; Kague et al. 2012; Mitchell et al. 2013; Sharif et al. 2014). A medaka transgenic line for *twist (twist:eGFP)*, which is a specific marker for sclerotome tissue within somites and expressed in mesenchymal cells in both medaka and

zebrafish, can be another interesting line to use for studying early development of bones (Inohaya et al. 2007; Morin-Kensicki and Eisen 1997; Renn et al. 2006). Therefore, transgenic lines of zebrafish proves to be a useful tool for *in vivo* imaging of various cell types that constitute the differentiated skeleton, such as osteoblasts and osteoclasts, and furthermore to create various skeletal disease models in order to support in developing personalized medicines for specific diseases like osteoporosis.

Experimentally immortalised cell lines for the study of osteoblasts proliferation and differentiation

Osteoblasts which constitute the main cellular component of bone are known to be rich in alkaline phosphatase (ALP) enzyme and for their ability to secrete and synthesise extra cellular matrix proteins such as osteopontin and osteocalcin, and also type 1 collagens (Kartsogiannis and Ng 2004). Osteoblasts also have receptors to 1,25-dihydroxy vitamin D3 (VD3), parathyroid hormone (PTH), tumour necrosis factors (TNFs) etc (Martin et al. 1989; Heath and Reynolds 1990). Osteoblast differentiation and the pathways involved can be clearly studied using cell culture systems. Immortalized cell lines are either cancerous cells that don't stop dividing or cells that have been artificially (experimentally) manipulated to keep growing for a long time. This means that they can be grown over many generations (Carter and Shieh 2015). Many established clonal cell lines from bone tumours such as osteosarcoma (eg. SOSP-9607) are also available. Both primary cell cultures of osteoblasts derived from bones

and experimentally immortalised cell lines have been often utilised and established to study osteoblasts. Among the experimentally immortalized cell lines, a frequently utilized one is MC3T3-E1 (Hakki et al. 2010; Lin and Hankenson 2011), which is a mouse cell line, and even though this cell line is still a pre-osteoblast, it is routinely employed to mimic osteoblasts and sometimes even osteocytes. To analyse bone-related gene expression and signalling pathways as well as to screen for pro/anti-mineralogenic molecules, fish cell lines generated from calcified tissues are a useful research tool (Laizé et al. 2022). Adult human osteoblast-like (hOB) cell line and the human fetal osteoblast (hFOB) cell line are of great significance to study various stages of osteoblast differentiation (Keeting et al. 1992; Harris et al. 1995). The hOB cell line was immortalized by transfecting normal adult human osteoblast-like cells from a 68-year-old female with both the SV40 virus's small and large T antigens. The human fetal osteoblast cell line (hFOB) was derived from miscarriage biopsies (Harris et al., 1995). By transfecting primary cultures obtained from fetal tissue and with a temperature-sensitive variant of the SV40 big T antigen, primary cultures were immortalized. Osteopontin, osteonectin, Bone sialo protein (BSP), and type I collagen expression were all found to be increased in differentiated hFOB cells. Additionally, when hFOB cultures reached confluence, they develop mineralized nodules. hFOB1.19, the highest alkaline phosphatase-expressing clone, demonstrated enhanced alkaline phosphatase (ALP) activity and osteocalcin secretion in a dosage dependently manner upon VD exposure. Based on previous evidence, hFOB cells could deposit a mineralized extracellular matrix (ECM) with microscopic features comparable with those formed by primary

osteoblasts *in vitro,* making them a suitable laboratory model (Subramaniam et al. 2002). Another study also investigated the mineral content of vesicles formed by two separate human cell lines: hFOB 1.19 and osteosarcoma line Saos-2, to establish the influence of the source and features of vesicles on the initiation of mineralization at the microscopic level and inferred that the mineralization process is distinct depending on the cell type (Strzelecka-Kiliszek et al. 2017; Bozycki et al. 2018).

Gene expression dynamics during osteoblast differentiation in humans

During the ongoing development of the osteoblasts, the stepwise expression of cell growth and differentiation-specific genes has been previously traced (Owen et al. 1990; Setzer et al. 2009). The sequential pattern of the expression of genes corresponds to four distinct developmental phases (Setzer et al. 2009). Firstly, proliferation of osteoblast cells and the production of type I collagen bone extracellular matrix. At this stage, genes that encode cell adhesion proteins (fibronectin) and other genes involved in the control of extracellular matrix production as well as its association with the cytoskeleton (TGF-β, type I collagen) are also activated. As a result of the first proliferative stage, the activation of genes associated in the maturation and architecture of the osseous extracellular matrix increases, leading to the extracellular matrix's readiness for mineralization and ultimately to the formation of bone in the second stage. The third developmental stage is

characterized by gene expression that relates to the formation of hydroxyapatites (HA) in an orderly fashion (HA deposition). Osteopontin (*spp1*) and osteocalcin (*bglap*) have the highest levels of expression in this stage. The fourth developmental stage happens when osteoblasts mature and during this time, collagenase and expression of type I collagen genes are enhanced, apoptotic behavior is seen, while compensatory proliferative action is apparent (Lynch et al. 1998). Even though the fourth developmental stage gene expression profile is not quite identified, it operates on extracellular matrix to preserve functional and structural features of the bone tissue (Lynch et al. 1998).

Prior to confluence, all cells display pre-confluent proliferation and express genes involved in cell cycle progression and extracellular matrix formation. Throughout early development, pre-confluent proliferation happens alongside osteoblast extracellular matrix manufacturing, culminating in a monolayer of cells with extracellular matrix containing type I collagen. It increases cell multi-layering as well as post-confluent proliferation in growing cells. Apoptotic osteo-nodules remodeling begins during a third cycle of proliferation (Soltanoff et al., 2009). Each stage has its own regulatory criteria for proliferation control and early response genes, competence factors, and growth regulatory factors that all lead to cell cycle regulation. Extracellular matrix synthesis reduces proliferative genes, whereas extracellular matrix mineralization inhibits proliferative genes (Owen et al. 1990; Soltanoff et al. 2009). Some of the key osteogenic markers, transcription factors, signaling molecules of various

stages of osteoblast differentiation during bone development is shown schematically in Fig.6.

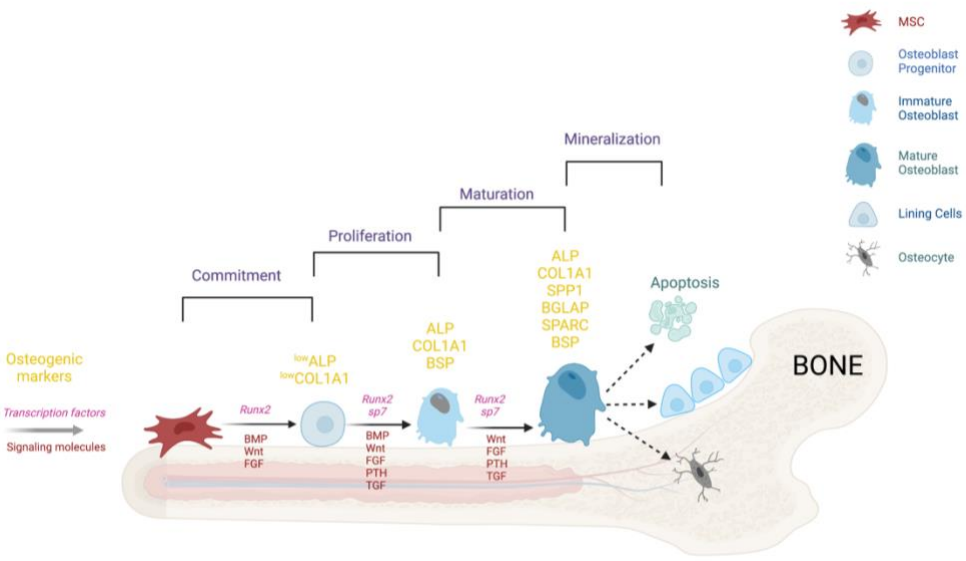

Fig.6. The differentiation of osteoblasts (OBs) in humans is shown schematically. Figure is adopted and modified from Amarasekara et al. (2021) and created with BioRender.com.

Vitamin D3 as an established pro-osteogenic compound

Vitamin D (VD) is present in two forms: ergocalciferol or vitamin D2 (VD2), which is acquired by irradiating plants, plant materials, or foods, and vitamin D3 or cholecalciferol (VD3), which is produced in the skin of humans in response to sunlight or UV light exposure. Calcitriol (1,25-dihydroxyvitamin D3) is the active metabolite form of VD generated in the kidney and liver after the two-step hydroxylation of VD3. Calcitriol is involved in the absorption of calcium (Ca) in the stomach where it binds to the VD receptor (Lips 2006). This complex forms a heterodimer with the retinoid receptor and binds to a VD receptor on a gene such as osteocalcin. Transcriptional regulation ensue, resulting in the synthesis of proteins such as the Ca binding protein or osteocalcin (Lips 2006). Ca is taken in by cells via membrane proteins. When calcitriol attaches to the VD receptor, it induces the production of the Ca binding protein, which governs active transport across the cell. Calcitriol has been shown to have direct impacts on bone cells (osteoblasts) by enhancing differentiation and ECM mineralization *in vitro* cultures of human osteoblasts (Driel et al. 2006; Woeckel et al. 2010; Meijden et al. 2014). The effect of dietary VD3 on the ontogenesis of the digestive system was previously reported to influence the ossification process in sea bass (Darias et al. 2010).

VD has direct effects on osteoblasts by regulating the formation of extracellular matrix proteins (osteocalcin, collagen type I, osteopontin, etc.) and by enhancing the activity of the ALP, which is a promoter for deposition of HA crystals in the extracellular matrix (van Driel and van

Leeuwen 2014). VD has been shown to have favorable impacts on mineralization and differentiation *in vitro* utilizing human mesenchymal stem cells, human osteoblasts, and even induced promotion of pluripotent stem cells to the osteogenic lineage (Driel et al. 2006; Piek et al. 2010; Zhou et al. 2012; Geng et al. 2013; Meijden et al. 2014; Kato et al. 2015). Mineralization abnormalities in humans caused by VD insufficiency could result in osteoporosis and an increased risk of fractures over time. VD supplementation improves bone mineral density, decreases bone turnover, and reduce fracture incidences. Multiple randomized placebo-controlled studies in humans utilizing VD, first with Ca and later without Ca, showed a significant reduction in the prevalence of fractures and Ca needs to be supplemented with VD in order for it to be effective in this case (Lips and van Schoor 2011).

Mineralization boosters and antagonists maintain a biphasic equilibrium in the synthesis and accumulation of HA crystals in the extracellular matrix (Stewart et al. 2006; Roberts et al. 2007; Yadav et al. 2011). Calcitriol was shown to increase *enpp1* (encoding for ENPP1 which is a pyrophosphatase that cleave pyrophosphate PPi, which is a mineralization inhibitor) expression levels in adult murine MLO-A5 osteoblasts, causing a mineral accumulation repression (Lieben et al. 2012; Yang et al. 2015). A prior work utilizing human osteoblasts shown that calcitriol administration increased ALP levels in extracellular vesicles, resulting in increased mineralization through increased synthesis and accumulation of HA crystals (Woeckel et al. 2010). The direct action of VD exist prior to mineralization and resulted in an advancement of the

extracellular matrix (Woeckel et al. 2010). VD therapy has little impact once mineralization began. Calcitriol's direct impact on the human osteoblast activity is phase dependent, just as was established in rat osteoblasts (Owen et al. 1991). VD has real impacts on osteoblasts by attachment to the nuclear VD receptor (VDR) (Haussler et al. 2013; Kato et al. 2015). Variations in VDR protein expression throughout osteoblast formation might account for calcitriol's osteoblast differentiation-dependent impacts. In mouse bone, it was discovered that the VDR is abundantly expressed in immature osteoblasts but is produced at a low or non-existent level in mature osteoblasts, including lining cells and osteocytes (Wang et al. 2014). Some of the hypothetical processes behind the increased bone mass associated with long-term VD therapy is shown below as Fig.7.

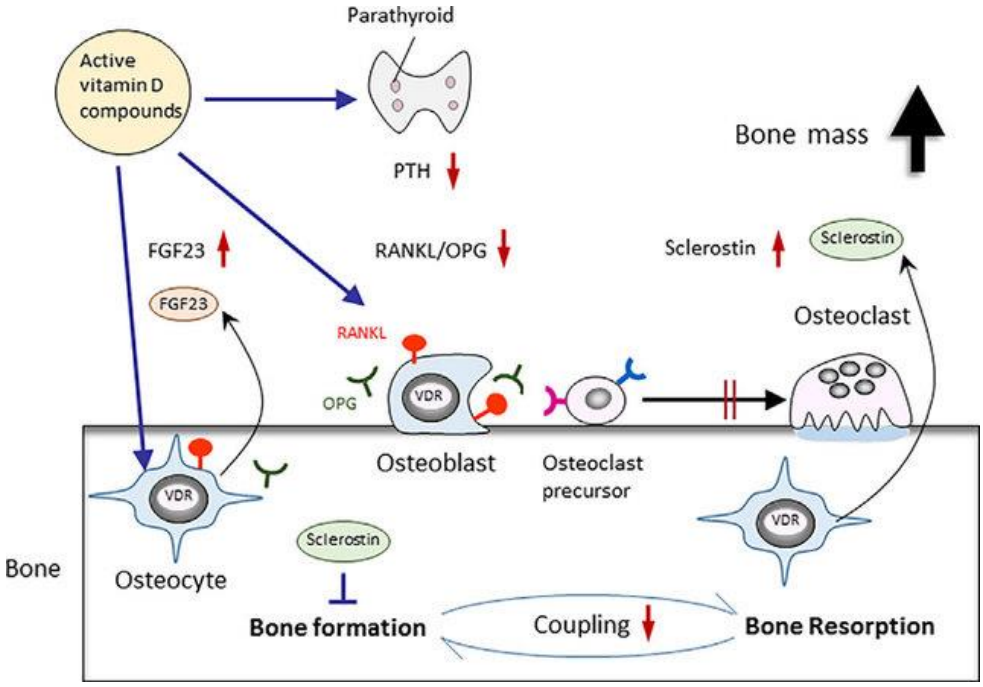

Fig.7. Possible processes regulating bone growth by long-term VD therapy hypothesised from the effects observed in mice and *in vitro* osteoblast lineage cells (Figure adopted from Nakamichi et al. 2017)

VDR activity had also been detected in hypertrophic chondrocytes although not in stromal cells, chondroclasts, or osteoclasts. The nuclear VDR heterodimerizes with the Retinoid X Receptor in response to calcitriol binding. Through the regulatory areas of the main VD target genes, the dimeric VDR complex interacts to genomic DNA (Haussler et al. 2013; Carlberg and Molnár 2015). VD's influence on osteoblast differentiation and mineralization is dependent on the VDR's association with RUNX2, a vital transcription factor in osteoblast differentiation. Modulation of RUNX2 by VD further influenced the expression of the non-collagenous proteins such as osteocalcin and osteopontin in rat osteoblasts (Paredes et al. 2004; Shen and Christakos 2005). Additionally, the calcitriol-activated VDR regulates osteoblast differentiation via interacting with the Wnt signaling cascade (Haussler et al. 2010). Also, VD treatment was previously found to increase the bone formation in zebrafish larvae (Aceto et al. 2015) and Tarasco et al., 2017 has showed that calcitriol increases opercular bone formation in zebrafish larvae.

Potential of micronutrients and probiotics as osteogenic compounds

Micronutrients are nutrients that are required only in microgram or milligram quantities for the proper functioning of the body's physiologic activities (FAO/WHO 2004). Micronutrients, which comprise electrolytes, minerals, vitamins, and carotenoids, are necessary for enzyme activity, intermediate metabolism, and the metabolic response to sickness, among many other things. Nutrients, minerals, and vitamins play an important part in bone modeling and remodeling and are required for the maintenance of bone strength and density.

The term "probiotics" basically translates as "for life" and is taken from Latin and Greek. Nevertheless, the term "probiotics" has been defined differently since it was created some years back. The Food and Agricultural Organization/World Health Organization defines probiotics as live bacteria that, when supplied in sufficient proportions, impart health benefits on the host (Gasbarrini et al. 2016). Besides mucosal barrier function, gut microbiota is also involved in food digestion and energy metabolism, as well as in bone health and metabolism.

Some earlier studies have established the importance of micronutrients and probiotics in maintaining bone health. The role of two important micronutrients, boron and selenium, and probiotics in bone health are further discussed in detail below.

Boron

Boron (B) is a micronutrient which is required by all living creatures. There have been numerous studies on the biological effects of B, including forms of transportation, cellular membrane functions (Goldbach et al. 2001), functions in cell-wall creation (O'Neill et al. 2004), osteogenesis, maintenance of bone, mitigation of Ca loss and bone decalcification (Hakki et al. 2010). It is particularly crucial in the process of bone formation and bone maintenance since numerous research data confirm the beneficial effects of B on the bone health in animals. Instead of appearing as isolated, B is found in combination with sodium or oxygen-containing organoboron complexes, which are the physiologically necessary forms of B in organisms (Hunt 2003). Boric acid ($B(OH)_3$) is the most common form of B found in nature; nevertheless, a minor amount of B in the form of borate anion $B(OH)_4$ is also present (Khaliq et al. 2018). B is required for bone formation and regeneration (Uysal et al. 2009), particularly for proliferation of osteoblasts and ECM mineralization (Hakki et al. 2010). B's influence on osteogenesis and bone maintenance has been studied *in vivo* in the past years (Gallardo-Williams et al. 2003; Nielsen 2004). B deficiency resulted in reduced growth of the bone and therefore resulted in defective bone formation in animals (Białek et al. 2019). It has been shown that supplementary B in the form of boric acid improves bone strength and structure in rats (Gorustovich et al. 2006). B deficiency raised plasma homocysteine levels while simultaneously decreasing S-adenosylmethionine (SAM-e) levels, confirming the notion that B's biological capacity could be mediated through an influence on

SAM-e synthesis, as was shown via laboratory experiments in rats (Pizzorno 2015; Nielsen 2009). A reduction in SAM-e has been seen in conditions such as rheumatoid arthritis, osteoporosis, urolithiasis, and diabetes that could be regulated by B nutritional consumption (Pizzorno 2015). Another study introduced B to the drinking water of ostrich chicks at different doses to determine its impact on the tibia (Cheng et al. 2011). The increase in bone strength after B intake may be as a result of B's influence on leptin and steroid hormone levels, as these are necessary for bone metabolism. 0.2 g/L of B supplementation in drinking water was an effective dose for enhancing bone strength in ostrich chick since the majority of indicators rose considerably (Cheng et al. 2011). B supplementation improved bone properties in pigs (Armstrong and Spears 2001) and B was recognized to boost bone strength and bone ash content in hens (Wilson and Ruszler 1996). B supplementation has also been demonstrated to increase cortical and trabecular bone microstructure and strength in diabetic mice (Abdelnour et al. 2018) and B can also help to prevent bone abnormalities caused by diabetes (McCoy et al. 1994).

In cell cultures (HEK293 cells), B deficiency was identified to induce the mitogen-activated protein kinase (MAPK) pathway which is known to play a significant role in the development of skeleton (Park et al. 2004). B has been shown to be capable of regulating extracellular matrix turnover and boosting TNF-alpha secretion in another research with human fibroblasts (Nzietchueng et al. 2002). The direct influence of B on particular enzymes involved in extracellular matrix turnover (trypsin-like enzymes, elastase,

alkaline phosphatase, and collagenase) was previously investigated and B was found to be possibly modifying these enzymes in fibroblasts *in vitro* (Dousset et al. 2002). Similarly, administration of B at a concentration of 1.0 ng/ml to osteoblasts cells (MC3T3-E1) had beneficial effects and adequate B levels resulted in an increase in bone morphogenetic proteins (Hakki et al. 2010).

B also interacts with other minerals and vitamins, including Ca, magnesium, and VD, and also hormones, hence contributing to bone health. Owing to B's biological role in the metabolism and absorption of certain other minerals, it is suggested that B could be having some indirect effects on a range of metabolic processes in bones. B administration boost Ca and phosphorus (P) retention and absorption in VD insufficient rats, and also magnesium (Mg) levels in the femur (Hegsted et al. 1991). B seems to be a critical cofactor in Ca homeostasis, and so plays a critical role in the occurrence of osteoporosis in humans (Miggiano and Gagliardi 2005). The mineral changes in bone, in combination with the fact that B deficiency decreases the alveolar bone surface and osteoblast activity in mice, imply that B have an influence on bone developmental processes through its effect on the activity of osteoblasts and/or osteoclasts, rather than just modulating bone Ca concentration (Gorustovich et al. 2006). According to what has been discussed so far, B has a critical role in the control of skeleton formation, the maintenance of bone overall health, and the metabolism of minerals such as Ca, magnesium, and VD.

Selenium

The micronutrient selenium (Se,) which is another requirement for living organisms, has various physiological functions that are principally regulated by the protein family called selenoproteins (e.g., selenocysteine). Some among the 25 selenoproteins discovered in humans function as redox gatekeepers and therefore are critical for regulating cellular antioxidant equilibrium (Gromer et al. 2005; Lu and Holmgren 2009; Reeves and Hoffmann 2009). Oxidative stress induced by an elevated level of reactive oxygen species (ROS) is harmful to normal bone physiology because high ROS decrease osteoblastic differentiation and increase osteoclastic differentiation (Wauquier et al. 2009; Manolagas 2010). ROS promotes the production of RANKL in osteoblasts (Bai et al. 2005) and functions as a critical intracellular signal transducer for RANKL-induced osteoclastic differentiation (Lean et al. 2005; Lee et al. 2005).

The bulk of the known selenoprotein genes, and also many critical contributing factors in selenoprotein production, have already been identified in osteoblasts and osteoclasts (Dreher et al. 1998; Ebert et al. 2006; Pietschmann et al. 2014). But still there are only limited research on the impact of Se on bone cells. In conventional cultured cells which are Se deficit, supplementation of Se reinstated thioredoxin reductase (TrxR) and glutathione peroxidase (GPx) activity as observed in human fetal osteoblast (hFOB) cells (Leist et al. 1996; Jakob et al. 2002). Similarly, Se supplementation increased GPx and TrxR activity in primary bone marrow

stromal cells (BMSCs) capable of converting into mesenchymal originated cells such as osteoblasts, lowering intracellular ROS levels and DNA damage (Ebert et al. 2006) and compensating for hydrogen peroxide-induced osteoblastic differentiation suppression (Liu et al. 2012). It also has been claimed that a deficiency of Se might alter bone metabolism and block development (Mody et al. 2001). Se deficiency has been associated with a higher risk of bone disease (Cao et al. 2012), decreased pituitary growth hormone, plasma insulin-like growth factor I, and Ca levels, as well as increased parathyroid hormone, 1,25-dihydroxyvitamin D3, and urinary Ca concentrations. The fact that these changes were associated with decreased BMD, lower bone volume, and impaired bone microarchitecture, indicates that they were associated with higher bone resorption (Moreno-Reyes et al. 2001; Cao et al. 2012). Downey et al. established that the conservation of selenoprotein function in osteo-chondro progenitors is necessary for skeletogenesis and cartilage viability preservation (Downey et al. 2009). Zheng and colleagues demonstrated that Se nanoparticles promoted mineralization in human umbilical cord mesenchymal stem cells (HUMSCs), which seem to be capable of promoting the deposition of Ca nodules (Zheng et al. 2014). Another study has shown that Se administration in nanomolar quantities promotes type I collagen expression, ALP activity, and Ca deposition in rat marrow stromal cells (MSCs), demonstrating that Se is able to boost osteoblastic differentiation at the cellular level (Liu et al. 2012).

Probiotics

Ca, P, and Mg are all important contributors to bone mineralization and for the uptake of these nutrients, the gut releases endocrine hormones, such as incretin and serotonin that communicate to bone cells. Gut microbiota can control bone metabolism by altering Ca absorption and it can be aided by the presence of VD (Hao et al. 2019). Several studies have demonstrated that eating a low-calcium diet alone is associated with increased bone turnover, decreased trabecular microarchitecture, and bone resorption in multiple bones. Therefore, measures taken to increase Ca uptake when combined with a balanced gut microbiota, can result in decreased osteoclast activity and increased osteoblast activity within the bone matrix, which eventually results in enhanced bone morphological qualities (Hao et al. 2019). Maradonna and others discovered that probiotic *Lactobacillus rhamnosus* supplementation could result in an increase in the mineralisation of zebrafish larvae bones (Maradonna et al. 2013). Earlier research has also shown that *Lactobacillus* and *Bifidobacterium* strains may increase bone mass density in ovariectomized (OVX) mice and rats, simulating post-menopausal scenario (Chiang and Pan 2011; McCabe et al. 2013). Another research on male osteoporosis rats found that *Lactobacillus helveticus* fermented milk enhanced bone mineral density (BMD) and bone mineral content (BMC), as evaluated by dual-energy X-ray absorptiometry (DEXA) (Narva et al. 2004a). Few randomized clinical trials in humans have already examined the impact of probiotic-containing therapies on skeletal effects including on BMD and bone turnover, with several studies indicating that probiotic

administration may improve BMD and indicators of bone turnover whereas others found no influence (Lambert et al. 2017; Jafarnejad et al. 2017; Nilsson et al. 2018; Takimoto et al. 2018; Jansson et al. 2019; Billington et al. 2021).

Possible mechanism of action of probiotics on bone

Probiotics may have a variety of effects on the bones via a range of mechanism of action such as modulation of immune system functions. Osteoimmunology is a branch of research that investigates the close relationship between the immune and skeletal systems. Inflammatory diseases have been discovered to be connected with osteoporosis, which has led to the development of new treatments (Terashima and Takayanagi 2018). Another possible mechanism of probiotic action on bone could be through interacting with hormones like VD and their receptors such as VD receptor (VDR), as reported previously in some epithelial cells from animal skin where expression of VDR was boosted when treated with *Lactobacillus* strains (Wu et al. 2015). Probiotics, perhaps via their association with oestrogens, was shown to prevent bone loss associated with steroid deficiency in mice, as previously reported (Li et al. 2016). The gut microbiota and its association with Ca intake have also been proven to have an impact on bone function in the past, which is important since Ca is required again for maintaining of bone health through lowering bone resorption (Chaplin et al. 2016). In addition, some of the strains provide a significant source of vitamin K2, which serves as a cofactor in the carboxylation of the most abundant non-collagenous bone

matrix protein BGLAP (osteocalcin), allowing appropriate osteocalcin-bone mineral binding during bone growth (Booth 2009; Atkins et al. 2009; Castaneda et al. 2020). There is still more research that needs to be done to verify the link between microbiome-derived vitamin K2 and bone tissue strength (Castaneda et al. 2020).

In vitro studies of probiotics on osteoblast differentiation and extracellular matrix mineralization

By growing osteoblast and osteoclast precursor cells derived from bone marrow of mice, researchers were able to determine the effects of the probiotics on osteoblasts and osteoclasts (Narva et al. 2004b). The findings in osteoblast cultures revealed that *Lactobacillus helveticus* from fermented milk whey, was able to boost osteoblast function (Narva et al. 2004b). *In vitro* osteoclast cultures, on the other hand, showed no substantial influence by probiotics (Takahashi et al. 1988; Qu et al. 1998; Narva et al. 2004b). There are few recent reports of studying the beneficial activity of probiotics in cell line cultures by making use of probiotic extracts, supernatants or even fractions (Chen et al. 2017; Nozari et al. 2019; Brognara et al. 2020; Isazadeh et al. 2020).

Reference

Abdelnour SA, Abd El-Hack ME, Swelum AA, et al (2018) The vital roles of boron in animal health and production: A comprehensive review. J Trace Elem Med Biol 50:296–304. https://doi.org/10.1016/j.jtemb.2018.07.018

Aceto J, Nourizadeh-Lillabadi R, Marée R, et al (2015) Zebrafish Bone and General Physiology Are Differently Affected by Hormones or Changes in Gravity. PLOS ONE 10:e0126928. https://doi.org/10.1371/journal.pone.0126928

Amarasekara DS, Kim S, Rho J (2021) Regulation of Osteoblast Differentiation by Cytokine Networks. Int J Mol Sci 22:2851.https ://doi .org /10.3390 /ijms 22062851

Ansari S, Ito K, Hofmann S (2021) Cell Sources for Human In vitro Bone Models. Curr Osteoporos Rep 19:88–100. https://doi.org/10.1007/s11914-020-00648-6

Apschner A, Schulte-Merker S, Witten PE (2011) Chapter 10 - Not All Bones are Created Equal – Using Zebrafish and Other Teleost Species in Osteogenesis Research. In: Detrich HW, Westerfield M, Zon LI (eds) Methods in Cell Biology. Academic Press, pp 239–255

Armstrong TA, Spears JW (2001) Effect of dietary boron on growth performance, calcium and phosphorus metabolism, and bone mechanical properties in growing barrows. J Anim Sci 79:3120–3127. https://doi.org/10.2527/2001.79123120x

Atkins GJ, Welldon KJ, Wijenayaka AR, et al (2009) Vitamin K promotes mineralization, osteoblast-to-osteocyte transition, and an anticatabolic phenotype by γ-carboxylation-dependent and -independent mechanisms. Am J Physiol-Cell Physiol 297:C1358–C1367. https://doi.org/10.1152/ajpcell.00216.2009

Ayub N, Faraj M, Ghatan S, et al (2021) The Treatment Gap in Osteoporosis. J Clin Med 10:3002. https://doi.org/10.3390/jcm10133002

Azevedo AS, Grotek B, Jacinto A, et al (2011) The Regenerative Capacity of the Zebrafish Caudal Fin Is Not Affected by Repeated Amputations. PLOS ONE 6:e22820. https://doi.org/10.1371/journal.pone.0022820

Bai X, Lu D, Liu A, et al (2005) Reactive Oxygen Species Stimulates Receptor Activator of NF-κB Ligand Expression in Osteoblast *. J Biol Chem 280:17497–17506. https://doi.org/10.1074/jbc.M409332200

Białek M, Czauderna M, Krajewska KA, Przybylski W (2019) Selected physiological effects of boron compounds for animals and humans. A review. J Anim Feed Sci 28:307–320. https://doi.org/10.22358/jafs/114546/2019

Billington EO, Mahajan A, Benham JL, Raman M (2021) Effects of probiotics on bone mineral density and bone turnover: A systematic review. Crit Rev Food Sci Nutr 0:1–12. https://doi.org/10.1080/10408398.2021.1998760

Bird NC, Mabee PM (2003) Developmental morphology of the axial skeleton of the zebrafish, Danio rerio (Ostariophysi: Cyprinidae). Dev Dyn 228:337–357. https://doi.org/10.1002/dvdy.10387

Blum N, Begemann G (2015) Osteoblast de- and redifferentiation are controlled by a dynamic response to retinoic acid during zebrafish fin regeneration. Development 142:2894–2903. https://doi.org/10.1242/dev.120204

Booth SL (2009) Roles for Vitamin K Beyond Coagulation. Annu Rev Nutr 29:89–110. https://doi.org/10.1146/annurev-nutr-080508-141217

Bozycki L, Komiazyk M, Mebarek S, et al (2018) Analysis of Minerals Produced by hFOB 1.19 and Saos-2 Cells Using Transmission Electron Microscopy with Energy Dispersive X-ray Microanalysis. J Vis Exp JoVE 57423. https://doi.org/10.3791/57423

Brognara L, Salmaso L, Mazzotti A, et al (2020) Effects of Probiotics in the Management of Infected Chronic Wounds: From Cell Culture to Human Studies. Curr Clin Pharmacol 15:193–206. https://doi.org/10.2174/1574884714666191111130630

Bruneel B, Witten PE (2015) Power and challenges of using zebrafish as a model for skeletal tissue imaging. Connect Tissue Res 56:161–173. https://doi.org/10.3109/03008207.2015.1013193

Bussell ME (2021) Improving bone health: addressing the burden through an integrated approach. Aging Clin Exp Res 33:2777–2786. https://doi.org/10.1007/s40520-021-01971-3

Bussmann J, Schulte-Merker S (2011) Rapid BAC selection for tol2-mediated transgenesis in zebrafish. Dev Camb Engl 138:4327–4332. https://doi.org/10.1242/dev.068080

Cao JJ, Gregoire BR, Zeng H (2012) Selenium Deficiency Decreases Antioxidative Capacity and Is Detrimental to Bone Microarchitecture in Mice. J Nutr 142:1526–1531. https://doi.org/10.3945/jn.111.157040

Carlberg C, Molnár F (2015) Vitamin D receptor signaling and its therapeutic implications: Genome-wide and structural view. Can J Physiol Pharmacol 93:311–318. https://doi.org/10.1139/cjpp-2014-0383

Carter M, Shieh J (2015) Chapter 14 - Cell Culture Techniques. In: Carter M, Shieh J (eds) Guide to Research Techniques in Neuroscience (Second Edition). Academic Press, San Diego, pp 295–310

Castaneda M, Strong JM, Alabi DA, Hernandez CJ (2020) The Gut Microbiome and Bone Strength. Curr Osteoporos Rep 18:677–683. https://doi.org/10.1007/s11914-020-00627-x

Caverzasio J, Manen D (2007) Essential role of Wnt3a-mediated activation of mitogen-activated protein kinase p38 for the stimulation of alkaline phosphatase activity and matrix mineralization in C3H10T1/2 mesenchymal cells. Endocrinology 148:5323–5330. https://doi.org/10.1210/en.2007-0520

Chang J, Sonoyama W, Wang Z, et al (2007) Noncanonical Wnt-4 signaling enhances bone regeneration of mesenchymal stem cells in craniofacial defects through activation of p38 MAPK. J Biol Chem 282:30938–30948. https://doi.org/10.1074/jbc.M702391200

Chaplin A, Parra P, Laraichi S, et al (2016) Calcium supplementation modulates gut microbiota in a prebiotic manner in dietary obese mice. Mol Nutr Food Res 60:468–480. https://doi.org/10.1002/mnfr.201500480

Chen G, Deng C, Li Y-P (2012) TGF-β and BMP Signaling in Osteoblast Differentiation and Bone Formation. Int J Biol Sci 8:272–288. https://doi.org/10.7150/ijbs.2929

Chen Z-Y, Hsieh Y-M, Huang C-C, Tsai C-C (2017) Inhibitory Effects of Probiotic Lactobacillus on the Growth of Human Colonic Carcinoma Cell Line HT-29. Molecules 22:107. https://doi.org/10.3390/molecules22010107

Cheng J, Peng K, Jin E, et al (2011) Effect of Additional Boron on Tibias of African Ostrich Chicks. Biol Trace Elem Res 144:538–549. https://doi.org/10.1007/s12011-011-9024-y

Chiang S-S, Pan T-M (2011) Antiosteoporotic Effects of Lactobacillus-Fermented Soy Skim Milk on Bone Mineral Density and the Microstructure of Femoral Bone in Ovariectomized Mice. J Agric Food Chem 59:7734–7742. https://doi.org/10.1021/jf2013716

Christou M, Iliopoulou M, Witten PE, Koumoundouros G (2018) Segmentation pattern of zebrafish caudal fin is affected by developmental temperature and defined by multiple fusions between segments. J Exp Zoolog B Mol Dev Evol 330:330–340. https://doi.org/10.1002/jez.b.22825

Cohen-Tanugi A, Forest N (1998) Retinoic acid suppresses the osteogenic differentiation capacity of murine osteoblast-like 3/A/1D-1M cell cultures. Differentiation 63:115–123. https://doi.org/10.1046/j.1432-0436.1998.6330115.x

Cosman F, de Beur SJ, LeBoff MS, et al (2014) Clinician's Guide to Prevention and Treatment of Osteoporosis. Osteoporos Int 25:2359–2381. https://doi.org/10.1007/s00198-014-2794-2

Crockett JC, Mellis DJ, Scott DI, Helfrich MH (2011) New knowledge on critical osteoclast formation and activation pathways from study of rare genetic diseases of osteoclasts: focus on the RANK/RANKL axis. Osteoporos Int 22:1–20. https://doi.org/10.1007/s00198-010-1272-8

Cuadrado A, Nebreda AR (2010) Mechanisms and functions of p38 MAPK signalling. Biochem J 429:403–417. https://doi.org/10.1042/BJ20100323

Cubbage CC, Mabee PM (1996) Development of the cranium and paired fins in the zebrafish Danio rerio (Ostariophysi, Cyprinidae). J Morphol 229:121–160. https://doi.org/10.1002/(SICI)1097-4687(199608)229:2<121::AID-JMOR1>3.0.CO;2-4

Darias MJ, Mazurais D, Koumoundouros G, et al (2010) Dietary vitamin D3 affects digestive system ontogenesis and ossification in European sea bass (Dicentrachus labrax, Linnaeus, 1758). Aquaculture 298:300–307. https://doi.org/10.1016/j.aquaculture.2009.11.002

Day TF, Yang Y (2008) Wnt and Hedgehog Signaling Pathways in Bone Development. JBJS 90:19–24. https://doi.org/10.2106/JBJS.G.01174

DeLaurier A, Eames BF, Blanco-Sánchez B, et al (2010) Zebrafish sp7:EGFP: A transgenic for studying otic vesicle formation, skeletogenesis, and bone regeneration. genesis 48:505–511. https://doi.org/10.1002/dvg.20639

Dousset B, Benderdour M, Hess K, et al (2002) Effects of Boron in Wound Healing. In: Roussel AM, Anderson RA, Favier AE (eds) Trace Elements in Man and Animals 10. Springer US, New York, NY, pp 1061–1065

Downey CM, Horton CR, Carlson BA, et al (2009) Osteo-Chondroprogenitor–Specific Deletion of the Selenocysteine tRNA Gene, Trsp, Leads to Chondronecrosis and Abnormal Skeletal Development: A Putative Model for Kashin-Beck Disease. PLOS Genet 5:e1000616. https://doi.org/10.1371/journal.pgen.1000616

Dreher I, Schütze N, Baur A, et al (1998) Selenoproteins Are Expressed in Fetal Human Osteoblast-like Cells. Biochem Biophys Res Commun 245:101–107. https://doi.org/10.1006/bbrc.1998.8393

Driel M, Koedam M, Buurman CJ, et al (2006) Evidence for auto/paracrine actions of vitamin D in bone: 1a-hydroxylase expression and activity in human bone cells. FASEB J 20:2417–2419. https://doi.org/10.1096/fj.06-6374fje

Duan P, Bonewald LF (2016) The role of the wnt/β-catenin signaling pathway in formation and maintenance of bone and teeth. Int J Biochem Cell Biol 77:23–29. https://doi.org/10.1016/j.biocel.2016.05.015

Ebert R, Ulmer M, Zeck S, et al (2006) Selenium Supplementation Restores the Antioxidative Capacity and Prevents Cell Damage in Bone Marrow Stromal Cells In Vitro. STEM CELLS 24:1226–1235. https://doi.org/10.1634/stemcells.2005-0117

Fernández I, Gavaia PJ, Laizé V, Cancela ML (2018) Fish as a model to assess chemical toxicity in bone. Aquat Toxicol 194:208–226. https://doi.org/10.1016/j.aquatox.2017.11.015

Fu Y, Zhao X-H (2013) In vitro responses of hFOB1.19 cells towards chum salmon (Oncorhynchus keta) skin gelatin hydrolysates in cell proliferation, cycle progression and apoptosis. J Funct Foods 5:279–288. https://doi.org/10.1016/j.jff.2012.10.017

Gallardo-Williams MT, Maronpot RR, Turner CH, et al (2003) Effects of Boric Acid Supplementation on Bone Histomorphometry, Metabolism, and Biomechanical Properties in Aged Female F-344 Rats. Biol Trace Elem Res 93:155–170. https://doi.org/10.1385/BTER:93:1-3:155

Gasbarrini G, Bonvicini F, Gramenzi A (2016) Probiotics History. J Clin Gastroenterol 50 Suppl 2, Proceedings from the 8th Probiotics, Prebiotics&New Foods for Microbiota and Human Health meeting held in Rome, Italy on September 13-15, 2015:S116–S119. https://doi.org/10.1097/MCG.0000000000000697

Gavaia PJ, Simes DC, Ortiz-Delgado JB, et al (2006) Osteocalcin and matrix Gla protein in zebrafish (Danio rerio) and Senegal sole (Solea senegalensis): Comparative gene and protein

expression during larval development through adulthood. Gene Expr Patterns 6:637–652. https://doi.org/10.1016/j.modgep.2005.11.010

Gemberling M, Bailey TJ, Hyde DR, Poss KD (2013) The zebrafish as a model for complex tissue regeneration. Trends Genet 29:611–620. https://doi.org/10.1016/j.tig.2013.07.003

Geng S, Zhou S, Bi Z, Glowacki J (2013) Vitamin D metabolism in human bone marrow stromal (mesenchymal stem) cells. Metabolism 62:768–777. https://doi.org/10.1016/j.metabol.2013.01.003

Gistelinck C, Gioia R, Gagliardi A, et al (2016) Zebrafish Collagen Type I: Molecular and Biochemical Characterization of the Major Structural Protein in Bone and Skin. Sci Rep 6:21540. https://doi.org/10.1038/srep21540

Glass DA, Bialek P, Ahn JD, et al (2005) Canonical Wnt signaling in differentiated osteoblasts controls osteoclast differentiation. Dev Cell 8:751–764. https://doi.org/10.1016/j.devcel.2005.02.017

Goldbach HE, Yu Q, Wingender R, et al (2001) Rapid response reactions of roots to boron deprivation. J Plant Nutr Soil Sci 164:173–181. https://doi.org/10.1002/1522-2624(200104)164:2<173::AID-JPLN173>3.0.CO;2-F

Gorustovich AA, Steimetz T, Nielsen FH, Guglielmotti MB (2006) A histomorphometric study of alveolar bone modeling and remodeling in mice fed a boron-deficient diet. FASEB J 20:A195–A195. https://doi.org/10.1096/fasebj.20.4.A195

Gromer S, Eubel JK, Lee BL, Jacob J (2005) Human selenoproteins at a glance. Cell Mol Life Sci CMLS 62:2414–2437. https://doi.org/10.1007/s00018-005-5143-y

Guicheux J, Lemonnier J, Ghayor C, et al (2003) Activation of p38 mitogen-activated protein kinase and c-Jun-NH2-terminal kinase by BMP-2 and their implication in the stimulation of osteoblastic cell differentiation. J Bone Miner Res Off J Am Soc Bone Miner Res 18:2060–2068. https://doi.org/10.1359/jbmr.2003.18.11.2060

Hakki SS, Bozkurt BS, Hakki EE (2010) Boron regulates mineralized tissue-associated proteins in osteoblasts (MC3T3-E1). J Trace Elem Med Biol 24:243–250. https://doi.org/10.1016/j.jtemb.2010.03.003

Hall BK (2005) Bones and Cartilage: Developmental and Evolutionary Skeletal Biology. Elsevier

Hall BK, Miyake T (1992) The membranous skeleton: the role of cell condensations in vertebrate skeletogenesis. Anat Embryol (Berl) 186:107–124. https://doi.org/10.1007/BF00174948

Hao M, Wang G, Zuo X, et al (2019) Gut microbiota: an overlooked factor that plays a significant role in osteoporosis. J Int Med Res 47:4095–4103. https://doi.org/10.1177/0300060519860027

Harris SA, Enger RJ, Riggs LB, Spelsberg TC (1995) Development and characterization of a conditionally immortalized human fetal osteoblastic cell line. J Bone Miner Res 10:178–186. https://doi.org/10.1002/jbmr.5650100203

Haussler MR, Haussler CA, Whitfield GK, et al (2010) The nuclear vitamin D receptor controls the expression of genes encoding factors which feed the “Fountain of Youth” to mediate healthful aging. J Steroid Biochem Mol Biol 121:88–97. https://doi.org/10.1016/j.jsbmb.2010.03.019

Haussler MR, Whitfield GK, Kaneko I, et al (2013) Molecular Mechanisms of Vitamin D Action. Calcif Tissue Int 92:77–98. https://doi.org/10.1007/s00223-012-9619-0

Heath JK, Reynolds JJ (1990) Chapter 2 - Bone cell physiology and in vitro techniques in its investigation. In: Stevenson JC (ed) New Techniques in Metabolic Bone Disease. Butterworth-Heinemann, pp 21–39

Hegsted M, Keenan MJ, Siver F, Wozniak P (1991) Effect of boron on vitamin D deficient rats. Biol Trace Elem Res 28:243–255. https://doi.org/10.1007/BF02990471

Hirasawa T, Kuratani S (2015) Evolution of the vertebrate skeleton: morphology, embryology, and development. Zool Lett 1:2. https://doi.org/10.1186/s40851-014-0007-7

Holmen SL, Zylstra CR, Mukherjee A, et al (2005) Essential role of beta-catenin in postnatal bone acquisition. J Biol Chem 280:21162–21168. https://doi.org/10.1074/jbc.M501900200

Holroyd C, Cooper C, Dennison E (2008) Epidemiology of osteoporosis. Best Pract Res Clin Endocrinol Metab 22:671–685. https://doi.org/10.1016/j.beem.2008.06.001

Howe DG, Bradford YM, Eagle A, et al (2017) The Zebrafish Model Organism Database: new support for human disease models, mutation details, gene expression phenotypes and searching. Nucleic Acids Res 45:D758–D768. https://doi.org/10.1093/nar/gkw1116

Hu H, Hilton MJ, Tu X, et al (2005) Sequential roles of Hedgehog and Wnt signaling in osteoblast development. Dev Camb Engl 132:49–60. https://doi.org/10.1242/dev.01564

Hunt CD (2003) Dietary boron: An overview of the evidence for its role in immune function. J Trace Elem Exp Med 16:291–306. https://doi.org/10.1002/jtra.10041

Huycke TR, Eames BF, Kimmel CB (2012) Hedgehog-dependent proliferation drives modular growth during morphogenesis of a dermal bone. Development 139:2371–2380. https://doi.org/10.1242/dev.079806

Iba K, Chiba H, Yamashita T, et al (2001) Phase-independent Inhibition by Retinoic Acid of Mineralization Correlated with Loss of Tetranectin Expression in a Human Osteoblastic Cell Line. Cell Struct Funct 26:227–233. https://doi.org/10.1247/csf.26.227

Inohaya K, Takano Y, Kudo A (2007) The teleost intervertebral region acts as a growth center of the centrum: in vivo visualization of osteoblasts and their progenitors in transgenic fish. Dev Dyn Off Publ Am Assoc Anat 236:3031–3046. https://doi.org/10.1002/dvdy.21329

Isazadeh A, Hajazimian S, Shadman B, et al (2020) Anti-Cancer Effects of Probiotic Lactobacillus acidophilus for Colorectal Cancer Cell Line Caco-2 through Apoptosis Induction. Pharm Sci 27:262–267. https://doi.org/10.34172/PS.2020.52

Jafarnejad S, Djafarian K, Fazeli MR, et al (2017) Effects of a Multispecies Probiotic Supplement on Bone Health in Osteopenic Postmenopausal Women: A Randomized, Double-blind, Controlled Trial. J Am Coll Nutr 36:497–506. https://doi.org/10.1080/07315724.2017.1318724

Jakob F, Becker K, Paar E, et al (2002) Expression and Regulation of Thioredoxin Reductases and Other Selenoproteins in Bone. In: Methods in Enzymology. Elsevier, pp 168–179

Jansson P-A, Curiac D, Ahrén IL, et al (2019) Probiotic treatment using a mix of three Lactobacillus strains for lumbar spine bone loss in postmenopausal women: a randomised, double-blind, placebo-controlled, multicentre trial. Lancet Rheumatol 1:e154–e162. https://doi.org/10.1016/S2665-9913(19)30068-2

Jerome C, Hoch B, Carlson CS (2018) 5 - Skeletal System. In: Treuting PM, Dintzis SM, Montine KS (eds) Comparative Anatomy and Histology (Second Edition). Academic Press, San Diego, pp 67–88

Johnson SL, Bennett P (1998) Chapter 16 Growth Control in the Ontogenetic and Regenerating Zebrafish Fin. In: Detrich HW, Westerfield M, Zon LI (eds) Methods in Cell Biology. Academic Press, pp 301–311

Kague E, Gallagher M, Burke S, et al (2012) Skeletogenic Fate of Zebrafish Cranial and Trunk Neural Crest. PLoS ONE 7:e47394. https://doi.org/10.1371/journal.pone.0047394

Kanis JA, Norton N, Harvey NC, et al (2021) SCOPE 2021: a new scorecard for osteoporosis in Europe. Arch Osteoporos 16:82. https://doi.org/10.1007/s11657-020-00871-9

Kangari P, Talaei-Khozani T, Razeghian-Jahromi I, Razmkhah M (2020) Mesenchymal stem cells: amazing remedies for bone and cartilage defects. Stem Cell Res Ther 11:492. https://doi.org/10.1186/s13287-020-02001-1

Kartsogiannis V, Ng KW (2004) Cell lines and primary cell cultures in the study of bone cell biology. Mol Cell Endocrinol 228:79–102. https://doi.org/10.1016/j.mce.2003.06.002

Kato H, Ochiai-Shino H, Onodera S, et al (2015) Promoting effect of 1,25(OH) 2 vitamin D 3 in osteogenic differentiation from induced pluripotent stem cells to osteocyte-like cells. Open Biol 5:140201. https://doi.org/10.1098/rsob.140201

Keeting PE, Scott RE, Colvard DS, et al (1992) Development and characterization of a rapidly proliferating, well-differentiated cell line derived from normal adult human osteoblast-like cells transfected with SV40 large T antigen. J Bone Miner Res 7:127–136. https://doi.org/10.1002/jbmr.5650070203

Khaliq H, Juming Z, Ke-Mei P (2018) The Physiological Role of Boron on Health. Biol Trace Elem Res 186:31–51. https://doi.org/10.1007/s12011-018-1284-3

Kimmel CB, DeLaurier A, Ullmann B, et al (2010) Modes of Developmental Outgrowth and Shaping of a Craniofacial Bone in Zebrafish. PLOS ONE 5:e9475. https://doi.org/10.1371/journal.pone.0009475

Knopf F, Hammond C, Chekuru A, et al (2011) Bone Regenerates via Dedifferentiation of Osteoblasts in the Zebrafish Fin. Dev Cell 20:713–724. https://doi.org/10.1016/j.devcel.2011.04.014

Komori T (2009) Regulation of bone development and extracellular matrix protein genes by RUNX2. Cell Tissue Res 339:189. https://doi.org/10.1007/s00441-009-0832-8

König D, Page L, Chassot B, Jaźwińska A (2018) Dynamics of actinotrichia regeneration in the adult zebrafish fin. Dev Biol 433:416–432. https://doi.org/10.1016/j.ydbio.2017.07.024

Lai C-F, Cheng S-L (2002) Signal transductions induced by bone morphogenetic protein-2 and transforming growth factor-beta in normal human osteoblastic cells. J Biol Chem 277:15514–15522. https://doi.org/10.1074/jbc.M200794200

Laizé V, Gavaia PJ, Cancela ML (2014) Fish: a suitable system to model human bone disorders and discover drugs with osteogenic or osteotoxic activities. Drug Discov Today Dis Models 13:29–37. https://doi.org/10.1016/j.ddmod.2014.08.001

Laizé V, Rosa JT, Tarasco M, Cancela ML (2022) Chapter 12 - Status, challenges, and perspectives of fish cell culture—Focus on cell lines capable of in vitro mineralization. In: Monzón IF, Fernandes JMO (eds) Cellular and Molecular Approaches in Fish Biology. Academic Press, pp 381–404

Lambert MNT, Thybo CB, Lykkeboe S, et al (2017) Combined bioavailable isoflavones and probiotics improve bone status and estrogen metabolism in postmenopausal osteopenic women: a randomized controlled trial. Am J Clin Nutr 106:909–920. https://doi.org/10.3945/ajcn.117.153353

Lean JM, Jagger CJ, Kirstein B, et al (2005) Hydrogen Peroxide Is Essential for Estrogen-Deficiency Bone Loss and Osteoclast Formation. Endocrinology 146:728–735. https://doi.org/10.1210/en.2004-1021

Lee NK, Choi YG, Baik JY, et al (2005) A crucial role for reactive oxygen species in RANKL-induced osteoclast differentiation. Blood 106:852–859. https://doi.org/10.1182/blood-2004-09-3662

Leist M, Raab B, Maurer S, et al (1996) Conventional cell culture media do not adequately supply cells with antioxidants and thus facilitate peroxide-induced genotoxicity. Free Radic Biol Med 21:297–306. https://doi.org/10.1016/0891-5849(96)00045-7

Li J-Y, Chassaing B, Tyagi AM, et al (2016) Sex steroid deficiency–associated bone loss is microbiota dependent and prevented by probiotics. J Clin Invest 126:2049–2063. https://doi.org/10.1172/JCI86062

Li W, Zhang S, Liu J, et al (2019) Vitamin K2 stimulates MC3T3-E1 osteoblast differentiation and mineralization through autophagy induction. Mol Med Rep 19:3676–3684. https://doi.org/10.3892/mmr.2019.10040

Liang W, Lin M, Li X, et al (2012) Icariin promotes bone formation via the BMP-2/Smad4 signal transduction pathway in the hFOB 1.19 human osteoblastic cell line. Int J Mol Med 30:889–895. https://doi.org/10.3892/ijmm.2012.1079

Lieben L, Masuyama R, Torrekens S, et al (2012) Normocalcemia is maintained in mice under conditions of calcium malabsorption by vitamin D–induced inhibition of bone mineralization. J Clin Invest 122:1803–1815. https://doi.org/10.1172/JCI45890

Lieschke GJ, Currie PD (2007) Animal models of human disease: zebrafish swim into view. Nat Rev Genet 8:353–367. https://doi.org/10.1038/nrg2091

Lin GL, Hankenson KD (2011) Integration of BMP, Wnt, and notch signaling pathways in osteoblast differentiation. J Cell Biochem 112:3491–3501. https://doi.org/10.1002/jcb.23287

Lips P (2006) Vitamin D physiology. Prog Biophys Mol Biol 92:4–8. https://doi.org/10.1016/j.pbiomolbio.2006.02.016

Lips P, van Schoor NM (2011) The effect of vitamin D on bone and osteoporosis. Best Pract Res Clin Endocrinol Metab 25:585–591. https://doi.org/10.1016/j.beem.2011.05.002

Liu H, Bian W, Liu S, Huang K (2012) Selenium Protects Bone Marrow Stromal Cells Against Hydrogen Peroxide-Induced Inhibition of Osteoblastic Differentiation by Suppressing Oxidative Stress and ERK Signaling Pathway. Biol Trace Elem Res 150:441–450. https://doi.org/10.1007/s12011-012-9488-4

Lu J, Holmgren A (2009) Selenoproteins *. J Biol Chem 284:723–727. https://doi.org/10.1074/jbc.R800045200

Lynch MP, Capparelli C, Stein JL, et al (1998) Apoptosis during bone-like tissue development in vitro. J Cell Biochem 68:31–49. https://doi.org/10.1002/(SICI)1097-4644(19980101)68:1<31::AID-JCB4>3.0.CO;2-X

Machado RG, Eames BF (2017) Using Zebrafish to Test the Genetic Basis of Human Craniofacial Diseases. J Dent Res 96:1192–1199. https://doi.org/10.1177/0022034517722776

Mahamid J, Sharir A, Addadi L, Weiner S (2008) Amorphous calcium phosphate is a major component of the forming fin bones of zebrafish: Indications for an amorphous precursor phase. Proc Natl Acad Sci 105:12748–12753. https://doi.org/10.1073/pnas.0803354105

Mak KK, Chen M-H, Day TF, et al (2006) Wnt/beta-catenin signaling interacts differentially with Ihh signaling in controlling endochondral bone and synovial joint formation. Dev Camb Engl 133:3695–3707. https://doi.org/10.1242/dev.02546

Mann V, Grimm D, Corydon TJ, et al (2019) Changes in Human Foetal Osteoblasts Exposed to the Random Positioning Machine and Bone Construct Tissue Engineering. Int J Mol Sci 20:1357. https://doi.org/10.3390/ijms20061357

Manolagas SC (2010) From Estrogen-Centric to Aging and Oxidative Stress: A Revised Perspective of the Pathogenesis of Osteoporosis. Endocr Rev 31:266–300. https://doi.org/10.1210/er.2009-0024

Maradonna F, Gioacchini G, Falcinelli S, et al (2013) Probiotic Supplementation Promotes Calcification in Danio rerio Larvae: A Molecular Study. PLoS One 8:. https://doi.org/10.1371/journal.pone.0083155

Martin TJ, Ng KW, Suda T (1989) Bone Cell Physiology. Endocrinol Metab Clin North Am 18:833–858. https://doi.org/10.1016/S0889-8529(18)30346-3

McCabe LR, Irwin R, Schaefer L, Britton RA (2013) Probiotic use decreases intestinal inflammation and increases bone density in healthy male but not female mice. J Cell Physiol 228:1793–1798. https://doi.org/10.1002/jcp.24340

McCoy H, Kenney MA, Montgomery C, et al (1994) Relation of boron to the composition and mechanical properties of bone. Environ Health Perspect 102:49–53. https://doi.org/10.1289/ehp.94102s749

Meijden K van der, Lips P, Driel M van, et al (2014) Primary Human Osteoblasts in Response to 25-Hydroxyvitamin D3, 1,25-Dihydroxyvitamin D3 and 24R,25-Dihydroxyvitamin D3. PLOS ONE 9:e110283. https://doi.org/10.1371/journal.pone.0110283

Melton III LJ, Atkinson EJ, O'Connor MK, et al (1998) Bone Density and Fracture Risk in Men. J Bone Miner Res 13:1915–1923. https://doi.org/10.1359/jbmr.1998.13.12.1915

Melton III LJ, Chrischilles EA, Cooper C, et al (1992) Perspective how many women have osteoporosis? J Bone Miner Res 7:1005–1010. https://doi.org/10.1002/jbmr.5650070902

Miggiano GAD, Gagliardi L (2005) [Diet, nutrition and bone health]. Clin Ter 156:47–56

Mitchell RE, Huitema LFA, Skinner REH, et al (2013) New tools for studying osteoarthritis genetics in zebrafish. Osteoarthritis Cartilage 21:269–278.

Mody N, Parhami F, Sarafian TA, Demer LL (2001) Oxidative stress modulates osteoblastic differentiation of vascular and bone cells. Free Radic Biol Med 31:509–519. https://doi.org/10.1016/S0891-5849(01)00610-4

Moreno-Reyes R, Egrise D, Nève J, et al (2001) Selenium Deficiency-Induced Growth Retardation Is Associated with an Impaired Bone Metabolism and Osteopenia. J Bone Miner Res 16:1556–1563. https://doi.org/10.1359/jbmr.2001.16.8.1556

Morin-Kensicki EM, Eisen JS (1997) Sclerotome development and peripheral nervous system segmentation in embryonic zebrafish. Dev Camb Engl 124:159–167. https://doi.org/10.1242/dev.124.1.159

Nakamichi Y, Udagawa N, Horibe K, et al (2017) VDR in Osteoblast-Lineage Cells Primarily Mediates Vitamin D Treatment-Induced Increase in Bone Mass by Suppressing Bone Resorption. J Bone Miner Res 32. https://doi.org/10.1002/jbmr.3096

Nakashima K, Zhou X, Kunkel G, et al (2002) The Novel Zinc Finger-Containing Transcription Factor Osterix Is Required for Osteoblast Differentiation and Bone Formation. Cell 108:17–29. https://doi.org/10.1016/S0092-8674(01)00622-5

Narva M, Collin M, Lamberg-Allardt C, et al (2004a) Effects of Long-Term Intervention with Lactobacillus helveticus-Fermented Milk on Bone Mineral Density and Bone Mineral Content in Growing Rats. Ann Nutr Metab 48:228–234. https://doi.org/10.1159/000080455

Narva M, Halleen J, Väänänen K, Korpela R (2004b) Effects of Lactobacillus helveticus fermented milk on bone cells in vitro. Life Sci 75:1727–1734. https://doi.org/10.1016/j.lfs.2004.04.011

Nguyen K-D, Bagheri B, Bagheri H (2018) Drug-induced bone loss: a major safety concern in Europe. Expert Opin Drug Saf 17:1005–1014. https://doi.org/10.1080/14740338.2018.1524868

Nielsen FH (2004) Dietary fat composition modifies the effect of boron on bone characteristics and plasma lipids in rats. BioFactors 20:161–171. https://doi.org/10.1002/biof.5520200305

Nielsen FH (2009) Boron deprivation decreases liver S-adenosylmethionine and spermidine and increases plasma homocysteine and cysteine in rats. J Trace Elem Med Biol 23:204–213. https://doi.org/10.1016/j.jtemb.2009.03.001

Nilsson AG, Sundh D, Bäckhed F, Lorentzon M (2018) Lactobacillus reuteri reduces bone loss in older women with low bone mineral density: a randomized, placebo-controlled, double-blind, clinical trial. J Intern Med 284:307–317. https://doi.org/10.1111/joim.12805

Nöth U, Tuli R, Seghatoleslami R, et al (2003) Activation of p38 and Smads mediates BMP-2 effects on human trabecular bone-derived osteoblasts. Exp Cell Res 291:201–211. https://doi.org/10.1016/s0014-4827(03)00386-0

Nozari S, Faridvand Y, Etesami A, et al (2019) Potential anticancer effects of cell wall protein fractions from Lactobacillus paracasei on human intestinal Caco-2 cell line. Lett Appl Microbiol 69:148–154. https://doi.org/10.1111/lam.13198

Nzietchueng RM, Dousset B, Franck P, et al (2002) Mechanisms implicated in the effects of boron on wound healing. J Trace Elem Med Biol 16:239–244. https://doi.org/10.1016/S0946-672X(02)80051-7

O'Neill MA, Ishii T, Albersheim P, Darvill AG (2004) RHAMNOGALACTURONAN II: Structure and Function of a Borate Cross-Linked Cell Wall Pectic Polysaccharide. Annu Rev Plant Biol 55:109–139. https://doi.org/10.1146/annurev.arplant.55.031903.141750

Owen TA, Aronow M, Shalhoub V, et al (1990) Progressive development of the rat osteoblast phenotype in vitro: Reciprocal relationships in expression of genes associated with osteoblast proliferation and differentiation during formation of the bone extracellular matrix. J Cell Physiol 143:420–430. https://doi.org/10.1002/jcp.1041430304

Owen TA, Aronow MS, Barone LM, et al (1991) Pleiotropic Effects of Vitamin D on Osteoblast Gene Expression Are Related to the Proliferative and Differentiated State of the Bone Cell Phenotype: Dependency upon Basal Levels of Gene Expression, Duration of Exposure, and Bone Matrix Competency in Normal Rat Osteoblast Cultures*. Endocrinology 128:1496–1504. https://doi.org/10.1210/endo-128-3-1496

Paredes R, Arriagada G, Cruzat F, et al (2004) The Runx2 transcription factor plays a key role in the 1α,25-dihydroxy Vitamin D3-dependent upregulation of the rat osteocalcin (OC) gene expression in osteoblastic cells. J Steroid Biochem Mol Biol 89–90:269–271. https://doi.org/10.1016/j.jsbmb.2004.03.076

Park M, Li Q, Shcheynikov N, et al (2004) NaBC1 Is a Ubiquitous Electrogenic Na+-Coupled Borate Transporter Essential for Cellular Boron Homeostasis and Cell Growth and Proliferation. Mol Cell 16:331–341. https://doi.org/10.1016/j.molcel.2004.09.030

Pfefferli C, Jaźwińska A (2015) The art of fin regeneration in zebrafish. Regeneration 2:72–83. https://doi.org/10.1002/reg2.33

Piek E, Sleumer LS, van Someren EP, et al (2010) Osteo-transcriptomics of human mesenchymal stem cells: Accelerated gene expression and osteoblast differentiation induced by vitamin D reveals c-MYC as an enhancer of BMP2-induced osteogenesis. Bone 46:613–627. https://doi.org/10.1016/j.bone.2009.10.024

Pietschmann N, Rijntjes E, Hoeg A, et al (2014) Selenoprotein P is the essential selenium transporter for bones†. Metallomics 6:1043–1049. https://doi.org/10.1039/c4mt00003j

Pizzorno L (2015) Nothing Boring About Boron. Integr Med Clin J 14:35–48

Printzi A, Fragkoulis S, Dimitriadi A, et al (2021) Exercise-induced lordosis in zebrafish Danio rerio (Hamilton, 1822). J Fish Biol 98:987–994. https://doi.org/10.1111/jfb.14240

Qu Q, Perälä-Heape M, Kapanen A, et al (1998) Estrogen enhances differentiation of osteoblasts in mouse bone marrow culture. Bone 22:201–209. https://doi.org/10.1016/S8756-3282(97)00276-7

Rahman MS, Akhtar N, Jamil HM, et al (2015) TGF-β/BMP signaling and other molecular events: regulation of osteoblastogenesis and bone formation. Bone Res 3:1–20. https://doi.org/10.1038/boneres.2015.5

Reeves MA, Hoffmann PR (2009) The human selenoproteome: recent insights into functions and regulation. Cell Mol Life Sci 66:2457–2478. https://doi.org/10.1007/s00018-009-0032-4

Renn J, Schaedel M, Volff J-N, et al (2006) Dynamic expression of sparc precedes formation of skeletal elements in the Medaka (Oryzias latipes). Gene 372:208–218. https://doi.org/10.1016/j.gene.2006.01.011

Roberts S, Narisawa S, Harmey D, et al (2007) Functional Involvement of PHOSPHO1 in Matrix Vesicle–Mediated Skeletal Mineralization. J Bone Miner Res 22:617–627. https://doi.org/10.1359/jbmr.070108

Rodda SJ, McMahon AP (2006) Distinct roles for Hedgehog and canonical Wnt signaling in specification, differentiation and maintenance of osteoblast progenitors. Dev Camb Engl 133:3231–3244. https://doi.org/10.1242/dev.02480

Samarut E, Fraher D, Laudet V, Gibert Y (2015) ZebRA: An overview of retinoic acid signaling during zebrafish development. Biochim Biophys Acta BBA - Gene Regul Mech 1849:73–83. https://doi.org/10.1016/j.bbagrm.2014.05.030

Setzer B, Bächle M, Metzger MC, Kohal RJ (2009) The gene-expression and phenotypic response of hFOB 1.19 osteoblasts to surface-modified titanium and zirconia. Biomaterials 30:979–990. https://doi.org/10.1016/j.biomaterials.2008.10.054

Sharif F, de Bakker MAG, Richardson MK (2014) Osteoclast-like Cells in Early Zebrafish Embryos. Cell J 16:211–224

Shen Q, Christakos S (2005) The Vitamin D Receptor, Runx2, and the Notch Signaling Pathway Cooperate in the Transcriptional Regulation of Osteopontin *. J Biol Chem 280:40589–40598. https://doi.org/10.1074/jbc.M504166200

Skillington J, Choy L, Derynck R (2002) Bone morphogenetic protein and retinoic acid signaling cooperate to induce osteoblast differentiation of preadipocytes. J Cell Biol 159:135–146. https://doi.org/10.1083/jcb.200204060

Soltanoff CS, Yang S, Chen W, Li Y-P (2009) Signaling Networks that Control the Lineage Commitment and Differentiation of Bone Cells. Crit Rev Eukaryot Gene Expr 19:1–46. https://doi.org/10.1615/CritRevEukarGeneExpr.v19.i1.10

Song HM, Nacamuli RP, Xia W, et al (2005) High-dose retinoic acid modulates rat calvarial osteoblast biology. J Cell Physiol 202:255–262. https://doi.org/10.1002/jcp.20115

Spoorendonk KM, Hammond CL, Huitema LFA, et al (2010) Zebrafish as a unique model system in bone research: the power of genetics and in vivo imaging. J Appl Ichthyol 26:219–224. https://doi.org/10.1111/j.1439-0426.2010.01409.x

Stein GS, Lian JB, Stein JL, et al (1996) Transcriptional control of osteoblast growth and differentiation. Physiol Rev 76:593–629. https://doi.org/10.1152/physrev.1996.76.2.593

Stewart AJ, Roberts SJ, Seawright E, et al (2006) The presence of PHOSPHO1 in matrix vesicles and its developmental expression prior to skeletal mineralization. Bone 39:1000–1007. https://doi.org/10.1016/j.bone.2006.05.014

Strzelecka-Kiliszek A, Bozycki L, Mebarek S, et al (2017) Characteristics of minerals in vesicles produced by human osteoblasts hFOB 1.19 and osteosarcoma Saos-2 cells stimulated for mineralization. J Inorg Biochem 171:100–107. https://doi.org/10.1016/j.jinorgbio.2017.03.006

Subramaniam M, Jalal SM, Rickard DJ, et al (2002) Further characterization of human fetal osteoblastic hFOB 1.19 and hFOB/ER? cells: Bone formation in vivo and karyotype

analysis using multicolor fluorescent in situ hybridization. J Cell Biochem 87:9–15. https://doi.org/10.1002/jcb.10259

Sun L, Wu L, Bao C, et al (2009) Gene expressions of Collagen type I, ALP and BMP-4 in osteo-inductive BCP implants show similar pattern to that of natural healing bones. Mater Sci Eng C 29:1829–1834. https://doi.org/10.1016/j.msec.2009.02.011

Suniaga S, Rolvien T, vom Scheidt A, et al (2018) Increased mechanical loading through controlled swimming exercise induces bone formation and mineralization in adult zebrafish. Sci Rep 8:3646. https://doi.org/10.1038/s41598-018-21776-1

Takahashi N, Yamana H, Yoshiki S, et al (1988) Osteoclast-Like Cell Formation and its Regulation by Osteotropic Hormones in Mouse Bone Marrow Cultures*. Endocrinology 122:1373–1382. https://doi.org/10.1210/endo-122-4-1373

Takimoto T, Hatanaka M, Hoshino T, et al (2018) Effect of Bacillus subtilis C-3102 on bone mineral density in healthy postmenopausal Japanese women: a randomized, placebo-controlled, double-blind clinical trial. Biosci Microbiota Food Health 37:87–96. https://doi.org/10.12938/bmfh.18-006

Tarasco M, Laizé V, Cardeira J, et al (2017) The zebrafish operculum: A powerful system to assess osteogenic bioactivities of molecules with pharmacological and toxicological relevance. Comparative Biochemistry and Physiology Part C: Toxicology & Pharmacology 197:45–52. https://doi.org/10.1016/j.cbpc.2017.04.006

Terashima A, Takayanagi H (2018) Overview of Osteoimmunology. Calcif Tissue Int 102:503–511. https://doi.org/10.1007/s00223-018-0417-1

Thouverey C, Caverzasio J (2015) Focus on the p38 MAPK signaling pathway in bone development and maintenance. BoneKEy Rep 4:711. https://doi.org/10.1038/bonekey.2015.80

Tonelli F, Bek JW, Besio R, et al (2020) Zebrafish: A Resourceful Vertebrate Model to Investigate Skeletal Disorders. Front Endocrinol 11:489. https://doi.org/10.3389/fendo.2020.00489

Uysal T, Ustdal A, Sonmez MF, Ozturk F (2009) Stimulation of Bone Formation by Dietary Boron in an Orthopedically Expanded Suture in Rabbits. Angle Orthod 79:984–990. https://doi.org/10.2319/112708-604.1

Valenti MT, Marchetto G, Mottes M, Dalle Carbonare L (2020) Zebrafish: A Suitable Tool for the Study of Cell Signaling in Bone. Cells 9:1911. https://doi.org/10.3390/cells9081911

van Driel M, van Leeuwen JPTM (2014) Vitamin D endocrine system and osteoblasts. BoneKEy Rep 3:493. https://doi.org/10.1038/bonekey.2013.227

Varshney GK, Burgess SM (2014) Mutagenesis and phenotyping resources in zebrafish for studying development and human disease. Brief Funct Genomics 13:82–94. https://doi.org/10.1093/bfgp/elt042

Walker M, Kimmel C (2007) A two-color acid-free cartilage and bone stain for zebrafish larvae. Biotech Histochem 82:23–28. https://doi.org/10.1080/10520290701333558

Wang Y, Zhu J, DeLuca HF (2014) Identification of the Vitamin D Receptor in Osteoblasts and Chondrocytes But Not Osteoclasts in Mouse Bone. J Bone Miner Res 29:685–692. https://doi.org/10.1002/jbmr.2081

Wauquier F, Leotoing L, Coxam V, et al (2009) Oxidative stress in bone remodelling and disease. Trends Mol Med 15:468–477. https://doi.org/10.1016/j.molmed.2009.08.004

Weigele J, Franz-Odendaal TA (2016) Functional bone histology of zebrafish reveals two types of endochondral ossification, different types of osteoblast clusters and a new bone type. J Anat 229:92–103. https://doi.org/10.1111/joa.12480

Wilkinson GF, Pritchard K (2015) In Vitro Screening for Drug Repositioning. J Biomol Screen 20:167–179. https://doi.org/10.1177/1087057114563024

Wilson JH, Ruszler PL (1996) Effects of dietary boron supplementation on laying hens. Br Poult Sci 37:723–729. https://doi.org/10.1080/00071669608417902

Witten PE, Huysseune A (2009) A comparative view on mechanisms and functions of skeletal remodelling in teleost fish, with special emphasis on osteoclasts and their function. Biol Rev 84:315–346. https://doi.org/10.1111/j.1469-185X.2009.00077.x

Woeckel VJ, Alves RD a. M, Swagemakers SMA, et al (2010) 1α,25-(OH)2D3 acts in the early phase of osteoblast differentiation to enhance mineralization via accelerated production of mature matrix vesicles. J Cell Physiol 225:593–600. https://doi.org/10.1002/jcp.22244

World Health Organization. (2004). Vitamin and mineral requirements in human nutrition. World Health Organization

Wu S, Yoon S, Zhang Y-G, et al (2015) Vitamin D receptor pathway is required for probiotic protection in colitis. Am J Physiol-Gastrointest Liver Physiol 309:G341–G349. https://doi.org/10.1152/ajpgi.00105.2015

Xu C, Volkery S, Siekmann AF (2015) Intubation-based anesthesia for long-term time-lapse imaging of adult zebrafish. Nat Protoc 10:2064–2073. https://doi.org/10.1038/nprot.2015.130

Yadav MC, Simão AMS, Narisawa S, et al (2011) Loss of skeletal mineralization by the simultaneous ablation of PHOSPHO1 and alkaline phosphatase function: A unified model of the mechanisms of initiation of skeletal calcification. J Bone Miner Res 26:286–297. https://doi.org/10.1002/jbmr.195

Yang D, Turner AG, Wijenayaka AR, et al (2015) 1,25-Dihydroxyvitamin D3 and extracellular calcium promote mineral deposition via NPP1 activity in a mature osteoblast cell line MLO-A5. Mol Cell Endocrinol 412:140–147. https://doi.org/10.1016/j.mce.2015.06.005

Yuan Y, Jin S, Qi X, et al (2019) Osteogenesis stimulation by copper-containing 316L stainless steel via activation of akt cell signaling pathway and Runx2 upregulation. J Mater Sci Technol 35:2727–2733. https://doi.org/10.1016/j.jmst.2019.04.028

Zheng C, Wang J, Liu Y, et al (2014) Functional Selenium Nanoparticles Enhanced Stem Cell Osteoblastic Differentiation through BMP Signaling Pathways. Adv Funct Mater 24:6872–6883. https://doi.org/10.1002/adfm.201401263

Zhou S, Glowacki J, Kim SW, et al (2012) Clinical characteristics influence in vitro action of 1,25-dihydroxyvitamin D3 in human marrow stromal cells. J Bone Miner Res 27:1992–2000. https://doi.org/10.1002/jbmr.1655

HYPOTHESIS

Hypothesis 1:

Micronutrients such as B and Se play key roles during the ossification process as suggested by various *in vitro* and *in vivo* studies. Furthermore, there are very few ambiguous reports on a possibility of positive osteogenic effect by the synergistic activity of the micronutrients and VD, a proven osteogenic micronutrient. Therefore, we hypothesize that B or Se can synergistically upregulate the osteogenic activity of VD.

Hypothesis 2:

Despite the fact that there are still gaps in our understanding of the molecular and physiological processes underlying the interaction between gut microbiota and bone, it has been previously reported that some probiotic strains, as dietary supplements, could contribute to the intestinal microecological balance, which is essential for bone health. Hence our second hypothesis is that the probiotic strains selected in this study may have a role to play in improving bone health or regeneration, when used alone or in combination with VD.

OBJECTIVES

Chapter 1:

- Establish the effective osteogenic concentrations of the micronutrient B and further explore the mode of action by analyzing the transcriptome of zebrafish larvae and using transgenic lines of zebrafish.
- Explore the potential synergy between the selected B concentrations with the pro-osteogenic VD in zebrafish larvae.

Chapter 2:

- Unveil the effect of selected probiotics mix in bone regeneration using juvenile zebrafish caudal fin as a tool.

Chapter 3 :

- Screen for potential probiotics with osteogenic properties and further test how they modulate skeletogenesis in wild-type and transgenic zebrafish larvae.
- Develop two new transgenic lines expressing the GFP protein under transcriptional control of the endogenous regulatory regions for the osteoblast marker *sp7* gene and its downstream target gene *col10a1a* and further apply them for testing the efficacy of selected osteogenic strains of probiotics.

Chapter 4:

- Use the extracts of probiotics and their combinations with VD in hFOB1.19 cell line to establish an *in vitro* model system to study osteogenicity of probiotics and to look for a possible synergistic combinations of probiotic strains and VD.
- Using hFOB1.19 cell line, explore the mineralogenic effect of the micronutrients B and Se and their combinations with VD.

CHAPTER 1: ZEBRAFISH AS A MODEL TO UNVEIL THE PRO-OSTEOGENIC EFFECTS OF BORON-VITAMIN D3 SYNERGISM

Jerry Maria Sojan[1], Manu Kumar Gundappa[2], Alessio Carletti[3,4], Vasco Gaspar[4], Paulo Gavaia[3,4], Francesca Maradonna[1*], Oliana Carnevali[1]

[1]Department of Life and Environmental Sciences, Università Politecnica delle Marche, via Brecce Bianche, 60131 Ancona, Italy
[2]The Roslin Institute and Royal (Dick) School of Veterinary Studies, The University of Edinburgh, Midlothian, United Kingdom
[3]CCMAR, University of Algarve, Campus Gambelas, 8005-139 Faro, Portugal
[4]Faculty of Medicine and Biomedical Sciences, University of Algarve, Campus de Gambelas, 8005-139 Faro, Portugal

Abstract

The micronutrient boron (B) plays a key role during the ossification process as suggested by various in vitro and in vivo studies. To deepen our understanding of the molecular mechanism involved in the osteogenicity of B and its possible interaction with vitamin D3 (VD), wild-type AB zebrafish (*Danio rerio*) were used for morphometric analysis and transcriptomic analysis in addition to taking advantage of the availability of specific zebrafish osteoblast reporter lines. Firstly, osteoactive concentrations of B, VD and their combinations were established by morphometric analysis of the opercular bone in AR-stained zebrafish larvae exposed to two selected concentrations of B (10 and 100 ng/ml), one concentration of VD (10 pg/ml) and their respective combinations. Bone formation, as measured by opercular bone growth, was significantly increased in the two combination treatments than VD alone. Subsequently, a transcriptomic approach was adopted to unveil the molecular key regulators involved in the synergy. Clustering of differentially expressed genes (DEGs) revealed enrichment towards bone and skeletal functions in the groups co-treated with B and VD. Downstream analysis confirmed MAPK as the most regulated pathway by the synergy groups in addition to TGF-β signaling, focal adhesion and calcium signaling. The best performing synergistic treatment, B at 10 ng/ml and VD at 10 pg/ml, was applied to two zebrafish transgenic lines, *Tg(sp7:mCherry)* and *Tg(bglap:EGFP),* at multiple time points to further explore the results of the transcriptomic analysis. The synergistic treatment with B and VD induced an enrichment of intermediate (*sp7*$^{+}$)

osteoblast at 6- and 9-days post fertilization (dpf) and of mature (*bglap*$^{+}$) osteoblasts at 15 dpf. The results obtained here validate the role of B in VD-dependent control over bone mineralization and can help widening the spectrum of therapeutic approaches to alleviate pathological conditions caused by VD deficiency by using low concentrations of B as nutritional additive.

Keywords

Bone, Boron, Vitamin D3, Micronutrients, Zebrafish, RNA-Seq, Transgenic lines, Cell differentiation

Introduction

Osteogenesis is a process which can be modulated by several factors including macro and micronutrients supplementation. Among the various micronutrients, it has been demonstrated that boron (B) has an important role in the development and maintenance of bone (McCoy et al. 1991; Gallardo-Williams et al. 2003; Nielsen 2004). B plays a crucial biological role in bone health by modulating the functions of various essential nutrients including vitamin D3 (VD), calcium (Ca), phosphorous (P) etc which are known to affect bone mineralisation in both humans and other vertebrates (Nielsen 1990; Elliot and Edwards 1992; Meacham et al. 1995; Naghii and Samman 1997; Kurtoğlu et al. 2001; Devirian and Volpe 2003; Naghii et al. 2006). B presence is restricted to the mineral component of skeletal tissues and not to the organic matrix (Jugdaohsingh et al. 2015). Contrasting results were found in previous studies about the effect of B on absorption of Ca and P, both essential nutrients for the skeletal formation. Dietary supplementation with B increased Ca and P absorption and balance in wethers and rats (Brown et al. 1989; Hegsted et al. 1991) and promoted the improvement of the mechanical properties of bone tissue (Rossi et al. 1993; Chapin et al. 1997, 1998; Wilson and Ruszler 1997; Wilson and Ruszler 1998), while no such effects were observed in barrows (Armstrong and Spears 2001). However, in vertebrates, B deficiency results in impaired osteogenesis, negatively affecting bone development (Gorustovich et al. 2008; Nielsen and Stoecker 2009). Supplementation of B resulted in the improvement of bone strength and microstructure in mice (Dessordi et al. 2017). This was also observed in

ostrich, where low concentrations of B supplemented through water led to increased osteogenesis through BMP-2 regulation (Zhu et al. 2020). In addition, B was found to be able to reduce inflammation correlated with reduced bone mineral density, thereby improving the bone health (Scorei and Scorei 2013) suggesting its use in the treatment for osteochondrosis (Johnson and Jayroe 2009). B supplementation was also able to enhance the fracture healing process in rats (Gölge et al. 2015). In addition to the *in vivo* evidence of the beneficial effects of B in the mineralization process, clear evidence was obtained *in vitro* as well. In pre-osteoblastic cell line MC3T3-E1, B was found to positively regulate mineralized tissue-associated proteins and mRNA expression of genes involved in osteoblastic functions such as osteocalcin (*bglap*), osteopontin (*spp1*) and collagen type 1 (Hakki et al. 2010). In the same study, B concentrations of 10ng/ml and 100ng/ml were able to increase *in vitro* mineralization in MC3T3-E1 cells (Hakki et al. 2010). Similar concentrations were used in human bone marrow mesenchymal stem cells (BMSCs), although cell proliferation was not affected, an increased expression of bone morphogenetic proteins (BMPs) and osteocalcin along with elevation in the activity of alkaline phosphatase (ALP) were reported (Ying et al. 2011). Similarly, osteo-inductive properties of encapsulated B within scaffolds were confirmed in MC3T3-E1 cells (Gümüşderelioğlu et al. 2015).

Skeletal diseases such as osteoporosis, osteomalacia and rickets are a significant medical burden worldwide and VD deficiency is one of the major and perhaps the most preventable factors leading to bone fragility (Kanis et al. 2021; Bussell 2021). In a previous study, the supplementation

of B in broiler chickens with VD deficiency alleviated symptoms associated with the insufficiency such as, disruptions in the mineral metabolism (Kurtoğlu et al. 2001). B supplementation further improved the biochemical characters like Ca, P levels, thereby resulting in a healthier bone despite the VD deficiency (Kurtoğlu et al. 2001). Similar observations were found in VD deficient rats where B was able to increase Ca, Mg and P (Dupre et al. 1994). B interacts with VD probably by compensating the disturbances in the energy-substrate consumption or by enhancing the macro-mineral content of bone, in addition to the possibility of VD-independent regulation of the indices of maturation of cartilage (Hunt et al. 1994). B was also shown to inhibit enzymes that catabolize VD thereby causing an up-regulatory impact in VD status (Miljkovic et al. 2004). The exact mode of interaction between B and VD is not clear yet and needs further exploration.

Zebrafish (*Danio rerio*) is an increasingly relevant vertebrate model for bone-related studies due to the many technical advantages associated with its use (Fernández et al. 2018). In particular, translucent larval stages and cost-effective genetic manipulation translated into an increased availability of fluorescent reporter lines, which are particularly useful for *in vivo* cellular tracking, allowing the study of the fate and differentiation of specific bone cell types (Valenti et al. 2020). Considering the necessity to provide valid solution to promote bone health, two concentrations of B were supplemented alone and in synergy with VD to zebrafish larvae and the impacts were studied at transcriptional level. Recent advances in next-generation sequencing (NGS) guaranteed an easy access to RNA

sequencing data which is being exploited here, and it allows the investigation of the action of compounds of interest on the bone metabolism and define key pathways modulated by therapeutic interventions. To further validate the effects of B and VD on early skeletal development, *Tg(Ola.sp7:mCherry-Eco.NfsB)pd46,* and *Tg(Ola.bglap:EGFP)hu4008,* hereinafter mentioned as *Tg(sp7:mCherry)* and *Tg(bglap:EGFP)* respectively, *D.rerio* lines were chosen for this study. Sp7 is a zinc-finger-containing transcription factor expressed in pre-osteoblasts and immature osteoblasts, making it an excellent marker for cell tracking of osteoblasts (Nakashima et al. 2002). *Bglap* is a mature osteoblast marker, suitable for studies on the effects of treatments on osteoblast maturation (Valenti et al. 2020).

The analyzed data provide greater understanding of the actions of these compounds in modulating the overall transcriptome with particular attention on the exact molecular regulation of skeletal development and time course of expression of sp7 and bglap proteins through transgenic lines. It also presents the possibility of employing micronutrients like B to boost VD's osteogenic effectiveness, thereby providing a low-cost solution to tackle the nutritional VD deficiency in biomedicine.

Materials and methods

Wild-type zebrafish husbandry, experimental design and alizarin red S (AR-S) staining

Adult wild-type AB female and male zebrafish specimens reared in the fish facility at Università Politecnica delle Marche (Ancona, Italy) were set up for overnight breeding at 2:1 ratio. The embryos were collected and divided into six groups in triplicates. Treatment concentrations were modified and adopted from previous studies (Ying et al. 2011; Tarasco et al. 2017):

- **Control**: control group with ethanol at 0.1%
- **VD**: VD group with VD3 (1α,25-dihydroxyvitamin D3; Sigma-Aldrich, USA) at 10pg/ml
- **B10**: B at 10ng/ml
- **B10VD**: B at 10ng/ml with VD at 10pg/ml
- **B100**: B at 100ng/ml
- **B100VD**: B at 100ng/ml with VD at 10pg/ml

Boric acid (Sigma-Aldrich, Germany) was used to make the concentrations of B across different treatment groups. The larvae were continuously treated via waterborne exposure with the respective compounds from 3 days post-fertilization (dpf) until 8 dpf, maintained at 28.0°C, pH 7.0, photoperiod 12:12 light:dark, $NO_2 < 0.01$ mg/L and $NO_3 < 10$ mg/L in 6 well-plates at a density of 15 larvae/10ml in triplicates per condition. 70% of the water with respective treatments was renewed daily and no

significant mortality was noticed in any group. VD was dissolved in ethanol before using in the treatments, therefore ethanol (0.1%) was added to the control and two B groups without VD to ensure constant ethanol concentrations in all the groups. The sampling was done at 9 dpf for AR-S staining, image acquisition and RNA extraction.

AR-S staining is one of the most used methods for studying bone mineralization (Bensimon-Brito et al. 2016). For fluorescence imaging, larvae (n=5 per replicate per group) were exposed to a lethal dose of 300 mg/L MS-222 (Ethyl 3-aminobenzoate methane sulfonate; Sigma-Aldrich, USA) and were stained with AR-S (Fluka Chemika, Switzerland) at 0.01% for 15 minutes. After washing with H_2O, stained larvae were placed in lateral position onto an agarose gel (2%). Images of the stained larvae were taken using a Zeiss Axio Imager M2 fluorescent microscope (Milan, Italy) set with a green light filter (λ_{ex} = 530–560 nm and λ_{em} = 580 nm). Images were acquired using constant parameters and analyzed using ImageJ (version 2.1.0/1.53c) software after splitting the color channels of the RGB images. 8-bit images were adjusted uniformly for all the images to achieve optimum contrast and brightness for improved visibility of the operculum.

Zebrafish transgenic lines husbandry, experimental design and image analysis

Broodstock from the transgenic lines used in our experiments, *Tg(sp7:mCherry)* and *Tg(bglap:EGFP),* were maintained in a recirculating

water system (Tecniplast, Italy) at the aquatic animal experimental facilities of the Centre of Marine Sciences (CCMAR), Faro, Portugal. Eggs were produced with an in-house breeding program and maintained in static conditions until hatching at 3 dpf. Larvae were then screened with a Leica MZ10F fluorescence stereomicroscope (Leica, Germany) and 400 fish expressing the reporter proteins were selected and randomly distributed into four 300 ml beaker cups (100 fish/beaker) with the respective treatments in water. The selected four experimental groups were:

- **Control**: control group with ethanol at 0.1%
- **VD**: VD group with VD3 (1α,25-dihydroxyvitamin D3, Sigma-Aldrich, USA) at 10pg/ml
- **B10**: B at 10ng/ml
- **B10VD**: B at 10ng/ml with VD3 at 10pg/ml

Boric acid (USB Corporation, USA) was used to make the required concentrations of B groups. Fish (n=20) were sampled at four different time points, 6, 9, 12 and 15 dpf, stained with 0.01% AR-S (Sigma-Aldrich, USA) or 0.1% calcein (Sigma-Aldrich, USA) to label mineralized structures and imaged using a Leica MZ10F fluorescence stereomicroscope equipped with a green fluorescence filter (λex= 546/10 nm) and a barrier filter (λem =590 nm) for *Tg(sp7:mCherry)* and AR-S stained fish; and with a blue fluorescence filter (λex= 470/40 nm) and a barrier filter (λem =515 nm) for *Tg(bglap:EGFP)* and calcein-stained fish. All Images were acquired with a DFC7000T color camera (Leica, Germany), according to the following parameters: 24-bit colored image, exposure time 2s (green

channel) and 1s (red channel), gamma 1.00, image format 1920×1440 pixels and binning 1×1. Fluorescence images were processed with ZFBONE macro toolset for Fiji (Tarasco et al. 2020).

RNA extraction and quantification

At 9 dpf, the larvae were sampled using a lethal dose of 300 mg/L MS-222 (Ethyl 3-aminobenzoate methane sulfonate; Sigma-Aldrich, USA) and stored at −80 °C. There were 3 biological replicates for each experimental group and each replicate consisted of a pool of 7 larvae. Total RNA was extracted from each replicate sample using RNAeasy Minikit (Qiagen, Germany) and eluted in 20µl of molecular grade nuclease-free water. Final RNA concentrations were determined using a nanophotometer (Implen, Germany). Total RNA was treated with DNase (10 IU at 37°C for 10 min; Sigma-Aldrich, USA) and quality was confirmed using gel electrophoresis (1% agarose gel) and stored at -80°C until library preparation for RNA sequencing. iScript cDNA Synthesis Kit (Bio-Rad, USA) was used to perform cDNA synthesis using 1µg of total RNA and stored at -20°C until further use in Real Time PCR (RT-PCR).

RNA sequencing and quality controlling

Samples to be used for RNA sequencing were confirmed for concentration using Invitrogen Qubit 3.0 Fluorometer with the RNA assay kit and for integrity using Agilent Tapestation. Illumina TruSeq RNA libraries were prepared by Novogene Ltd (Cambridge, UK) and sequenced on an Illumina Novaseq6000. All the triplicate samples of each group were sequenced to

generate approximately 30 million paired end reads of 150 base pairs (bp) each. The read data was assessed for its quality using FastQC v.0.11.5 (http://www.bioinformatics.babraham.ac.uk/projects/fastqc/). Reads were then trimmed using TrimGalore v0.4.4 (https://github.com/FelixKrueger/TrimGalore) setting the parameters -q 30 --stringency 5 --length 40. Specifically, reads were trimmed for any adapters, and bases with a Phred score of less than 25 were trimmed off. Trimmed reads less than 40 bp were also removed.

Differential expression analysis

The final cleaned up reads were then mapped to the *D.rerio* reference genome (GRCz11) retrieved from Ensemble genome database. Mapping was performed using STAR aligner (Dobin et al. 2013) with the following parameters (--outSAMtype BAM SortedByCoordinate, --outSAMunmappedWithin, --outSAMattributes Standard). Gene level read count data was generated using featureCounts (Liao et al. 2014) with the following parameters (--primary, -C, -t exon, -g gene_id) and rest was set to default.

Differential gene expression analysis was performed using DESeq2 1.26.0 (Love et al. 2014) within R 3.6.1 (R Core Team 2019). Finally, genes with false discovery rate (FDR) <0.05 and absolute log2 fold change values (FC) >0.5 were considered as differentially expressed. Principal component analysis (PCA) plots were generated to remove any outlier samples from the data using plotPCA function within DESeq2 1.26.0

followed by hierarchical clustering across samples using the function heatmap.2 within the package gplots 3.0.1.1 (Warnes et al. 2020) to confirm the clustering of replicates. A list of differentially expressed genes (DEGs) was generated for all treatment combinations and concatenated to generate a final list of genes that were differentially expressed in at least one combination. The DEGs were then clustered using partition around medoids (PAM) algorithm (Kaufman and Rousseeuw 2009) into different clusters based on the DESeq2 median ratio normalised expression values across different treatments using the package cluster 2.1.0 (Maechler et al. 2019). The optimum number of clusters were identified using Gap statistic method (Tibshirani et al. 2001) within the package factoextra 1.0.6 (Kassambara and Mundt 2020). The normalised counts were mean centralised across different treatments within each cluster and visualised using the package ggplot2 3.2.1 (Hadley 2016).

Gene set enrichment analysis was performed using Clusterprofiler 3.14.3 package (Yu et al. 2012). Annotations for *Danio rerio* were retrieved from the package org.Dr.eg.db 3.8.2 (Carlson 2019) and gene set enrichment analysis was performed for DEGs in the clusters individually. Gene Ontology (GO) terms falling under the categories Biological Process (BP), Cellular Component (CC) and Molecular Function (MF) with a $p< 0.05$ were considered as significant and used for downstream analysis. Enriched GO terms and genes within each cluster were then used to generate bipartite networks using the package ggnetwork 0.5.1 (Briatte 2016) within R. Kyoto Encyclopedia of Genes and Genomes (KEGG) pathway enrichment analysis was performed against the DEGs present in

the three clusters and filtered for $p < 0.05$ to be considered significant. Bubble plots for enriched KEGG pathways across all the clusters were generated using ggplot2 3.2.1.

RT-PCR

RT-PCRs were performed with SYBR green in a CFX thermal cycler (Bio-Rad, Italy) in triplicate as previously described (Carnevali et al. 2017). For each reaction, the mix contained: 1 µL of cNDA (1:10) + 5 µL iQ SYBR Green Supermix + 3.8 µL miliQ water + 0.1 µL forward primer + 0.1 µL reverse primer. The thermal profile for all reactions was 3 min at 95°C followed by 45 cycles of 20 s at 95°C, 20 s at 60°C and 20 s at 72°C. Dissociation curve analysis showed a single peak in all the cases. Ribosomal protein L13 (*rpl13*) and ribosomal protein, large, P0 (*rplp0*) were used as the housekeeping genes (validated previously by Forner-Piquer et al. 2020) to standardize the results by eliminating variation in mRNA and cDNA quantity. No amplification product was observed in negative controls and primer-dimer formation was never seen. Data was analyzed using iQ5 Optical System version 2.1 (Bio-Rad) including Genex Macro iQ5 Conversion and Genex Macro iQ5 files. Modification of gene expression between the groups is reported as relative mRNA abundance (Arbitrary Units). Primers were used at a final concentration of 10pmol/ml. Primer sequences are listed in Supplemental Table 5.

Statistical analysis

Data of all groups were normally distributed as assessed by Shapiro-Wilk's test (p>0.05) and there was homogeneity of variances, as assessed by Levene's test for equality of variances (p>0.05). The differences between the control and the treatments were tested with a One-way analysis of variance (ANOVA) followed by Tukey's post hoc test (p<0.05) for the experiments with the transgenic lines and for the image data of AR-S staining. All the tests were performed using R version 3.6.1(R Core Team 2019) and plots were generated using ggplot2 3.2.1.

Results

Increased operculum calcification in synergy treatment groups

No major differences in opercular bone growth were observed between the two concentrations of B (B10 and B100) whereas an increase in mineralization of the operculum was observed in groups treated with VD with respect to control, B10 and B100. However, both the synergy groups (B10VD and B100VD) showed an increase in mineralized area of the opercular bone when compared to VD treatment (Fig.1A). Quantitative analysis of the integrated pixel density within the operculum area was performed as it adequately proxies the intensity of fluorescence signal thus providing an index of the density of AR-S staining (i.e., mineralization). Using ImageJ (version 2.1.0/1.53c), the area of the operculum (OpA) and the area of the head (HA) were manually selected

and the raw integrated density within the area of the operculum (OpI) was extracted. OpI was then normalized with area of the head, to compensate for differences in size among fish. Normalized pixel density within the operculum (OpI/HA) did not vary among fish treated with ethanol (Control) and the two concentrations of B (B10, B100) while VD significantly increased mineralization of the operculum in respect to the control group and both B concentrations (Fig.1B). Importantly, opercular bone mineralization was significantly increased in fish treated with both synergy groups (B10VD, B100VD) compared to VD alone in what appear to be a dose-dependent manner, although no significant differences were found between the synergy groups with different concentrations of B (Fig.1B).

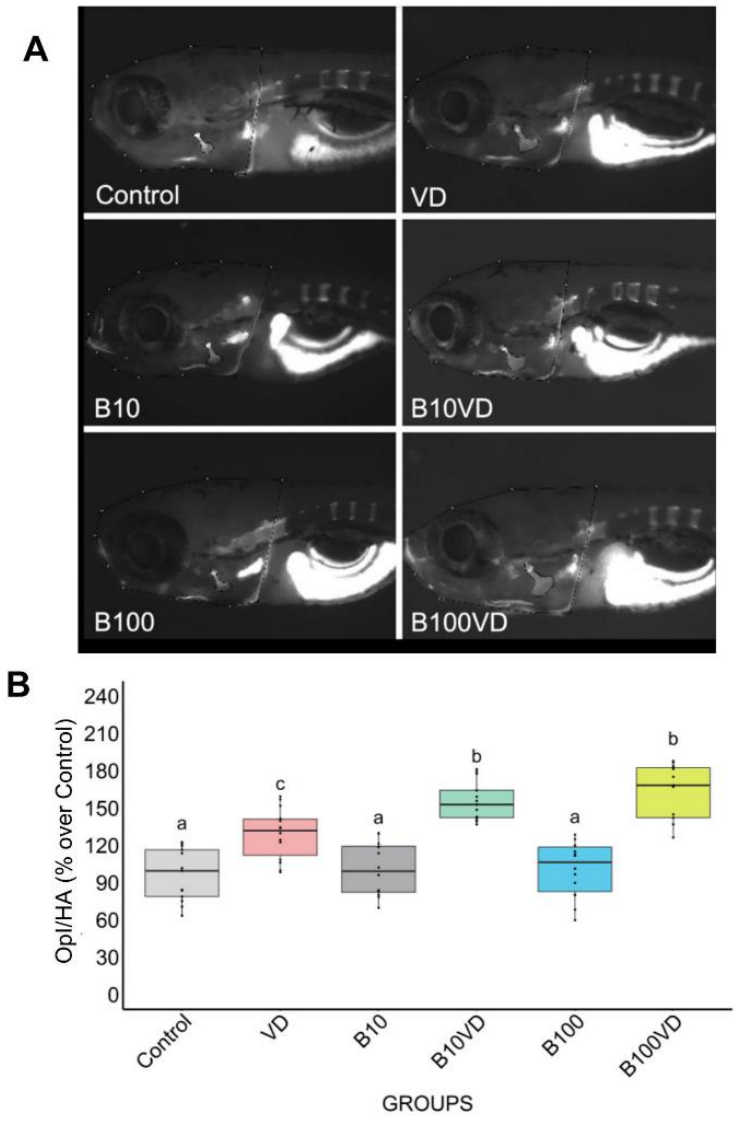

Fig.1 Fluorescence microphotograph of AR-S-stained larvae and ImageJ quantification of the opercular bone mineralization; n=15 **(A)** Mineralized bones stained by AR-S staining at 9 dpf following different treatments; (**B**) Quantitative analysis of the operculum integrated pixel density normalized by head area (Opl/HA) showed as % over control in fish treated with different concentrations of B and VD. Different letters above each graph indicate statistically significant differences among different groups. One way ANOVA and Tukey's Post hoc test were used, and statistical significance was set at $p < 0.05$.

Differential expression analysis and clustering of DEGs

Approximately 30 million paired end reads of 150 bp were generated across each sample of RNA in triplicates from each treatment group at 9 dpf. PCA on the read count data stratified the different treatment and replicates into distinct clusters (Fig.2A). Hierarchical clustering of the top 1500 DEGs clustered the different replicates of different treatments together (Fig.2B) confirming uniformity among the replicates. However, control and B10 samples showed an interspersing in both the PCA and hierarchical clustering indicating very low variability in expression between these groups, this is also consistent with the developmental state of the operculum between the two treatment groups (Fig.1B). Differential expression analysis on all these groups combined resulted in a set of 7341 genes differentially expressed in at least one of the different contrasts listed in Fig.2C. Comparing the differential expression of different treatment against control revealed B10VD to be a highly responsive group against control with 1477 and 724 genes up and downregulated, respectively (Fig.2C). B10 treatment in contrast just revealed 4 downregulated and 1 upregulated gene, showing to be the treatment with lowest transcriptional response against control (Fig.2C).

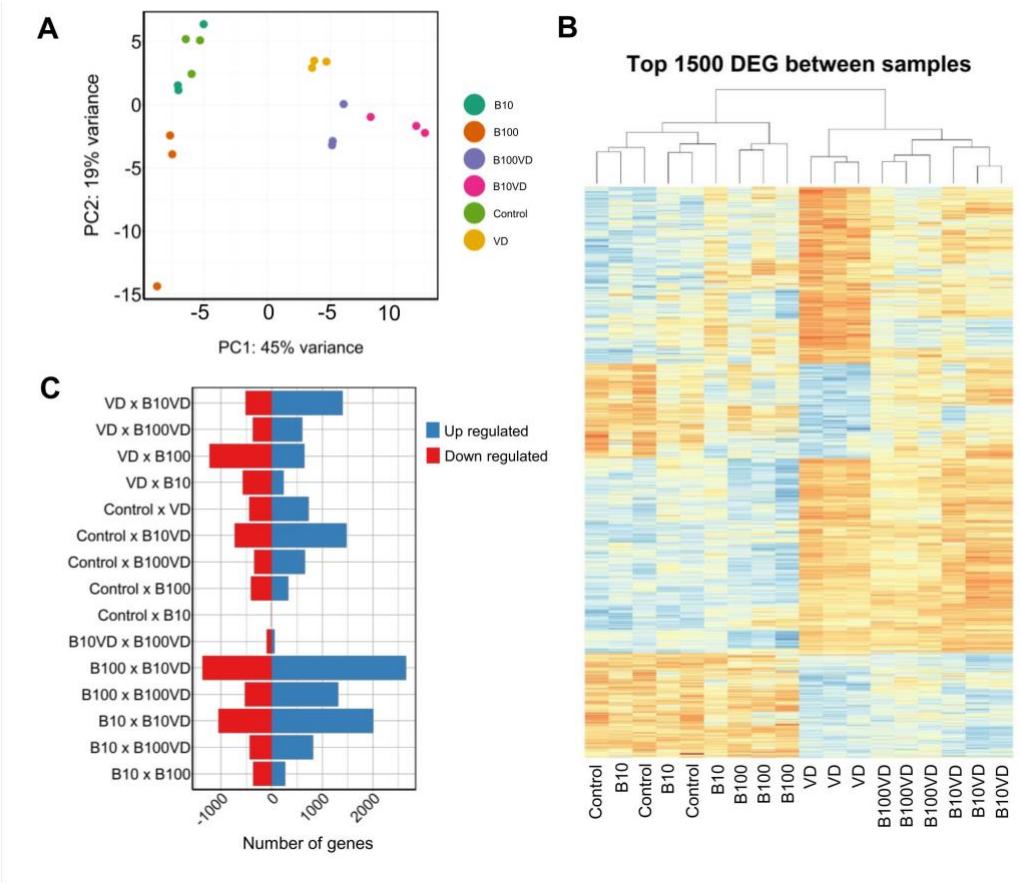

Fig.2 Sample clustering and DEGs across different combinations. (**A**) PCA of all the samples used in the experiment; (**B**) Hierarchical clustering of the top 1500 DEGs across all the samples used in the experiment; (**C**) Number of upregulated and downregulated genes across different combinations of experimental groups.

Gap statistic method determined three clusters to be optimum for PAM clustering (Supplemental Fig. 1). PAM clustering defined three clusters C1, C2, C3 with 2993, 2014 and 2245 genes in each cluster (Fig.3A), respectively. The three clusters revealed distinct expression patterns across different treatments, normalised expression values in cluster1 were highest for B100 and lowest for B10VD (Fig.3B). Cluster2 genes

displayed a contrasting expression pattern between VD (decreased) and B10VD (increased) compared to control, while cluster3 harboured genes showing increased expression in VD, B10VD, B100VD groups compared to the control and other treatment groups.

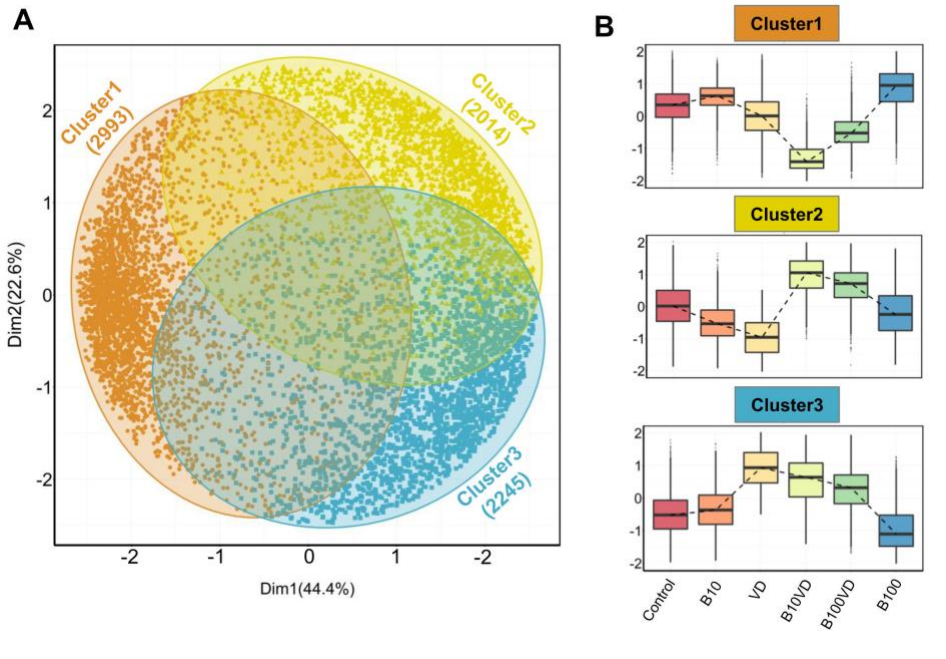

Fig.3 Outputs from PAM clustering of all the DEGs. (**A**) PCA visualizing the three clusters labelled Cluster1, Cluster2 and Cluster3 (orange, yellow and blue color respectively) as defined by the PAM clustering; (**B**) Expression patterns of normalized gene expression values across different treatment groups in each of the three clusters. The expression counts were mean-centred before plotting them as box plots. The dashed lines within each panel connect the medians values across different treatment groups.

Functional annotation of DEGs

Gene function enrichment analysis for all the differentially expressed genes across each cluster revealed distinct functional enrichment for GO terms and KEGG analysis. Cluster1 was enriched for a total of 47 GO terms across Biological Process (BP), Molecular Function (MF) and Cellular Component (CC) categories with a very high representation of terms involved in catabolic processes (GO:0019941, GO:0010499, GO:0043632, GO:0006511) and proteasome assembly (GO:0043248) (Details of GO terms in Supplemental Table 3). A total of 117 GO terms were enriched in cluster2 and there was no overrepresentation of GO terms contributing to a particular function across all the three GO categories (Supplemental Table 3). Cluster1 and cluster2 revealed no significant enrichment for functions or processes related to skeletal system. Interestingly, cluster3 stood out amongst the three with a high enrichment for GO terms involved in bone and skeleton system functioning (Supplemental Table 3). In cluster3, a total of 44 GO terms were enriched in Biological Process category out of which 23 GO terms were involved in processes leading to bone and skeletal system functioning, such as extracellular matrix organization (GO:0030198; p=1.29e-16) and skeletal system development (GO:0001501; p=0.000504). In addition, within cluster3 - GO terms involved in skeletogenesis were again enriched in the Cellular Component (<10 terms) and Molecular Functions (<5 terms) category (Supplemental Table 3), however the key focus was diverted towards Biological Processes considering more than half of the enriched processes were related to bone and skeletal system. The bipartite network showing

interactions of genes and enriched GO terms (BP) across the clusters displayed minimum overlap between enriched GO terms across three different clusters (Fig.4). This further indicates that genes showing distinct expression profiles across the three clusters are in fact enriched for distinct functions. Also, many genes in cluster3 are shared across multiple GO terms with bone and skeletal system functions as highlighted in Fig.4, which otherwise is not observed in the other two clusters.

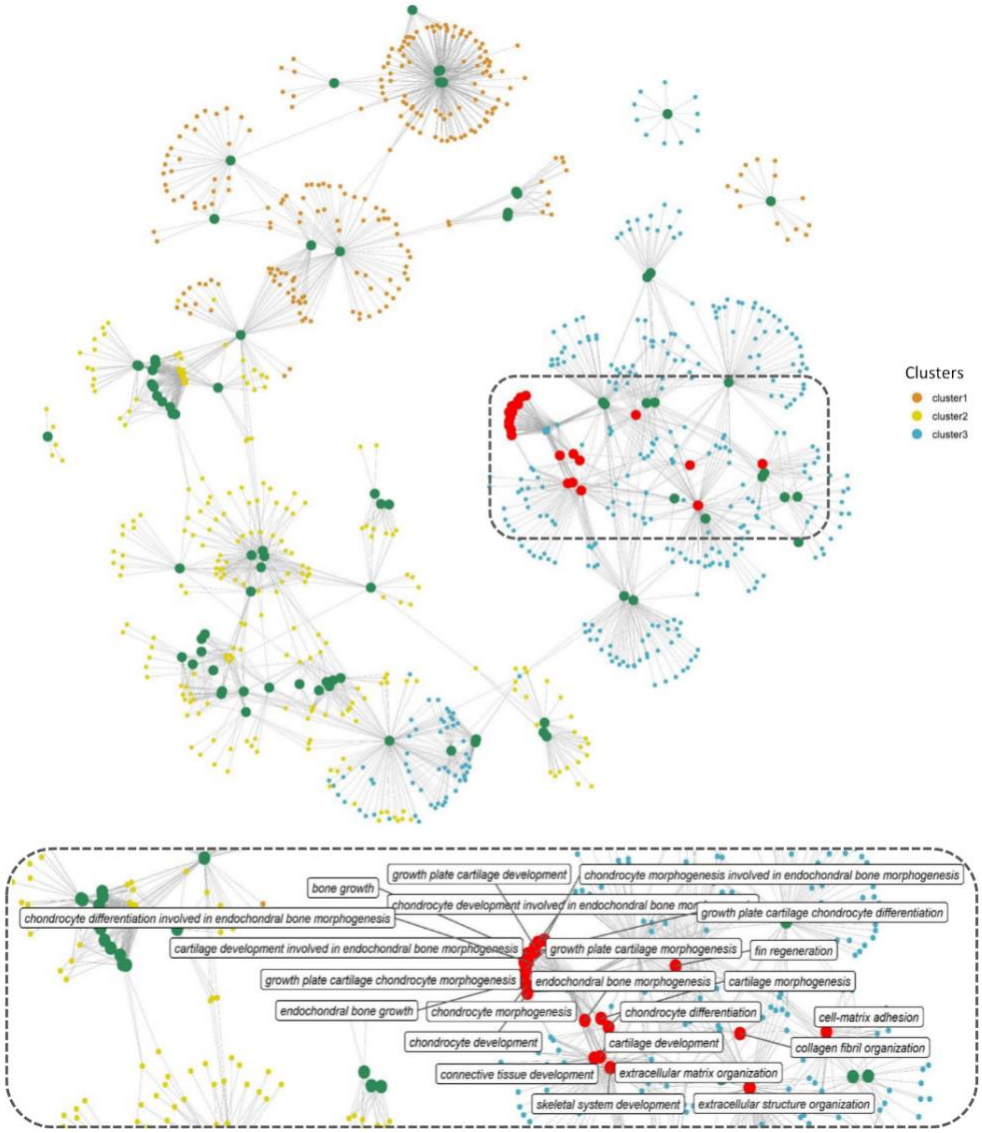

Fig.4 Network representation of enriched GO terms (BP) performed against the DEGs across three different clusters (Supplemental Table 3), the large sized green and red colored nodes indicate enriched GO terms, the red nodes in particular highlight GO terms in bone and skeleton system functioning, the region within dashed rectangle is zoomed at the bottom of the network to highlight the nomenclature of key GO terms. Each small node of orange, green and blue colors indicate a gene contributing to the enriched GO term across different clusters.

We further investigated the strong enrichment for skeletal GO terms (BP) by generating a quantitative matrix of number of genes falling within each GO terms across three clusters (Fig.5A). Increased number of genes involved in skeletal functions within cluster 3 correlate well with the strong enrichment in GO terms. KEGG analysis revealed Cluster1 to be enriched for 11 KEGG pathways, while cluster 2 displayed enrichment for only one pathway, phototransduction, involving 21 genes (Fig.5B; Supplemental Table 4). Cluster 3 that showed a strong bias towards skeletal functions in GO analysis was enriched for 5 KEGG pathways, out of which Focal adhesion (dre04510), Extracellular matrix (ECM)-receptor interaction (dre04512) and regulation of actin cytoskeleton (dre04810) contribute towards bone/skeletal functions (Fig.5B). Heatmaps showing normalised expression values of genes falling within key enriched bone and skeletal related GO terms such as skeletal system development (GO:0001501), Extracellular matrix organisation (GO:0030198), Bone growth (GO:0098868), Endochondral bone growth (GO:0003416), Endochondral bone morphogenesis (GO:0060350) and Chondrocyte differentiation involved in endochondral bone morphogenesis (GO:0003413) revealed an increased expression in the B10VD group compared to all other groups (Fig.5C). There is a bias towards increased expression of skeletal system genes in B10VD despite the overall expression pattern of cluster3 showing highest expression for VD group (Fig.5C and Fig.5A).

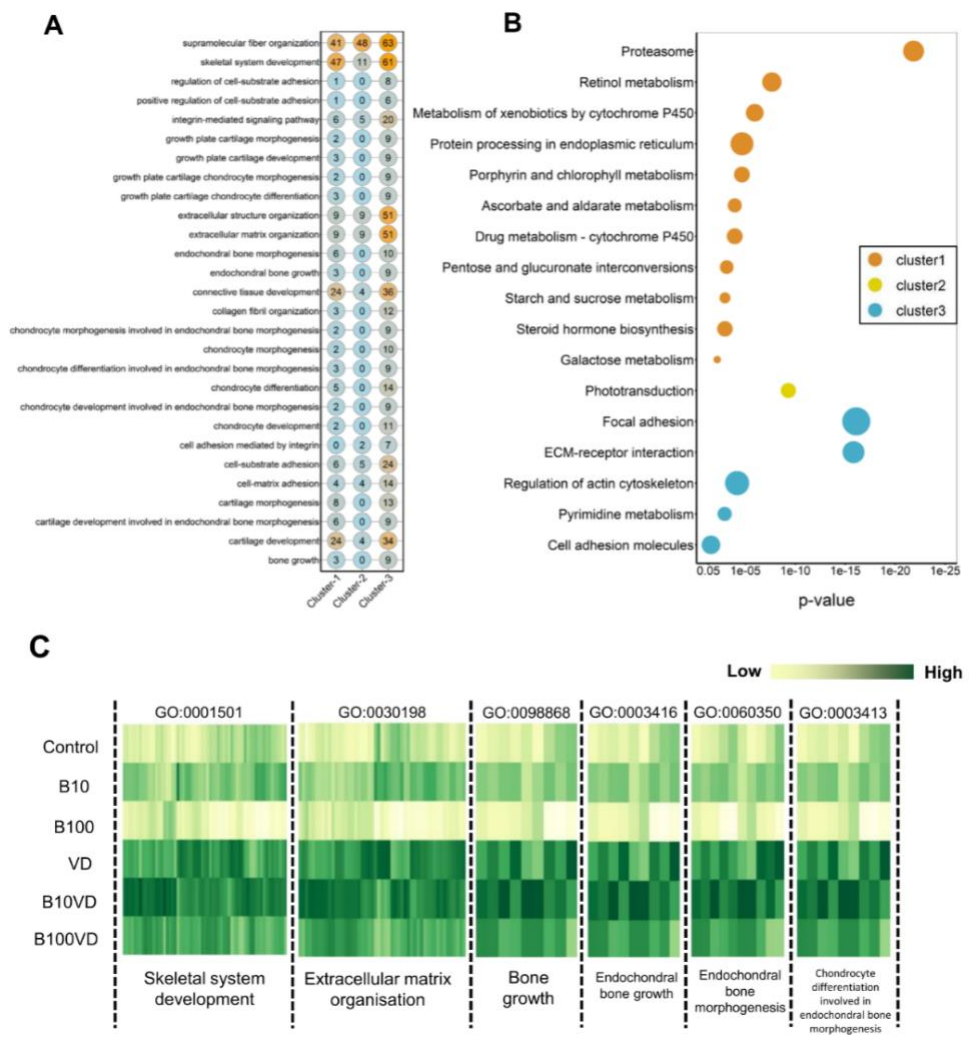

Fig.5 (**A)** Matrix visualizing the number of DEGs falling under enriched GO terms involved in skeletal system development. y-axis highlights the key enriched GO terms and x-axis describes the cluster number. The numbers within each circle indicate the total genes falling within that GO term in each cluster; (**B)** Bubble plot visualizing KEGG pathways significantly enriched ($p<0.05$) across the three different clusters. Colour of the bubbles indicate the cluster they fall into, and size of the bubble indicate the number of genes (**C**) Heatmap visualizing normalized expression values of genes contributing to enriched skeletal GO terms in the cluster3. Y-axis highlights the different treatment groups and X-axis describes the enriched GO terms.

A total 354 genes related to bone and skeletal system were identified from the 28 GO terms listed in Fig. 5A. In comparison to control, 101 DEGS for VD, 126 DEGs for B10VD and 64 DEGs for B100VD were found. Since we observed more DEGs with B10VD, which is the synergy group with less concentration of B, downstream analysis was focused on B10VD alone. A total of 55 genes (3 downregulated and 52 upregulated) were commonly differentially expressed for B10VD and VD compared to control. 71 DEGs were unique for B1OVD and 46 were specific for VD. Some important genes playing key roles in osteogenesis like *col1a1a* and *ucmab* were common DEGs among B10VD and VD whereas *dcn* was upregulated only in B10VD. The osteoclast marker gene *ctsk* (cathepsin K), on the contrary, was found to be upregulated only in VD and not in B10VD.

We further decided to investigate synergy by exploring the KEGG pathways that were not enriched in the current analysis but were key for bone and skeletal development in zebrafish. KEGG pathway maps for MAPK (dre04010), TFG-β (dre04350), focal adhesion (dre0510), Wnt signalling pathway (dre04310) and Ca signalling (dre04020) were generated incorporating the log fold change data for B10VD, VD treatments in contrast to control (Supplemental Fig..2). Expression patterns of the genes from these pathways further confirmed that B10VD synergy to be more effective in supporting bone and skeletal development. Key candidate genes from these pathways such as *cacn3b, egfra, mapk14b, mras, ppp3cca, rps6ka3b* were confirmed for their upregulation in B10VD than VD or B100VD (Supplemental Table 2 and Supplemental Fig. 2).

RT-PCR validation of RNA-Seq data using selected genes from MAPK pathway

Given their importance for osteogenesis and mineralogenesis, eight marker genes (*cacn3b, dusp2, egfra, hspb1, mapk14b, mrasb, ppp3cca, rps6ka3b*) involved in the MAPK pathway were selected for validation of the transcriptomic data by RT-PCR. As shown in Supplemental Fig. 3, the relative fold change in RT-PCR were consistent with RNA-Seq results, suggesting that the transcript identification and quantification were extremely consistent between the two techniques. Most genes from RNAseq analysis were in good accordance with the expression intensities by RT-PCR although the result was dissimilar for *mapk14b* in the VD group, probably due to the difference in sensitivity of each technique.

Time course study of operculum growth using the transgenic lines Tg(sp7:mCherry) and Tg(bglap:EGFP)

Since B10VD is the synergy group with the lower concentration of B, yet with more DEGs, to further investigate the synergy effect at various stages of skeletal development, additional analysis was performed at multiple time points using two zebrafish fluorescent reporter lines, one expressing mCherry under control of the medaka (*Oryzias latipes*) *sp7* (osterix) promoter, the other expressing EGFP downstream to the promoter of medaka *bglap* (osteocalcin). Areas of the operculum and $sp7^{+}$ and $bglap^{+}$ areas, showing early and mature osteoblasts respectively,

were measured (Fig.6). Synergy group (B10VD) exhibits the largest mineralized area of the operculum as well as the largest *sp7*$^{+}$ and *bglap*$^{+}$ areas at all time points analyzed (Fig.6). The *sp7*$^{+}$ area normalised with head area (*sp7*$^{+}$A/HA) was significantly higher in VD and B10VD with respect to control at 6 dpf whereas at 9 dpf only the synergy group showed a significantly higher fluorescence signal with respect to control. At 12 and 15 dpf, B10VD remained the group with largest *sp7*$^{+}$ area, but significant differences were only found with B group at 12 dpf. No differences between control and B groups were detected throughout the experiment (Fig.6C). GFP fluorescence marking mature osteoblasts normalised with head area (*bglap*$^{+}$A/HA) showed a significant increase for the synergy group compared to every other group at 15 dpf. Importantly, this time point was characterized by the strongest signal among all endpoints studied. Synergy group (B10VD) also showed a significantly larger *bglap*$^{+}$ area than control at every time point studied whereas VD showed larger bglap-positive area than control at all time points except 15 dpf. This indicate towards a possible acceleration of skeleton developmental rate during early ontogeny by VD groups, which later fades out when VD is supplemented alone. Synergy group also showed a significantly stronger signal compared to VD or B alone at 15 dpf. In accordance with what was observed for *sp7* expression pattern, no differences were detected between control and B at any of the endpoints evaluated. Except VD, all other groups showed a general increase of *bglap*$^{+}$ area from 6 to 15 dpf (Fig.6C).

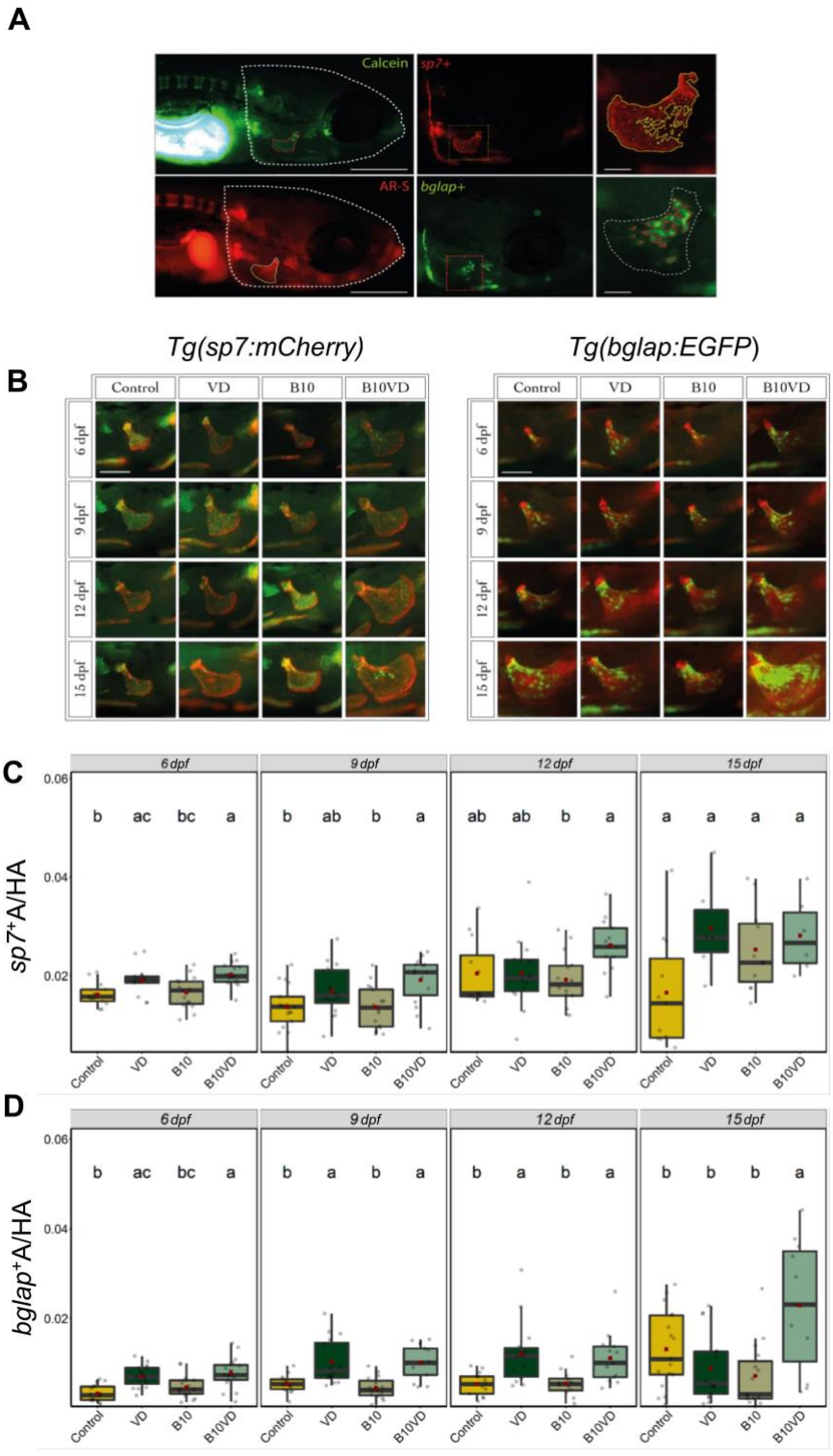
A
Calcein
sp7+
AR-S
bglap+
B
Tg(sp7:mCherry)
Tg(bglap:EGFP)
Control
VD
B10
B10VD
6 dpf
9 dpf
12 dpf
15 dpf
C
sp7+A/HA
6 dpf
9 dpf
12 dpf
15 dpf
0.06
0.04
0.02
b ac bc a
b ab b a
ab ab b a
a a a a
Control
VD
B10
B10VD
D
bglap+A/HA
b ac bc a
b a b a
b a b a
b b b a

Fig.6 Early and mature osteoblasts respectively tracked by the fluorescence expression of *Tg(sp7:mCherry)* and *Tg(bglap:EGFP)*. Four groups of treatment are ethanol at 0.1% (Control), VD group with VD3 at 10pg/ml (VD), B at 10ng/ml (B10), B at 10ng/ml with VD3 at 10pg/ml (B10VD); (**A)** An example of how the areas of the operculum and *sp7*$^{+}$ and *bglap*$^{+}$ were measured (Big scale bar = 0.35 mm; Small bar = 0.05 mm); (**B)** A table with merged pictures from the *sp7*:mCherry line stained with calcein and the *bglap*:EGFP line stained with AR-S (Scale bar = 0.17 mm); (**C)** The *sp7*+ area inside the operculum was normalized with total head area at time points 6,9,12 and 15 dpf; (**D)** The *bglap*$^{+}$ area inside the operculum was normalized with total head area at time points 6, 9, 12 and 15 dpf. One way ANOVA and Tukey's Post hoc test were used. Data are presented as means ± SD and different letters represent statistical significance at $p<0.05$.

Discussion

Morphometrical assessment of the mineralizing opercular bone in early-stages zebrafish larvae was previously described as a suitable tool for the screening of osteogenic compounds (Tarasco et al. 2017; Bergen et al. 2019). The pro-osteogenic properties of VD are long-time known but less understood is the possible synergistic actions of VD with micronutrients to promote bone mineralisation. Here we tested two concentrations of B, one concentration of VD and their respective combinations and observed the induction of osteogenic effect as observed by increased mineralised operculum areas in both the synergy groups compared to the supplementation of VD alone but even more pronounced effect when compared to the control and the B treatments alone. Following this preliminary screening, and with the scope of exploring the molecular determinants of the observed phenotype, we analyzed the transcriptome of the treated larvae to obtain a large multivariate dataset of DEGs with

particular attention given to pathways associated with skeletal system. The PAM clustering approach was previously proven to be appropriate to cluster and define expression patterns among the DEGs (Martínez et al. 2018) and the same was observed here, where a dominance of skeletal or bone related pathways was observed in one out of the three clusters. This cluster of interest (C3) had a specific pattern for groups with VD, where VD and its synergy groups stayed in the high expression side, whereas control and groups with B stayed in the low expression side. Interestingly, when looking at the expression patterns of genes contributing to enriched skeletal function GO terms, only B10VD showed higher expression than VD group suggesting a potential role that the synergy between VD and B could be playing in inducing the pro-mineralogenic effect observed. In addition, transcriptomic responses showed that more genes with positive effects on the skeleton were highly expressed in the combination group of VD with lower concentration of B (B10VD) than the other synergy group with higher concentration of B (B100VD). Thus, on a molecular level, 10ng/ml B with VD showed the strongest positive effect on metabolic pathways associated with skeletal development.

Among B10VD and VD, there were common DEGs including *col1a1a*, expressed in developing bony elements and ectoderm, and *ucmab* which play a pivotal role in zebrafish skeletal development (Neacsu et al. 2011; Gistelinck et al. 2016). Some important genes were expressed only for B10VD such as *dcn*, which encodes for an important extracellular matrix glycoprotein which has a role in regulation of bone mass by modulating

TGF-β activity (Bi et al. 2005). The most affected pathway was observed to be the MAPK signalling, where many genes were found to be overexpressed in the synergy groups compared to VD. RSK2 (encoded by *rps6ka3a* gene) was shown to be highly upregulated in the B10VD group relative to B100VD and VD groups, which is particularly relevant, given its importance for osteoblast differentiation and function (Yang et al. 2004). It is in fact involved at the distal end of MAPK pathway, where it plays a key role in bone turnover by phosphorylating different substrates, such as cAMP response element-binding protein (CREB) which is a known inducer of osteoblast differentiation and c-Fos which is an osteoclast differentiation inducer (Wang et al. 1992; Xing et al. 1996; Nottmeier et al. 2020). C-Fos was found to be downregulated in both VD and B10VD but osteoclast marker gene *ctsk* was upregulated only in VD. This indicate that synergy group possibly have a reduced VD-induced osteoclast formation through VD receptors in the nuclei as found in previous studies (Suda et al. 2003). The synergy groups also showed significant upregulation for p38 which is involved in the *runx2* activation (Lee et al. 2002) giving further evidence to the pro-osteogenic effect of B and VD synergy in the induction of osteoblast differentiation. Fgfr4 receptor, a gene in the ERK signalling pathway, which is involved in the *runx2* transcriptional activation, was also found to be highly upregulated in the synergy groups pointing out at a possibility of *runx2* regulation, and thereby to be involved in the differentiation and proliferation of osteoblasts (Cool et al. 2002; Kawane et al. 2018). Although *runx2* was not one of the DEGs observed here and that could be due to the specific skeletal development stage of the larvae under study. Fgfr4 being the

receptor for Fgf6, also plays a pivotal role in osteoblast and osteoclast differentiation (Pawlikowski et al. 2017). The calcineurin, which is part of multiple bone-related pathways such as MAPK, Wnt and Ca signalling, was found to be upregulated in the B10VD synergy group. Calcineurin is known to be expressed in osteoblasts and enhances differentiation of osteoblasts, thereby increasing bone formation (Sun et al. 2005). The focal adhesion pathway was also regulated in both the synergy groups where fibronectin 1 (FN-1) was highly upregulated. FN-1, through activation of Wnt pathway, stimulate osteoblast differentiation and extracellular matrix mineralisation as observed in previous *in vitro* studies and it is known to be produced by osteoblasts during bone generation (Bentmann et al. 2010; Yang et al. 2020). Additionally, FN-1 was found to play a role in osteoblast compaction through fibronectin fibrillogenesis cell-mediated matrix assembly, which is crucial for the bone extracellular matrix mineralization mediated by osteoblast (Brunner et al. 2011; Sens et al. 2017). In the KEGG analysis of the TGF-β/BMP pathway, *smad4* was largely upregulated in B10VD group. Proteins belonging to the Smad family are associated with bone morphogenetic protein (BMP) pathway, whose activation is paramount for bone mineralisation and osteoblast differentiation (Chen et al. 2012; Karner et al. 2017). The transcriptomic analysis clearly evidenced the upregulation of genes involved in bone formation by osteoblast differentiation, extracellular matrix formation and mineralization in the synergy groups, particularly in B10VD, with a higher effect than VD treated alone.

From the combined morphological and transcriptomic data, we decided to further investigate the synergy of VD with B at lower concentration, 10ng/ml. To explore the effect of the B-VD synergy on bone development in a time-dependent manner, cellular dynamics of intermediate and late osteoblasts, as labelled by *sp7* and *bglap* expression respectively, were verified. *Sp7* is a highly conserved, zinc finger-containing transcription factor essential within the stepwise genetic program regulating osteoblast differentiation. It is required for the activation of a repertoire of genes directly associated to osteoblast maturity and bone extracellular matrix formation and mineralization such as *bglap*, *spp1*, *col10a1a/b* and *sparc* (Niu et al. 2017; Liu et al. 2020). In zebrafish, *sp7* expression is considered to be labelling intermediate stages of osteoblast differentiation and it tend to be downregulated in mature osteoblasts (Liu et al. 2020). It is first observed at the time of the onset of the primary cranial ossified structures (36 hours post fertilisation), with its expression pattern perfectly co-localizes with the whole mineralized domain of the bone (Liu et al. 2020). On the other side, osteocalcin (*bglap*) is a small osteoblast-secreted protein well accepted as a marker of mature and matrix-secreting osteoblasts (Rutkovskiy et al. 2016). Plenty of evidence suggest that VD exerts a direct stimulating effect on osteoblasts proliferation and differentiation through the VD Receptor (VDR) in humans and other mammals (van Driel and van Leeuwen 2014). Similarly, it has been previously observed in zebrafish that treatment with VD is able to increase the expression of *sp7* and *blglap* at very early stages of skeletal development (6 dpf) (Tarasco et al. 2017). Accordingly, in the present study a significant increase in the area of *sp7*$^{+}$ cells within the opercular

bone were observed for VD alone and when in combination with B at early stages of opercular development (6 dpf), but only the synergy group increased the amount of intermediate osteoblast (*sp7*$^{+}$) populating the operculum at 9 dpf. Similarly, when looking at more advanced (*bglap*$^{+}$*)* osteoblasts stages, both VD alone and synergy group increased *bglap*$^{+}$ osteoblasts in early stages (6, 9 and 12 dpf) but the synergy group extended the induction of mature osteoblast up to 15 dpf. As a result, larger mineralized opercular bone was observed in the synergy group at 15 dpf. Overall, B administered alone was not able to affect the intermediate or mature osteoblast populations and the effect was observed only in synergy with VD.

In conclusion, our study indicate that B may be able to potentiate the osteoblast-stimulating effect of VD or exerts its pro-osteogenic effect in a VD-dependent manner. Our transcriptome analysis suggest that these effects could be through the induction of molecular programs involving the activation of MAPK and TGF-β/BMP pathways. These findings could lead to a promising approach in developing medicines to alleviate VD deficiency by synergically adding micronutrients along with VD to increase the overall efficiency of the treatment. In a world where improving bone health has become a matter of crucial importance, there is a high translational value for the findings of this study in the development of prophylactic measures focusing on improving VD supplementation efficiency in nutrition. Future studies should explore other outcomes of the combinatorial treatments such as its effects on stress or immunity to have a complete overview.

Reference

Armstrong TA, Spears JW (2001) Effect of dietary boron on growth performance, calcium and phosphorus metabolism, and bone mechanical properties in growing barrows. J Anim Sci 79:3120–3127. https://doi.org/10.2527/2001.79123120x

Bensimon-Brito A, Cardeira J, Dionísio G, et al (2016) Revisiting in vivo staining with alizarin red S - a valuable approach to analyse zebrafish skeletal mineralization during development and regeneration. BMC Developmental Biology 16:2. https://doi.org/10.1186/s12861-016-0102-4

Bentmann A, Kawelke N, Moss D, et al (2010) Circulating fibronectin affects bone matrix, whereas osteoblast fibronectin modulates osteoblast function. Journal of Bone and Mineral Research 25:706–715. https://doi.org/10.1359/jbmr.091011

Bergen DJM, Kague E, Hammond CL (2019) Zebrafish as an Emerging Model for Osteoporosis: A Primary Testing Platform for Screening New Osteo-Active Compounds. Frontiers in Endocrinology 10:6. https://doi.org/10.3389/fendo.2019.00006

Bi Y, Stuelten CH, Kilts T, et al (2005) Extracellular Matrix Proteoglycans Control the Fate of Bone Marrow Stromal Cells*. Journal of Biological Chemistry 280:30481–30489. https://doi.org/10.1074/jbc.M500573200

Briatte F (2016) ggnetwork: Geometries to Plot Networks with'ggplot2'. R package version 0.5, 1

Brown TF, McCormick ME, Morris DR, Zeringue LK (1989) Effects of dietary boron on mineral balance in sheep. Nutrition Research 9:503–512. https://doi.org/10.1016/S0271-5317(89)80175-7

Brunner M, Millon-Frémillon A, Chevalier G, et al (2011) Osteoblast mineralization requires β1 integrin/ICAP-1–dependent fibronectin deposition. Journal of Cell Biology 194:307–322. https://doi.org/10.1083/jcb.201007108

Bussell ME (2021) Improving bone health: addressing the burden through an integrated approach. Aging Clin Exp Res 33:2777–2786. https://doi.org/10.1007/s40520-021-01971-3

Carlson M (2019) org.Dr.eg.db: Genome wide annotation for Zebrafish. R package version 3.8.2.

Carnevali O, Notarstefano V, Olivotto I, et al (2017) Dietary administration of EDC mixtures: A focus on fish lipid metabolism. Aquatic Toxicology 185:95–104. https://doi.org/10.1016/j.aquatox.2017.02.007

Chapin RE, Ku WW, Kenney MA, et al (1997) The Effects of Dietary Boron on Bone Strength in Rats. Toxicol Sci 35:205–215. https://doi.org/10.1093/toxsci/35.2.205

Chapin RE, Ku WW, Kenney MA, McCoy H (1998) The effects of dietary boric acid on bone strength in rats. Biol Trace Elem Res 66:395–399. https://doi.org/10.1007/BF02783150

Chen G, Deng C, Li Y-P (2012) TGF-β and BMP Signaling in Osteoblast Differentiation and Bone Formation. Int J Biol Sci 8:272–288. https://doi.org/10.7150/ijbs.2929

Cool S, Jackson R, Pincus P, et al (2002) Fibroblast growth factor receptor 4 (FGFR4) expression in newborn murine calvaria and primary osteoblast cultures. Int J Dev Biol 46:519–523

Dessordi R, Spirlandeli AL, Zamarioli A, et al (2017) Boron supplementation improves bone health of non-obese diabetic mice. Journal of Trace Elements in Medicine and Biology 39:169–175. https://doi.org/10.1016/j.jtemb.2016.09.011

Devirian TA, Volpe SL (2003) The Physiological Effects of Dietary Boron. Critical Reviews in Food Science and Nutrition 43:219–231. https://doi.org/10.1080/10408690390826491

Dobin A, Davis CA, Schlesinger F, et al (2013) STAR: ultrafast universal RNA-seq aligner. Bioinformatics 29:15–21. https://doi.org/10.1093/bioinformatics/bts635

Dupre JN, Keenan MJ, Hegsted M, Brudevold AM (1994) Effects of dietary boron in rats fed a vitamin D-deficient diet. Environmental Health Perspectives 102:55–58. https://doi.org/10.1289/ehp.94102s755

Elliot MA, Edwards HM (1992) Studies to Determine Whether an Interaction Exists Among Boron, Calcium, and Cholecalciferol on the Skeletal Development of Broiler Chickens. Poult Sci 71:677–690. https://doi.org/10.3382/ps.0710677

Fernández I, Gavaia PJ, Laizé V, Cancela ML (2018) Fish as a model to assess chemical toxicity in bone. Aquatic Toxicology 194:208–226. https://doi.org/10.1016/j.aquatox.2017.11.015

Forner-Piquer I, Beato S, Piscitelli F, et al (2020) Effects of BPA on zebrafish gonads: Focus on the endocannabinoid system. Environ Pollut 264:114710. https://doi.org/10.1016/j.envpol.2020.114710

Gallardo-Williams MT, Maronpot RR, Turner CH, et al (2003) Effects of boric acid supplementation on bone histomorphometry, metabolism, and biomechanical properties in aged female F-344 rats. Biol Trace Elem Res 93:155–169. https://doi.org/10.1385/BTER:93:1-3:155

Gistelinck C, Gioia R, Gagliardi A, et al (2016) Zebrafish Collagen Type I: Molecular and Biochemical Characterization of the Major Structural Protein in Bone and Skin. Sci Rep 6:21540. https://doi.org/10.1038/srep21540

Gölge UH, Kaymaz B, Arpaci R, et al (2015) Effects of Boric Acid on Fracture Healing: An Experimental Study. Biol Trace Elem Res 167:264–271. https://doi.org/10.1007/s12011-015-0326-3

Gorustovich AA, Steimetz T, Nielsen FH, Guglielmotti MB (2008) A histomorphometric study of alveolar bone modelling and remodelling in mice fed a boron-deficient diet. Archives of Oral Biology 53:677–682. https://doi.org/10.1016/j.archoralbio.2008.01.011

Gümüşderelioğlu M, Tunçay EÖ, Kaynak G, et al (2015) Encapsulated boron as an osteoinductive agent for bone scaffolds. Journal of Trace Elements in Medicine and Biology 31:120–128. https://doi.org/10.1016/j.jtemb.2015.03.008

Hadley W (2016) Ggplot2: Elegrant graphics for data analysis. Springer

Hakki SS, Bozkurt BS, Hakki EE (2010) Boron regulates mineralized tissue-associated proteins in osteoblasts (MC3T3-E1). Journal of Trace Elements in Medicine and Biology 24:243–250. https://doi.org/10.1016/j.jtemb.2010.03.003

Hegsted M, Keenan MJ, Siver F, Wozniak P (1991) Effect of boron on vitamin D deficient rats. Biol Trace Elem Res 28:243–255. https://doi.org/10.1007/BF02990471

Hunt CD, Herbel JL, Idso JP (1994) Dietary boron modifies the effects of vitamin D3 nutrition on indices of energy substrate utilization and mineral metabolism in the chick. Journal of Bone and Mineral Research 9:171–182. https://doi.org/10.1002/jbmr.5650090206

Johnson EW, Jayroe LM (2009) Prevention and treatment of osteochondrosis in animals and humans

Jugdaohsingh R, Pedro LD, Watson A, Powell JJ (2015) Silicon and boron differ in their localization and loading in bone. Bone Reports 1:9–15. https://doi.org/10.1016/j.bonr.2014.10.002

Kanis JA, Norton N, Harvey NC, et al (2021) SCOPE 2021: a new scorecard for osteoporosis in Europe. Arch Osteoporos 16:82. https://doi.org/10.1007/s11657-020-00871-9

Karner CM, Lee S-Y, Long F (2017) Bmp Induces Osteoblast Differentiation through both Smad4 and mTORC1 Signaling. Molecular and Cellular Biology 37:. https://doi.org/10.1128/MCB.00253-16

Kassambara A, Mundt F (2020) Factoextra: extract and visualize the results of multivariate data analyses (R package version 1.0. 6)

Kaufman L, Rousseeuw PJ (2009) Finding Groups in Data: An Introduction to Cluster Analysis. John Wiley & Sons

Kawane T, Qin X, Jiang Q, et al (2018) Runx2 is required for the proliferation of osteoblast progenitors and induces proliferation by regulating Fgfr2 and Fgfr3. Scientific Reports 8:13551. https://doi.org/10.1038/s41598-018-31853-0

Kurtoğlu V, Kurtoğlu F, Coşkun B (2001) Effects of boron supplementation of adequate and inadequate vitamin D3-containing diet on performance and serum biochemical characters of broiler chickens. Research in Veterinary Science 71:183–187. https://doi.org/10.1053/rvsc.2001.0517

Lee K-S, Hong S-H, Bae S-C (2002) Both the Smad and p38 MAPK pathways play a crucial role in Runx2 expression following induction by transforming growth factor-β and bone morphogenetic protein. Oncogene 21:7156–7163. https://doi.org/10.1038/sj.onc.1205937

Liao Y, Smyth GK, Shi W (2014) featureCounts: an efficient general purpose program for assigning sequence reads to genomic features. Bioinformatics 30:923–930. https://doi.org/10.1093/bioinformatics/btt656

Liu Q, Li M, Wang S, et al (2020) Recent Advances of Osterix Transcription Factor in Osteoblast Differentiation and Bone Formation. Frontiers in Cell and Developmental Biology 8:1575. https://doi.org/10.3389/fcell.2020.601224

Love MI, Huber W, Anders S (2014) Moderated estimation of fold change and dispersion for RNA-seq data with DESeq2. Genome Biology 15:550. https://doi.org/10.1186/s13059-014-0550-8

Maechler M, Rousseeuw P, Struyf A, et al (2019) cluster: Cluster Analysis Basics and Extensions. R package version 2.1.0.

Martínez R, Esteve-Codina A, Herrero-Nogareda L, et al (2018) Dose-dependent transcriptomic responses of zebrafish eleutheroembryos to Bisphenol A. Environmental Pollution 243:988–997. https://doi.org/10.1016/j.envpol.2018.09.043

McCoy H, Irwin A, Kenney MA, Williams L (Univ of A (1991) Effects of boron supplements on bones from rats fed calcium and magnesium deficient diets. FASEB Journal (Federation of American Societies for Experimental Biology); (United States) 5:5:

Meacham SL, Taper LJ, Volpe SL (1995) Effect of boron supplementation on blood and urinary calcium, magnesium, and phosphorus, and urinary boron in athletic and sedentary women. The American Journal of Clinical Nutrition 61:341–345. https://doi.org/10.1093/ajcn/61.2.341

Miljkovic D, Miljkovic N, McCarty MF (2004) Up-regulatory impact of boron on vitamin D function – does it reflect inhibition of 24-hydroxylase? Medical Hypotheses 63:1054–1056. https://doi.org/10.1016/j.mehy.2003.12.053

Naghii MR, Samman S (1997) The effect of boron on plasma testosterone and plasma lipids in rats. Nutrition Research 17:523–531. https://doi.org/10.1016/S0271-5317(97)00017-1

Naghii MR, Torkaman G, Mofid M (2006) Effects of boron and calcium supplementation on mechanical properties of bone in rats. BioFactors 28:195–201. https://doi.org/10.1002/biof.5520280306

Nakashima K, Zhou X, Kunkel G, et al (2002) The Novel Zinc Finger-Containing Transcription Factor Osterix Is Required for Osteoblast Differentiation and Bone Formation. Cell 108:17–29. https://doi.org/10.1016/S0092-8674(01)00622-5

Neacsu CD, Grosch M, Tejada M, et al (2011) Ucmaa (Grp-2) is required for zebrafish skeletal development. Evidence for a functional role of its glutamate γ-carboxylation. Matrix Biology 30:369–378. https://doi.org/10.1016/j.matbio.2011.07.002

Nielsen FH (1990) Studies on the relationship between boron and magnesium which possibly affects the formation and maintenance of bones. Magnes Trace Elem 9:61–69

Nielsen FH (2004) Dietary fat composition modifies the effect of boron on bone characteristics and plasma lipids in rats. BioFactors 20:161–171. https://doi.org/10.1002/biof.5520200305

Nielsen FH, Stoecker BJ (2009) Boron and fish oil have different beneficial effects on strength and trabecular microarchitecture of bone. Journal of Trace Elements in Medicine and Biology 23:195–203. https://doi.org/10.1016/j.jtemb.2009.03.003

Niu P, Zhong Z, Wang M, et al (2017) Zinc finger transcription factor Sp7/Osterix acts on bone formation and regulates col10a1a expression in zebrafish. Science Bulletin 62:174–184. https://doi.org/10.1016/j.scib.2017.01.009

Nottmeier C, Decker MG, Luther J, et al (2020) Accelerated tooth movement in Rsk2-deficient mice with impaired cementum formation. Int J Oral Sci 12:1–8. https://doi.org/10.1038/s41368-020-00102-4

Pawlikowski B, Vogler TO, Gadek K, Olwin BB (2017) Regulation of skeletal muscle stem cells by fibroblast growth factors. Developmental Dynamics 246:359–367. https://doi.org/10.1002/dvdy.24495

R Core Team (2019) R: A language and environment for statistical computing. Vienna, Austria: R Foundation for Statistical Computing; 2011.

Rossi AF, Miles RD, Damron BL, Flunker LK (1993) Effects of Dietary Boron Supplementation on Broilers. Poult Sci 72:2124–2130. https://doi.org/10.3382/ps.0722124

Rutkovskiy A, Stensløkken K-O, Vaage IJ (2016) Osteoblast Differentiation at a Glance. Med Sci Monit Basic Res 22:95–106. https://doi.org/10.12659/MSMBR.901142

Scorei ID, Scorei RI (2013) Calcium Fructoborate Helps Control Inflammation Associated with Diminished Bone Health. Biol Trace Elem Res 155:315–321. https://doi.org/10.1007/s12011-013-9800-y

Sens C, Huck K, Pettera S, et al (2017) Fibronectins containing extradomain A or B enhance osteoblast differentiation via distinct integrins. Journal of Biological Chemistry 292:7745–7760. https://doi.org/10.1074/jbc.M116.739987

Suda T, Ueno Y, Fujii K, Shinki T (2003) Vitamin D and bone. Journal of Cellular Biochemistry 88:259–266. https://doi.org/10.1002/jcb.10331

Sun L, Blair HC, Peng Y, et al (2005) Calcineurin regulates bone formation by the osteoblast. PNAS 102:17130–17135. https://doi.org/10.1073/pnas.0508480102

Tarasco M, Cordelières FP, Cancela ML, Laizé V (2020) ZFBONE: An ImageJ toolset for semi-automatic analysis of zebrafish bone structures. Bone 138:115480. https://doi.org/10.1016/j.bone.2020.115480

Tarasco M, Laizé V, Cardeira J, et al (2017) The zebrafish operculum: A powerful system to assess osteogenic bioactivities of molecules with pharmacological and toxicological relevance. Comparative Biochemistry and Physiology Part C: Toxicology & Pharmacology 197:45–52. https://doi.org/10.1016/j.cbpc.2017.04.006

Tibshirani R, Walther G, Hastie T (2001) Estimating the number of clusters in a data set via the gap statistic. Journal of the Royal Statistical Society: Series B (Statistical Methodology) 63:411–423. https://doi.org/10.1111/1467-9868.00293

Valenti MT, Marchetto G, Mottes M, Dalle Carbonare L (2020) Zebrafish: A Suitable Tool for the Study of Cell Signaling in Bone. Cells 9:1911. https://doi.org/10.3390/cells9081911

van Driel M, van Leeuwen JPTM (2014) Vitamin D endocrine system and osteoblasts. Bonekey Rep 3:493. https://doi.org/10.1038/bonekey.2013.227

Wang Z-Q, Ovitt C, Grigoriadis AE, et al (1992) Bone and haematopoietic defects in mice lacking c-fos. Nature 360:741–745. https://doi.org/10.1038/360741a0

Warnes GR, Bolker B, Bonebakker L, et al (2020) gplots: Various R Programming Tools for Plotting Data. Version 3.1.1URL https://CRAN.R-project.org/package=gplots

WILSON JH, RUSZLER PL (1998) Long term effects of boron on layer bone strength and production parameters. British Poultry Science 39:11–15. https://doi.org/10.1080/00071669889312

Wilson JH, Ruszler PL (1997) Effects of boron on growing pullets. Biol Trace Elem Res 56:287–294. https://doi.org/10.1007/BF02785300

Xing J, Ginty DD, Greenberg ME (1996) Coupling of the RAS-MAPK Pathway to Gene Activation by RSK2, a Growth Factor-Regulated CREB Kinase. Science 273:959–963. https://doi.org/10.1126/science.273.5277.959

Yang C, Wang C, Zhou J, et al (2020) Fibronectin 1 activates WNT/β-catenin signaling to induce osteogenic differentiation via integrin β1 interaction. Laboratory Investigation 100:1494–1502. https://doi.org/10.1038/s41374-020-0451-2

Yang X, Matsuda K, Bialek P, et al (2004) ATF4 Is a Substrate of RSK2 and an Essential Regulator of Osteoblast Biology: Implication for Coffin-Lowry Syndrome. Cell 117:387–398. https://doi.org/10.1016/S0092-8674(04)00344-7

Ying X, Cheng S, Wang W, et al (2011) Effect of boron on osteogenic differentiation of human bone marrow stromal cells. Biol Trace Elem Res 144:306–315. https://doi.org/10.1007/s12011-011-9094-x

Yu G, Wang L-G, Han Y, He Q-Y (2012) clusterProfiler: an R Package for Comparing Biological Themes Among Gene Clusters. OMICS: A Journal of Integrative Biology 16:284–287. https://doi.org/10.1089/omi.2011.0118

Zhu D, Ansari AR, Xiao K, et al (2020) Boron Supplementation Promotes Osteogenesis of Tibia by Regulating the Bone Morphogenetic Protein-2 Expression in African Ostrich Chicks. Biol Trace Elem Res. https://doi.org/10.1007/s12011-020-02258-w

Data Availability Statement

The RNA sequencing data generated for this study has been deposited to NCBI under the project accession PRJNA796753. Data that support the findings of this study are available in the supplementary material of this article. **Supplemental table 2** is openly available in figshare at https://doi.org/10.6084/m9.figshare.18316271.v1

Supplementary Material

Supplementary Table 1 – Details of the data generated after sequencing, after initial QC across different groups.

Sample	*Raw reads (Pairs)*	*Sequence data*	*Q30 (%)*	*GC (%)*
C-13	96708280	14,506,242,000	93.65	46.93
B100-3	64455670	9,668,350,500	94.83	47.99
VD-3	79895168	11,984,275,200	94.13	47.77
VD-2	81963304	12,294,495,600	94.28	48.27
B10VD-3	92865370	13,929,805,500	94.18	46.99
B10-4	88668494	13,300,274,100	94.6	47.65
C-2	102022422	15,303,363,300	94.22	48.1
B10VD-1	104282710	15,642,406,500	93.81	48.15
B100-1	71415618	10,712,342,700	94.54	48.33
C-4	80591422	12,088,713,300	94.5	47.78
B10-1	113506504	17,025,975,600	94.52	47.62
B10-2	64377336	9,656,600,400	94.67	47.21
VD-1	86162182	12,924,327,300	94.49	47.82
B100VD-2	111101012	16,665,151,800	94.49	49.34
B100-4	76966844	11,545,026,600	94.84	49.99
VD-4	71121896	10,668,284,400	94.62	47.9
B10-3	83129550	12,469,432,500	94.11	47.83
B100VD-4	63256244	9,488,436,600	94.64	47.73
B100VD-1	86462822	12,969,423,300	93.79	47.3
C-1	84886368	12,732,955,200	94.35	47.01
B10VD-4	86311546	12,946,731,900	94.68	47.88
B100VD-3	88289786	13,243,467,900	94.18	47.5
B100-2	91357382	13,703,607,300	94.29	47.73
B10VD-2	96428740	14,464,311,000	94.2	48.78

Supplementary Table 3 – GO enrichment results across genes differentially expressed in the three clusters.

Cluster	*Go Category*	*ID*	*Description*	*GeneRatio*	*pvalue*	*p.adjust*	*qvalue*	*Count*
1	Biological Process	GO:0019941	modification-dependent protein catabolic process	90/1987	1.44E-09	1.66E-06	1.62E-06	90
1	Biological Process	GO:0010499	proteasomal ubiquitin-independent protein catabolic process	16/1987	1.53E-09	1.66E-06	1.62E-06	16
1	Biological Process	GO:0043632	modification-dependent macromolecule catabolic process	91/1987	1.63E-09	1.66E-06	1.62E-06	91
1	Biological Process	GO:0006511	ubiquitin-dependent protein catabolic process	88/1987	2.24E-09	1.71E-06	1.67E-06	88
1	Biological Process	GO:0043248	proteasome assembly	12/1987	1.54E-08	9.43E-06	9.2E-06	12
1	Biological Process	GO:0002088	lens development in camera-type eye	30/1987	1.67E-07	8.54E-05	8.34E-05	30
1	Biological Process	GO:0043161	proteasome-mediated ubiquitin-dependent protein catabolic process	58/1987	1.24E-06	0.000544	0.000531	58
1	Biological Process	GO:0010498	proteasomal protein catabolic process	59/1987	5.06E-06	0.00194	0.001893	59
1	Biological Process	GO:0043010	camera-type eye development	76/1987	7.95E-06	0.002709	0.002643	76
1	Biological Process	GO:0006457	protein folding	33/1987	3.49E-05	0.010693	0.010433	33
1	Biological Process	GO:0006081	cellular aldehyde metabolic process	14/1987	5.09E-05	0.014189	0.013844	14
1	Biological Process	GO:0051149	positive regulation of muscle cell differentiation	7/1987	6.32E-05	0.014912	0.01455	7
1	Biological Process	GO:0051155	positive regulation of striated muscle cell differentiation	7/1987	6.32E-05	0.014912	0.01455	7
1	Biological Process	GO:0009408	response to heat	13/1987	9.41E-05	0.020593	0.020092	13
1	Biological Process	GO:0016202	regulation of striated muscle tissue development	10/1987	0.000106	0.021745	0.021217	10
1	Biological Process	GO:0050953	sensory perception of light stimulus	37/1987	0.00021	0.040213	0.039236	37
1	Biological Process	GO:1901861	regulation of muscle tissue development	10/1987	0.000226	0.040777	0.039786	10
2	Biological Process	GO:0006836	neurotransmitter transport	27/1240	5.18E-09	1.39E-05	1.28E-05	27
2	Biological Process	GO:0018298	protein-chromophore linkage	14/1240	2.8E-07	0.000315	0.000291	14
2	Biological Process	GO:0007602	phototransduction	15/1240	3.54E-07	0.000315	0.000291	15
2	Biological Process	GO:0009583	detection of light stimulus	16/1240	1.39E-06	0.000927	0.000854	16
2	Biological Process	GO:0043269	regulation of ion transport	38/1240	2.74E-06	0.001466	0.001352	38
2	Biological Process	GO:0015893	drug transport	21/1240	4.97E-06	0.002216	0.002042	21
2	Biological Process	GO:0009416	response to light stimulus	27/1240	1.06E-05	0.00332	0.00306	27
2	Biological Process	GO:0009581	detection of external stimulus	18/1240	1.12E-05	0.00332	0.00306	18
2	Biological Process	GO:0009582	detection of abiotic stimulus	18/1240	1.12E-05	0.00332	0.00306	18
2	Biological Process	GO:0071482	cellular response to light stimulus	14/1240	1.79E-05	0.004356	0.004014	14
2	Biological Process	GO:0001505	regulation of neurotransmitter levels	24/1240	1.95E-05	0.004356	0.004014	24
2	Biological Process	GO:0051606	detection of stimulus	19/1240	1.95E-05	0.004356	0.004014	19
2	Biological Process	GO:0050953	sensory perception of light stimulus	29/1240	2.32E-05	0.004781	0.004406	29
2	Biological Process	GO:0034762	regulation of transmembrane transport	31/1240	4.32E-05	0.008253	0.007606	31
2	Biological Process	GO:0007601	visual perception	27/1240	6.72E-05	0.011989	0.011049	27
2	Biological Process	GO:0015672	monovalent inorganic cation transport	40/1240	8.05E-05	0.013467	0.012411	40
2	Biological Process	GO:0015807	L-amino acid transport	8/1240	0.000121	0.019019	0.017529	8
2	Biological Process	GO:0016079	synaptic vesicle exocytosis	13/1240	0.000139	0.01927	0.01776	13
2	Biological Process	GO:0007269	neurotransmitter secretion	15/1240	0.000144	0.01927	0.01776	15
2	Biological Process	GO:0099643	signal release from synapse	15/1240	0.000144	0.01927	0.01776	15

2	Biological Process	GO:0034765	regulation of ion transmembrane transport	29/1240	0.000165	0.020984	0.01934	29
2	Biological Process	GO:0045055	regulated exocytosis	16/1240	0.000196	0.0228	0.021013	16
2	Biological Process	GO:0003333	amino acid transmembrane transport	11/1240	0.000196	0.0228	0.021013	11
2	Biological Process	GO:0055003	cardiac myofibril assembly	9/1240	0.000295	0.032902	0.030324	9
2	Biological Process	GO:0006865	amino acid transport	13/1240	0.000314	0.033658	0.031021	13
2	Biological Process	GO:0071478	cellular response to radiation	14/1240	0.00033	0.033966	0.031304	14
2	Biological Process	GO:0071214	cellular response to abiotic stimulus	15/1240	0.00038	0.036355	0.033506	15
2	Biological Process	GO:0104004	cellular response to environmental stimulus	15/1240	0.00038	0.036355	0.033506	15
2	Biological Process	GO:0098655	cation transmembrane transport	51/1240	0.000414	0.038105	0.03512	51
2	Biological Process	GO:0015850	organic hydroxy compound transport	15/1240	0.000433	0.038105	0.03512	15
2	Biological Process	GO:0009314	response to radiation	28/1240	0.000441	0.038105	0.03512	28
2	Biological Process	GO:0051260	protein homooligomerization	21/1240	0.000471	0.038555	0.035534	21
2	Biological Process	GO:0098656	anion transmembrane transport	20/1240	0.000475	0.038555	0.035534	20
2	Biological Process	GO:1901879	regulation of protein depolymerization	11/1240	0.000491	0.038638	0.03561	11
2	Biological Process	GO:0006936	muscle contraction	21/1240	0.000516	0.039487	0.036392	21
2	Biological Process	GO:0006353	DNA-templated transcription, termination	5/1240	0.000608	0.043529	0.040118	5
2	Biological Process	GO:0048739	cardiac muscle fiber development	7/1240	0.000611	0.043529	0.040118	7
2	Biological Process	GO:0015844	monoamine transport	8/1240	0.000622	0.043529	0.040118	8
2	Biological Process	GO:1903825	organic acid transmembrane transport	13/1240	0.000651	0.043529	0.040118	13
2	Biological Process	GO:1905039	carboxylic acid transmembrane transport	13/1240	0.000651	0.043529	0.040118	13
2	Biological Process	GO:0043244	regulation of protein-containing complex disassembly	12/1240	0.000731	0.047637	0.043904	12
2	Biological Process	GO:1902903	regulation of supramolecular fiber organization	22/1240	0.000776	0.047637	0.043904	22
2	Biological Process	GO:0014046	dopamine secretion	7/1240	0.000801	0.047637	0.043904	7
2	Biological Process	GO:0014059	regulation of dopamine secretion	7/1240	0.000801	0.047637	0.043904	7
2	Biological Process	GO:0030241	skeletal muscle myosin thick filament assembly	7/1240	0.000801	0.047637	0.043904	7
2	Biological Process	GO:0006820	anion transport	42/1240	0.000839	0.048803	0.044979	42
3	Biological Process	GO:0030198	extracellular matrix organization	51/1501	9.03E-20	1.3E-16	1.22E-16	51
3	Biological Process	GO:0043062	extracellular structure organization	51/1501	9.03E-20	1.3E-16	1.22E-16	51
3	Biological Process	GO:0030199	collagen fibril organization	12/1501	3.08E-08	2.47E-05	2.33E-05	12
3	Biological Process	GO:0007229	integrin-mediated signaling pathway	20/1501	3.44E-08	2.47E-05	2.33E-05	20
3	Biological Process	GO:0031589	cell-substrate adhesion	24/1501	8.48E-08	4.88E-05	4.59E-05	24
3	Biological Process	GO:0061448	connective tissue development	36/1501	6.76E-07	0.000276	0.000259	36
3	Biological Process	GO:0090171	chondrocyte morphogenesis	10/1501	7.55E-07	0.000276	0.000259	10
3	Biological Process	GO:0006820	anion transport	59/1501	7.66E-07	0.000276	0.000259	59
3	Biological Process	GO:0001501	skeletal system development	61/1501	1.58E-06	0.000504	0.000474	61
3	Biological Process	GO:0003414	chondrocyte morphogenesis involved in endochondral bone morphogenesis	9/1501	2.76E-06	0.00062	0.000583	9
3	Biological Process	GO:0003429	growth plate cartilage chondrocyte morphogenesis	9/1501	2.76E-06	0.00062	0.000583	9
3	Biological Process	GO:0003433	chondrocyte development involved in endochondral bone morphogenesis	9/1501	2.76E-06	0.00062	0.000583	9
3	Biological Process	GO:0051216	cartilage development	34/1501	2.8E-06	0.00062	0.000583	34
3	Biological Process	GO:0015711	organic anion transport	44/1501	4.41E-06	0.000826	0.000777	44
3	Biological Process	GO:0031101	fin regeneration	21/1501	4.61E-06	0.000826	0.000777	21
3	Biological Process	GO:0003413	chondrocyte differentiation involved in endochondral bone morphogenesis	9/1501	4.88E-06	0.000826	0.000777	9

3	Biological Process	GO:0003418	growth plate cartilage chondrocyte differentiation	9/1501	4.88E-06	0.000826	0.000777	9
3	Biological Process	GO:0002062	chondrocyte differentiation	14/1501	6.81E-06	0.001088	0.001023	14
3	Biological Process	GO:0002063	chondrocyte development	11/1501	1.29E-05	0.001934	0.001818	11
3	Biological Process	GO:0003422	growth plate cartilage morphogenesis	9/1501	1.34E-05	0.001934	0.001818	9
3	Biological Process	GO:0060536	cartilage morphogenesis	13/1501	2.7E-05	0.003701	0.00348	13
3	Biological Process	GO:0003416	endochondral bone growth	9/1501	3.24E-05	0.004048	0.003807	9
3	Biological Process	GO:0003417	growth plate cartilage development	9/1501	3.24E-05	0.004048	0.003807	9
3	Biological Process	GO:0018158	protein oxidation	6/1501	3.66E-05	0.004383	0.004121	6
3	Biological Process	GO:0097435	supramolecular fiber organization	63/1501	4.1E-05	0.004706	0.004425	63
3	Biological Process	GO:0006270	DNA replication initiation	10/1501	4.25E-05	0.004706	0.004425	10
3	Biological Process	GO:0098868	bone growth	9/1501	4.82E-05	0.005135	0.004828	9
3	Biological Process	GO:0015849	organic acid transport	28/1501	7.31E-05	0.007506	0.007058	28
3	Biological Process	GO:0007160	cell-matrix adhesion	14/1501	7.84E-05	0.00778	0.007316	14
3	Biological Process	GO:0048514	blood vessel morphogenesis	58/1501	8.3E-05	0.007955	0.00748	58
3	Biological Process	GO:0040007	growth	58/1501	0.000144	0.013292	0.012499	58
3	Biological Process	GO:0046942	carboxylic acid transport	27/1501	0.000148	0.013292	0.012499	27
3	Biological Process	GO:0009611	response to wounding	42/1501	0.00016	0.01399	0.013154	42
3	Biological Process	GO:0033627	cell adhesion mediated by integrin	7/1501	0.000173	0.014597	0.013725	7
3	Biological Process	GO:0060350	endochondral bone morphogenesis	10/1501	0.000253	0.02061	0.01938	10
3	Biological Process	GO:0060351	cartilage development involved in endochondral bone morphogenesis	9/1501	0.000258	0.02061	0.01938	9
3	Biological Process	GO:0042060	wound healing	35/1501	0.000338	0.026313	0.024743	35
3	Biological Process	GO:0090504	epiboly	17/1501	0.000486	0.035997	0.033848	17
3	Biological Process	GO:0048589	developmental growth	53/1501	0.000488	0.035997	0.033848	53
3	Biological Process	GO:0010810	regulation of cell-substrate adhesion	8/1501	0.000606	0.042405	0.039874	8
3	Biological Process	GO:0010811	positive regulation of cell-substrate adhesion	6/1501	0.000618	0.042405	0.039874	6
3	Biological Process	GO:0030903	notochord development	15/1501	0.000619	0.042405	0.039874	15
3	Biological Process	GO:0002011	morphogenesis of an epithelial sheet	19/1501	0.000684	0.045687	0.04296	19
3	Biological Process	GO:0001525	angiogenesis	46/1501	0.000699	0.045687	0.04296	46
1	Cellular Component	GO:0000502	proteasome complex	42/1966	4.03E-23	9.95E-21	9.75E-21	42
1	Cellular Component	GO:1905369	endopeptidase complex	42/1966	4.03E-23	9.95E-21	9.75E-21	42
1	Cellular Component	GO:0005838	proteasome regulatory particle	23/1966	7.19E-19	1.18E-16	1.16E-16	23
1	Cellular Component	GO:1905368	peptidase complex	42/1966	5.61E-18	6.93E-16	6.79E-16	42
1	Cellular Component	GO:0022624	proteasome accessory complex	23/1966	4.09E-16	4.04E-14	3.96E-14	23
1	Cellular Component	GO:0005839	proteasome core complex	16/1966	9.8E-11	8.07E-09	7.91E-09	16
1	Cellular Component	GO:0008540	proteasome regulatory particle, base subcomplex	12/1966	1.4E-09	9.91E-08	9.71E-08	12
1	Cellular Component	GO:0008541	proteasome regulatory particle, lid subcomplex	9/1966	1.01E-08	6.23E-07	6.11E-07	9
1	Cellular Component	GO:0019773	proteasome core complex, alpha-subunit complex	9/1966	5.05E-08	2.77E-06	2.71E-06	9
1	Cellular Component	GO:0000323	lytic vacuole	35/1966	0.000641	0.027382	0.02684	35
1	Cellular Component	GO:0005764	lysosome	35/1966	0.000641	0.027382	0.02684	35
1	Cellular Component	GO:0005765	lysosomal membrane	19/1966	0.000721	0.027382	0.02684	19
1	Cellular Component	GO:0098852	lytic vacuole membrane	19/1966	0.000721	0.027382	0.02684	19
2	Cellular Component	GO:0070382	exocytic vesicle	23/1275	2.01E-05	0.003069	0.002651	23

2	Cellular Component	GO:0005865	striated muscle thin filament	14/1275	2.6E-05	0.003069	0.002651	14
2	Cellular Component	GO:0036379	myofilament	14/1275	2.6E-05	0.003069	0.002651	14
2	Cellular Component	GO:0099503	secretory vesicle	26/1275	3.15E-05	0.003069	0.002651	26
2	Cellular Component	GO:0030017	sarcomere	24/1275	4.4E-05	0.003069	0.002651	24
2	Cellular Component	GO:0044449	contractile fiber part	24/1275	4.92E-05	0.003069	0.002651	24
2	Cellular Component	GO:0045202	synapse	54/1275	5.93E-05	0.003069	0.002651	54
2	Cellular Component	GO:0030016	myofibril	24/1275	6.1E-05	0.003069	0.002651	24
2	Cellular Component	GO:0043292	contractile fiber	24/1275	6.79E-05	0.003069	0.002651	24
2	Cellular Component	GO:0097731	9+0 non-motile cilium	11/1275	0.000183	0.006678	0.005769	11
2	Cellular Component	GO:0097733	photoreceptor cell cilium	11/1275	0.000183	0.006678	0.005769	11
2	Cellular Component	GO:0030018	Z disc	15/1275	0.000197	0.006678	0.005769	15
2	Cellular Component	GO:0031674	I band	16/1275	0.000302	0.009403	0.008122	16
2	Cellular Component	GO:0031430	M band	8/1275	0.000323	0.009403	0.008122	8
2	Cellular Component	GO:0008021	synaptic vesicle	18/1275	0.000402	0.010334	0.008927	18
2	Cellular Component	GO:0015629	actin cytoskeleton	38/1275	0.000406	0.010334	0.008927	38
2	Cellular Component	GO:0098793	presynapse	24/1275	0.000453	0.010847	0.00937	24
2	Cellular Component	GO:0034703	cation channel complex	24/1275	0.000493	0.011068	0.009561	24
2	Cellular Component	GO:0001750	photoreceptor outer segment	9/1275	0.000517	0.011068	0.009561	9
2	Cellular Component	GO:0044456	synapse part	42/1275	0.000638	0.012978	0.011211	42
2	Cellular Component	GO:0097730	non-motile cilium	12/1275	0.000722	0.013985	0.01208	12
2	Cellular Component	GO:0005929	cilium	34/1275	0.000808	0.014954	0.012918	34
2	Cellular Component	GO:0030133	transport vesicle	25/1275	0.001037	0.018352	0.015853	25
2	Cellular Component	GO:0031672	A band	8/1275	0.001328	0.021892	0.018911	8
2	Cellular Component	GO:0044463	cell projection part	49/1275	0.001406	0.021892	0.018911	49
2	Cellular Component	GO:0120038	plasma membrane bounded cell projection part	49/1275	0.001406	0.021892	0.018911	49
2	Cellular Component	GO:0008076	voltage-gated potassium channel complex	10/1275	0.00156	0.021892	0.018911	10
2	Cellular Component	GO:0030672	synaptic vesicle membrane	10/1275	0.00156	0.021892	0.018911	10
2	Cellular Component	GO:0099501	exocytic vesicle membrane	10/1275	0.00156	0.021892	0.018911	10
2	Cellular Component	GO:0044441	ciliary part	26/1275	0.00208	0.028223	0.02438	26
2	Cellular Component	GO:0098797	plasma membrane protein complex	48/1275	0.002477	0.032523	0.028094	48
2	Cellular Component	GO:0001518	voltage-gated sodium channel complex	5/1275	0.002884	0.036687	0.031691	5
2	Cellular Component	GO:1902495	transmembrane transporter complex	29/1275	0.003341	0.041209	0.035598	29
2	Cellular Component	GO:0034702	ion channel complex	28/1275	0.00345	0.041299	0.035675	28
3	Cellular Component	GO:0031012	extracellular matrix	85/1543	5.84E-33	2.52E-30	2.38E-30	85
3	Cellular Component	GO:0062023	collagen-containing extracellular matrix	41/1543	6.32E-20	1.37E-17	1.29E-17	41
3	Cellular Component	GO:0005581	collagen trimer	32/1543	2.6E-16	3.75E-14	3.53E-14	32
3	Cellular Component	GO:0008305	integrin complex	17/1543	1.07E-09	9.28E-08	8.75E-08	17
3	Cellular Component	GO:0098636	protein complex involved in cell adhesion	17/1543	1.07E-09	9.28E-08	8.75E-08	17
3	Cellular Component	GO:0044420	extracellular matrix component	10/1543	1.54E-06	0.000111	0.000104	10
3	Cellular Component	GO:0098644	complex of collagen trimers	7/1543	1.93E-06	0.000119	0.000112	7
3	Cellular Component	GO:0042555	MCM complex	8/1543	1.99E-05	0.001076	0.001014	8
3	Cellular Component	GO:0005925	focal adhesion	14/1543	0.000138	0.006614	0.006237	14

3	Cellular Component	GO:0005924	cell-substrate adherens junction	14/1543	0.000168	0.006614	0.006237	14
3	Cellular Component	GO:0030055	cell-substrate junction	14/1543	0.000168	0.006614	0.006237	14
3	Cellular Component	GO:0005732	small nucleolar ribonucleoprotein complex	7/1543	0.000426	0.015333	0.014459	7
3	Cellular Component	GO:0005882	intermediate filament	17/1543	0.000752	0.024984	0.02356	17
3	Cellular Component	GO:0045111	intermediate filament cytoskeleton	17/1543	0.000855	0.026388	0.024883	17
3	Cellular Component	GO:0030054	cell junction	55/1543	0.000943	0.027165	0.025616	55
3	Cellular Component	GO:0005923	bicellular tight junction	15/1543	0.001266	0.034193	0.032243	15
3	Cellular Component	GO:0045178	basal part of cell	6/1543	0.001442	0.03664	0.034551	6
3	Cellular Component	GO:0070160	tight junction	15/1543	0.001647	0.039525	0.037272	15
1	Molecular Function	GO:0004298	threonine-type endopeptidase activity	16/1989	2.4E-10	1.02E-07	9.75E-08	16
1	Molecular Function	GO:0070003	threonine-type peptidase activity	16/1989	2.4E-10	1.02E-07	9.75E-08	16
1	Molecular Function	GO:0004175	endopeptidase activity	83/1989	1.27E-06	0.000361	0.000344	83
1	Molecular Function	GO:0016798	hydrolase activity, acting on glycosyl bonds	32/1989	1.39E-05	0.002954	0.002818	32
1	Molecular Function	GO:0005212	structural constituent of eye lens	20/1989	4.12E-05	0.007016	0.006692	20
1	Molecular Function	GO:0051787	misfolded protein binding	10/1989	5.89E-05	0.008364	0.007977	10
1	Molecular Function	GO:0000977	RNA polymerase II regulatory region sequence-specific DNA binding	78/1989	7.6E-05	0.009254	0.008827	78
1	Molecular Function	GO:0019842	vitamin binding	26/1989	0.00015	0.016006	0.015266	26
1	Molecular Function	GO:0005506	iron ion binding	41/1989	0.000232	0.021975	0.02096	41
1	Molecular Function	GO:0001228	DNA-binding transcription activator activity, RNA polymerase II-specific	23/1989	0.000298	0.025369	0.024197	23
1	Molecular Function	GO:0008237	metallopeptidase activity	36/1989	0.000328	0.025369	0.024197	36
1	Molecular Function	GO:0004553	hydrolase activity, hydrolyzing O-glycosyl compounds	25/1989	0.00043	0.030559	0.029147	25
1	Molecular Function	GO:0046906	tetrapyrrole binding	35/1989	0.000673	0.044085	0.042048	35
1	Molecular Function	GO:0020037	heme binding	34/1989	0.000926	0.049895	0.047589	34
1	Molecular Function	GO:0008236	serine-type peptidase activity	38/1989	0.000937	0.049895	0.047589	38
1	Molecular Function	GO:0017171	serine hydrolase activity	38/1989	0.000937	0.049895	0.047589	38
2	Molecular Function	GO:0009881	photoreceptor activity	16/1293	5.01E-08	3.77E-05	3.42E-05	16
2	Molecular Function	GO:0005326	neurotransmitter transporter activity	17/1293	5.53E-07	0.000208	0.000189	17
2	Molecular Function	GO:0008307	structural constituent of muscle	11/1293	1.14E-06	0.000249	0.000226	11
2	Molecular Function	GO:0008020	G protein-coupled photoreceptor activity	13/1293	1.32E-06	0.000249	0.000226	13
2	Molecular Function	GO:0046873	metal ion transmembrane transporter activity	59/1293	4.96E-06	0.000747	0.000678	59
2	Molecular Function	GO:0015171	amino acid transmembrane transporter activity	18/1293	1.05E-05	0.001319	0.001197	18
2	Molecular Function	GO:0008509	anion transmembrane transporter activity	41/1293	3.86E-05	0.004154	0.003769	41
2	Molecular Function	GO:0017080	sodium channel regulator activity	6/1293	5.37E-05	0.004234	0.003841	6
2	Molecular Function	GO:0022839	ion gated channel activity	48/1293	5.4E-05	0.004234	0.003841	48
2	Molecular Function	GO:0022836	gated channel activity	49/1293	6.01E-05	0.004234	0.003841	49
2	Molecular Function	GO:0046943	carboxylic acid transmembrane transporter activity	25/1293	6.18E-05	0.004234	0.003841	25
2	Molecular Function	GO:0005342	organic acid transmembrane transporter activity	25/1293	7.59E-05	0.004763	0.004321	25
2	Molecular Function	GO:0005328	neurotransmitter:sodium symporter activity	11/1293	0.000101	0.005778	0.005242	11
2	Molecular Function	GO:0005244	voltage-gated ion channel activity	30/1293	0.000107	0.005778	0.005242	30
2	Molecular Function	GO:0005216	ion channel activity	55/1293	0.000132	0.006646	0.00603	55
2	Molecular Function	GO:0022832	voltage-gated channel activity	30/1293	0.000162	0.007622	0.006915	30
2	Molecular Function	GO:0015077	monovalent inorganic cation transmembrane transporter activity	50/1293	0.000175	0.00774	0.007022	50

2	Molecular Function	GO:0015179	L-amino acid transmembrane transporter activity	11/1293	0.000234	0.009261	0.008402	11
2	Molecular Function	GO:0099106	ion channel regulator activity	11/1293	0.000234	0.009261	0.008402	11
2	Molecular Function	GO:0022843	voltage-gated cation channel activity	25/1293	0.00026	0.00967	0.008773	25
2	Molecular Function	GO:0051015	actin filament binding	30/1293	0.00028	0.00967	0.008773	30
2	Molecular Function	GO:0008514	organic anion transmembrane transporter activity	28/1293	0.000283	0.00967	0.008773	28
2	Molecular Function	GO:0015081	sodium ion transmembrane transporter activity	24/1293	0.000344	0.010952	0.009936	24
2	Molecular Function	GO:0005267	potassium channel activity	22/1293	0.000349	0.010952	0.009936	22
2	Molecular Function	GO:0015238	drug transmembrane transporter activity	14/1293	0.000465	0.013801	0.01252	14
2	Molecular Function	GO:0005249	voltage-gated potassium channel activity	18/1293	0.000477	0.013801	0.01252	18
2	Molecular Function	GO:0016247	channel regulator activity	12/1293	0.000556	0.015514	0.014075	12
2	Molecular Function	GO:0042805	actinin binding	9/1293	0.000662	0.01779	0.01614	9
2	Molecular Function	GO:0005261	cation channel activity	42/1293	0.000705	0.018306	0.016608	42
2	Molecular Function	GO:0051371	muscle alpha-actinin binding	8/1293	0.001113	0.027895	0.025307	8
2	Molecular Function	GO:0003779	actin binding	47/1293	0.001148	0.027895	0.025307	47
2	Molecular Function	GO:0051393	alpha-actinin binding	8/1293	0.001372	0.032283	0.029288	8
2	Molecular Function	GO:0005283	amino acid:sodium symporter activity	6/1293	0.001423	0.032481	0.029468	6
2	Molecular Function	GO:0005313	L-glutamate transmembrane transporter activity	5/1293	0.00151	0.032484	0.029471	5
2	Molecular Function	GO:0015172	acidic amino acid transmembrane transporter activity	5/1293	0.00151	0.032484	0.029471	5
2	Molecular Function	GO:0015079	potassium ion transmembrane transporter activity	25/1293	0.001709	0.035745	0.03243	25
2	Molecular Function	GO:0015370	solute:sodium symporter activity	15/1293	0.001882	0.037304	0.033844	15
2	Molecular Function	GO:0005416	amino acid:cation symporter activity	6/1293	0.001883	0.037304	0.033844	6
3	Molecular Function	GO:0005201	extracellular matrix structural constituent	36/1495	1.82E-22	1.42E-19	1.3E-19	36
3	Molecular Function	GO:0050839	cell adhesion molecule binding	24/1495	2.67E-06	0.000876	0.000801	24
3	Molecular Function	GO:0008514	organic anion transmembrane transporter activity	36/1495	3.36E-06	0.000876	0.000801	36
3	Molecular Function	GO:0015291	secondary active transmembrane transporter activity	41/1495	5.91E-06	0.001049	0.000959	41
3	Molecular Function	GO:0005178	integrin binding	14/1495	6.7E-06	0.001049	0.000959	14
3	Molecular Function	GO:0008509	anion transmembrane transporter activity	47/1495	1.23E-05	0.001599	0.001462	47
3	Molecular Function	GO:0022804	active transmembrane transporter activity	56/1495	1.44E-05	0.001615	0.001477	56
3	Molecular Function	GO:0003688	DNA replication origin binding	9/1495	3.93E-05	0.003848	0.003518	9
3	Molecular Function	GO:0005342	organic acid transmembrane transporter activity	28/1495	4.67E-05	0.003866	0.003534	28
3	Molecular Function	GO:0038024	cargo receptor activity	15/1495	4.94E-05	0.003866	0.003534	15
3	Molecular Function	GO:0046943	carboxylic acid transmembrane transporter activity	27/1495	9.67E-05	0.006883	0.006292	27
3	Molecular Function	GO:0015293	symporter activity	26/1495	0.000218	0.013789	0.012606	26
3	Molecular Function	GO:0005539	glycosaminoglycan binding	20/1495	0.000229	0.013789	0.012606	20
3	Molecular Function	GO:0005044	scavenger receptor activity	12/1495	0.000364	0.020345	0.018599	12
3	Molecular Function	GO:0015106	bicarbonate transmembrane transporter activity	7/1495	0.000669	0.033112	0.03027	7
3	Molecular Function	GO:0005540	hyaluronic acid binding	8/1495	0.000677	0.033112	0.03027	8
3	Molecular Function	GO:0004222	metalloendopeptidase activity	19/1495	0.000991	0.045645	0.041727	19
3	Molecular Function	GO:0015370	solute:sodium symporter activity	17/1495	0.001136	0.048203	0.044066	17
3	Molecular Function	GO:0015081	sodium ion transmembrane transporter activity	25/1495	0.001174	0.048203	0.044066	25
3	Molecular Function	GO:0005518	collagen binding	7/1495	0.001231	0.048203	0.044066	7

Supplementary Table 4 – Results from KEGG pathway enrichment analysis performed across the DEGs across the three different clusters.

cluster	*ID*	*Description*	*GeneRatio*	*BgRatio*	*pvalue*	*p.adjust*	*qvalue*	*Count*
1	dre03050	Proteasome	40/820	57/6867	9.62E-25	1.47E-22	1.3E-22	40
1	dre00830	Retinol metabolism	34/820	91/6867	2.96E-10	2.27E-08	2E-08	34
1	dre00980	Metabolism of xenobiotics by cytochrome P450	28/820	77/6867	2.24E-08	1.14E-06	1.01E-06	28
1	dre04141	Protein processing in endoplasmic reticulum	49/820	202/6867	6.03E-07	2.2E-05	1.93E-05	49
1	dre00860	Porphyrin and chlorophyll metabolism	23/820	65/6867	7.18E-07	2.2E-05	1.93E-05	23
1	dre00053	Ascorbate and aldarate metabolism	19/820	53/6867	5.33E-06	0.000118	0.000104	19
1	dre00982	Drug metabolism - cytochrome P450	23/820	72/6867	5.4E-06	0.000118	0.000104	23
1	dre00040	Pentose and glucuronate interconversions	18/820	55/6867	3.92E-05	0.00075	0.000661	18
1	dre00500	Starch and sucrose metabolism	14/820	38/6867	6.55E-05	0.001114	0.000981	14
1	dre00140	Steroid hormone biosynthesis	22/820	78/6867	7.5E-05	0.001147	0.00101	22
1	dre00052	Galactose metabolism	12/820	35/6867	0.000472	0.006559	0.005776	12
2	dre04744	Phototransduction	21/492	49/6867	3.55E-12	4.97E-10	4.71E-10	21
3	dre04510	Focal adhesion	77/654	278/6867	5.61E-19	7.79E-17	6.79E-17	77
3	dre04512	ECM-receptor interaction	44/654	107/6867	2.2E-18	1.53E-16	1.33E-16	44
3	dre04810	Regulation of actin cytoskeleton	55/654	303/6867	1.46E-06	6.75E-05	5.88E-05	55
3	dre00240	Pyrimidine metabolism	19/654	73/6867	3.48E-05	0.00121	0.001054	19
3	dre04514	Cell adhesion molecules	31/654	183/6867	0.001012	0.028126	0.024494	31

Supplementary Table 5 - List of primers used in the RT-PCRs

Gene Acronym	*NCBI gene accession no*	*Forward*	*Reverse*
mapk14b	NM_001313759.1	CCAAGAGGAACTTCGCAGAC	GATCCAGCAGCTTTCAGGAC
egfra	NM_194424.1	GGACGACCGCATGCATTTAC	AGGCTGAAAGTCTCCCTCCT
ppp3cca	NM_001166628.1	ACAGAATGCCATCCAAGGCT	TCTTCTCGTTGGCAGCGTTA
dusp2	NM_001003451.1	CGCAACGTCAACTGGAACTC	GGTTCTGATTGGAGTCGAGGC
cacnb3b	XM_682310.7	CCTTTACACCTCAGGACCACC	CTGAGGACCCCCTGAGAAAC
rps6ka3b	NM_001083026.2	AGTGAAGGTGTATGATGATGGC	GCCACAGTTTTGGTGATGGT
mrasb	XM_003200999.5	CGAGTGCGAAAGATCCACCA	TAGAGGGTTTGCGCTCACAG
hspb1	NM_001008615.2	GAGTTACGGACGAGCCCTTT	AGCACCCCGTCTTTGGTTTTA
rpl13a	NM_212784.1	TCTGGAGGACTGTAAGAGGTATGC	AGACGCACAATCTTGAGAGCAG
rplp0	NM_131580.2	CTGAACATCTCGCCCTTCTC	TAGCCGATCTGCAGACACAC

Supplementary Fig. 1 – Gap statistic method-based cluster determination

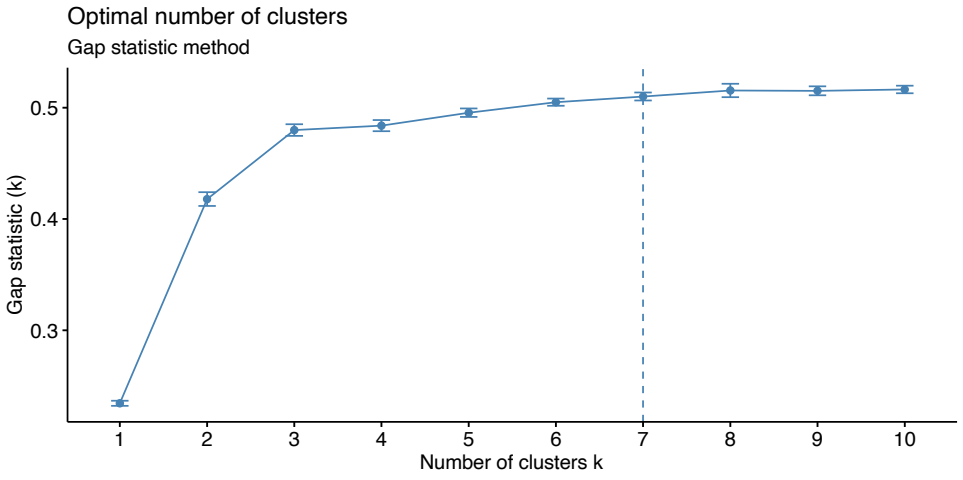

Supplementary Fig. 2 - KEGG pathway maps for key skeletal pathways generated using Pathview showing differentially expressed genes in: A) VD treatment in comparison to the control; B) B10VD treatment in comparison to the control; C) B100VD treatment in comparison to the control; Green colours indicated increased expression and red colour indicates decreased expression compared to control.

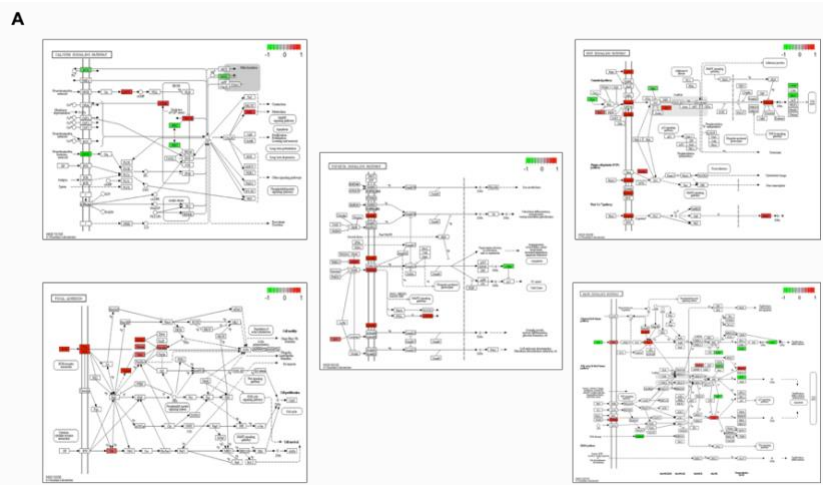
A

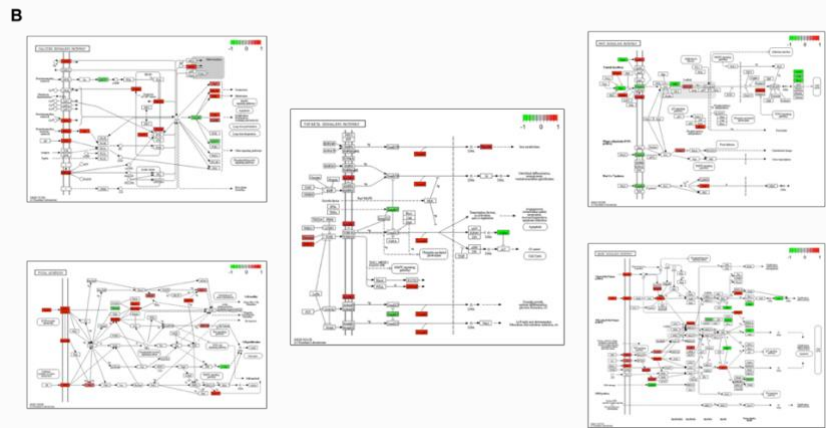
B

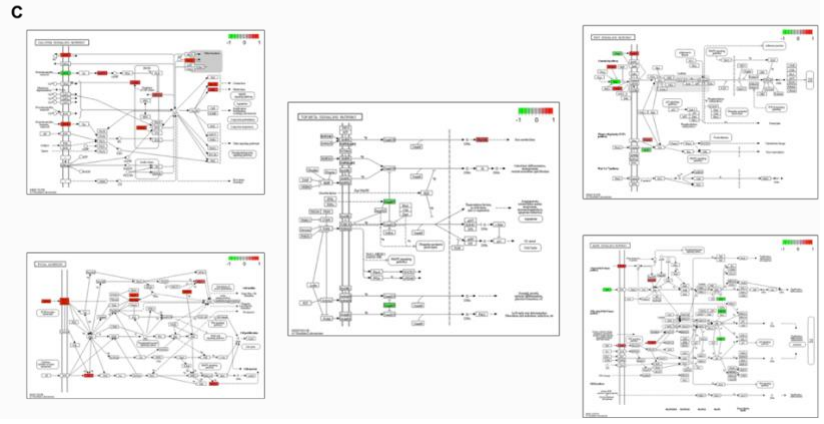
C

Supplementary Fig. 3 - Validation of RNA-Seq based expression patterns using RT-PCR using eight selected genes from MAPK pathway involved in skeletal development and wild-type AB zebrafish 9 dpf larvae RNA.

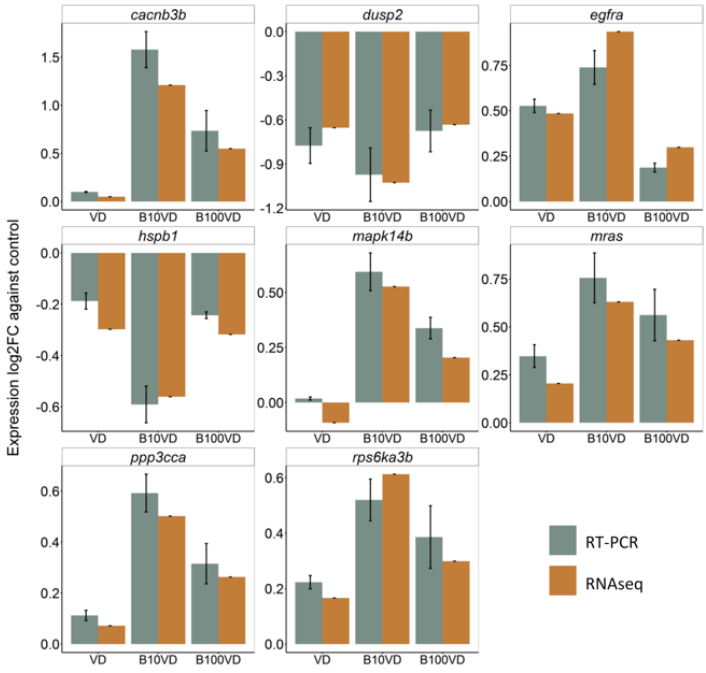

CHAPTER 2: ZEBRAFISH CAUDAL FIN AS A MODEL TO INVESTIGATE THE ROLE OF PROBIOTICS IN BONE REGENERATION

Jerry Maria Sojan[1], Giorgia Gioacchini[1], Elisabetta Giorgini[1], Patrick Orlando[1], Luca Tiano[1], Francesca Maradonna [1,2,*] and Oliana Carnevali [1,2,]

[1]Department of Life and Environmental Sciences, Università Politecnica delle Marche, via Brecce Bianche, 60131 Ancona, Italy;
[2] Biostructures and Biosystems National Institute—Interuniversity Consortium, Viale delle Medaglie d'Oro 305, 00136 Roma, Italy

Abstract

Probiotics are live microorganisms that confer several beneficial effects to the host, including enhancement of bone mineralization, when administered in adequate amounts. However, probiotic action on bone regeneration is not well studied. We therefore studied various effects of probiotic treatment on the caudal fin regeneration of zebrafish using a multidisciplinary approach. Morphological analysis revealed an increased regenerated area with shorter and thicker lepidotrichia segments after probiotic treatment. Fourier transform infrared spectroscopy imaging (FTIRI) analysis highlighted the distribution of phosphate groups in the regenerated fins and probiotic group showed higher amounts of well-crystallized hydroxyapatite. At the midpoint (5 Days Post Amputation (DPA)) of regeneration, probiotics were able to modulate various stages of osteoblast differentiation as confirmed by the upregulation of some key marker genes such as *runx2b, sp7, col10a1a, spp1* and *bglap*, besides suppressing osteoclast activity as evidenced from the downregulation of *ctsk*. Probiotics also caused an enhanced cell cycle by regulating the expression of genes involved in Retinoic acid (*rarga, cyp26b1*) and Wnt/β-catenin (*ctnnb1, ccnd1, axin2, sost*) signaling pathways, and also modulated phosphate homeostasis by increasing the *entpd5a* levels. These findings provide new outlooks for the use of probiotics as a prophylactic treatment in accelerating bone regeneration and improving skeletal health in both aquaculture and biomedical fields.

Key words

Danio rerio, probiotics, fin regeneration, FTIRI, bones

Introduction

Probiotics are beneficial microbes that can exert numerous health benefits to the host including effects on bone metabolism as reported in various animal models such as poultry and rodents (McCabe et al. 2013; Messora et al. 2013; Abdelqader et al. 2013). In addition, in the zebrafish model, few studies have provided clear evidence for the role of probiotics in accelerating skeletogenesis and mineralization (Avella et al. 2012; Maradonna et al. 2013). Probiotic administration basically modulates the host-microbiome (Falcinelli et al. 2015) which is proven to affect bone metabolism through many possible ways including metabolite production (Charles et al. 2015), hormonal interactive pathways, osteo-immunological responses (Jones et al. 2011) or via synthesis of vitamins (Hancock and Viola 2001). Many probiotic species such as *Bacillus subtilis* are known to produce vitamins with osteogenic properties such as vitamin K_2 (Sato et al. 2001).

The zebrafish caudal fin has emerged as a highly successful model system for studying the basic mechanisms of tissue regeneration. Under lab conditions, it has several study advantages such as easy live tracking, fin accessibility and the absence of major amputation-causing detrimental effects on the fish (Sehring and Weidinger 2020). Zebrafish, as a genetic

model for bone regeneration, offers the additional worth to translate the findings into bio-medicinal perspective in human regenerative medicines (Tavares and Lopes 2013; Cavanah et al. 2020). Expression of orthologues for important mammalian osteogenic molecular players like β-catenin has been detected in the regenerating fin in addition to the orthologues for its downstream targets (Schebesta et al. 2006; Stewart et al. 2014; Wehner et al. 2014). Zebrafish regenerate amputated caudal fins by creating lineage-restricted blastemal cells (Tanaka and Reddien 2011; Gemberling et al. 2013). Following partial amputation, the fin with bony rays and soft inter-ray tissue, regenerates very robustly through establishment of blastema, which are populations of lineage-restricted mesenchymal progenitor cells formed via de-differentiation of mature stump cells (Knopf et al. 2011; Tu and Johnson 2011). The pool of de-differentiated osteoblasts in the blastema proliferates, re-differentiates exclusively into non-proliferating osteoblasts and deposit bone matrix, during the progression of regeneration (Knopf et al. 2011). These differentiation steps are distinguished by various osteoblast stage markers such as RUNX family transcription factor 2b (*runx2b*) for osteoblast progenitors towards the distal part of proximal blastema, followed by sp7 transcription factor (*sp7* or osterix) positive osteoblasts and finally bone gamma-carboxyglutamate (gla) protein (*bglap* or osteocalcin) positive mature osteoblasts to the proximal end (Brown et al. 2009). Re-expression of *sp7* and the decrease in *bglap* are found to be the indicators of de-differentiation of cells in blastema during regeneration (Sousa et al. 2011). Several other signaling pathways including RA (Retinoic Acid) (Blum and Begemann 2015) and Wnt/β-

catenin (Kawakami et al. 2006; Stoick-Cooper et al. 2007) have been identified to be essential for fin regeneration.

Based on the evidence from literature, the aim of the present study was to investigate the potential effects of the administration of probiotics on the caudal fin regeneration process. Fish were subject to pre-treatment with probiotics for two weeks before amputation in order to favor colonization of beneficial bacteria in the gut of treated fish and generate desired positive outcomes as previously confirmed with another probiotics species *Lactobacillus rhamnosus* (Schneider et al. 2014). Using a multidisciplinary approach, ranging from analysis of morphological parameters related to fin growth, to evaluation of expression of representative genes involved in ossification followed by quantification of phosphates and other macromolecules, we aimed at gaining evidence on the role of probiotic bacteria in bone regeneration, which could aid in the development of regenerative medicine protocols. In this regard, the possible probiotic action on bone through either increased osteoblast activity or decreased osteoclast activity are both explored in the current study using specific marker genes of osteoblasts and osteoclasts, such as secreted protein, acidic, cysteine-rich (*sparc* or osteonectin) and cathepsin K (*ctsk)*, respectively (Schmidt et al. 2019).

Materials and Methods

Probiotics administration and caudal fin regeneration

Three months old wild-type (AB) zebrafish with a mean weight of 100 ± 7 mg and a mean total length of 20 ± 2 mm, maintained at 28.0°C, pH 7.0, photoperiod 12:12 light: dark, NO_2 < 0.01 mg/L and NO_3 < 10 mg/L, were collected from the fish facility and divided into a control group (C) (n=24) and a probiotic-treated group (P) (n=24). The trial was conducted using a commercial probiotic mixture, Bactosafe H (Bernaqua), which consists of a mix of 5 different bacteria- *Bacillus subtilis, Bacillus licheniformis, Bacillus coagulans and Lactobacillus acidophilus* plus the yeast *Saccharomyces cerevisiae*. Within the probiotic mix, *B.subtilis*, the strain of our interest is known to produce vitamin K_2 or menaquinones, a group of pro-osteogenic vitamins (Sato et al. 2001). C and P groups were fed a commercial diet (Zebrafeed, Sparos, Portugal) at 3% body weight twice a day and only P group received a dietary supplementation with the probiotics at 10^6 CFU/ml by water administration. A 14-day pre-conditioning treatment with the probiotics was administered to the P group to enhance gut colonization. At the end of pre-conditioning, all fish were anesthetized using 0.1 g/l MS-222 (Sigma-Aldrich, USA) and the caudal fins were amputated 1–2 segments anterior to the bifurcation of the second bifurcated lepidotrichia (Cardeira et al. 2016). Amputated fins (0 DPA) were stored at -80°C for RNA extraction. After amputation, each fish was maintained separately, to have biological replicates at a density of 1 fish per 200 mL in glass containers filled with water from the rearing

system. Fish were allowed to regenerate at 33.0 (±1) °C in a water table to accelerate regeneration as previously reported (Boominathan and Ferreira 2012). During the regeneration, fish were fed with the same quantity of commercial feed and administered with the same P concentration, as in the 14 days of pre-conditioning. Individual regeneration process was tracked (n=7 per group) by taking images of the same fish at pre-amputation, post amputation and 1, 5 and 10 DPA. Regenerated caudal fin samples were collected at 5 DPA, representing the mid time point of regeneration and at 10 DPA as the last point of regeneration for RNA extraction and FTIRI analysis. Fins for RNA extraction (n=9 per group per time point) were stored at -80°C and for FTIRI analysis, the fins (n=3 per group per time point) were fixed in 4% paraformaldehyde (PFA) for 12 hours and then washed twice with PBS and then stored in PBS at +4°C.

Microscopy and Image analysis

Images were taken using a stereomicroscope (Leica, Germany) during pre-amputation, post amputation and 1, 5 and 10-DPA for tracking the progress of regeneration in C and P fins (n=7 per group). Fish were anaesthetized before the imaging using MS-222 at 0.6mM and could recover in fresh water with aeration after the imaging. Fin images were analyzed using ImageJ (version 2.1.0/1.53c) (Wayne Rasband, National Institutes of Health, USA). Morphological studies were performed by measuring some of the previously described parameters: REG (regenerated area), PED (peduncle width), STU (stump width), RAY (fin ray

width) and SEG (segment length) and two ratios REG/STU and REG/PED were also assessed (Cardeira et al. 2016). ImageJ macros used to analyze the images was scripted specifically for the regeneration parameters of caudal fin.

FTIRI analysis

FTIRI analysis was performed by a Bruker INVENIO interferometer coupled with a Hyperion 3000 IR-Vis microscope and equipped with a FPA detector (Bruker Optics, Ettlingen, Germany). Fin samples from C and P experimental groups (n=3 per group per time point) were deposited onto CaF2 optical windows. By using a 15x condenser objective, on each fin sample, specific areas were selected. The two regions assayed after amputation in the fourth bifurcated fin ray of the dorsal fin lobe are described as: proximal- corresponding to the first distal bifurcation and distal- corresponding to the last segment joint preceding the actinotrichia (see Fig 1.a). On these areas, the IR maps were acquired in transmission mode in the 4000-800 cm^{-1} spectral range. Each map was 164 x 164-micron side, and it was the result of 4096 pixel/spectra (256 scans), with a spatial resolution of 2.56 x 2.56 micron. Raw IR maps were corrected for carbon dioxide and water vapour and then vector normalized in the full spectral range (Atmospheric Compensation and Vector Normalization routines, OPUS 7.5 software package). False colour images representing the topographical distribution of phosphate groups were obtained by integrating all IR maps in the 1185-980 cm^{-1} spectral range (assigned to the stretching vibrations of phosphate groups). An arbitrary color scale

was used where white/light pink colours represent the zones with the highest absorption of phosphates whereas black/dark blue denote the zones with the lowest absorption of phosphates.

On each IR map, a submap (ca. 300 spectra/pixel) was extracted in correspondence with the bone at the two analyzed regions. The average spectrum and average ± standard deviation spectra were calculated, and curve was fitted in the 1800-900 cm^{-1} spectral range. The number and the position (expressed in wavenumbers, cm^{-1}) of the underlying bands were identified by second derivative minima analysis and fixed during procedure with Gaussian functions (GRAMS/AI 9.1, Galactic Industries, Inc., Salem, New Hampshire). The integrated areas (A) of the underlying bands were used to calculate the following band area ratios: A_{1655}/A_{1024} (Protein to Phosphate ratio), A_{1240}/A_{1024} (Collagen to Phosphate ratio), and A_{1024}/A_{1090} (Well crystallized HA to Poorly crystallized HA ratio).

RNA extraction and quantification

Pools of 3 fins were made to have 3 replicates per group for each time point. Total RNA was extracted from amputated caudal fin (0 DPA) and regenerated caudal fins (5 and 10 DPA) using RNAeasy Microkit (Qiagen, Italy). It was then eluted in 20 µL of molecular grade nuclease free water. Final RNA concentrations were determined using a nanophotometer. Total RNA was treated with DNase (10 IU at 37°C for 10 min, MBI Fermentas). One microgram of total RNA was used for cDNA synthesis

using iScript cDNA Synthesis Kit (Bio-Rad, Italy) and stored at -20°C until further use as described previously (Maradonna et al. 2014).

RT-PCR

RT-PCRs were performed in C and P fins (n=3 for both C and P, at each time point) with SYBR green (Bio-Rad, Milan, Italy) in a CFX thermal cycler (Bio-Rad, Milan, Italy) as described before (Carnevali et al. 2017). For each reaction, the mix contained: 1 µL of cNDA (1:10) + 5 µL iQ SYBR Green Supermix + 3.8 µL miliQ water + 0.1 µL forward primer + 0.1 µL reverse primer. The thermal profile for all reactions was 3 min at 95°C followed by 45 cycles of 20 s at 95°C, 20 s at 60°C and 20 s at 72°C. Dissociation curve analysis showed a single peak in all the cases. Ribosomal protein L13 (*rpl13*) and ribosomal protein, large, P0 (*rplp0*) were used as the housekeeping genes (validated previously by Forner-Piquer et al. 2020) to standardize the results by eliminating variation in mRNA and cDNA quantity. No amplification product was observed in negative controls and primer-dimer formation was never seen. Data was analyzed using iQ5 Optical System version 2.1 (Bio-Rad) including Genex Macro iQ5 Conversion and Genex Macro iQ5 files. Modification of gene expression between the experimental groups is reported as relative mRNA abundance (Arbitrary Units). Primers used at a final concentration of 10 pmol/ml. All primer sequences used in the study are listed in Supplementary Table S1.

Statistical analysis

Data of all groups were normally distributed as assessed using Shapiro-Wilk's test ($p > 0.05$), and there was homogeneity of variances, as assessed using Levene's test for equality of variances ($p > 0.05$). T-test was used to analyze the morphological regeneration parameter differences between the groups. Two-way analysis of variance (ANOVA) followed by Tukey's post hoc tests were applied to IR data and RT-PCR analysis to compare differences among experimental groups. All the tests were performed using R version 3.6.1 (R Core Team 2019) and plots were generated using ggplot2 3.2.1. Statistical significance was set at $p<0.05$ for all the tests.

Results

Morphometric analysis

To get a preliminary confirmation on whether the probiotic treatment can influence the regeneration process, few morphometric parameters of regenerating fins were analyzed. The regenerative performance of the control (C) and probiotic-treated (P) experimental groups was evaluated at 5 days post amputation (DPA) and 10 DPA by analyzing the fin ray width (RAY), calculated by averaging the width of the second bifurcated fin ray in the dorsal lobe at the first formed segment joint after amputation; segment length (SEG), calculated by averaging the length of the first formed segment after amputation in the second bifurcated fin ray in the

dorsal lobe; REG/STU, which is the ratio between regenerated area (REG) and stump width (STU), and lastly REG/PED, which is the ratio between REG and peduncle width (PED). The complete course of regeneration was tracked for both C (n=7) and P (n=7) fish every day at the same time. In Fig.1a, images of representative C and P fins from the same tracked fish for pre-amputation, post-amputation and 1, 5 and 10 DPA are reported. A representative image of a regenerating fin with RAY, SEG, REG, PED and STU measurements is shown (Fig.1b). A specific equation was modified from a previous study to calculate % regeneration by using the ratios REG/STU and Initial amputated area/STU (Petrie et al. 2014). The modified equation (1) is presented below:

$$\%\ Regeneration = \frac{\frac{REG}{STU}\ at\ 10\ DPA\ *\ 100}{\text{Initial amputated area/STU at 0 DPA}}$$

This parameter was 8-9% higher in P fins than in C group at 10 DPA (Fig.1c)

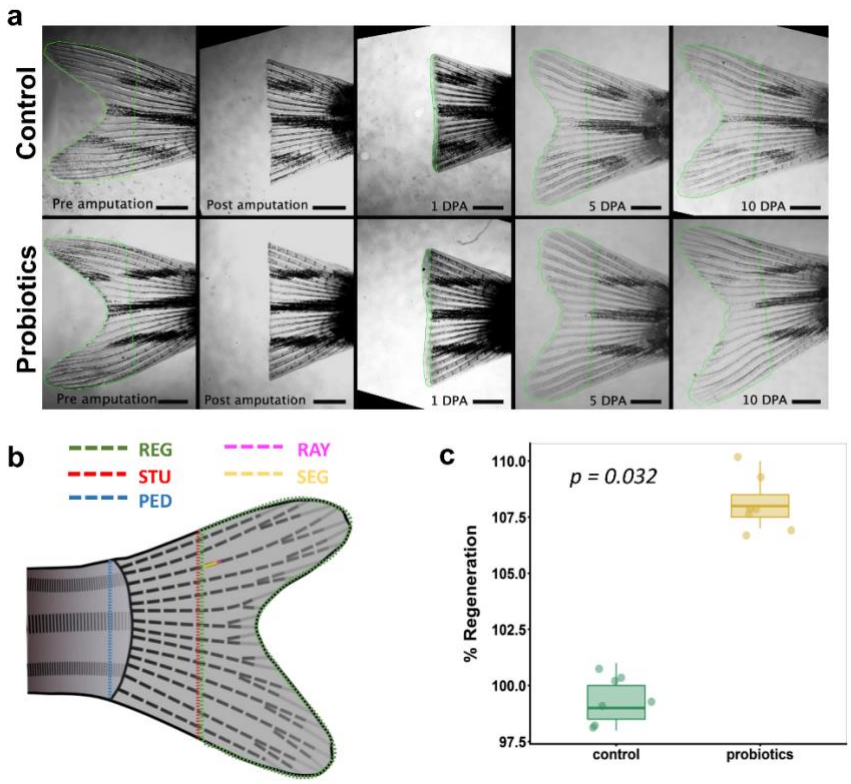

Fig. 1. **(a)** Representative photographs showing the fins before amputation, post amputation and at 1, 5 and 10 DPA in control (C) (n=7) and probiotic-treated (P) (n=7) groups (Scale bar = 1,000 µm); **(b)** Picture of a representative amputated fin, showing the regenerated area (REG, green tracing), the stump width or width of the amputation plane (STU, red dotted line), the peduncle width (PED, blue dotted line), the fin ray width (RAY, pink line), and the segment length (SEG, yellow line); **(c)** Statistical analysis of regeneration rate (expressed as %) between C and P groups calculated at 10 DPA with respect to non-amputated fin of the same individual fish. T-test was used after conversion of % values to respective decimal values and statistical significance was set at $p<0.05$.

REG/STU ratio was significantly higher in P fins than C fins at both 5 DPA (*p=0.013*) and 10 DPA (*p=0.012*). No significant difference was observed between the groups for REG/PED ratio even though it displayed the same

pattern as that of REG/STU (Fig.2a and 2b). Stump width (STU) was used to normalize the inter-specimen variability arising due to variable size and alignment of fin; therefore REG/STU is considered as the best standard to normalize the regenerated area (Cardeira et al. 2016). Hence, the lack of significant difference for the ratio REG/PED between P and C could be due to a non-significant increase in PED linked to a possible inter-specimen variability in body size. Another interesting observation was that P group had thicker fin rays (Mean RAY; Fig.2c) and shorter segments (Mean SEG; Fig. 2d) with respect to C at 10 DPA. No significant differences in body weight and total length were observed between C and P fish during the trial. These results suggest that P treatment accelerated the regeneration process and the larger regenerated P fins had shorter but thicker segments.

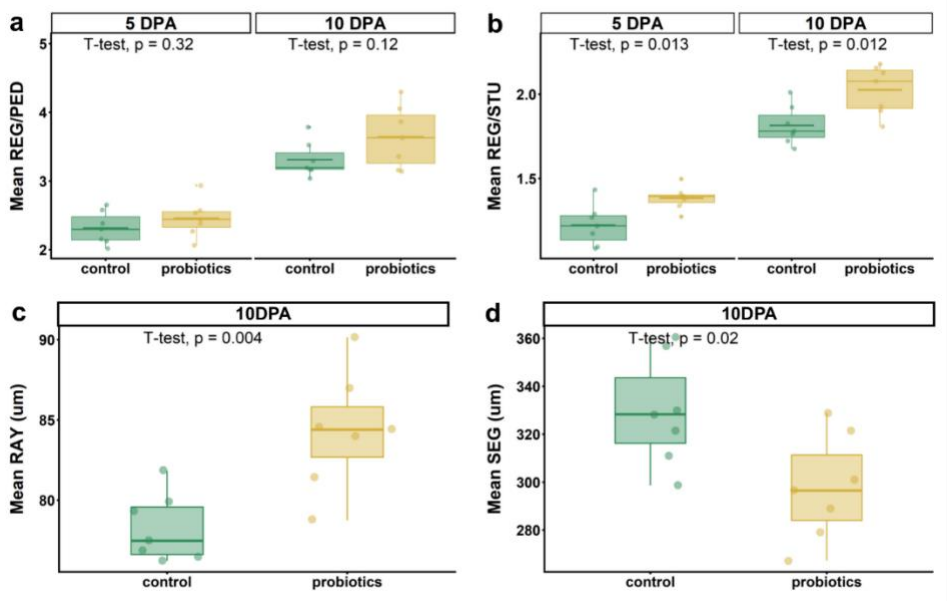

Fig. 2. Various morphometric parameters used to analyze the regenerated areas in C and P fins (n=7 per group per time point) are as follows: **(a)** Regenerated area (REG)/Peduncle width (PED) ratio; **(b)** Regenerated area (REG)/Stump width (STU) ratio; **(c)** Mean fin ray width (RAY) and **(d)** Mean segment length (SEG). T-test was used to analyze the regeneration parameter differences among the groups and statistical significance was set at $p<0.05$.

FTIRI (Fourier Transform Infrared Spectroscopic Imaging) analysis

FTIRI is a suitable tool to study bone composition, particularly the mineral and organic matrix content by calculating relative concentrations using peak intensity ratios of various chemical components (Taylor and Donnelly 2020). In Fig.3a, a representative image of the fin showing the two regions of FTIRI analysis, proximal and distal, on the fourth bifurcated fin ray in the dorsal fin lobe, is presented. In Fig. 3b and 3c, the hyperspectral imaging analysis of C and P amputated fins are reported at two time points of regeneration, 5 and 10 DPA. As expected, a non-homogeneous distribution was observed within the mapped areas and the distribution of phosphates clearly matched with bone structures in both the regions analysed. In the actinotrichia (see black dotted square in the distal maps; Fig.3b and 3c), a lower phosphate level was detected indicating a lower mineralization of this zone.

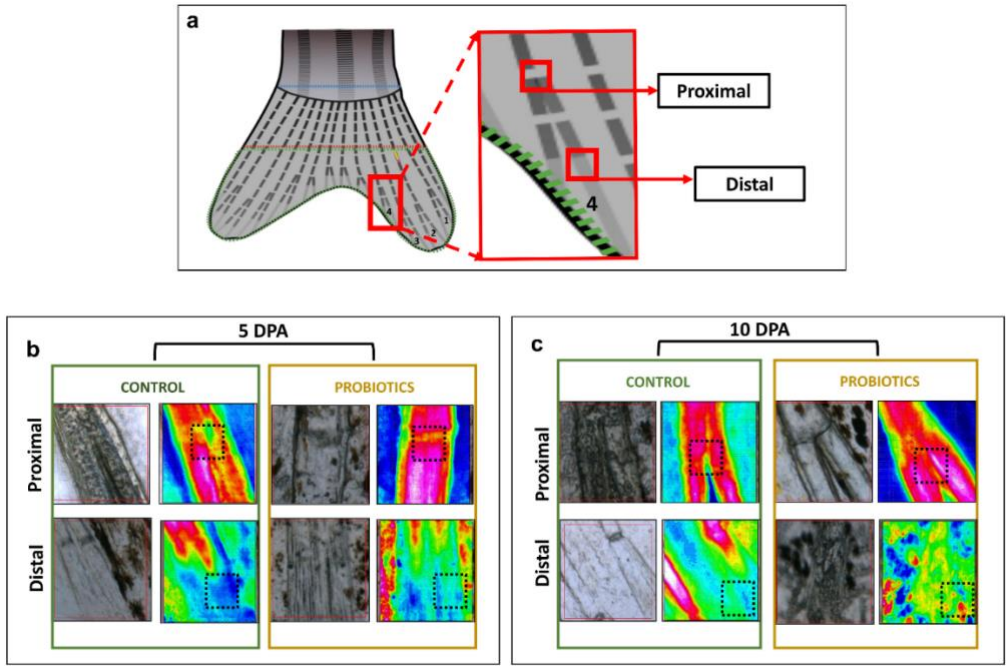

Fig. 3. **(a)** Representative picture showing the areas analyzed by FTIRI in the fourth bifurcated fin ray of the dorsal lobe of the regenerating fin. The two regions assayed after amputation were: proximal-corresponding to the first formed bifurcation after amputation and distal-corresponding to the last segment joint preceding the actinotrichia; **(b-c)** Representative microphotograph (left) and false color images (right) representing the topographical distribution of phosphate groups in the proximal and distal areas of the regenerated fin from C and P fins (n=3) at **(b)** 5 DPA and **(c)** 10 DPA time points. The same color scale (0-3) was used for all false color images: white/light pink colors indicate the areas with the highest amount of phosphates, red/orange/yellow indicate the areas with an intermediate amount and black/dark blue shows the areas with the lowest amount of phosphates. The black dotted squares indicate the region where spectra were extracted for the curve fitting analysis.

To evaluate the biochemical composition and degree of mineralization of bone in the two analyzed regions, the following band area ratios were

calculated: A_{1655}/A_{1024} (ratio between the area of the Amide I band of proteins centered at 1655 cm^{-1} and the area of the phosphate band centered at 1024 cm^{-1}; Fig.4a); A_{1240}/A_{1024} (ratio between the area of the collagen band centered at 1240 cm^{-1} and the area of the phosphate band centered at 1024 cm^{-1}; Fig.4b) and A_{1024}/A_{1090} (ratio between the area of the phosphate bands centered at 1024 cm^{-1} and 1090 cm^{-1}, ascribable respectively to well and poorly crystallized hydroxyapatites (HA); Fig.4c). The A_{1655}/A_{1024} and A_{1240}/A_{1024} ratios are usually related to the relative amount of the organic component (proteins and collagen) with respect to the inorganic/mineral one (bone HA) (Kontopoulos et al. 2018). These two ratios showed a decrease in the proximal area with respect to distal one. Moreover, at 5 DPA, in the distal region, statistically significant lower values were found for these ratios in P group compared to C ($p<0.05$), indicative of a higher amount of the mineral component in the P fins. Conversely, no statistically significant difference was observed for these two ratios at 10 DPA between C and P groups in both analyzed regions ($p>0.05$) (Fig. 4a and 4b). The A_{1024}/A_{1090} ratio is referred to the mineral maturity of bone, representing the transformation of HA from a nanocrystalline form (represented by the peak at 1090 cm-1) to a well-crystallized stoichiometric one (represented by the peak at 1024 cm-1) (Farlay et al. 2010). In the distal region, statistically significant higher values were found in P samples at both 5 DPA and 10 DPA with respect to C. In the proximal region, the ratio remained same between C and P samples ($p>0.05$) (Fig. 4c). Altogether, these results suggest an increase of mineral content and mineral maturity in the regenerated fins due to P treatment.

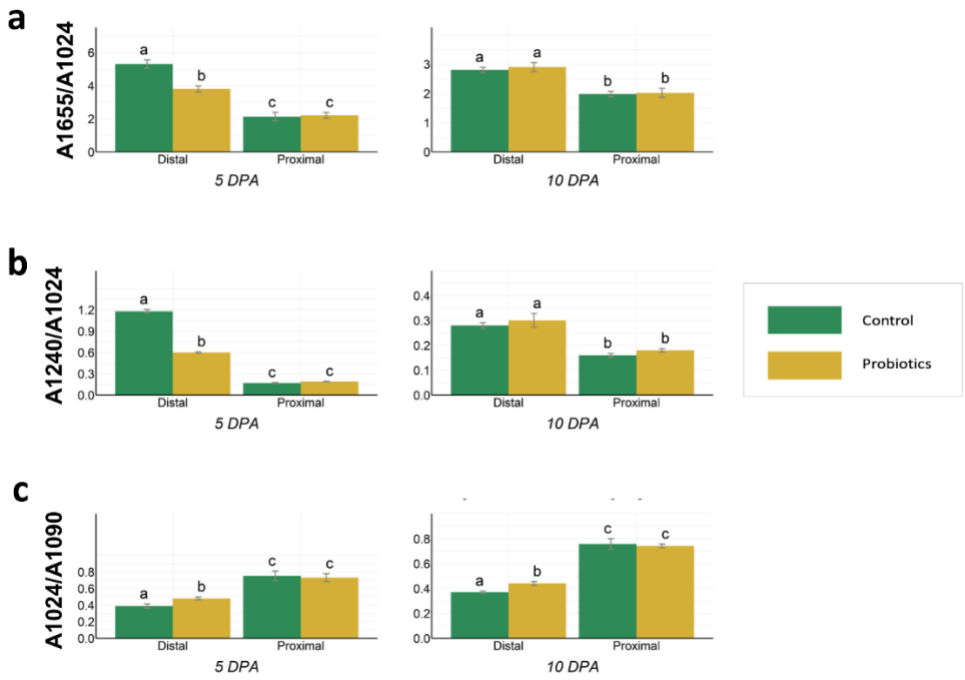

Fig. 4. Biochemical composition and bone mineralization assessed from FTIRI analysis (a) A1655/A1024, (b) A1240/A1024 and (c) A1024/A1090 band area ratios calculated on proximal and distal of the fourth bifurcated fin ray in the dorsal lobe of the regenerating fin C (n=3) and P (n=3) fish at 5 DPA and 10 DPA. Data are presented as mean ± S.D. Different letters over the histograms indicate statistically significant difference among groups. Two-way ANOVA and Tukey's multiple comparison test are used, and statistical significance was set at $p<0.05$.

Marker genes analysis by RT-PCR

Expression of early, intermediate, and late markers of osteoblast differentiation

Fin regeneration is a process where cells ranging from pre-osteoblast to mature osteoblast are involved. Therefore, it is essential to consider that probiotic treatment can act differently on various osteoblast stages. In

our study, mRNA levels of early and intermediate markers of osteoblast differentiation such as *runx2b, sp7* and collagen 10a1a (*col10a1a)* increased during the regeneration at 5 DPA with respected to 0 DPA in both C and P. Both *runx2b* and *col10a1a* mRNA showed a significantly higher expression in P group. *Col10a1a* was highly expressed in the P fins at 0 and 5 DPA. The late marker *bglap* was significantly higher in both groups when nearing the completion of the regeneration process (10 DPA) but a significant difference between P and C was observed particularly at 5 DPA. The expression of mature osteoblast specific marker secreted phosphoprotein 1 (*spp1* or osteopontin) mRNA was significantly increased in treated fins at 5 DPA (Fig.5). The results indicate that P treatment can boost osteoblast advancement from early differentiation to extracellular matrix mineralization.

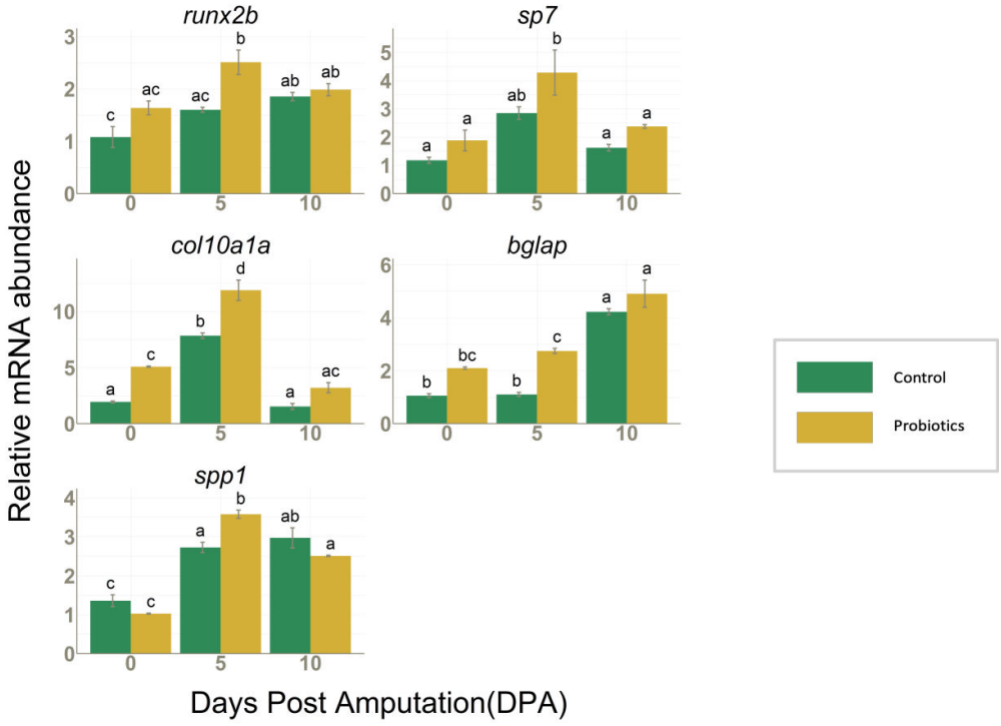

Fig. 5. *runx2b, sp7, col10a1a, bglap* and *spp1*mRNA values normalized against *rplp0* and *rpl13* in fins collected from C (n = 3) and P (n = 3) groups at 0, 5 and 10 DPA. Data are presented as mean±S.D. Different letters over the histograms indicate statistically significant difference among groups. Two-way ANOVA and Tukey's multiple comparison test are used, and statistical significance was set at $p<0.05$.

Expression of genes associated with the regulation of RA signaling and phosphate homeostasis during regeneration

Previous studies reported the RA signaling involvement in the blastemal cell proliferation, a key process in fin regeneration which is also regulated by Wnt/ β-catenin signaling (Blum and Begemann 2012). At 5 DPA, the RA degrading enzyme, codified by cytochrome P450, family 26, subfamily b,

polypeptide 1 (*cyp26b1*) mRNA, was significantly higher in P group and was associated to a decreased expression of retinoic acid receptor gamma-a (*rarga*) with respect to C. *Rarga* mRNA expression was also found to be higher in the initial amputated fins (0 DPA) of P treated group than in C. A general increase in the expression of ectonucleoside triphosphate diphosphohydrolase 5a (*entpd5a*), which is involved in the homeostasis of phosphates (Huitema et al. 2012), was observed from 0 DPA to 5 DPA in both C and P groups. At 10 DPA, the *entpd5a* gene expression declined and only at this time point, the mRNA level in P group was significantly higher with respect to the control (Fig.6). The expression changes observed across these genes indicate that probiotic treatment can modulate the RA signaling pathway and also regulate phosphate homeostasis during regeneration.

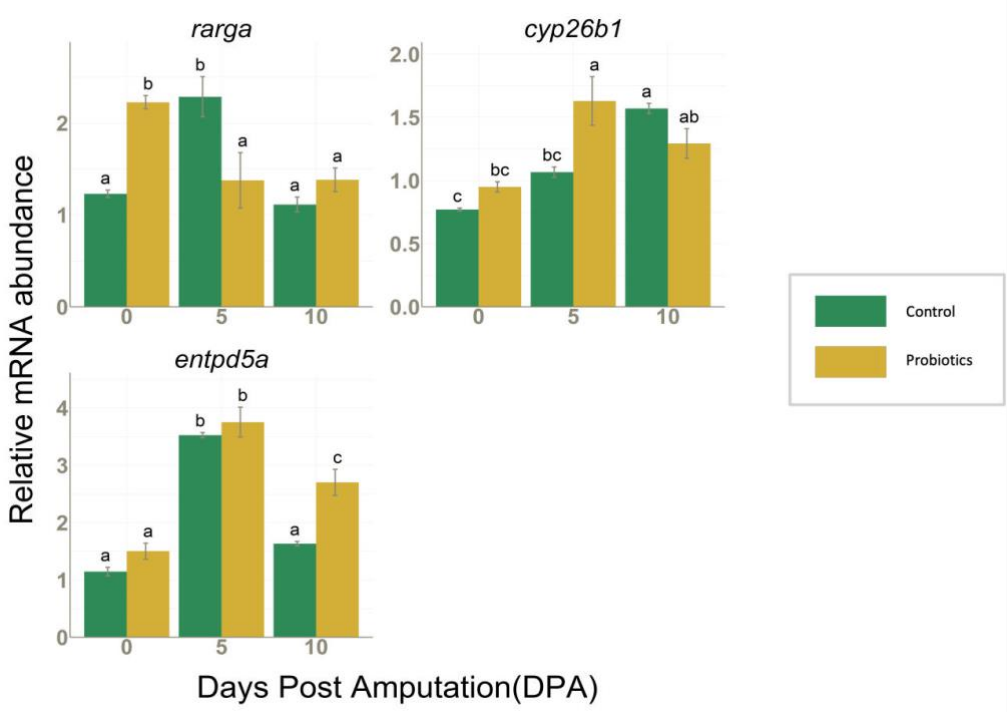

Fig. 6. *rarga, cyp26b1* and *entpd5a* mRNA values normalized against *rplp0* and *rpl13* in fins collected from C (n = 3) and P (n = 3) groups at 0, 5 and 10 DPA. Data are presented as mean±S.D. Different letters over histograms indicate statistically significant difference among groups. Two-way ANOVA and Tukey's multiple comparison test are used, and statistical significance was set at $p<0.05$.

Expression of genes associated with the regulation of Wnt/β-catenin signaling during regeneration

Wnt/β-catenin mediated signaling plays an important role in blastema cell proliferation (Wehner et al. 2014) and analyzing the expression of some key genes involved in this pathway can provide essential information on the effect of probiotic treatment on early differentiation and proliferation during fin regeneration. The catenin (cadherin-associated protein), beta 1 (*ctnnb1*) was significantly higher in P group at both 5DPA and 10 DPA whereas its universal transcriptional target gene *axin2,* which is also a negative feedback regulator in the canonical Wnt signaling, was significantly higher in P fins at 10 DPA. *Sparc,* representing the gene encoding for sparc protein which are known to prevent the degradation of β-catenin, was also significantly higher at 5 DPA in both groups with respect to 0 DPA but without any significant difference between C and P groups. The negative regulator of Wnt signaling, sclerostin (*sost*) and the osteoclast marker gene *ctsk* were significantly higher in C at 5 DPA whereas at 10 DPA, *sost* was higher in P group than in C. Another downstream transcriptional target gene of β-catenin is cyclin D1(*ccnd1*) which is a marker of cell proliferation, and its mRNA was upregulated in P fins with respect to C at 5 DPA (Fig.7). Altogether, these

results provide evidence that the increase in β-catenin transcription activity drives the expression of several downstream regulator genes which are also involved in fin regeneration process. Thus, Wnt/β-catenin signaling pathway was found to be modulated by P treatment leading to an increased cell proliferation, thereby accelerating the regeneration process, and led to an increased regenerated area as evidenced by the morphological results.

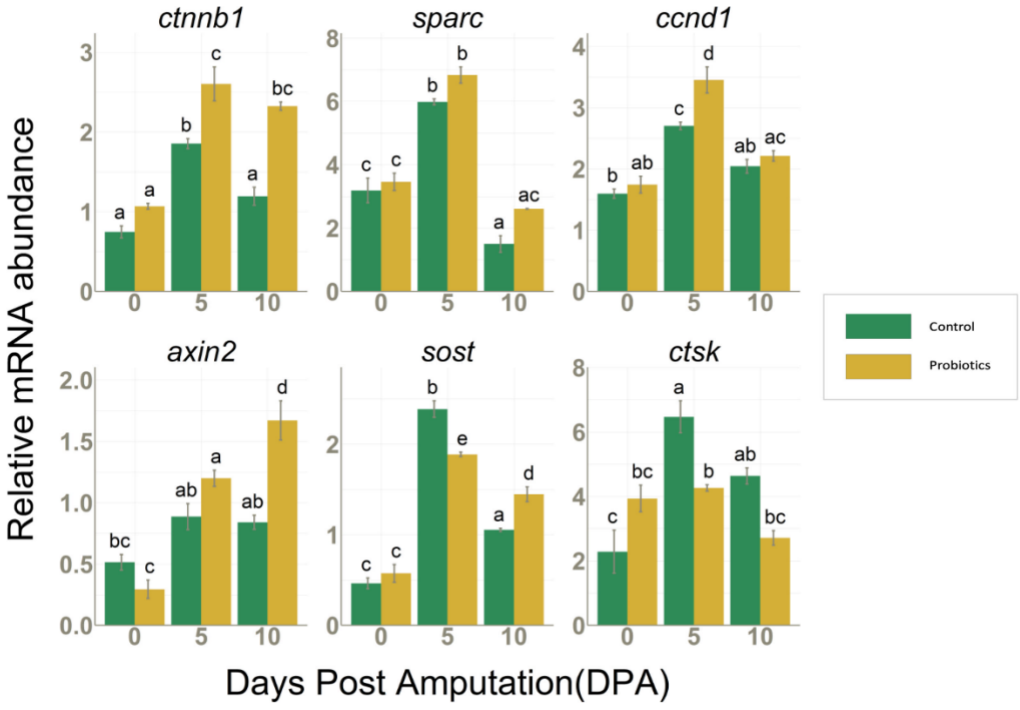

Fig. 7. *ctnnb1, sparc, ccnd1, axin2, sost* and *ctsk* mRNA values normalized against *rplp0* and *rpl13* in fins collected from C (n = 3) and P (n = 3) groups at 0, 5 and 10 DPA. Data are presented as mean±S.D. Different letters over histograms indicate statistically significant difference among groups. Two-way ANOVA and Tukey's multiple comparison test are used, and statistical significance was set at $p<0.05$.

Discussion

Using the established zebrafish fin regeneration model, we evaluated the modulation of regeneration in zebrafish caudal fin by probiotic treatment. Since treated fish showed an increased area of regenerated fin compared to the initial amputated area, but not changes of length, weight and peduncle width, the increased regenerated area can be conclusively linked to the effect of P treatment on regeneration and not to fish growth or fin alignment. In addition, C fins switched back to isometric growth once the amputated area is regenerated whereas the P fins maintained the allometric growth pattern of regeneration even after reaching the original amputated area. This led to a significantly increased outgrowth of fin area with shorter but thicker segments of fin rays than in C. Previous studies have described a similar outgrowth during fin regeneration by inhibiting the protein phosphatase calcineurin and also by an integrated effect of calcineurin inhibition and bioelectric signaling like potassium channels (Kujawski et al. 2014; Daane et al. 2018). Thus, we can speculate that P treatment could play a role in the activation of the above mentioned signaling causing a delay to the conventional switching back of the fin growth to isometric pattern.

Calcineurin-inhibition related fin outgrowth was previously reported to be also associated with the promotion of RA signaling (Kujawski et al. 2014; McMillan et al. 2018). In the initial amputated fins (0 DPA) which received the probiotics preconditioning for 14 days, interestingly an upregulation in the RA receptor, *rarga* as well as *col10a1a* was observed.

Indeed, the positive effects of P exposure on RA pathway were previously described in probiotic treated zebrafish favoring an enhanced calcification of vertebrae (Avella et al. 2012). This verifies the activity of probiotics in regulating genes with a role in the bone calcification besides modulating regeneration process. During the regeneration, rarga, which is expressed during the blastema formation, (Poss et al. 2000) increased in C fins accordance with the established molecular regulation of regeneration process but a decrease was noted in P fins at 5 DPA. Considering that cyp26b1-mediated RA degradation plays an important role in promoting the re-differentiation of the pre-osteoblasts to the non-proliferative osteoblasts which is an essential requirement for the formation of new bones (Blum and Begemann 2015), the higher RA levels in C fins respect to P fins, suggests the promotion of the proliferation of the pre-osteoblasts and less re-differentiation whereas P fins are at a relatively more advanced stage of regeneration involving re-differentiation. Furthermore, higher levels in the completely regenerated P fin suggests a higher phosphate concentration, since *entpd5a* is a direct regulator of phosphate homeostasis (Huitema et al. 2012). Nevertheless, at both time point analyzed, FTIR results show that in the distal zone, P fins present higher amount of phosphates as crystallized HA. Since this part of fin, according to the physiology of bone regeneration is the newly formed, these results let us speculate that P treatment accelerate the transformation of phosphates from amorphous to a more organized form thereby boosting the bone maturation process (Mahamid et al. 2008).

The significantly higher expression of early and intermediate osteoblast differentiation stage markers such as *runx2b, sp7, ctnnb1* and *col10a1* in

P fins at the mid-point of regeneration (5 DPA) confirms the role of probiotics in modulating the regeneration process at various stages of osteoblast de-differentiation and proliferation. *Runx2b* is a pre-osteoblast stage marker, which expression is found in the blastema during the de-differentiation of osteoblasts in the early stages of regeneration (Brown et al. 2009) and *sp7* acts hierarchically downstream to the *runx2b* in the differentiation pathway. *Runx2b* also regulates the expression of other important marker genes of various stages of osteoblast differentiation like *col10a1, spp1, bglap* and hence is considered as a key regulator. *Col10a1a*, which acts further downstream to *sp7*, marks the intermediate stages of skeletogenesis (bone matrix deposition stages) (Niu et al. 2017). It is expressed in early osteoblasts and chondrocytes during intramembranous and perichondral ossification of fish bone (Padhi et al. 2004; Avaron et al. 2006; Smith et al. 2006; Renn and Winkler 2010) and our results showed its strong downregulation towards the final stage of regeneration (10 DPA). The sequential activation of early markers points to the same conclusion that P treatment significantly promotes the early stages of osteoblast differentiation processes after fin amputation.

Regarding mineralization, established marker genes of later stages of osteoblast differentiation and mineralization such as *bglap* (osteocalcin) and *spp1* (osteopontin), both acting downstream and regulated by sp7 and runx2, were evaluated (Brown et al. 2009; Sousa et al. 2011; Chen et al. 2019). In our study, both were upregulated during the regeneration process with a significantly higher expression in the treated fins at 5 DPA. These results are strongly supported by the higher crystallized HA levels

found in P fins, providing clear evidence of the effect of P on the mineralization stage as well.

Ctnnb1 (β-catenin) transcript was significantly higher in P fins during regeneration suggesting an activation of Wnt/β-catenin signaling by P. From the expression of two downstream target genes of β-catenin, cell proliferation marker *ccnd1* and negative regulator of β-catenin signaling *axin2,* we could observe that the increased β-catenin signaling at 5 DPA was suppressed towards 10 DPA in both the groups. This confirms that the measured levels of genes involved in β-catenin signaling are well related with the different regeneration stages, being higher during proliferative phase and lower during the later stages of differentiation/maturation. Elevated expression of *sparc* at 5 DPA further confirms the previous reports of the involvement of this pathway in the fin regeneration as *sparc* codes for a matrix protein which is known to increase osteoblastogenesis through enhancing β-catenin mediated signaling and preventing the degradation of β-catenin (Nie and Sage 2009). *Sparc* was earlier found to be enriched at 4 DPA regenerates (Schmidt et al. 2019) which further agrees with our observation of significantly higher amount of *sparc* at 5 DPA although no differences were observed between groups. Also, the higher expression of *sost* at the midpoint of regeneration is an additional indicator for the modulation of Wnt/β-catenin signaling during blastema formation, since sclerostin is found to be expressed in the blastema during early fin regeneration in zebrafish (Wehner et al. 2014). In our study, P caused the downregulation of sost mRNA levels in P fins resulting in agreement with a previous trial

on zebrafish larvae where sost levels were regulated by probiotic treatment (Maradonna et al. 2013). Wnt/β-catenin signaling is also involved in the suppression of osteoclast activity (Holmen et al. 2005; Spencer et al. 2006). This evidence is strongly supported by our results showing P ability to downregulate ctsk, the osteoclast marker gene (Schmidt et al. 2019).

The overall results suggest that P treatment positively affects the caudal fin regeneration process. At molecular level, P mainly affected the regeneration at midpoint (summarized in Supplementary Fig.S2) and the major pathways involved are Wnt/β-catenin and RA signaling pathways. The treatment induced an increase in the regenerated area, affected the morphology of the fins, and enhanced well-crystallized HA content. FTIRI can be proposed as a suitable tool to investigate on regeneration process. Since probiotics can have their regulatory effects through multiple ways, studies investigating the exact mode of action of probiotics on regeneration at cellular level could be done in the future as a follow-up of these positive results. Since this probiotic mix contains major vitamin K_2 producers such as *Bacillus subtilis* and vitamin K2 is a crucial class of vitamins known to partake in the positive regulation of bone development (Villa et al. 2017), further studies can be done focusing on probiotic ability to produce vitamin K_2. In brief, the significant impact of probiotic treatment on the regeneration process was revealed using zebrafish caudal fin as a model. This observation could be useful in bone regenerative medicine studies where probiotics can be a potential prophylactic candidate to improve bone health.

References

Abdelqader A, Irshaid R, Al-Fataftah A-R (2013) Effects of dietary probiotic inclusion on performance, eggshell quality, cecal microflora composition, and tibia traits of laying hens in the late phase of production. Trop Anim Health Prod 45:1017–1024. https://doi.org/10.1007/s11250-012-0326-7

Avaron F, Hoffman L, Guay D, Akimenko MA (2006) Characterization of two new zebrafish members of the hedgehog family: Atypical expression of a zebrafish indian hedgehog gene in skeletal elements of both endochondral and dermal origins. Developmental Dynamics 235:478–489. https://doi.org/10.1002/dvdy.20619

Avella MA, Place A, Du S-J, et al (2012) Lactobacillus rhamnosus Accelerates Zebrafish Backbone Calcification and Gonadal Differentiation through Effects on the GnRH and IGF Systems. PLOS ONE 7:e45572. https://doi.org/10.1371/journal.pone.0045572

Blum N, Begemann G (2015) Retinoic acid signaling spatially restricts osteoblasts and controls ray-interray organization during zebrafish fin regeneration. Development 142:2888–2893. https://doi.org/10.1242/dev.120212

Blum N, Begemann G (2012) Retinoic acid signaling controls the formation, proliferation and survival of the blastema during adult zebrafish fin regeneration. Development 139:107–116. https://doi.org/10.1242/dev.065391

Boominathan VP, Ferreira TL (2012) Factors Promoting Increased Rate of Tissue Regeneration: The Zebrafish Fin as a Tool for Examining Tissue Engineering Design Concepts. Zebrafish 9:207–219. https://doi.org/10.1089/zeb.2012.0741

Brown AM, Fisher S, Iovine MK (2009) Osteoblast maturation occurs in overlapping proximal-distal compartments during fin regeneration in zebrafish. Developmental Dynamics 238:2922–2928. https://doi.org/10.1002/dvdy.22114

Cardeira J, Gavaia PJ, Fernández I, et al (2016) Quantitative assessment of the regenerative and mineralogenic performances of the zebrafish caudal fin. Scientific Reports 6:39191. https://doi.org/10.1038/srep39191

Carnevali O, Notarstefano V, Olivotto I, et al (2017) Dietary administration of EDC mixtures: A focus on fish lipid metabolism. Aquatic Toxicology 185:95–104. https://doi.org/10.1016/j.aquatox.2017.02.007

Cavanah P, Itou J, Rusman Y, et al (2020) A nontoxic fungal natural product modulates fin regeneration in zebrafish larvae upstream of FGF-WNT developmental signaling. Dev Dyn. https://doi.org/10.1002/dvdy.244

Charles JF, Ermann J, Aliprantis AO (2015) The intestinal microbiome and skeletal fitness: Connecting bugs and bones. Clinical Immunology 159:163–169. https://doi.org/10.1016/j.clim.2015.03.019

Chen Z, Song Z, Yang J, et al (2019) Sp7/osterix positively regulates dlx2b and bglap to affect tooth development and bone mineralization in zebrafish larvae. J Biosci 44:127. https://doi.org/10.1007/s12038-019-9948-5

Daane JM, Lanni J, Rothenberg I, et al (2018) Bioelectric-calcineurin signaling module regulates allometric growth and size of the zebrafish fin. Scientific Reports 8:1–9. https://doi.org/10.1038/s41598-018-28450-6

Falcinelli S, Picchietti S, Rodiles A, et al (2015) Lactobacillus rhamnosus lowers zebrafish lipid content by changing gut microbiota and host transcription of genes involved in lipid metabolism. Scientific Reports 5:9336. https://doi.org/10.1038/srep09336

Farlay D, Panczer G, Rey C, et al (2010) Mineral maturity and crystallinity index are distinct characteristics of bone mineral. J Bone Miner Metab 28:433–445. https://doi.org/10.1007/s00774-009-0146-7

Forner-Piquer I, Beato S, Piscitelli F, et al (2020) Effects of BPA on zebrafish gonads: Focus on the endocannabinoid system. Environ Pollut 264:114710. https://doi.org/10.1016/j.envpol.2020.114710

Gemberling M, Bailey TJ, Hyde DR, Poss KD (2013) The zebrafish as a model for complex tissue regeneration. Trends in Genetics 29:611–620. https://doi.org/10.1016/j.tig.2013.07.003

Hancock R, Viola R (2001) The use of micro-organisms for L-ascorbic acid production: Current status and future perspectives. Applied microbiology and biotechnology 56:567–76. https://doi.org/10.1007/s002530100723

Holmen SL, Zylstra CR, Mukherjee A, et al (2005) Essential Role of β-Catenin in Postnatal Bone Acquisition. J Biol Chem 280:21162–21168. https://doi.org/10.1074/jbc.M501900200

Huitema LFA, Apschner A, Logister I, et al (2012) Entpd5 is essential for skeletal mineralization and regulates phosphate homeostasis in zebrafish. PNAS 109:21372–21377. https://doi.org/10.1073/pnas.1214231110

Jones D, Glimcher LH, Aliprantis AO (2011) Osteoimmunology at the nexus of arthritis, osteoporosis, cancer, and infection. J Clin Invest 121:2534–2542. https://doi.org/10.1172/JCI46262

Kawakami Y, Esteban CR, Raya M, et al (2006) Wnt/β-catenin signaling regulates vertebrate limb regeneration. Genes Dev 20:3232–3237. https://doi.org/10.1101/gad.1475106

Knopf F, Hammond C, Chekuru A, et al (2011) Bone Regenerates via Dedifferentiation of Osteoblasts in the Zebrafish Fin. Developmental Cell 20:713–724. https://doi.org/10.1016/j.devcel.2011.04.014

Kontopoulos I, Presslee S, Penkman K, Collins MJ (2018) Preparation of bone powder for FTIR-ATR analysis: The particle size effect. Vibrational Spectroscopy 99:167–177. https://doi.org/10.1016/j.vibspec.2018.09.004

Kujawski S, Lin W, Kitte F, et al (2014) Calcineurin Regulates Coordinated Outgrowth of Zebrafish Regenerating Fins. Developmental Cell 28:573–587. https://doi.org/10.1016/j.devcel.2014.01.019

Mahamid J, Sharir A, Addadi L, Weiner S (2008) Amorphous calcium phosphate is a major component of the forming fin bones of zebrafish: Indications for an amorphous precursor phase. PNAS 105:12748–12753. https://doi.org/10.1073/pnas.0803354105

Maradonna F, Gioacchini G, Falcinelli S, et al (2013) Probiotic Supplementation Promotes Calcification in Danio rerio Larvae: A Molecular Study. PLoS One 8:. https://doi.org/10.1371/journal.pone.0083155

Maradonna F, Nozzi V, Dalla Valle L, et al (2014) A developmental hepatotoxicity study of dietary bisphenol A in Sparus aurata juveniles. Comparative Biochemistry and Physiology Part C: Toxicology & Pharmacology 166:1–13. https://doi.org/10.1016/j.cbpc.2014.06.004

McCabe LR, Irwin R, Schaefer L, Britton RA (2013) Probiotic use decreases intestinal inflammation and increases bone density in healthy male but not female mice. Journal of Cellular Physiology 228:1793–1798. https://doi.org/10.1002/jcp.24340

McMillan SC, Zhang J, Phan H-E, et al (2018) A regulatory pathway involving retinoic acid and calcineurin demarcates and maintains joint cells and osteoblasts in regenerating fin. Development 145:dev161158. https://doi.org/10.1242/dev.161158

Messora MR, Oliveira LFF, Foureaux RC, et al (2013) Probiotic Therapy Reduces Periodontal Tissue Destruction and Improves the Intestinal Morphology in Rats With Ligature-Induced Periodontitis. Journal of Periodontology 84:1818–1826. https://doi.org/10.1902/jop.2013.120644

Nie J, Sage EH (2009) SPARC Inhibits Adipogenesis by Its Enhancement of β-Catenin Signaling*. Journal of Biological Chemistry 284:1279–1290. https://doi.org/10.1074/jbc.M808285200

Niu P, Zhong Z, Wang M, et al (2017) Zinc finger transcription factor Sp7/Osterix acts on bone formation and regulates col10a1a expression in zebrafish. Science Bulletin 62:174–184. https://doi.org/10.1016/j.scib.2017.01.009

Padhi BK, Joly L, Tellis P, et al (2004) Screen for genes differentially expressed during regeneration of the zebrafish caudal fin. Developmental Dynamics 231:527–541. https://doi.org/10.1002/dvdy.20153

Petrie TA, Strand NS, Tsung-Yang C, et al (2014) Macrophages modulate adult zebrafish tail fin regeneration. Development 141:2581–2591. https://doi.org/10.1242/dev.098459

Poss KD, Shen J, Keating MT (2000) Induction of lef1 during zebrafish fin regeneration. Developmental Dynamics 219:282–286. https://doi.org/10.1002/1097-0177(2000)9999:9999<::AID-DVDY1045>3.0.CO;2-C

R Core Team (2019) R: A language and environment for statistical computing. Vienna, Austria: R Foundation for Statistical Computing; 2011.

Renn J, Winkler C (2010) Characterization of collagen type 10a1 and osteocalcin in early and mature osteoblasts during skeleton formation in medaka. Journal of Applied Ichthyology 26:196–201. https://doi.org/10.1111/j.1439-0426.2010.01404.x

Sato T, Yamada Y, Ohtani Y, et al (2001) Production of Menaquinone (vitamin K2)-7 by Bacillus subtilis. Journal of Bioscience and Bioengineering 91:16–20. https://doi.org/10.1016/S1389-1723(01)80104-3

Schebesta M, Lien C-L, Engel FB, Keating MT (2006) Transcriptional Profiling of Caudal Fin Regeneration in Zebrafish. In: The Scientific World Journal. https://www.hindawi.com/journals/tswj/2006/947207/abs/. Accessed 2 Dec 2019

Schmidt JR, Geurtzen K, von Bergen M, et al (2019) Glucocorticoid Treatment Leads to Aberrant Ion and Macromolecular Transport in Regenerating Zebrafish Fins. Front Endocrinol 10:. https://doi.org/10.3389/fendo.2019.00674

Schneider ACR, Machado ABMP, de Assis AM, et al (2014) Effects of Lactobacillus Rhamnosus GG on Hepatic and Serum Lipid Profiles in Zebrafish Exposed to Ethanol. Zebrafish 11:371–378. https://doi.org/10.1089/zeb.2013.0968

Sehring IM, Weidinger G (2020) Recent advancements in understanding fin regeneration in zebrafish. WIREs Developmental Biology 9:e367. https://doi.org/10.1002/wdev.367

Smith A, Avaron F, Guay D, et al (2006) Inhibition of BMP signaling during zebrafish fin regeneration disrupts fin growth and scleroblast differentiation and function. Developmental Biology 299:438–454. https://doi.org/10.1016/j.ydbio.2006.08.016

Sousa S, Afonso N, Bensimon-Brito A, et al (2011) Differentiated skeletal cells contribute to blastema formation during zebrafish fin regeneration. Development 138:3897–3905. https://doi.org/10.1242/dev.064717

Spencer GJ, Utting JC, Etheridge SL, et al (2006) Wnt signalling in osteoblasts regulates expression of the receptor activator of NFκB ligand and inhibits osteoclastogenesis in vitro. J Cell Sci 119:1283–1296. https://doi.org/10.1242/jcs.02883

Stewart S, Gomez AW, Armstrong BE, et al (2014) Sequential and Opposing Activities of Wnt and BMP Coordinate Zebrafish Bone Regeneration. Cell Reports 6:482–498. https://doi.org/10.1016/j.celrep.2014.01.010

Stoick-Cooper CL, Weidinger G, Riehle KJ, et al (2007) Distinct Wnt signaling pathways have opposing roles in appendage regeneration. Development 134:479–489. https://doi.org/10.1242/dev.001123

Tanaka EM, Reddien PW (2011) The Cellular Basis for Animal Regeneration. Developmental Cell 21:172–185. https://doi.org/10.1016/j.devcel.2011.06.016

Tavares B, Lopes SS (2013) The importance of Zebrafish in biomedical research. Acta medica portuguesa. https://doi.org/10.20344/amp.4628

Taylor EA, Donnelly E (2020) Raman and Fourier transform infrared imaging for characterization of bone material properties. Bone 139:115490. https://doi.org/10.1016/j.bone.2020.115490

Tu S, Johnson SL (2011) Fate Restriction in the Growing and Regenerating Zebrafish Fin. Developmental Cell 20:725–732. https://doi.org/10.1016/j.devcel.2011.04.013

Villa JKD, Diaz MAN, Pizziolo VR, Martino HSD (2017) Effect of vitamin K in bone metabolism and vascular calcification: A review of mechanisms of action and evidences. Critical Reviews in Food Science and Nutrition 57:3959–3970. https://doi.org/10.1080/10408398.2016.1211616

Wehner D, Cizelsky W, Vasudevaro MD, et al (2014) Wnt/β-Catenin Signaling Defines Organizing Centers that Orchestrate Growth and Differentiation of the Regenerating Zebrafish Caudal Fin. Cell Reports 6:467–481. https://doi.org/10.1016/j.celrep.2013.12.036

Supplementary Material

Supplementary Table S1. List of primers used in the RT-PCR

Gene Acronym	NCBI gene accession no	Forward	Reverse
col10a1a	NM_001083827.1	CCCATCCACATCACATCAAA	GCGTGCATTTCTCAGAACAA
runx2b	NM_212862.2	GTGGCCACTTACCACAGAGC	TCGGAGAGTCATCCAGCTT
spp1	NM_001002308.1	GAGCCTACACAGACCACGCCAACAG	GGTAGCCCAAACTGTCTCCCCG
cyp26b1	NM_212666.1	GCTGTCAACCAGAACATTCCC	GGTTCTGATTGGAGTCGAGGC
rarga	NM_131339.1	ATTCCGCCAGAGAGCTATGA	TAGGCCCAGGTCTAGCTGAA
ctnnb1	XM_005157831.4	CGCACACATTCACTCTCAGC	TGGGTAGCCATGATTTTCTCA
entpd5a	XM_679770.8	ATATGCCTGAAAAGGGTGGA	TACTTCTTTGACCTCATTCAGCAG
ctsk	NM_001017778.1	GATGAGGCTTGGGAGAGCTGGAA	TTTCGGTTACGAGCCATCAGGAC
sparc	NM_001001942.1	TGCTTAGGCTGAAACTCAAGATGAG	GCATCAATGGAAGACGTCCTTAGAT
sp7	NM_212863.2	AACCCAAGCCCGTCCCGACA	CCGTACACCTTCCCGCAGCC
bglap	NM_001083857.3	GCCTGATGACTGTGTGTCTGAGCG	AGTTCCAGCCCTCTTCTGTCTCAT
sost	XM_021480342.1	ACAATGAATCGGGCGAAGAA	GTTCTGAGGCTCCATAAGTCC
ccnd1	NM_131025	CCAACTTCCTCTCGCAAGTC	TGGTCTCTGTGGAGATGTGC

rplp0	NM_131580.2	CTGAACATCTCGCCCTTCTC	TAGCCGATCTGCAGACACAC
axin2	NM_131561	ACCCTCGGACACTTCAAGGAA	TCACTGGCCCTTTTGAAGAAGTAT
rpl13a	NM_212784.1	TCTGGAGGACTGTAAGAGGTATGC	AGACGCACAATCTTGAGAGCAG

Supplementary Fig. S2. Schematic diagram summarizing all the upregulated and downregulated genes in the probiotic treated fins at 5 DPA and 10 DPA.

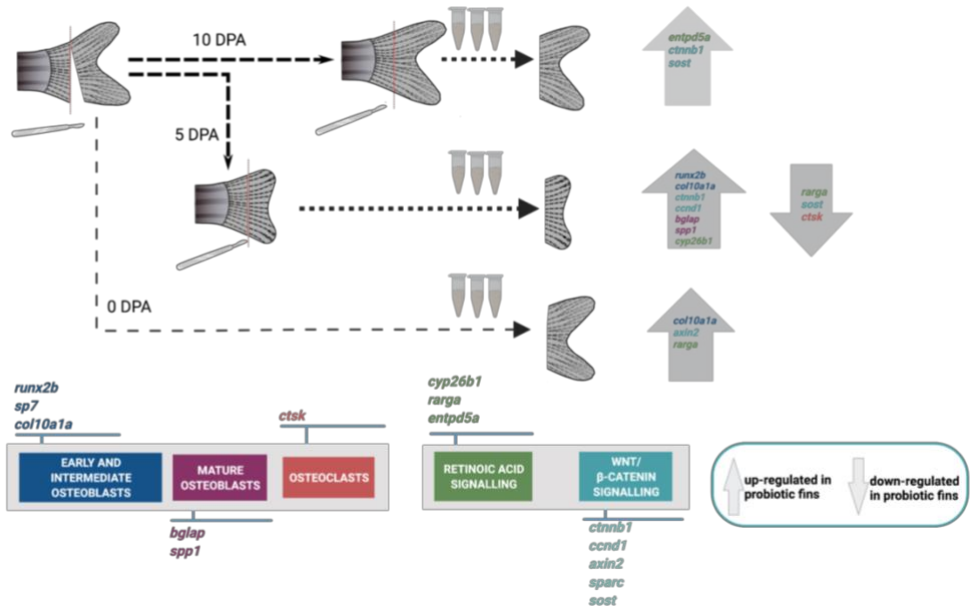

CHAPTER 3: PROBIOTICS ENHANCE BONE GROWTH AND RESCUE BMP INHIBITION: NEW TRANSGENIC ZEBRAFISH LINES TO STUDY BONE HEALTH

Jerry Maria Sojan[1], Ratish Raman[2], Marc Muller[2*], Oliana Carnevali[1], Jörg Renn[2]

[1]Department of Life and Environmental Sciences, Università Politecnica delle Marche, via Brecce Bianche, 60131 Ancona, Italy; j.m.sojan@pm.univpm.it (J.M.S.); o.carnevali@staff.univpm.it
[2]Laboratoire d'Organogenèse et Régénération, GIGA-R 1, University of Liège, Belgium; ratish.raman@uliege.be; m.muller@uliege.be; joergrenn@yahoo.de

Abstract

Zebrafish larvae, especially gene specific mutants and transgenic lines, are increasingly used to study vertebrate skeletal development, in particular human pathologies such as osteoporosis, osteopetrosis and osteoarthritis. Probiotics have been recognized in recent years as a prophylactic treatment for various bone health issues in humans. Here we present two new zebrafish transgenic lines containing the coding sequences for fluorescent proteins inserted into the endogenous genes for *sp7* and *col10a1a*. These larvae display fluorescence in developing osteoblasts and in the bone extracellular matrix (mineralized or non-mineralized), respectively. Furthermore, we use these transgenic lines to show that exposure to two different probiotics, *Bacillus subtilis* and *Lactococcus lactis*, leads to an increase in osteoblast formation and bone matrix growth and mineralization. Gene expression analysis revealed the effect of probiotics, particularly *Bacillus subtilis*, in modulating several skeletal development genes such as *runx2, sp7, spp1* and *col10a1a*, further supporting their ability to improve bone health. In comparison, *Bacillus subtilis* was the most potent probiotic and was able to significantly reverse the inhibition of bone matrix formation when larvae were exposed to a BMP inhibitor (LDN212854).

Keywords

Danio rerio; zebrafish; transgenic lines; bone matrix, probiotics; mineralization; BMP inhibitors, bone growth

Introduction

Probiotics are beneficial microbes that contribute health benefits to hosts when provided in suitable quantities (Hill et al. 2014). Bone growth and health are proven to be affected by probiotics since they rely on the gut mainly for the absorption of minerals and vitamins (McCabe et al. 2015). The novel term “osteomicrobiology” was coined for microbiota and bone health research (Ohlsson and Sjögren 2018). There are many reports on the positive effects of various probiotic bacteria strains on bone health in various animal models and human studies (Cosme-Silva et al. 2020; Rizzoli and Biver 2020; Gholami et al. 2020; Jia et al. 2021; Huidrom et al. 2021). Lactobacillus and Bifidobacterium strains were proven to be preventive against ovariectomized (OVX)-mediated bone loss in mice and rat models (Chiang and Pan 2011; Britton et al. 2014; Ohlsson et al. 2014; Parvaneh et al. 2015). *Bacillus subtilis* supplementation was able to decrease bone loss due to periodontitis in rats (Foureaux et al. 2014). In humans, there are multiple reports on the prevention of bone loss by various probiotics in post-menopausal women (Nilsson et al. 2018; Takimoto et al. 2018). In zebrafish, Maradonna and others showed an increase in calcification after probiotic administration (Maradonna et al. 2013).

There are various possible modes of action for probiotics to influence bones. Probiotics are known to influence immune systems and inflammatory conditions were previously reported to be associated with osteoporosis (Terashima and Takayanagi 2018). Some Lactobacillus strains are shown to increase the vitamin D receptor (VDR) expression in

epithelial cells of human and mouse (Wu et al. 2015). Probiotics, through their possible interaction with estrogens, inhibit bone loss linked to steroid deficiency as was previously demonstrated in studies with mice (Li et al. 2016). The gut microbiome and its interaction with dietary calcium was also previously shown as another way to affect bone health, since calcium is essential for maintenance of bone health by decreasing bone resorption (Chaplin et al. 2016). Some beneficial strains are also an important source of vitamin K2, which acts as a cofactor in carboxylation of the matrix protein BGLAP (osteocalcin), thereby supporting bone mineralization (Booth 2009; Atkins et al. 2009; Castaneda et al. 2020).

The zebrafish (*Danio rerio*) is increasingly used as a model species for skeletal development, as basic regulatory networks and metabolic pathways are largely conserved between teleost fish and mammals. A number of mutants have been described in zebrafish that mimic human pathologies such as osteoporosis, osteopetrosis, osteoarthritis (Lleras-Forero et al. 2020), thus illustrating how homologous genes play similar roles in both species. In addition, zebrafish larvae can advantageously replace cell culture to test pro- or anti-osteogenic properties of specific compounds because they are better suited to reproduce the complex regulatory interactions taking place between different tissues. Although developing larvae may be fixed at different stages to undergo specific staining for various tissues and features (cartilage, bone matrix, etc), the optical clarity of zebrafish embryos and larvae allow for continuous observation of live animals. To that purpose, several transgenic lines are available that express a fluorescent protein (GFP, mCherry, citrine) under

the control of a synthetic or natural transcription regulatory region (Bergen et al. 2019; Sun et al. 2020). Specific transgenic lines reveal *in vivo* the activation of canonical BMP, Hedgehog, or Wnt pathways (Schiavone et al. 2014; Lovely et al. 2016; Jacobs and Huang 2019; Alhazmi et al. 2021; Westphal et al. 2022), all involved in bone development. Others use cell-specific promoter regions or recombinant Bacterial Artificial Chromosomes (BACs) to target the expression of the reporter protein to chondrocytes, early or late osteoblasts, or osteoclasts (Ando et al. 2017).

Even with all the therapeutic effects of probiotics or gut microbiota on bones, there is still a lack of clear understanding on how they are able to influence bone homeostasis (Cooney et al. 2021). Here, we present two newly generated transgenic zebrafish lines that were obtained by inserting the reporter protein coding sequence directly into the coding region of two endogenous genes. These new transgenic lines express the GFP protein under transcriptional control of the endogenous regulatory regions for i) the osteoblast marker *sp7* (Sp7 transcription factor) gene and ii) its downstream target gene *col10a1a*, encoding the osteoblast- and hypertrophic chondrocyte-specific collagen type X alpha 1a chain. We describe the expression pattern of their reporter gene and apply them for testing the efficacy of osteogenic strains of probiotics. We analysed the modulatory effects of two probiotics, *Bacillus subtilis* and *Lactococcus lactis*, in osteoblast differentiation and early skeletal growth of zebrafish using the two lines. Furthermore, we checked the ability of the probiotics to counter-act the deleterious effect of BMP inhibitor treatment on the bone matrix. The results presented here emphasize yet again that

zebrafish, particularly transgenic lines, are an ideal model for live studies on skeletogenesis, including the impact of probiotics.

Materials and Methods

Generation of transgenic lines using the CRISPR/Cas9 method

To generate fluorescent reporter lines where the expression of the fluorescent protein GFP would be driven by endogenous bone-specific promoters, we engineered a plasmid containing the coding sequence for GFP to contain a specific sequence (Mbait) for which we also engineered a corresponding gRNA (gRNA1, see Fig. 1 a, (Kimura et al. 2014). By co-injecting the bait gRNA1, the specific col10a1a or sp7 gRNA, the plasmid, and the *Cas9* nuclease into fertilized eggs as previously described (Kimura et al. 2014) we generate double-stranded breaks within the endogenous gene, and we linearize the plasmid with the GFP cDNA. Injected individuals are then screened for fluorescence in bone structures, indicating that the GFP cDNA was inserted in frame and in the correct orientation into the endogenous target gene (Fig. 1a). Positive individuals are grown, tested for germ line transmission into the F1 generation and the exact sequence at the insertion point is determined.

Sequence of guide RNAs:

- MBait: gRNA1:GGCTGCTGCGGTTCCAGAGG
- *col10a1a*: gRNA2:GGAGTAAGGCTGGTACTGCG
- *sp7*: gRNA3:GGCTCATTCAGCTCAAGCGG

Sequence of primers for insertion site sequencing:

- GFP-rev: GGTCTTGTAGTTGCCGTCGT
- *col10a1a*-for: TTGTCAAGAAGGTGATGAAGG
- *sp7*-for: AAAAGGCCTACAGCATGACTTC

Morpholino injection

One to two cell-stage embryos were injected as previously described (Wiweger et al. 2012) with 3 ng of antisense morpholino oligonucleotides (MO, Gene Tools Inc.) complementary to the translational start site of the entpd5 gene. Morpholinos were diluted in Danieau buffer and Tetramethylrhodamine dextran (Invitrogen, Belgium) was added at 0.5% to verify proper injection of the embryos by fluorescence stereomicroscopy. Standard control morpholino (MOcon) was injected at the same concentrations. Although no increase of cell death was observed in the morphants, parallel co-injection experiments with 4.5 ng of a morpholino directed against p53 (Larbuisson et al. 2013) were performed to ensure inhibition of MO-induced unspecific cell death (Robu et al. 2007). The effects of morpholino injection were tested on at least 100 individuals, performed in at least three independent experiments.

Sequence of the morpholino oligonucleotides:

- MOentpd5 AATTTAGTCTTACCTTTTCAGGC
- MOcon random sequence
- MOp53 GACCTCCTCTCCACTAAACTACGAT

RNA extraction and quantification

Total RNA was extracted from larvae (n= 8) using RNAeasy Microkit ((Qiagen, Germany). It was then eluted in 20 µL of molecular grade nuclease free water. Final RNA concentrations were determined using a nanophotometer (Implen, Germany). Total RNA was treated with DNase according to the manufacturer's instructions (Sigma-Aldrich, USA). 1 mg of total RNA was used for cDNA synthesis using iScript cDNA Synthesis Kit (Bio-Rad, USA) and stored at -20°C until further use as described previously (Maradonna et al. 2014).

RT- PCR

RT-PCR reactions were performed with the SYBR green method in a CFX thermal cycler (Bio-Rad, Italy) in triplicate as described before (Carnevali et al. 2017). Primers were used at a final concentration of 10 pmol/ml. For each reaction, the mix contained: 1 µL of cNDA (1:10) + 5 µL iQ SYBR Green Supermix + 3.8 µL miliQ water + 0.1 µL forward primer + 0.1 µL reverse primer. The thermal profile for all reactions was 3 min at 95°C followed by 45 cycles of 20 s at 95°C, 20 s at 60°C and 20 s at 72°C. Dissociation curve analysis showed a single peak in all the cases. Ribosomal protein L13 (*rpl13*) and ribosomal protein, large, P0 (*rplp0*) were used as the housekeeping genes (validated previously by Forner-Piquer et al. 2020) to standardize the results by eliminating variation in mRNA and cDNA quantity. No amplification product was observed in negative controls and primer-dimer formation was never seen. Data was

analyzed using iQ5 Optical System version 2.1 (Bio-Rad) including Genex Macro iQ5 Conversion and Genex Macro iQ5 files. Modification of gene expression between the experimental groups is reported as relative mRNA abundance (Arbitrary Units). All primer sequences used in the study are listed in Table 1.

Table.1. List of primers used in the RT-PCR

Gene Acronym	NCBI gene accession no	Forward	Reverse
col10a1a	NM_001083827.1	CCCATCCACATCACATCAAA	GCGTGCATTTCTCAGAACAA
runx2b	NM_212862.2	GTGGCCACTTACCACAGAGC	TCGGAGAGTCATCCAGCTT
spp1	NM_001002308.1	GAGCCTACACAGACCACGCCAACAG	GGTAGCCCAAACTGTCTCCCCG
cyp26b1	NM_212666.1	GCTGTCAACCAGAACATTCCC	GGTTCTGATTGGAGTCGAGGC
sp7	NM_212863.2	AACCCAAGCCCGTCCCGACA	CCGTACACCTTCCCGCAGCC
bglap	NM_001083857.3	GCCTGATGACTGTGTGTCTGAGCG	AGTTCCAGCCCTCTTCTGTCTCAT
rpl13a	NM_212784.1	TCTGGAGGACTGTAAGAGGTATGC	AGACGCACAATCTTGAGAGCAG
rplp0	NM_131580.2	CTGAACATCTCGCCCTTCTC	TAGCCGATCTGCAGACACAC

Zebrafish transgenic lines maintenance

Broodstock of the transgenic lines used in our experiments, *Tg(col10a1a:col10a1a-GFP*), *Tg(sp7:sp7-GFP)* and *Tg(Ola.Sp7:mCherry)* were maintained at the zebrafish facilities, GIGA-R, University of Liège, Belgium in a recirculating water system (Tecniplast, Italy) at 28.0°C, pH 7.0, photoperiod 12:12 light: dark, $NO_2 < 0.01$ mg/L and $NO_3 < 10$ mg/L. To collect fertilized eggs in the morning, brooders were maintained at 1:2 male to female ratio the day before and set for overnight breeding at tanks with slopes. Collected eggs were maintained in small tanks until

hatching at 3 days post-fertilization (dpf). Using a fluorescent stereomicroscope (Olympus SZX10), larvae expressing the reporter proteins were screened and randomly distributed into 6 well plates at a density of 15 larvae per well with 10 ml of E3 medium per well until 7 dpf and later to small tanks with 15 larvae per 45 ml of E3 medium till 10 dpf. 70% of the medium was exchanged daily. Commercial feed (Zebrafeed, Sparos, Portugal) and live feed (paramecia) were given from 5 dpf to 10 dpf along with the treatments.

Exposure to LDN212854 and probiotics

Two probiotics, *Bacillus subtilis* (BS) and *Lactococcus lactis* (LL), were obtained from Fermedics (Belgium) as lyophilized powder at a commercially formulated concentration of 10^{11} CFU/g. After preliminary tests, larvae were exposed at a concentration of 10^{6} CFU/ml administered in water from 5 dpf to 10 dpf. The type 1 BMP receptor inhibitor LDN212854 (Cat. No. 6151; Bio-Techne Ltd. TOCRIS, United Kingdom) was dissolved in DMSO (0.1%) and used at concentrations of 10 µM and 20 µM, starting at 2 dpf until 4 dpf. Combined treatments were performed by exposing the larvae to LDN212854 from 2 dpf until 5 dpf, followed by probiotic treatment until 10 dpf. Each experiment was performed in triplicates.

Alizarin red (AR) staining

AR staining is one of the most applied techniques for observing the extent of bone mineralization (Bensimon-Brito et al. 2016). Larvae were sacrificed by exposure to MS-222 (Ethyl 3-aminobenzoate methane sulfonate; Merck, Overijse, Belgium) and stained with AR-S (Merck, Overijse, Belgium) at 0.01% for 15 minutes. They were placed in lateral side down onto glycerol (100%) for imaging.

Image acquisition and analysis

Imaging was done using a Leica fluorescence stereomicroscope (Leica, Wetzlar, Germany) equipped with a red fluorescence filter (λex= 546/10 nm, ET-DSR) for *Tg(Ola.Sp7:mCherry*) and AR-stained fish; and with a green fluorescence filter (λex= 470/40 nm) for *Tg(sp7:sp7-GFP)* and *Tg(col10a1a: col10a1a-GFP).* All images were acquired with a DFC7000T colour camera (Leica, Wetzlar, Germany), according to the following parameters: 24-bit coloured image, exposure time 2s (green filter EGFP) and 1s (red filter ET-DSR), gamma 1.00, image format 1920×1440 pixels, binning 1×1. Images were acquired using constant parameters and analysed using ImageJ version 2.1.0/1.53c software after splitting the colour channels of the RGB images. The green or red channel 8-bit images were adjusted uniformly on all the images for optimum contrast and brightness for improved visibility of the structures. The integrated pixel intensity was measured inside the total bone areas (in lateral and ventral view) of each fish and the integrated pixel intensity from the eye was

subtracted. The values were further corrected with head area (pixel intensity / head area) to eliminate possible inter-specimen size variability due to non-homogenous growth. The corrected values were plotted relative to control, arbitrarily set to 100%. A representative image showing how the pixel intensity was measured in both lateral and ventral head views is presented (Supplementary Fig..S1).

Statistical analysis

Data of all groups were normally distributed as assessed by a Shapiro-Wilk's test ($p>0.05$) and variances were homogenous, as assessed by Levene's test for equality of variances ($p>0.05$). The differences between the control and the treatments were tested with a one-way analysis of variance (ANOVA) followed by Tukey's post hoc test ($p<0.05$) for all the image analysis data and gene expression differences between groups. All the tests were performed using R version 4.0.2 and plots were generated using ggplot2 within R (R Core Team 2019).

Results

Generation and characterization of new transgenic lines

Tg(col10a1a:col10a1a-GFP) line

We generated a transgenic line where expression of the GFP reporter protein would be driven by the endogenous zebrafish *col10a1a* promoter

(see Fig. 1a). This *Tg(col10a1a:col10a1a-GFP)* line expresses a fusion protein between Col10a1a and the GFP (Fig. 1a, bottom line, Fig. 1b). Selected fluorescent F1 fish were crossed with the *Tg(Ola.Sp7:mCherry)* line that expresses the red fluorescent mCherry protein in osteoblast cells (Renn et al. 2014). GFP expression is found very specifically in the same regions as the osteoblasts expressing the mCherry protein. This includes the early appearance of the cleithrum, opercle and pharyngeal tooth bud at 3 days post-fertilization (dpf), the parasphenoid and branchiostegal rays at 4 dpf, as well as maxillary, dentary, and entopterygoids at 5-6 dpf (Fig. 1c), consistent with previous in situ hybridization studies (Debiais-Thibaud et al. 2019). AR live fluorescent staining on *Tg(col10a1a:col10a1a-GFP)* larvae (Fig. 1d) confirmed the transgene presence on mineralized bone matrix.

When we analysed in more detail the exact insertion site of the transgene in different lines that we obtained, the translation into the resulting amino acid sequence of the fusion proteins produced (Fig. 1b) revealed that the fusion proteins all contain an intact, N-terminal signal peptide that would normally be eliminated after secretion of the protein into the extracellular space, followed by an 11 amino acid peptide that was common to all the fusion proteins produced. We thus hypothesized that the fluorescent protein in our transgenic reporter lines would be secreted from the producing cells and, once outside the cells, would stay in the vicinity and bind to the extracellular matrix in the bones to generate the observed labelling pattern. To investigate this hypothesis in detail, we turned back to the *Tg(col10a1a:col10a1a-GFP; Ola.Sp7:mCherry)* double

transgenic line and dissected individual bone elements for analysis. Looking at the developing cleithrum (cl) (Fig. 1e), we observed that most of the Col10a1a-GFP protein was associated with extracellular bone matrix. This conclusion was even more apparent when looking at the developing opercle (Fig. 1f). Here, the Col10a1a-GFP was mainly present in the proximal part that contained less cells, while the majority of mCherry-expressing osteoblasts were found at the distal growth fringe of the opercle. In only some cases, fluorescence could be observed inside cells. This predominant bone matrix staining was further confirmed by comparing the Col10a1a-GFP pattern in *Tg(col10a1a:col10a1a-GFP)* transgenic larvae to an AR staining performed on the same animal (Fig. 1g,h).

In the next step, we wondered whether the fact that the transgene is expressed in osteoblasts would favour its preferential binding to the nearby bone matrix. Therefore, we engineered a synthetic mRNA coding for the Col10a1a-GFP fusion protein that we directly injected into fertilized eggs such that it would be translated in every cell within the embryo. Microinjection of a control mRNA coding for GFP lead to an intense, widely distributed green fluorescence at 5dpf (Fig. 1i). In contrast, microinjection of the col10a1a-GFP mRNA resulted in a weak fluorescence specifically restricted to the cleithrum and the opercle (Fig. 1i, right), further supporting the notion that this fusion protein specifically binds to the bone matrix. Finally, to test the binding of Col10a1a-GFP to unmineralized bone matrix, we took advantage of the finding that the *entpd5* gene is required for bone mineralization (Huitema et al. 2012). We

designed morpholino antisense oligonucleotides against *entpd5* mRNA and injected them into fertilized eggs derived from a heterozygous *Tg(col10a1a:col10a1a-GFP)* parent. As expected, about half of the larvae (44/85) revealed Col10a1a-GFP fluorescence in control-injected larvae, while 50/109 displayed similar fluorescence in *entpd5* morphants (Fig. 1j, top), indicating that *entpd5* knockdown did not affect bone staining. In con-trast, alizarin red (AR) staining for mineralized bone was completely absent or very weak in all the morphants, as compared to the control-injected larvae (Fig. 1j, bottom).

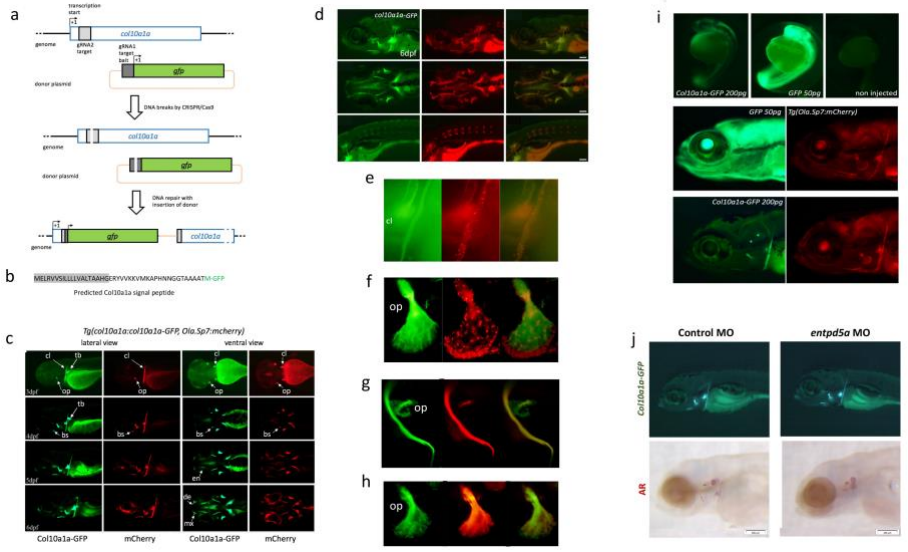

Fig. 1. *Tg(col10a1a:col10a1a-GFP)* **(a)** Schematic representation of the endogenous col10a1a gene (top line), the plasmids used for microinjection along with the two gRNAs (bait and col10a1a, respectively gRNA1 and gRNA2), the resulting cuts in the genomic DNA and plasmids, and the expected reporter construct in the transgenic genome. **(b)** N-terminal end of the fusion protein produced in the *Tg(col10a1a:col10a1-GFP)* transgenic line, with the predicted signal peptide shaded grey and the original GFP translational start site (M) in green. **(c)** Timeline of expression of GFP (green fluorescence) and mCherry (red fluorescence) in the double transgenic larvae Tg(col10a1a:col10a1a-GFP; Ola.Sp7:mCherry). Lateral and ventral views at different stages as indicated,

anterior to the left. White arrows point to specific elements: (bs) branchiostegal ray, (cl) cleithrum, (de) dentary, (en) entopterygoid, (mx) maxillary, (op) opercle and (tb) tooth bud. **(d)** Expression of Col10a1a-GFP protein (green) in *Tg(col10a1a:col10a1a-GFP)* 6dpf larvae live-stained with AR to visualize mineralized bone. (e-h) Close inspection of Col10a1a-GFP localization (green) compared to mCherry expression in osteoblasts in **(e)** cleithrum (cl) or in the opercle **(f)** of 9dpf *Tg(col10a1a:col10a1a-GFP) and Tg(Ola.Sp7:mCherry*) zebrafish larvae; **(g,h)** Expression of GFP protein (green) in *Tg(col10a1a:col10a1a-GFP)* 6dpf larvae live-stained with AR to visualize bone matrix. Close inspection of the cleithrum **(g)** and opercle (**h). (i)** Zebrafish *Tg(Ola.Sp7:mCherry)* larvae after microinjection of mRNA coding for GFP or for the fusion protein Col10a1a-GFP. Top: embryos at 1dpf, showing weak fluorescence of Col10a1a-GFP, extremely strong for GFP, and no fluorescence in controls. Bottom: the same larvae at 5dpf, still showing strong GFP expression in the entire body and weak, but specific fluorescence of Col10a1a-GFP located at bone elements (cleithrum and opercle) as confirmed by the red fluorescence of the osteoblast-specific mCherry. **(j)** Morpholino injection into *Tg(col10a1a:col10a1a-GFP)* larvae. The Col10a1a-GFP protein labels cranial bone elements at 4dpf in both control and *entpd5* MO injected larvae (top), while alizarin red (AR) staining is absent in entpd5 morphants (bottom).

Tg(sp7:sp7-GFP) line

Using the same CRISPR/Cas9 method, we generated another transgenic line by targeting the insertion of the GFP reporter cDNA into the endogenous *sp7* coding region, resulting in a line expressing a fusion protein between Sp7 and GFP (Fig. 2a). This new line, *Tg(sp7:sp7-GFP),* was analyzed for green fluorescence in parallel with the red fluorescence in the *Tg(Ola.Sp7:mCherry)* line to compare the expression of the two transgenes. Comparison of the two lines (Fig. 2b) revealed that the expression of both transgenes largely overlaps, starting at 3dpf in cleithrum and opercle and extending to maxillary, dentary, branchiostegal rays and entopterygoids at later stages. However, some

differences in the expression pattern are also apparent, mainly the earlier expression in the pharyngeal tooth bud at 3dpf and the stronger expression in the entopterygoid at 6dpf in the *Tg(sp7:sp7-GFP)* line. Both lines display a weakened expression at 10dpf and beyond (not shown).

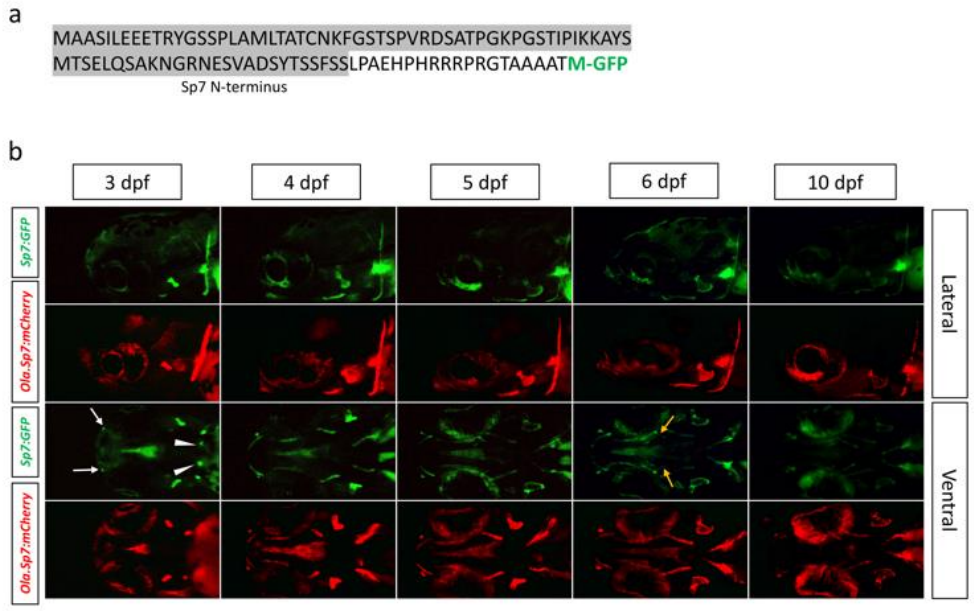

Fig. 2. *Tg(sp7:sp7-GFP)* **(a)** N-terminal end of the fusion protein produced in the *Tg(sp7:sp7-GFP)* transgenic line, with the predicted signal peptide shaded grey and the original GFP translational start site (M) in green **(b)** *Tg(sp7:sp7-GFP)* and the previously described *Tg(Ola.Sp7:mCherry)* lines are tracked for transgene expression in the head region (top: lateral view and bottom: ventral view) from 3dpf to 10dpf. Earlier expression in maxillary (white arrows) and pharyngeal tooth buds (white arrowheads) at 3dpf, and the entopterygoid (yellow arrows) at 6dpf are indicated in the *Tg(sp7:sp7-GFP)* line.

Effect of probiotics

Effect of probiotics on bone formation

Bacillus subtilis (BS) treated larvae showed an increase in mineralized area of the opercular bone when compared to control and *Lactococcus lactis* (LL) treated ones by AR staining (Fig.3a). Then we tested the effect of probiotics on specific mRNA levels. Total RNA was extracted from 7dpf larvae grown in control and the two probiotics. Using RT-PCR, we observed that all the bone-related gene's mRNA levels were significantly increased upon exposure to the probiotics. Interestingly, expression of the specific marker genes *sp7, col10a1a, spp1, runx2b* were more extensively induced by BS, while *bglap* mRNA levels were not significantly affected. In contrast, induction of *cyp26b1*, coding for an enzyme degrading retinoic acid, was significantly higher with LL (Fig. 3b).

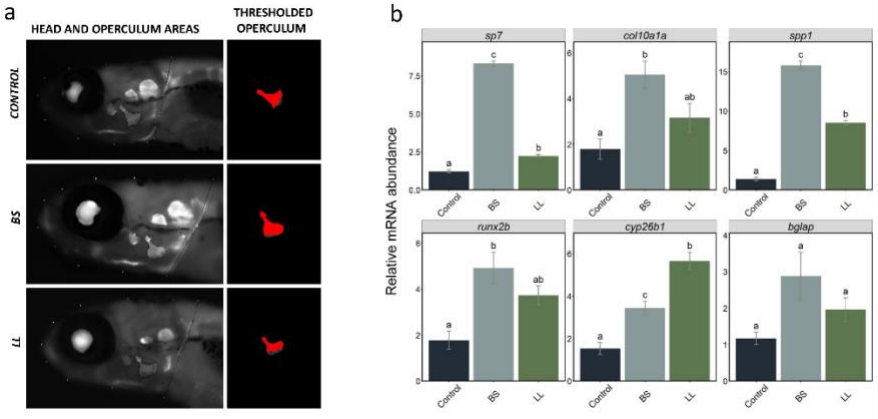

Fig. 3. (a) Representative fluorescence microphotograph of AR-S-stained wild-type zebrafish larvae at 7 dpf following BS and LL treatments; AR-stained operculum of each group is separately shown to the left as enlarged images to view the clear mineralisation differences between groups **(b**) Relative expression levels of *sp7, col10a1a, spp1, runx2b, cyp26b1*, and *bglap* genes in wild-type zebrafish larvae (n = 7) treated with two probiotics, the BS and LL and in control, sampled at 7dpf . Data are presented as mean±S.D. One-way ANOVA and Tukey's multiple comparison tests are used. Different letters denote statistically significant differences between experimental groups.

To facilitate and complement this observation, we decided to test the effects of the two different probiotics on bone development by direct live observation of developing bone elements using three transgenic lines. Two lines are based on the osteoblast-specific *sp7* promoter, one from medaka *Tg(Ola.Sp7:mCherry)* (Renn et al. 2014) and the other from the endogenous zebrafish *sp7* gene, *Tg(sp7:sp7-GFP)*. The third line is based on the endogenous *col10a1a* promoter, which reveals preferentially the bone matrix.

Control and probiotic enrichment conditions were applied to individuals of each of the three transgenic lines. For the two transgenic lines based on the *sp7* promoter, *Tg(Ola.Sp7:mcherry)* and *Tg(sp7:sp7-GFP)*, we determined the integrated pixel intensity in the head areas (lateral and ventral view) at 7dpf (Fig. 4a,b). We observed a significant increase in fluorescence upon exposure to both BS and LL probiotics for head and opercular areas in lateral views, while areas in ventral views reached significance only in the *Tg(Ola.Sp7:mCherry)* line. In all cases, the increase was consistently more intense with BS, compared to LL. Representative images of larvae in the corresponding conditions illustrate the measured

trends (Fig. 4c). Using the *Tg(col10a1a:col10a1a-GFP)* line, we decided to extend the observations to a later stage and 10 dpf was selected since most cranial bone elements are detectable. In addition, we performed a live alizarin red (AR) staining before observation in order to further illustrate the predominant staining of the bone matrix in this line. The pixel intensities were significantly higher than control in all areas for both probiotics (Fig. 4d). Furthermore, BS caused a significantly higher GFP pixel intensity compared to LL in the ventral view. Simultaneous staining with AR confirmed that mineralization in the BS-treated larvae have the highest integrated pixel intensity in the total head-(lateral and ventral). Representative images of larvae in the corresponding conditions illustrate the measured trends (Fig. 4e), while merged images confirm the near-perfect overlap of GFP and AR fluorescence for both signal positive areas as well as pixel intensity.

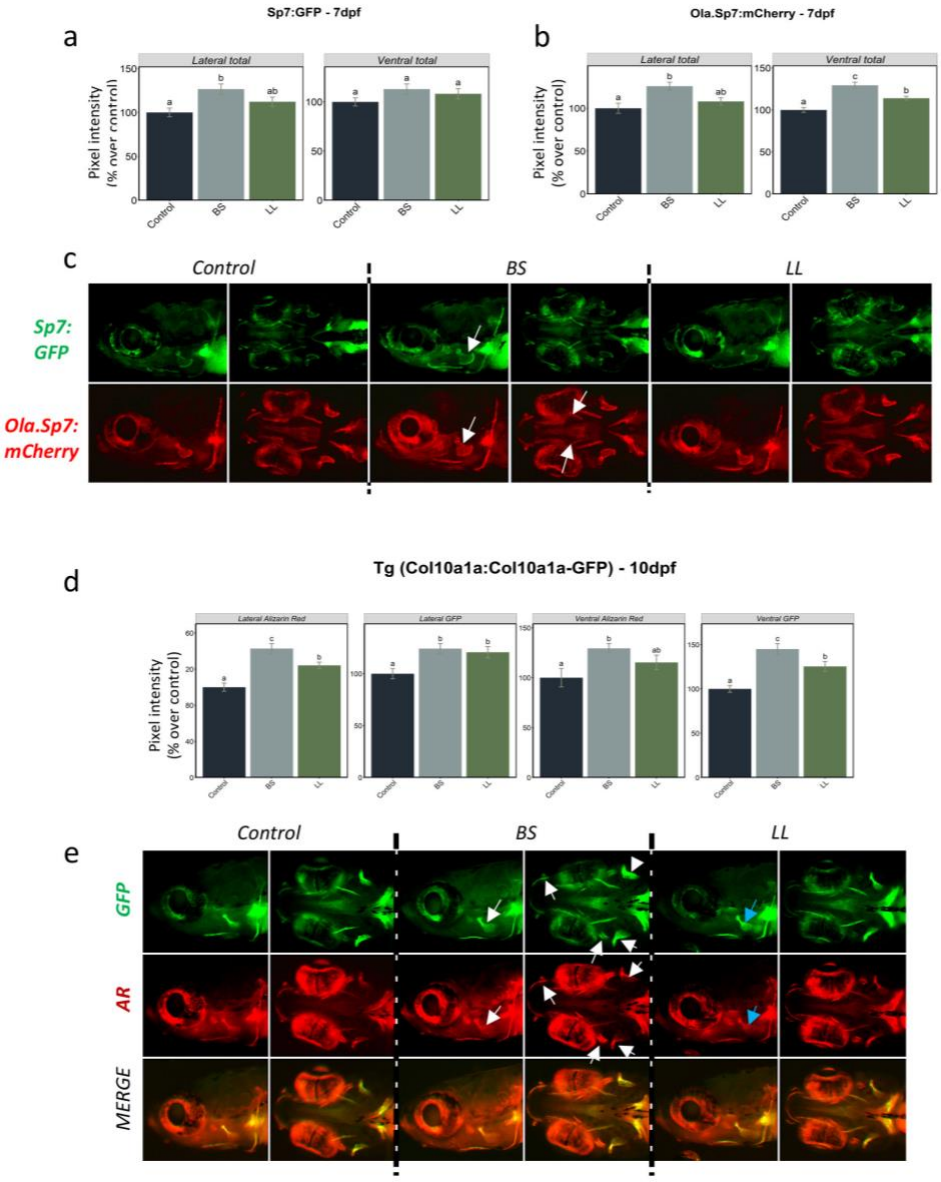

Fig. 4. Integrated pixel intensity values of various areas measured in 7dpf zebrafish of **(a)** *Tg(sp7:sp7-GFP)* and **(b)** *Tg(Ola.Sp7:mCherry)* larvae in controls and upon two different probiotic treatments; **(c)** Signal expression images (lateral and ventral views) of the head area of *Tg(sp7:sp7-GFP)* and *Tg(Ola.Sp7-mCherry)* larvae in the different conditions; **(d)** Integrated pixel intensity values of various areas measured in 10 dpf *Tg(col10a1a:col10a1a-GFP)* zebrafish larvae

from different treatment groups and stained with AR; **(e)** GFP, AR fluorescence and merged images of the head area (lateral and ventral views) of *Tg(col10a1a:col10a1a-GFP)* larvae in the different treatment groups. Increased GFP and AR fluorescence in various bony structures are denoted by white and blue arrows respectively in BS and LL treated fish. One-way ANOVA and Tukey's multiple comparison tests are used, and statistical significance was set at $p<0.05$. Different letters denote statistically significant differences between experimental groups.

BMP inhibitor exposure followed by probiotic treatment

BMP signalling is known to be required for osteoblast differentiation and for bone mineralization (Windhausen et al. 2015; Zinck et al. 2021). The widely used marker gene for investigating the osteoblast differentiation in mammals and teleost species is the *sp7* gene (Li et al. 2009; Hammond and Moro 2012; Azetsu et al. 2017). We treated *Tg(Ola.Sp7:mCherry)* transgenic larvae with the BMP inhibitor LDN212854 from 2dpf until 4dpf at two different concentrations (respectively 10μM and 20μM) to test its effect on the osteoblast population. We observed a weak, but significant increase in mCherry expression in the 20μM concentration group as compared to the control (DMSO) group at 5 dpf (Fig. 5), suggesting that at this concentration osteoblast proliferation and/or differentiation is affected by BMP inhibition.

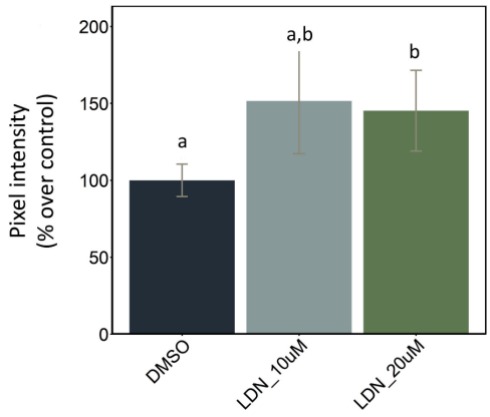

Fig. 5. Effects of LDN212854 on *sp7* expression. Integrated pixel intensity values (mCherry red fluorescence) of 5 dpf Tg*(Ola.Sp7-mCherry)* larvae measured in ventral view treated with 10μM and 20μM LDN212854 from 2dpf to 4 dpf. Different letters denote statistically significant differences between experimental groups (one-way ANOVA, $p < 0.05$, followed by Tukey's post hoc test).

Furthermore, we used the T*g(col10a1a:col10a1a-GFP)* line to observe the effects of the BMP inhibitor LDN212854 at 20μM on bone matrix formation and mineralization, and to investigate the potential protecting properties of the probiotics. LDN212854 was administered from 2dpf up to 4dpf, followed by probiotic supplementation (BS or LL) from 5 dpf to 10 dpf. DMSO (0.1%) was used as the control since the inhibitor was dissolved in DMSO. Sampling was performed at 10 dpf, and additional staining with AR was used to visualize the mineralized structures in the larvae. Compared to both control and DMSO, we observed a dramatic decrease in the integrated pixel intensity values in all analyzed areas in the presence of LDN, both for *Col10a1a*-GFP and live AR staining. Compared to BMP inhibition alone, additional treatment with probiotics

resulted in significantly increased *Col10a1a-GFP* fluorescence in both lateral and ventral observation, while the increase observed after live AR staining never reached significance. These observations suggest that in particular BS can revert the deleterious effect of BMP inhibition on bone matrix formation, while AR staining indicates that the effect is not evident on mineralization (Fig. 6a and 6b).

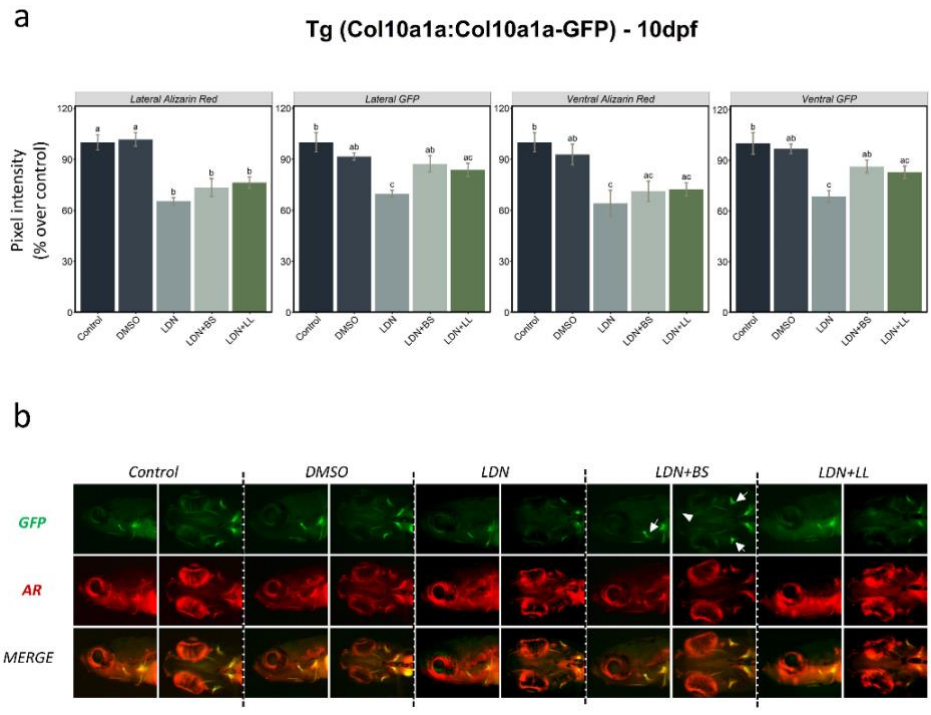

Fig. 6. BMP inhibitor exposure followed by two probiotics treatments in *Tg(col10a1a:col10a1a-GFP*) larvae **(a)** Corrected pixel intensity values of various areas measured in 10 dpf zebrafish *Tg(col10a1a:col10a1a-GFP)* larvae divided into various groups - control, DMSO, LDN, LDN+BS and LDN+LL and stained with AR. DMSO was used as additional control since it was used as the solvent for LDN. One-way ANOVA and Tukey's multiple comparison tests were used, and statistical significance was set at $p<0.05$. Different letters denote statistically significant differences among experimental groups; **(b)** GFP, AR staining and

merged images of the head area (lateral and ventral views) of *Tg(col10a1a:col10a1a-GFP)* larvae of the different treated groups. White arrows denote the recovered GFP in various bony structures and white arrowhead indicate the presence of signal in additional structures (which were absent in other groups) in BS treated fish after LDN exposure (LDN+BS).

Discussion

The use of transgenic zebrafish reporter lines using the specific expression of fluorescent proteins to follow the development of specific organs, tissues, and cells in living larvae is now widely used in developmental biology. Here we present two new trans-genic lines, namely *Tg(sp7:sp7-GFP)* and *Tg(col10a1a:col10a1a-GFP),* which we obtained by inserting the GFP coding sequence into the endogenous *sp7* or *col10a1a* gene coding sequence using the CRISPR/Cas9 technology. We used these lines to visualize the formation of the zebrafish skeleton, and to evaluate the effects of two types of probiotics on this process, also after treatment using a BMP inhibitor.

Several transgenic zebrafish lines expressing fluorescent reporter genes under the control of the sp7 promoter have been described in recent years. However, there are important differences between these lines and the *Tg(sp7:sp7-GFP)* line presented here: i) previously described lines, such as the *Tg(Ola.Sp7:mCherry)* (Spoorendonk et al. 2008; Renn et al. 2014) or *Tg(Ola.Sp7:mCherry-NTR)* (Singh et al. 2012) use the heterologous promoter from medaka (*Oryzias latipes*, Ola) to drive expression of the transgene (Renn and Winkler 2009) ii) these lines were

obtained by insertion of an artificial construct at a random, unknown location in the genome. In contrast, the *Tg(sp7:sp7-GFP)* carries the reporter gene in place of the endogenous *sp7* gene, it is under the control of the endogenous regulatory regions and thus should reproduce more correctly the *sp7* expression pattern. Indeed, consistent with the pattern observed here in the transgenic line, *in situ* hybridization has revealed *sp7* expression in the tooth buds at 4dpf (Wiweger et al. 2012), and in the maxillary (Clément et al. 2008; Yan et al. 2012) and the entopterygoid at 3dpf (Li et al. 2009). On the other hand, the higher mCherry expression could be due to the random location of the transgene. Despite these differences in the exact timing of expression patterns, the two lines display fluorescence in many overlapping regions, such as opercle, cleithrum or branchiostegal rays (Clément et al. 2008; Yan et al. 2012).

Col10a1a is a secreted protein and in our *Tg(col10a1a:col10a1a-GFP)* zebrafish the GFP insertion preserves the N-terminal signal peptide of Col10a1a (see Fig. 1a,b). Thus, the transgenic fish actually code for a fusion protein that is secreted by the producing cells. Although we can observe some fluorescent cells in this line, it appears that the main fluorescent structure is the extracellular bone matrix. It appears that the Col10a1a-GFP fusion protein, after secretion, strongly binds to the extracellular bone matrix, as shown by the overlapping pattern with AR staining. Microinjection of an mRNA coding for the fusion protein into one- or two-cell stage embryos , leading to its expression basically in all the embryonic cells, resulted in the same specific fluorescent staining of bone elements, showing that this is an inherent property of the Col10a1a-

GFP protein. Morpholino microinjection experiments revealed that knockdown of the *entpd5* gene, required for bone mineralization (Huitema et al. 2012), did not affect fluorescent labelling of the bone matrix, while mineralization was nearly absent as revealed by alizarin red staining (Fig. 1j). Therefore, we consider the *Tg(col10a1a:col10a1a-GFP)* line as the first reporter line revealing the extracellular bone matrix, mineralized or not, representing an important tool to differentiate between non-mineralized and mineralized bone matrix in live larvae. Therefore, we consider the *Tg(col10a1a:col10a1a-GFP)* line as the first reporter line revealing the extracellular bone matrix in live larvae without the need of any staining method.

A preliminary test for the effects of probiotics revealed that the transcription of several marker genes for bone development were significantly up regulated upon probiotic treatment at 7 dpf. Interestingly, expression of the pro-osteogenic genes *sp7*, *col10a1a*, *spp1*, and *runx2b* was more significantly induced by BS treatment, while induction of *cyp26b1* expression was significantly higher in LL. The *cyp26b1* gene codes for a protein with retinoic acid 4 hydroxylase activity, whose mutation leads to severe defects in head cartilage formation (Reijntjes et al. 2003), increased ossification of the vertebral column (Laue et al. 2008; Spoorendonk et al. 2008) with complex effects on skeletal formation, depending on timing and location (Laue et al. 2011). It is therefore difficult to predict how this differential response to the different probiotics will affect the skeletal development. None of the probiotics was effective on *bglap* expression in mature osteoblast, compared to

their more predominant effect on *spp1* expressing immature osteoblasts; this could be due to the degree of osteoblast differentiation at the particular stage studied here (Maruyama et al. 2007). Since *runx2b* expression has to be downregulated for immature osteoblasts to differentiate into mature osteoblasts for formation of mature bone (Komori 2009), the stage of osteoblast differentiation observed here appears to be more transitional, from immature to mature, with highest upregulation of *spp1* and *sp7* and no downregulation of *runx2b*, particularly in both probiotic treatments and even more significant in BS. All this preliminary evidence from the expression pattern of genes related to skeletal development directed us to further explore the possibility of using reporter lines to confirm the results.

Transgenic reporter lines offer the opportunity to follow the formation of specific tissues in live embryos and larvae, over time and in specific locations. The new lines presented here, both driving their transgene expression from endogenous regulatory regions, reveal either the location of osteoblasts (*Tg(sp7:sp7-GFP)* line) or of the bone matrix (*Tg(col10a1a:col10a1a-GFP)* line). When we tested probiotics exposure of these transgenic lines, *B.subtilis* was found to significantly induce *sp7*-driven expression in osteoblasts at 7dpf and Col10a1a-GFP labelling of the bone matrix at 10 dpf. These results observed in the bony structures of the head are clearly in agreement with the mRNA level results. Additional AR staining in the *Tg(col10a1a:col10a1a-GFP)* line revealed that probiotics induced a significant increase of mineralized bone matrix as well. The positive influence of *B.subtilis* on bone matrix formation and

mineralization was significant when bony structures were analyzed from both lateral and ventral views of the head, whereas the weaker effect of LL resulted in non-significant effects in both views. This indicate that different bacteria have varying ability in modulating the process of bone formation and in our study, *B.subtilis* positively influenced osteogenesis more than *L.lactis*. In addition, we show that treatment with the BMP inhibitor LDN212854 dramatically decreases bone matrix labelling by Col10a1a-GFP, and of bone mineralization as assessed by AR. BMP inhibitor treatment on the *Tg(Ola.Sp7:mCherry)* line revealed in contrast no or a weak increase in osteoblast-specific expression (Fig. 5), in line with previous observations showing that BMP inhibitors dorsomorphin and K02288 decreased bone mineralization without affecting osteoblast numbers (Windhausen et al. 2015). Interestingly, we also observed that BS was able to partially revert this negative effect of BMP inhibition on bone matrix deposition but could not rescue bone mineralization. These results suggested a decoupling of the bone matrix deposition from bone mineralization which may be differentially affected by probiotics (or BMP signaling).

Osteoblast or bone matrix reporter transgenic lines combined with staining techniques like AR are useful to follow both osteoblast differentiation, bone matrix deposition, and bone mineralization simultaneously. Future studies may take further advantage of these transgenic lines by focusing on continuous monitoring of transgene expression during development and in the adults, or on specific bone structures. In our study, the new transgenic lines (*Tg(sp7:sp7-GFP*) and

(*Tg(col10a1a:col10a1a-GFP*) clearly evidenced the pro-osteogenic effects of the two probiotics strains and were in agreement with the gene expression results. Thus, we can conclude that the probiotics are clearly pro-osteogenic, both alone and in the presence of a BMP inhibitor, with a clear advantage for *Bacillus subtilis*. These findings open a new outlook in the use of probiotics as a prophylactic treatment in improving bone growth and health, which is currently a very under-explored area of research.

References

Alhazmi N, Carroll SH, Kawasaki K, et al (2021) Synergistic roles of Wnt modulators R-spondin2 and R-spondin3 in craniofacial morphogenesis and dental development. Sci Rep 11:5871. https://doi.org/10.1038/s41598-021-85415-y

Ando K, Shibata E, Hans S, et al (2017) Osteoblast Production by Reserved Progenitor Cells in Zebrafish Bone Regeneration and Maintenance. Dev Cell 43:643-650.e3. https://doi.org/10.1016/j.devcel.2017.10.015

Atkins GJ, Welldon KJ, Wijenayaka AR, et al (2009) Vitamin K promotes mineralization, osteoblast-to-osteocyte transition, and an anticatabolic phenotype by γ-carboxylation-dependent and -independent mechanisms. American Journal of Physiology-Cell Physiology 297:C1358–C1367. https://doi.org/10.1152/ajpcell.00216.2009

Azetsu Y, Inohaya K, Takano Y, et al (2017) The sp7 gene is required for maturation of osteoblast-lineage cells in medaka (Oryzias latipes) vertebral column development. Developmental Biology 431:252–262. https://doi.org/10.1016/j.ydbio.2017.09.010

Bensimon-Brito A, Cardeira J, Dionísio G, et al (2016) Revisiting in vivo staining with alizarin red S - a valuable approach to analyse zebrafish skeletal mineralization during development and regeneration. BMC Developmental Biology 16:2. https://doi.org/10.1186/s12861-016-0102-4

Bergen DJM, Kague E, Hammond CL (2019) Zebrafish as an Emerging Model for Osteoporosis: A Primary Testing Platform for Screening New Osteo-Active Compounds. Frontiers in Endocrinology 10:6. https://doi.org/10.3389/fendo.2019.00006

Booth SL (2009) Roles for Vitamin K Beyond Coagulation. Annu Rev Nutr 29:89–110. https://doi.org/10.1146/annurev-nutr-080508-141217

Britton RA, Irwin R, Quach D, et al (2014) Probiotic L. reuteri Treatment Prevents Bone Loss in a Menopausal Ovariectomized Mouse Model. Journal of Cellular Physiology 229:1822–1830. https://doi.org/10.1002/jcp.24636

Carnevali O, Notarstefano V, Olivotto I, et al (2017) Dietary administration of EDC mixtures: A focus on fish lipid metabolism. Aquatic Toxicology 185:95–104. https://doi.org/10.1016/j.aquatox.2017.02.007

Castaneda M, Strong JM, Alabi DA, Hernandez CJ (2020) The Gut Microbiome and Bone Strength. Curr Osteoporos Rep 18:677–683. https://doi.org/10.1007/s11914-020-00627-x

Chaplin A, Parra P, Laraichi S, et al (2016) Calcium supplementation modulates gut microbiota in a prebiotic manner in dietary obese mice. Molecular Nutrition & Food Research 60:468–480. https://doi.org/10.1002/mnfr.201500480

Chiang S-S, Pan T-M (2011) Antiosteoporotic Effects of Lactobacillus-Fermented Soy Skim Milk on Bone Mineral Density and the Microstructure of Femoral Bone in Ovariectomized Mice. J Agric Food Chem 59:7734–7742. https://doi.org/10.1021/jf2013716

Clément A, Wiweger M, Hardt S von der, et al (2008) Regulation of Zebrafish Skeletogenesis by ext2/dackel and papst1/pinscher. PLOS Genetics 4:e1000136. https://doi.org/10.1371/journal.pgen.1000136

Cooney OD, Nagareddy PR, Murphy AJ, Lee MKS (2021) Healthy Gut, Healthy Bones: Targeting the Gut Microbiome to Promote Bone Health. Frontiers in Endocrinology 11:1159. https://doi.org/10.3389/fendo.2020.620466

Cosme-Silva L, Dal-Fabbro R, Cintra LTA, et al (2020) Reduced bone resorption and inflammation in apical periodontitis evoked by dietary supplementation with probiotics in rats. International Endodontic Journal 53:1084–1092. https://doi.org/10.1111/iej.13311

Debiais-Thibaud M, Simion P, Ventéo S, et al (2019) Skeletal Mineralization in Association with Type X Collagen Expression Is an Ancestral Feature for Jawed Vertebrates. Mol Biol Evol 36:2265–2276. https://doi.org/10.1093/molbev/msz145

Forner-Piquer I, Beato S, Piscitelli F, et al (2020) Effects of BPA on zebrafish gonads: Focus on the endocannabinoid system. Environ Pollut 264:114710. https://doi.org/10.1016/j.envpol.2020.114710

Foureaux R de C, Messora MR, de Oliveira LFF, et al (2014) Effects of Probiotic Therapy on Metabolic and Inflammatory Parameters of Rats With Ligature-Induced Periodontitis Associated With Restraint Stress. Journal of Periodontology 85:975–983. https://doi.org/10.1902/jop.2013.130356

Gholami A, Dabbaghmanesh MH, Ghasemi Y, et al (2020) Probiotics ameliorate pioglitazone-associated bone loss in diabetic rats. Diabetology & Metabolic Syndrome 12:78. https://doi.org/10.1186/s13098-020-00587-3

Hammond CL, Moro E (2012) Using transgenic reporters to visualize bone and cartilage signaling during development in vivo. Front Endocrinol 3:. https://doi.org/10.3389/fendo.2012.00091

Hill C, Guarner F, Reid G, et al (2014) The International Scientific Association for Probiotics and Prebiotics consensus statement on the scope and appropriate use of the term probiotic. Nat Rev Gastroenterol Hepatol 11:506–514. https://doi.org/10.1038/nrgastro.2014.66

Huidrom S, Beg MA, Masood T (2021) Post-menopausal Osteoporosis and Probiotics. Current Drug Targets 22:816–822. https://doi.org/10.2174/1389450121666201027124947

Huitema LFA, Apschner A, Logister I, et al (2012) Entpd5 is essential for skeletal mineralization and regulates phosphate homeostasis in zebrafish. Proc Natl Acad Sci 109:21372–21377. https://doi.org/10.1073/pnas.1214231110

Jacobs CT, Huang P (2019) Notch signalling maintains Hedgehog responsiveness via a Gli-dependent mechanism during spinal cord patterning in zebrafish. eLife 8:e49252. https://doi.org/10.7554/eLife.49252

Jia L, Tu Y, Jia X, et al (2021) Probiotics ameliorate alveolar bone loss by regulating gut microbiota. Cell Proliferation 54:e13075. https://doi.org/10.1111/cpr.13075

Kimura Y, Hisano Y, Kawahara A, Higashijima S (2014) Efficient generation of knock-in transgenic zebrafish carrying reporter/driver genes by CRISPR/Cas9-mediated genome engineering. Sci Rep 4:6545. https://doi.org/10.1038/srep06545

Komori T (2009) Regulation of bone development and extracellular matrix protein genes by RUNX2. Cell Tissue Res 339:189. https://doi.org/10.1007/s00441-009-0832-8

Larbuisson A, Dalcq J, Martial JA, Muller M (2013) Fgf receptors Fgfr1a and Fgfr2 control the function of pharyngeal endoderm in late cranial cartilage development. Differ Res Biol Divers 86:192–206. https://doi.org/10.1016/j.diff.2013.07.006

Laue K, Jänicke M, Plaster N, et al (2008) Restriction of retinoic acid activity by Cyp26b1 is required for proper timing and patterning of osteogenesis during zebrafish development. Development 135:3775–3787. https://doi.org/10.1242/dev.021238

Laue K, Pogoda H-M, Daniel PB, et al (2011) Craniosynostosis and Multiple Skeletal Anomalies in Humans and Zebrafish Result from a Defect in the Localized Degradation of Retinoic Acid. The American Journal of Human Genetics 89:595–606. https://doi.org/10.1016/j.ajhg.2011.09.015

Li J-Y, Chassaing B, Tyagi AM, et al (2016) Sex steroid deficiency–associated bone loss is microbiota dependent and prevented by probiotics. J Clin Invest 126:2049–2063. https://doi.org/10.1172/JCI86062

Li N, Felber K, Elks P, et al (2009) Tracking gene expression during zebrafish osteoblast differentiation. Developmental Dynamics 238:459–466. https://doi.org/10.1002/dvdy.21838

Lleras-Forero L, Winkler C, Schulte-Merker S (2020) Zebrafish and medaka as models for biomedical research of bone diseases. Developmental Biology 457:191–205. https://doi.org/10.1016/j.ydbio.2019.07.009

Lovely CB, Swartz ME, McCarthy N, et al (2016) Bmp signaling mediates endoderm pouch morphogenesis by regulating Fgf signaling in zebrafish. Development 143:2000–2011. https://doi.org/10.1242/dev.129379

Maradonna F, Gioacchini G, Falcinelli S, et al (2013) Probiotic Supplementation Promotes Calcification in Danio rerio Larvae: A Molecular Study. PLoS One 8:. https://doi.org/10.1371/journal.pone.0083155

Maradonna F, Nozzi V, Dalla Valle L, et al (2014) A developmental hepatotoxicity study of dietary bisphenol A in Sparus aurata juveniles. Comparative Biochemistry and Physiology Part C: Toxicology & Pharmacology 166:1–13. https://doi.org/10.1016/j.cbpc.2014.06.004

Maruyama Z, Yoshida CA, Furuichi T, et al (2007) Runx2 determines bone maturity and turnover rate in postnatal bone development and is involved in bone loss in estrogen deficiency. Developmental Dynamics 236:1876–1890. https://doi.org/10.1002/dvdy.21187

McCabe L, Britton RA, Parameswaran N (2015) Prebiotic and Probiotic Regulation of Bone Health: Role of the Intestine and its Microbiome. Curr Osteoporos Rep 13:363–371. https://doi.org/10.1007/s11914-015-0292-x

Nilsson AG, Sundh D, Bäckhed F, Lorentzon M (2018) Lactobacillus reuteri reduces bone loss in older women with low bone mineral density: a randomized, placebo-controlled, double-blind, clinical trial. Journal of Internal Medicine 284:307–317. https://doi.org/10.1111/joim.12805

Ohlsson C, Engdahl C, Fåk F, et al (2014) Probiotics Protect Mice from Ovariectomy-Induced Cortical Bone Loss. PLOS ONE 9:e92368. https://doi.org/10.1371/journal.pone.0092368

Ohlsson C, Sjögren K (2018) Osteomicrobiology: A New Cross-Disciplinary Research Field. Calcif Tissue Int 102:426–432. https://doi.org/10.1007/s00223-017-0336-6

Parvaneh K, Ebrahimi M, Sabran MR, et al (2015) Probiotics (Bifidobacterium longum) Increase Bone Mass Density and Upregulate Sparc and Bmp-2 Genes in Rats with Bone Loss Resulting from Ovariectomy. BioMed Research International 2015:e897639. https://doi.org/10.1155/2015/897639

R Core Team (2019) R: A language and environment for statistical computing. Vienna, Austria: R Foundation for Statistical Computing; 2011.

Reijntjes S, Rodaway A, Maden M (2003) The retinoic acid metabolising gene, CYP26B1, patterns the cartilaginous cranial neural crest in zebrafish. Int J Dev Biol 51:351–360. https://doi.org/10.1387/ijdb.062258sr

Renn J, Pruvot B, Muller M (2014) Detection of nitric oxide by diaminofluorescein visualizes the skeleton in living zebrafish. Journal of Applied Ichthyology 30:701–706. https://doi.org/10.1111/jai.12514

Renn J, Winkler C (2009) Osterix-mCherry transgenic medaka for in vivo imaging of bone formation. Developmental Dynamics 238:241–248. https://doi.org/10.1002/dvdy.21836

Rizzoli R, Biver E (2020) Are Probiotics the New Calcium and Vitamin D for Bone Health? Curr Osteoporos Rep 18:273–284. https://doi.org/10.1007/s11914-020-00591-6

Robu ME, Larson JD, Nasevicius A, et al (2007) p53 Activation by Knockdown Technologies. PLOS Genet 3:e78. https://doi.org/10.1371/journal.pgen.0030078

Schiavone M, Rampazzo E, Casari A, et al (2014) Zebrafish reporter lines reveal in vivo signaling pathway activities involved in pancreatic cancer. Dis Model Mech 7:883–894. https://doi.org/10.1242/dmm.014969

Singh SP, Holdway JE, Poss KD (2012) Regeneration of amputated zebrafish fin rays from de novo osteoblasts. Dev Cell 22:879–886. https://doi.org/10.1016/j.devcel.2012.03.006

Spoorendonk KM, Peterson-Maduro J, Renn J, et al (2008) Retinoic acid and Cyp26b1 are critical regulators of osteogenesis in the axial skeleton. Development 135:3765–3774. https://doi.org/10.1242/dev.024034

Sun X, Zhang R, Chen H, et al (2020) Fgfr3 mutation disrupts chondrogenesis and bone ossification in zebrafish model mimicking CATSHL syndrome partially via enhanced Wnt/β-catenin signaling. Theranostics 10:7111–7130. https://doi.org/10.7150/thno.45286

Takimoto T, Hatanaka M, Hoshino T, et al (2018) Effect of Bacillus subtilis C-3102 on bone mineral density in healthy postmenopausal Japanese women: a randomized, placebo-controlled, double-blind clinical trial. Bioscience of Microbiota, Food and Health 37:87–96. https://doi.org/10.12938/bmfh.18-006

Terashima A, Takayanagi H (2018) Overview of Osteoimmunology. Calcif Tissue Int 102:503–511. https://doi.org/10.1007/s00223-018-0417-1

Westphal M, Panza P, Kastenhuber E, et al (2022) Wnt/β-catenin signaling promotes neurogenesis in the diencephalospinal dopaminergic system of embryonic zebrafish. Sci Rep 12:1030. https://doi.org/10.1038/s41598-022-04833-8

Windhausen T, Squifflet S, Renn J, Muller M (2015) BMP Signaling Regulates Bone Morphogenesis in Zebrafish through Promoting Osteoblast Function as Assessed by Their Nitric Oxide Production. Molecules 20:7586–7601. https://doi.org/10.3390/molecules20057586

Wiweger MI, Zhao Z, Merkesteyn RJP van, et al (2012) HSPG-Deficient Zebrafish Uncovers Dental Aspect of Multiple Osteochondromas. PLOS ONE 7:e29734. https://doi.org/10.1371/journal.pone.0029734

Wu S, Yoon S, Zhang Y-G, et al (2015) Vitamin D receptor pathway is required for probiotic protection in colitis. American Journal of Physiology-Gastrointestinal and Liver Physiology 309:G341–G349. https://doi.org/10.1152/ajpgi.00105.2015

Yan Y-L, Bhattacharya P, He XJ, et al (2012) Duplicated zebrafish co-orthologs of parathyroid hormone-related peptide (PTHrP, Pthlh) play different roles in craniofacial skeletogenesis. Journal of Endocrinology 214:421–435. https://doi.org/10.1530/JOE-12-0110

Zinck NW, Jeradi S, Franz-Odendaal TA (2021) Elucidating the early signaling cues involved in zebrafish chondrogenesis and cartilage morphology. J Exp Zool B Mol Dev Evol 336:18–31. https://doi.org/10.1002/jez.b.23012

Supplementary Materials

Supplementary Fig. S1: Representative images of **(a)** lateral and **(b)** ventral views of zebrafish larvae head showing how the pixel intensity was measured in both views. Red indicate the area measured and yellow denote the eye area subtracted. Bony structures are in white against grey background (Created with BioRender.com)

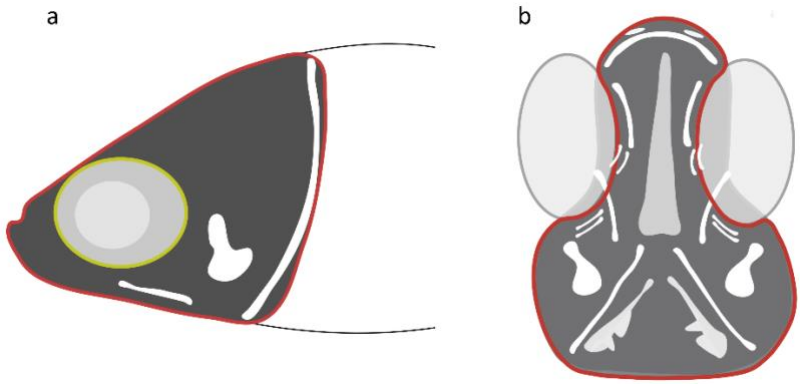

CHAPTER 4: ACTION OF MICRONUTRIENTS AND PROBIOTICS EXTRACTS IN SYNERGY WITH VITAMIN D3 ON hFOB1.19 CELLS DIFFERENTIATION AND MINERALIZATION

Jerry Maria Sojan[1], Caterina Licini[2], Patrick Orlando[1], Fabio Marcheggiani[1], Monica Mattioli Belmonte[2], Luca Tiano[1], Francesca Maradonna[1] and Oliana Carnevali[1]

[1]Department of Life and Environmental Sciences, Università Politecnica delle Marche, via Brecce Bianche, 60131 Ancona, Italy
[2] Department of Clinical and Molecular Sciences (DISCLIMO), Università Politecnica delle Marche, Via Tronto 10/a, Ancona 60126, Italy

Abstract

Probiotics such as *Bacillus subtilis* and *Lactococcus lactis*, as well as micronutrients such as boron (B) and selenium (Se), have been shown to have a positive impact on bone health in the prior literature. In this study, we investigated all of their possible synergistic effect with calcitriol (VD) on a human osteoblast cell line, with a particular emphasis on their capacity to control ECM mineralization and calcium absorption. B and Se showed a greater positive impact on the cells when used in conjunction with VD. Both the probiotics extracts did not show any osteogenic synergism with VD although, *B.subtilis* was found to be the probiotic with the greatest effect on mineralization, outperforming *L. lactis* and even VD itself. In addition to the ALP staining results, Western blot and immunofluorescence studies further revealed that ALP levels were significantly elevated in cells treated with *B. subtilis* extract. The results obtained here revealed the substantial osteogenic impacts of *B. subtilis* extract, as well as the combinatorial groups of micronutrients and VD on osteoblast cells. Furthermore, this study also confirms the suitability of using *in vitro* cell culture systems to test the effects of probiotics by utilizing probiotics extracts instead of live cells.

Key words

Probiotics, boron, selenium, hFOB 1.19, vitamin D3, micronutrients, mineralization, osteoblasts

Introduction

Bone continuously undergo formation by osteoblasts and resorption by osteoclasts and any disruption to this fine balance can lead to unfavorable bone health conditions such as osteoporosis, which is a huge global health issue (Jakab 2014; Kanis et al. 2021). Growth and differentiation of osteoblasts can be categorized into three distinct phases: proliferation, extracellular matrix maturation and extracellular matrix mineralization. The specific gene expression pattern of these phases is useful to study the stage-effect of the treatments on the osteoblast cells under study (Fig.1).

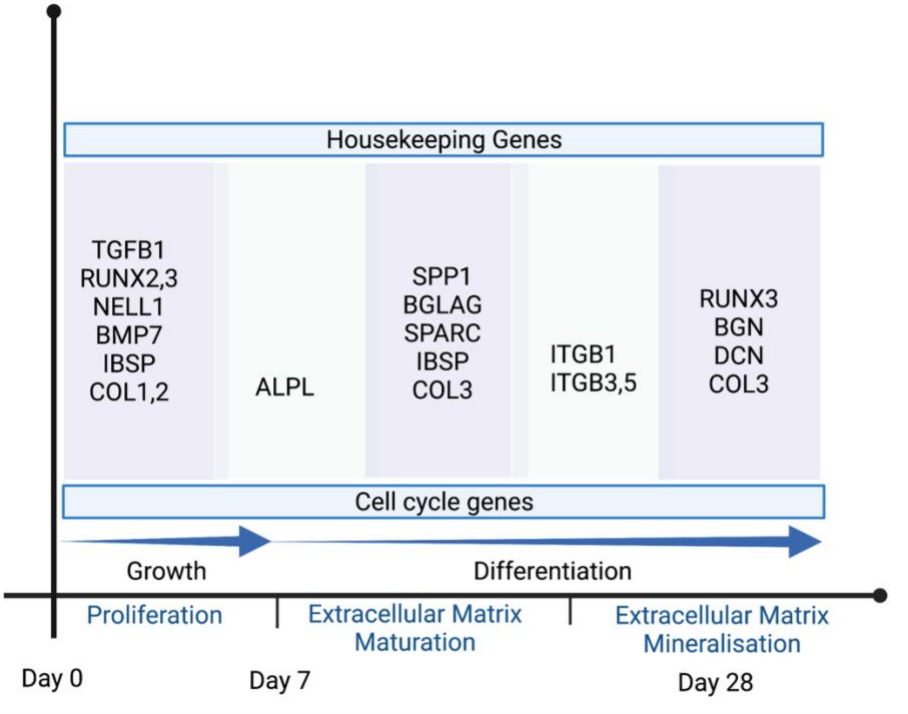

Fig.1. Three separate phases of osteoblast lineage cell growth and differentiation: (1) osteoblast proliferation (2) osteoblast extracellular matrix maturation (3) extracellular matrix mineralization (Figure adapted and modified from Stein et al. 2004 and Setzer et al. 2009) Created with BioRender.com.

Various micronutrients, minerals and vitamins play a vital role in bone remodeling and are essential for maintaining bone strength. Numerous studies have demonstrated the positive effects of boron (B) on bone health in both *in vitro* and *in vivo* models (Benderdour et al. 2000; Gallardo-Williams et al. 2003; Nielsen 2004; Gorustovich et al. 2008a; Hakki et al. 2010a). Additionally, prior research indicated that B controls ECM turnover, calcium nodule development, and the activity of enzymes such as ALP in fibroblasts (Nzietchueng et al. 2002). Similarly, selenium (Se) is another micronutrient with a reported osteogenic effect in several models including humans (Beukhof et al. 2016; Wang et al. 2020; Vescini et al. 2021). However, very few studies deeply explored the molecular mechanisms and possible synergic interactions of these micronutrients with calcitriol (VD). Two previous studies report a possible interaction of B with VD as they found out that B supplementation was able to correct the alterations in mineral metabolism and also increase calcium levels in serum in VD deficiency in rats and chicks (Hunt and Nielsen 1982; Dupre et al. 1994). Another recent report was on the role of B in VD-dependent control over bone mineralization in zebrafish larvae (Sojan et al. 2022). The possibility of a synergism between Se and VD was not well described till now. Therefore, checking the possible interactive action of these micronutrients with VD *in vitro*, opens the possibility to tackle the VD deficiency which is one of the main causes of deteriorating bone health.

Focusing on probiotics, they are beneficial microbes which have numerous positive effects on the host if administered in suitable

quantities and there are previous reports on some probiotics having a positive role in improving bone parameters like bone mass density or preventing bone loss (Foureaux et al. 2014; Nilsson et al. 2018; Takimoto et al. 2018; Rizzoli and Biver 2020). There are very limited studies on the effect of probiotics *in vitro* since they are live microbes which can contaminate the cell cultures. A previous study reported an increase in osteoblastic bone formation with supplementation of milk fermented with *Lactobacillus helveticus* in mouse osteoblast cell cultures (Narva et al. 2004). There have only been a few reports of researchers investigating the various beneficial effect of probiotics in cell line cultures by using probiotic extracts, supernatants, or even fractions of probiotic cultures (Chen et al. 2017; Nozari et al. 2019; Brognara et al. 2020; Isazadeh et al. 2020). Therefore, the present study aims to establish a suitable *in vitro* method to check the efficiency of probiotics by utilizing the ethanol extracts of the probiotics. We also aimed to explore the possibility of bacteria producing vitamin K2 in promoting synergistic effect with VD on ossification process.

Therefore, in this study, two micronutrients, B and Se and ethanol extracts of two probiotics, *Bacillus subtilis* and *Lactococcus lactis* were used at various concentrations and in combination with an established osteogenic concentration of VD to treat hFOB1.19 cells, which is a suitable model to study bone formation, capable of generating an ECM *in vitro* with ultrastructural elements similar to those deposited by primary osteoblasts *in vitro* (Subramaniam et al. 2002). The cell survival, alkaline phosphatase (ALP) production and calcium nodule formation were

analyzed in all experimental groups. In order to deeply elucidate the molecular mechanism controlled by the probiotic extracts, selected proteins were analyzed by Western Blot and immunocytochemistry to validate the morphological observations.

Materials and methods

High-performance liquid chromatography (HPLC) quantification of Vitamin K2 or menaquinones (MK) from probiotics

Using HPLC, MK-7 and MK-9 were measured to confirm the production ability of the bacteria. 50 mg of bacteria was extracted with 1 ml of ethanol (99%) and vortexed vigorously for at least 30s. Subsequently, to maximize the menaquinones extraction, 3 cycles of 3 min each of sonication interspersed with 30s of vortex were performed. The suspension was centrifuged at 20,900 g for 2 min at 4°C and 40 μL of supernatant was injected in the HPLC system (9300, YL Instrument, Anyang, Republic of Korea) and menaquinone forms were quantified by using of fluorescence detector (Nanospace SI-2, Shiseido). Results are expressed as μg/g for both MK-7 and MK-9.

Cell culture and treatments

Human fetal hFOB 1.19 SV40 large T antigen transfected osteoblastic cells (ATCC CRL-11372) were cultured in 1:1 mixture of Ham's F12 Medium and Dulbecco's Modified Eagle's Medium (DMEM) supplemented with 2.5 mM L-glutamine without phenol red (Gibco, Netherlands), 0.3 mg/ml

geneticin (Gibco, UK) and 10% fetal serum bovine (FBS, Gibco, UK) at 34°C and 5% CO_2. For the experiments, the cells were seeded in complete medium supplemented by a mineralization mix (MM) comprising of 50 µg/mL ascorbic acid (Sigma-Aldrich, UK) and 7.5 mM β-glycerophosphate (Sigma-Aldrich, UK) to stimulate mineralization. Cells were seeded at a density of $1x10^5$ cell/well in 12-well plates with 3 replicates for every treatment which lasted for 7 days. After seeding, on the second day the medium was removed from each well and media with corresponding treatments (1ml/well) were added to the monolayer. Media with respective treatments were changed on the fifth day. B in the form of boric acid (USB Corporation, USA), Se as sodium selenite (Sigma Aldrich, USA), VD (calcitriol or vitamin D3; Sigma Aldrich, USA), HPLC ethanol extracts of two probiotics (Fermedics, Belgium) - *Bacillus subtilis* (P1) and *Lactococcus lactis* (P2) were used for making the treatment groups. Compounds were tested alone or in various combination with VD for a total of 14 treatment groups as shown in table 1, in hFOB 1.19 cells for 7 days

Table 1: Compositions of groups of treatment.

NAME	CONCENTRATION
CONTROL	*DMEM + FBS 10 % + 0.03 µg/ml G418*
VD	*DMEM + FBS 10 % + 0.03 µg/ml G418 + MM + 100 nM VD*
B10	*DMEM + FBS 10 % + 0.03 µg/ml G418 + MM + B10ng/ml*
B100	*DMEM + FBS 10 % + 0.03 µg/ml G418 + MM + B100ng/ml*
B10VD	*DMEM + FBS 10 % + 0.03 µg/ml G418 + MM + B10ng/ml + 100 nM VD*
B100VD	*DMEM + FBS 10 % + 0.03 µg/ml G418+ MM + B100ng/ml + 100 nM VD*
Se	*DMEM + FBS 10 % + 0.03 µg/ml G418 + MM + Se10ng/ml*
SeB	*DMEM + FBS 10 % + 0.03 µg/ml G418 + MM + Se10ng/ml + B10ng/ml*

SeVD	*DMEM + FBS 10 % + 0.03 µg/ml G418 + MM + Se10ng/ml + 100 nM VD*
SeBVD	*DMEM + FBS 10 % + 0.03 µg/ml G418 + MM + Se10ng/ml + B10ng/ml + 100 nM VD*
P1	*DMEM + FBS 10 % + 0.03 µg/ml G418 + MM + P1 extract 1 µl/ml*
P2	*DMEM + FBS 10 % + 0.03 µg/ml G418 + MM + P2 extract 1 µl/ml*
P1VD	*DMEM + FBS 10 % + 0.03 µg/ml G418 + MM + P1 extract 1 µl/ml + 100 nM VD*
P2VD	*DMEM + FBS 10 % + 0.03 µg/ml G418 + MM + P2 extract 1 µl/ml + 100 nM VD*

XTT assay

The hFOB1.19 cell viability under different treatments for two time points- 24 hours and 48 hours, was determined using the XTT assay kit (Abcam). Cells were seeded in 96 well plates at a density of 10^4 cells/well in 100 µL of culture medium with all the 14 experimental groups to be tested in triplicates, and incubated in a CO_2 incubator set at 5% and 37°C. 10 µl of the prepared XTT mixture (equal volumes of XTT developer reagent and electron mediator solution) were added to each well of the respective plates after 24 and 48 hours and incubated for 2 hours at 37°C and 5% of CO_2. Then absorbance was measured using a microplate reader at 450 nm.

Alizarin red (AR) staining

After 7 days of culture in respective treatments, the cells were washed 3 times with PBS and fixed in 4% (v/v) PFA (1 ml / well) for 30 minutes at 4°C. The PFA was discarded and the cells were washed 3 times with milliQ water. The fixed cells were stained with 40 mM AR (pH 4.2, Fluka

Chemika, Switzerland) for 30 minutes in dark at room temperature (25 °C). Finally, monolayers were washed with milliQ water 4 times and were observed under Lionheart XF Automated Microscope (Biotek). Calcium nodules appeared in red. For the spectroscopic quantification of calcium deposits, the distilled water was removed and the AR stain was dissolved in 1 ml of 10% cetylpyridinium chloride (CPC) (Sigma Aldrich, USA) in 10 mM sodium phosphate buffer (pH 7.0) for 30 minutes at room temperature (25 °C). Finally, 250 µL of the solution were taken from each well and then transferred to a 96-well plate to measure absorbance at 550 nm.

Alkaline phosphatase (ALP) staining

Cells were fixed and washed using the same protocol as the AR staining protocol described in the previous section and the fixed cells were incubated with a staining mixture for ALP provided by the BCIP/NBT kit (Sigma Aldrich, UK) for 45 minutes at 37°C in dark conditions following the kit protocol. Once the color develop, the dye was removed and stained mono layers were washed twice and covered with milliQ water (1 ml / well) and photographed under a Lionheart XF Automated Microscope (Biotek).

Western blot (WB)

The following proteins - ALP, SPARC, SPP1 and BGLAP were quantified by WB in hFOB1.19 cells after 7 days of probiotic treatments. Total proteins were extracted using Radio-immunoprecipitation assay buffer system

(RIPA Lysis Buffer System). Protein concentration was determined using DC protein assay kit (BIO-RAD, USA) by reading absorbance at 750 nm. Total protein extracts (15 µg) were incubated with NuPAGE™ LDS Sample Buffer (4X) (Invitrogen) according to the manufacturer's instructions, fractionated in NuPAGE™ 4–12% Bis-Tris Protein Gels (Life technologies) and electrophoretically transferred to PVDF membranes. Membranes were incubated with 5% milk in Tris-buffered saline (TBS-T) to block non-specific sites or 3% BSA in TBS-T for SPP1 (since SPP1 is a phosphoprotein and milk blockage can cause background) and then with anti-SPARC (35 and 45 kDa fragments), anti-ALP (78 and 200 kDa fragments), anti-SPP1 and anti-BGLAP primary antibodies at 4 °C. Mouse anti-GAPDH was used as an endogenous control. After overnight incubation, the membrane was washed four times with TBS-T and then incubated with the secondary antibodies conjugated to horseradish peroxidase for 90 minutes at room temperature (25 °C) and washed four times with TBS-T. The detection of antibody binding was performed with Pierce ECL Western Blotting Substrate (Thermo Scientific, USA) and images were taken using Alliance Mini HD9 (Uvitec, UK). Gel band analysis was performed with ImageJ version 2.1.0/1.53c software.

Immunocytochemistry (ICC)

For immunocytochemistry (ICC) staining, cells were fixed in 4% PFA for 30 min at room temperature (25 °C) and washed thrice with PBS. Cells are then permeabilized in 0.1% Triton X-100 in 0.01 M PBS for 30 min and washed thrice with PBS followed by 30 minutes of blocking with 1%

bovine serum albumin (BSA) in PBS. Then cells were incubated overnight with mouse anti-human ALP primary antibody (1:100) (green fluorescence) at 4°C. Then cells were first washed thrice with PBS and then stained with a goat anti-mouse secondary antibody (1:1500) for 30 minutes protected from sunlight. After washing thrice with PBS, TRITC-labelled phalloidin (1:100) diluted in PBS was added to visualize F-actin fiber organization (red fluorescence) for 45 minutes and washed thrice with PBS. Nuclei were counterstained (blue fluorescence) with DAPI (1:1000) for 10 minutes and washed thrice with PBS. Samples were mounted using Vectashield mounting medium (Vector Laboratories Inc, CA) and observed with a Nikon E600 Fluorescence microscope (Milan, Italy).

Image analysis using ImageJ

ImageJ version 2.1.0/1.53c software was used for the image analysis for both AR staining and ALP staining. RGB stack was selected to split the image and green channel was chosen to analyze further. Intensity was measured for the thresholded range in all images and the data was statistically analyzed using R version 3.6.1 (R Core Team 2019) and plots were generated using ggplot2 3.2.1.

RNA extraction and quantification

Cells were cultured in 12-well plates as previously described in M&M. After 7 days of culture, the cells were detached and lysed directly into plates by removing the media and adding 100 µl of RNAzol to each well (vigorously

pipetting to detach all adherent cells). The contents of 3 wells for each treatment group were pooled in a 1.5 ml eppendorfs and four replicates per group were sampled for extraction. Total RNA was then extracted from the cells using RNAeasy Microkit (Qiagen, Italy). It was then eluted in 20 µL of molecular grade nuclease free water. Final RNA concentrations were determined using a nanophotometer. Total RNA was treated with DNase (10 IU at 37°C for 10 min, MBI Fermentas). One microgram of total RNA was used for cDNA synthesis using iScript cDNA Synthesis Kit (Bio-Rad, Italy) and stored at -20°C until further use as described previously.

RT-PCR

RT-PCRs were performed with SYBR green (Bio-Rad, Milan, Italy) in a CFX thermal cycler (Bio-Rad, Milan, Italy). For each reaction, the mix contained: 1 µL of cNDA (1:10) + 5 µL iQ SYBR Green Supermix + 3.8 µL miliQ water + 0.1 µL forward primer + 0.1 µL reverse primer. The thermal profile for all reactions was 3 min at 95°C followed by 45 cycles of 20 s at 95 °C, 20 s at 60°C and 20 s at 72°C. Dissociation curve analysis showed a single peak in all the cases. Actin beta (*actb*) and ribosomal protein, large, P0 (*rplp0*) were used as the housekeeping genes to standardize the results by eliminating variation in mRNA and cDNA quantity. No amplification product was observed in negative controls and primer-dimer formation was never seen. Data was analyzed using iQ5 Optical System version 2.1 (Bio-Rad) including Genex Macro iQ5 Conversion and Genex Macro iQ5 files. Modification of gene expression between the experimental groups is reported as relative mRNA abundance (Arbitrary Units). Primers used at a final concentration of 10 pmol/ml. All primer sequences used in the study are listed in Table 2.

***Table 2**: List of primers used in gene expression analysis by Real-Time PCR.*

GENE	**FORWARD PRIMER (5'-3')**	**REVERSE PRIMER (3'-5')**
actb	ATTGGCAATGAGCGGTTC	GGATGCCACAGGACTCCAT
rplp0	CTGGAAAACAACCCAGCTCT	GAGGTCCTCCTTGGTGAACA
runx2	GTGCCTAGGCGCATTTCA	GCTCTTCTTACTGAGAGTGGAAGG
alpl	CCATCCTGTATGGCAATGG	CGCCTGGTAGTTGTTGTGAG
tgfb1	GCAGCACGTGGAGCTGTA	CAGCCGGTTGCTGAGGTA
itgb1	TCCAAAGTCAGCAGAGACCTT	ATTTCCAGGGCTTGGGATA
col3a1	CTGGACCCCAGGGTCTTC	CATCTGATCCAGGGTTTCCA
spp1	TTGCAGCCTTCTCAGCCAA	CAAAAGCAAATCACTGCAATTCTC
sparc	GTACATCGCCCTGGATGAGT	CGAAGGGGAGGGTTAAAGAG
bgn	CAGCCCGCCAACTAGTCA	GGCCAGCAGAGACACGAG
bglap	TGAGAGCCCTCACACTCCTC	ACCTTTGCTGGACTCTGCAC
dcn	GGAGACTTTAAGAACCTGAAGAACC	CGTTCCAACTTCACCAAAGG

Statistical analysis

Data of all groups were normally distributed as assessed by Shapiro-Wilk's test (p>0.05) and there was homogeneity of variances, as assessed by Levene's test for equality of variances (p>0.05). The differences between the control and the treatments was tested with a One-way analysis of variance (ANOVA) followed by Tukey's post hoc test (p<0.05). All the tests were performed using R version 3.6.1 (R Core Team 2019) and plots were generated using ggplot2 3.2.1.

Results

Menaquinones production

The average production of menaquinone-7 (MK-7) and menaquinone-9 (MK-9) from the two probiotic bacteria was quantified respectively as:

- 0.59 μg/g and 7 μg/g for *L. lactis*
- 81μg/g and 0.5μg/g for *B. subtilis*

Furthermore, the unquantified peaks observed in the HPLC output could be other forms of menaquinones produced by the bacteria such as MK-8 (Fig.2).

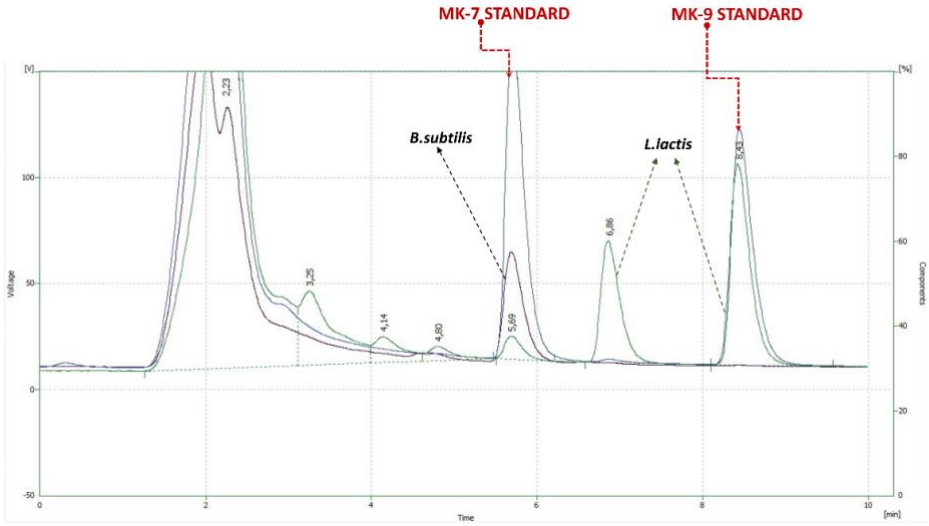

Fig. 2: MK-7 and MK-9 peaks of the standard and in the two probiotic strains observed in the HPLC output. The colour of the lines correspondingly indicate to as follows: Blue = Standard, Green = *L. lactis*, Black = *B. subtilis*.

Cell viability

The XTT test was used to determine the cytotoxic effects and cell viability in all treatment groups after 24 and 48 hours. After 24 hours incubation, we evidenced an increase of cell number relative to control in all groups except in SeB and B10VD from the micronutrient experiment. Except P2 and P1VD, other groups from the probiotic experiment also showed a similar increase in cell number after 24 hours. However, after 48 hours, all groups from both experiments were the same. Regarding cytotoxicity, at 24 hours exposure, only one group, the B100VD shown slight cytotoxicity, although the impact was reversed after 48 hours. Thus, cell viability was slightly affected after 24 hours, with B100VD exhibiting a slight negative effect and a few groups exhibiting an increase in cell numbers, but by 48 hours, all treatments were non-toxic to cells and had no effect on viability (Fig 3A,3B).

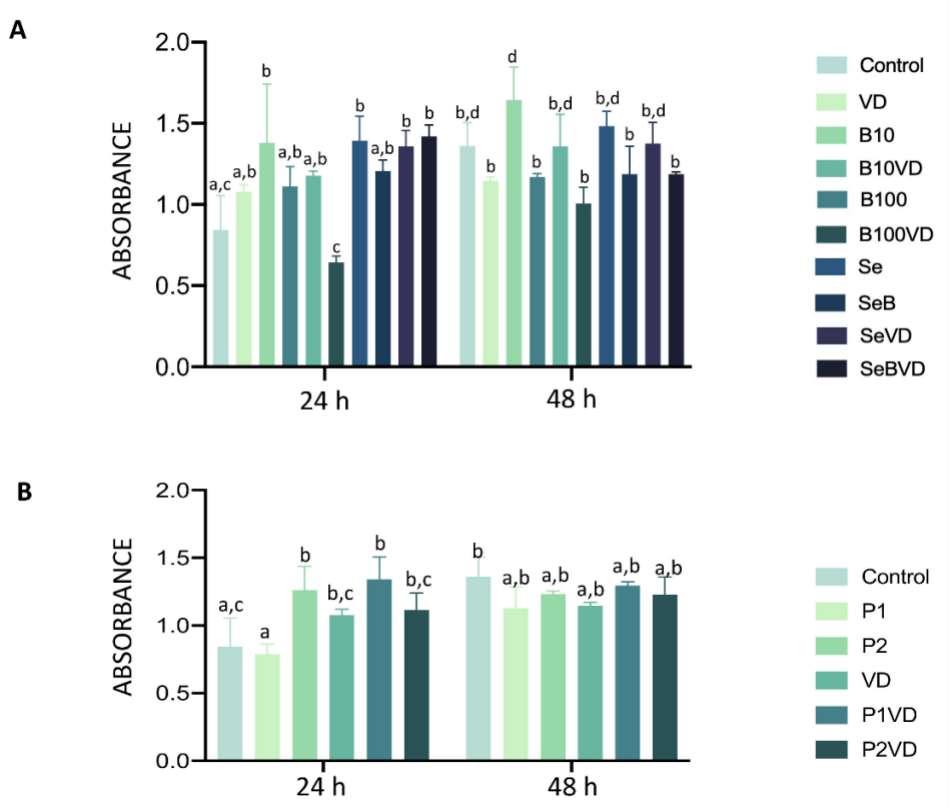

Fig 3. Cell viability of human fetal osteoblast (hFOB1.19) cells analysed by XTT assay exposed to different treatments (n=4) **A)** micronutrients B and Se treatments alone or in combination with VD; **B)** Probiotic extracts, P1 and P2, alone or in combination with VD. The graphs show the mean and standard deviation as error bars. The different letters above each graph indicate statistically significant differences in the different groups. Statistical significance was set at $p < 0.05$.

AR staining and quantitative analysis

AR staining was used to determine the capacity of the hFOB1.19 cells to produce calcium nodules. As expected, there was a significant difference between the control and VD groups, with the VD group exhibiting more mineralized nodules, as indicated qualitatively by the more prominent

red color in the images and quantitatively by the estimation of the pixel intensity of the images respect to the control group. The same findings were confirmed by spectrometric analysis, which demonstrated that VD had a greater absorbance than the control.

A significant increase in the appearance of calcium nodules, as evidenced by a strong intensity of red color, high pixel intensity from image analysis and high absorbance values from spectroscopy, was also observed in the synergy groups of micronutrients (B10VD, B100VD, SeVD, SeBVD) (Fig 4A and 4B) and in the group treated with the P1 extract (Fig 4D and 4E). The treatments B and Se alone, as well as the combination SeB, showed similar mineralization of the control (Fig 4A and 4B).

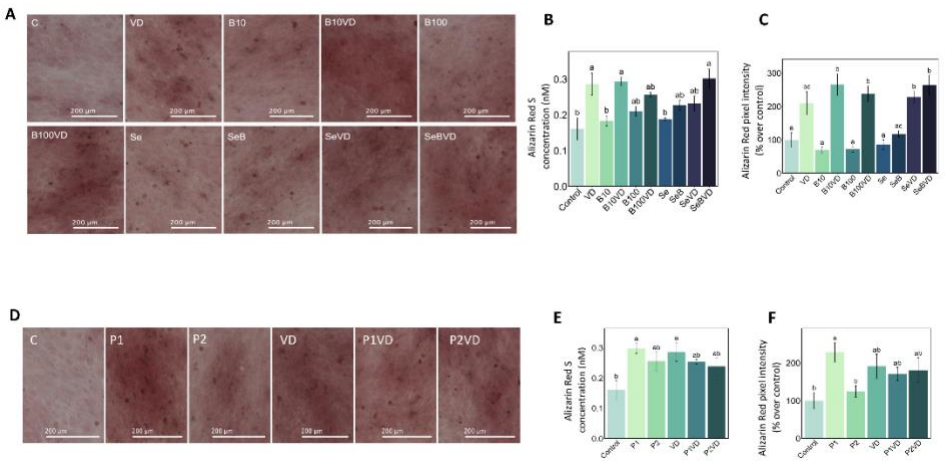

Fig 4. Alizarin Red staining of the hFOB1.19 cells cultured in the different treatments; **(A&D)** Each image is a representative of the different treatments applied to hFOB1.19 cells for 7 days; Scale bar: 200 μm; **(B&E)** Quantitative analysis of the extracellular matrix mineralization following the different treatments by measuring the absorbance using spectroscopy; n=4 **(C&F)** AR pixel

intensity measured using ImageJ and converted to % values over control. The graphs show the mean and standard deviation as error bars. One way ANOVA was used to analyse the difference between the groups and Tukey's post hoc test was used for multiple comparisons between every group. Different letters above each graph indicate statistically significant differences in the different groups and statistical significance was set at $p < 0.05$.

ALP staining and quantitative analysis

An ALP cytochemical staining of the hFOB1.19 cells was used to quantify the osteogenic differentiation in the treated cells. In the experiment using micronutrients, all groups except B10 and Se groups demonstrated an increase in the activity of ALP when compared to cells cultivated in a medium base medium (C) as indicated by the quantitative analysis of pixel intensity of the blue color (Fig.5A and 5B). Among the probiotic treatments, only P1 shown a significant increase in ALP activity, while VD interestingly showed an increase but not statistically significant (Fig.5C and 5D).

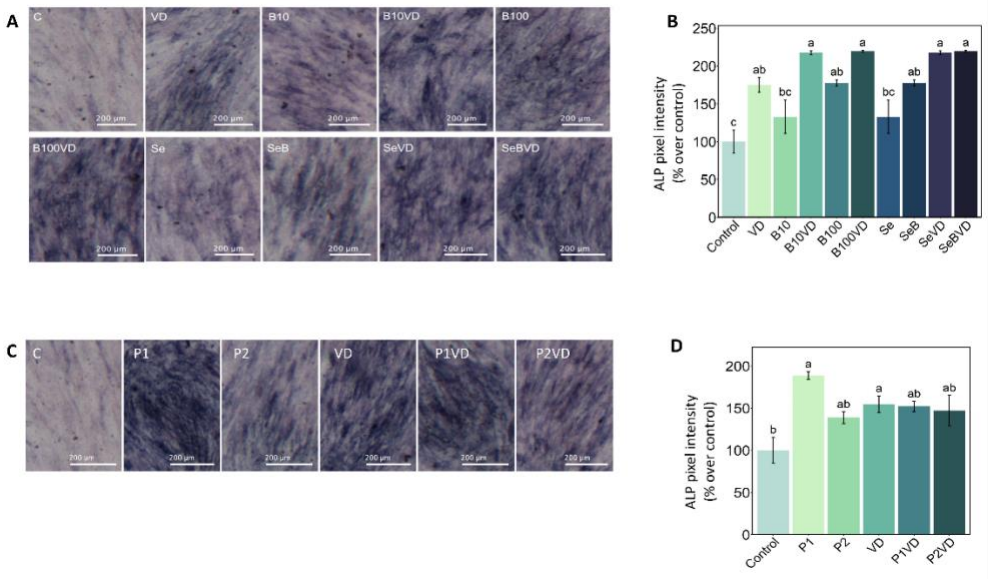

Fig 5. Alkaline phosphatase (ALP) staining of the hFOB1.19 cells cultured with the different treatments. **(A&C)** Each image as a representative of the different treatments applied to the cells for 7 days in mineralization inducing media. Scale bar: 200 µm; (**B&D)** ALP pixel intensity measured using ImageJ and converted to % values over control. The graphs show the mean and standard deviation as error bars (n=4). One way ANOVA was used to analyse the difference between the groups and Tukey's post hoc test was used for multiple comparisons between every groups. Different letters above each graph indicate statistically significant differences in the different groups and statistical significance was set at $p < 0.05$.

WB for probiotics experiment

The increased mineralized nodules and ALP activity observed in P1 group was further validated by doing a WB analysis for selected proteins including ALP (Fig.6A). The 200 kDa form of ALP and BGLAP was significantly more abundant in the P1 samples with respect to control. Another interesting observation was the 78 kDa form of both ALP and SPARC found to be significantly lowered in P2VD cells when compared to

VD suggesting a negative action of P2 extract when combined with VD. Regarding SPP1, a significant increase in P1 cells was found with respect to control and interestingly no change in SPP1 was detected in hFOB1.19 cells exposed to VD (Fig.6B).

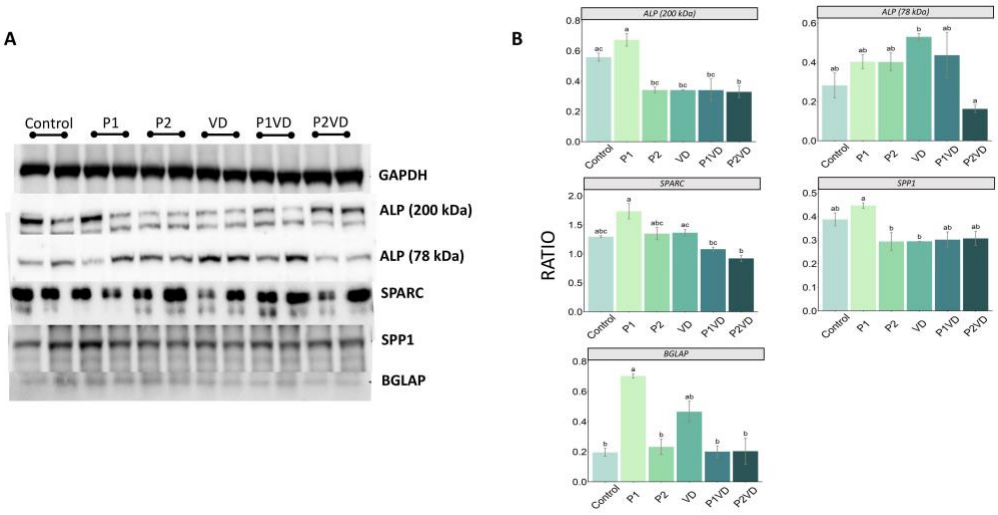

Fig.6. Western blot analysis of the expression of bone formation related proteins, ALP, SPARC, SPP1 and BGLAP, in hFOB1.19 cells cultured without any treatment (Control), treated with VD (VD), with two probiotics (P1 and P2) and their respective combinations with VD (P1VD and P2VD); **(A)** Western blot showing the expression levels of the selected bone formation-related proteins and GAPDH in all the groups; **(B)** Relative expression of the proteins calculated as a ratio of band density with respect to GAPDH. One-way ANOVA was used to compare between groups and Tukey's post hoc test was used for multiple comparisons between every groups. Different letters indicate statistical significance ($p < 0.05$).

Immunofluorescence for probiotics experiment

Fluorescent staining for the ALP, along with staining of cytoskeletal filamentous actin fibers and nuclei, were performed on the osteoblast cells after culture of 7 days with corresponding treatments. F-actin/DAPI staining confirms the cytocompatibility of the probiotic treatments morphologically. Fig. 7 shows representative pictures of structure of F-actin filaments and nuclear architecture in the cells after treatment with probiotic extracts and with their combinations with VD. After one week of treatment, the cells of all the groups exhibited a characteristic adherent morphology with a dispersion of F-actin filaments which are well-structured. Additionally, cells treated with the extracts and their combinations with VD exhibited a nuclear structure same as that of control and VD, confirming the cytocompatibility of the probiotic extracts. ALP, an early bone marker protein as a measure of biomineralization, was detected more in the cells treated with P1 (*B.subtilis*) extracts. ALP was particularly localized throughout the inner surface of the cellular membrane which was observed as brighter green spots along the membranes (Fig.7, white arrows).

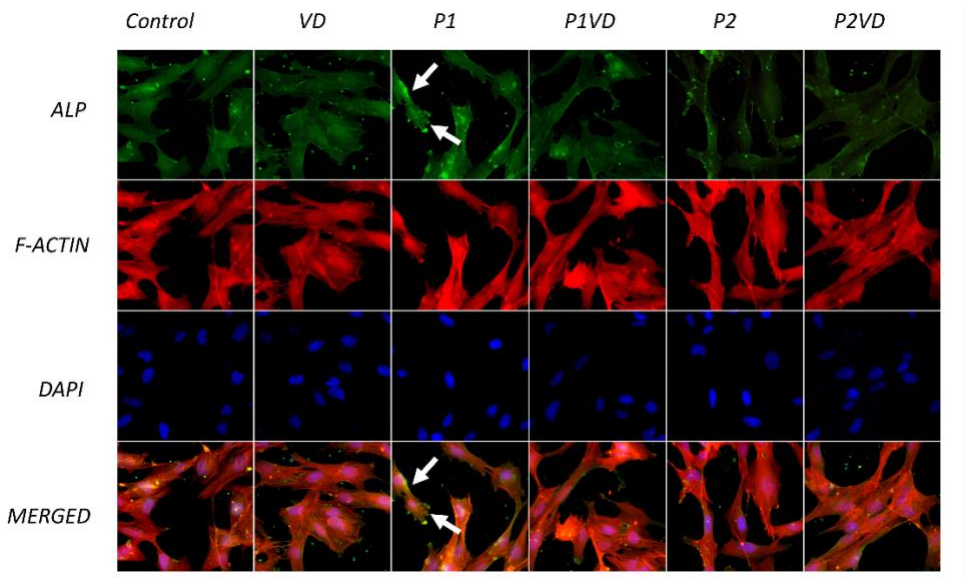

Fig.7. Representative immunofluorescence detection images of ALP, F-actin cytoskeleton (F-ACTIN) and DAPI in hFOB1.19 cells cultured without any treatment (Control), with VD (VD), probiotics (P1 and P2) extracts and their respective combinations with VD (P1VD and P2VD). White arrows indicate highest immunofluorescence of ALP detected in P1 cells.

Gene expression

Gene expression of selected marker genes of various stages of osteoblast growth and differentiation was evaluated following treatments with the two probiotics and VD (Fig.8). Regarding the genes involved in "proliferation stage", *runx2, tgfb1,* and *alpl* genes were significantly highly expressed in P1 extract-treated cells. Neither of the synergy groups or VD was showing any significant difference in the mRNA levels of these genes. About the maturation of extracellular matrix stage marker genes, *spp1, sparc* and *col3a1* genes showed the significant increase in expression in the P1 group. Mineralization of extracellular matrix stage marker genes *bgn, bglap* and *dcn* were also found to

be highly expressed in the P1. VD also exhibited a higher expression for the maturation of extracellular matrix stage marker gene *col3a1* and for the mineralization markers, *dcn* and *bgn*, compared to control. Interestingly, *dcn* was significantly high in P1VD as well (Fig.8).

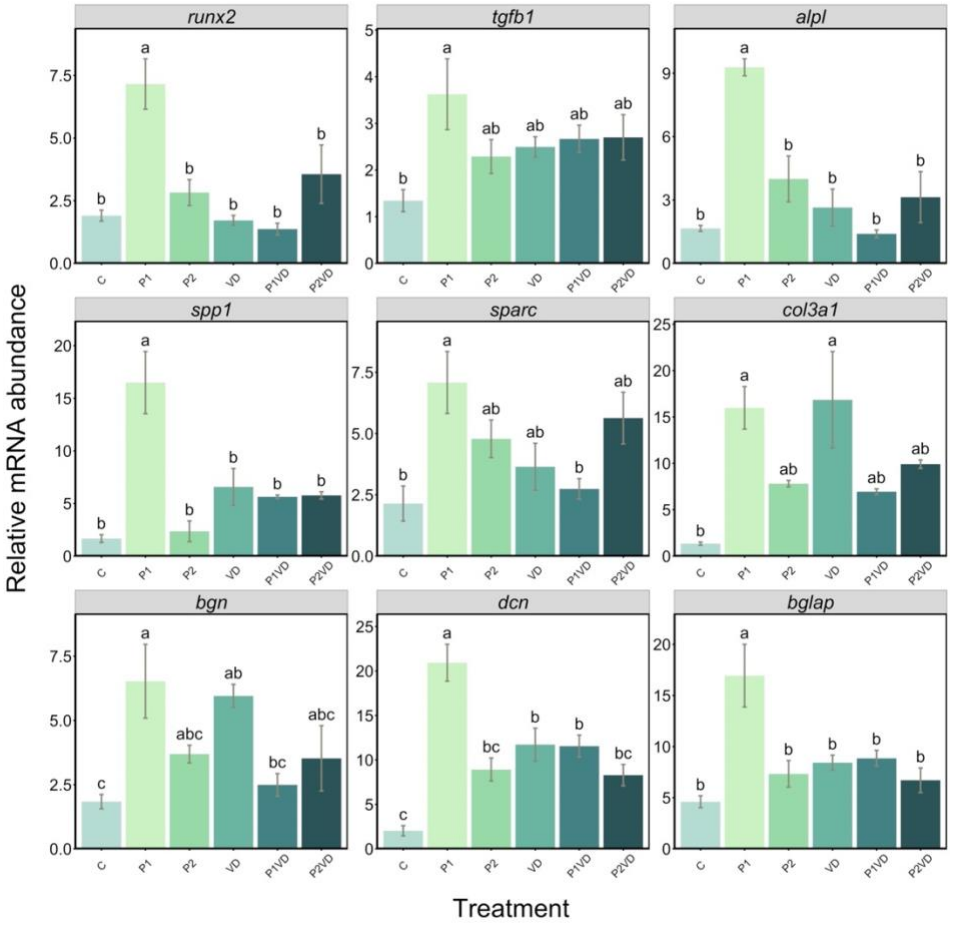

Fig 8. Expression of genes involved in the proliferation, maturation, and mineralization of the extracellular matrix after treatments. The graphs show the mean and standard deviation as error bars relating to gene expression in cells cultured with the different treatment groups. The different letters above each graph indicate statistically significant differences in the different groups. Statistical significance was set at $p < 0.05$.

Discussion

Osteoblasts are a natural target for drugs designed to promote bone anabolism. Compounds having an anabolic impact on the bone may be useful in enhancing the activity of osteoblasts and treating osteoporosis, a degenerative condition of aged bone which is a major public health concern on a global scale due to its high prevalence (Liang et al. 2012). During bone formation, osteoblasts go through a series of distinct phases of differentiation and maturation including proliferation, matrix synthesis and mineralization (Fu and Zhao 2013). To date, more studies are required to determine which substances may favorably affect these processes. A great deal of interest is now being shown in medications or nutritional supplements originating from natural sources such as probiotics. The goals of this study were to establish if the previous reports of positive role played by the selected micronutrients and probiotics in the bone health of animal models is also true in human osteoblasts and also to explore whether the osteogenic impact of these would enhance when used in combination with VD. Previously in mouse MC3T3-E1 cells and MSCs, toxicity was reported for cells when B and Se were used at a concentrations more than 100 ng/ml and 1 µM, respectively shown by two different studies (Hakki et al. 2010b; Liu et al. 2012a). Here we observed that B at 100 ng/ml was not detrimental to cells whereas the same concentration of B when combined with VD was slightly toxic after 24 hours but cells were able to recover by 48 hours. Regarding probiotic extracts, the results of cell viability assay, along with cytoskeleton and nuclei staining were indicative of good cytocompatibility of both

probiotics extracts and its combination groups with VD. No harmful effect was shown by VD on cell proliferation at the selected concentration which agrees with previous reports (Ruiz-GaspÃ et al. 2010). Most importantly, we could show that utilization of ethanol extract of probiotics is a very cytocompatible method to study the effects of probiotics *in vitro*.

ALP was employed as a biomarker of osteoblast cell differentiation in our study and cells treated with B and Se in combination with VD showed a substantial rise in ALP levels as compared to the groups utilized alone. The fact that VD has superior beneficial effects when combined with B shown here in human osteoblasts is also corroborated by previous studies in animal models where B exhibits additional integrative effects on bone metabolism in its VD-related actions, by acting as a helper, backup agent, and/or facilitator to maintain bone integrity in rats (Naghii et al. 2006). B with VD was also shown to be modulating various key signaling pathways in zebrafish which are involved in bone formation such as MAPK, TGF-β (Sojan et al.2022). The finding that Se in conjunction with B and VD (SeVD and SeBVD) resulted in a considerable rise in ALP levels lead to the conclusion that the already synergistic groups like SeVD or B10VD remain to have its enhanced osteogenic property when all three are combined together as well, but not more than their separate synergistic combinations with VD. Since we could not find a synergistic effect with B and Se together, we could conclude that both the micronutrients are able to enhance the osteogenicity of VD in a VD-dependent mode of action. AR staining was also used to check the mineralization profile of calcium nodules and even though previous results have validated the calcium

deposition ability of cells when treated with B and Se (Zheng et al. 2014; Liu et al. 2012b), we observed a further enhanced calcium depositing effect when the cells were treated with the same micronutrients in conjugation with VD. The increase in calcium nodule deposition for hFOB1.19 cells obtained with 100 ng/ml B suggests higher tolerance of these cells to this micronutrient which may exert its beneficial effects also at higher dose, different to what was previously observed in other cell types. Another prior study on MSC cells, showed the increase of calcium depositions in groups exposed to boric acid (1 and 10 ng/ml), whereas a decrease was found when 100 ng/ml were used (Ying et al. 2011) evidencing a downregulation in presence of high dose. The different result observed in our study may suggest a different sensitivity to B between hFOB1.19 cells and MSCs. Similarly, due to the varied origin and phenotypes of different cell types, there have previously been reports of differing amounts of calcium deposition after being stimulated for mineralization in the same manner in multiple studies with hFOB1.19 cells and Saos-2 cells (Strzelecka-Kiliszek et al. 2017; Bozycki et al. 2018; Yen et al. 2007).

Only the extract of *B.subtilis* had an effect on ALP production by cells and no evidence of synergy with VD was observed with both the probiotics. Studies have shown that the vitamin K2 series have enhanced osteogenic effect in osteoblasts by significantly increasing the activity of ALP in cells (Wu et al. 2019) and *B.subtilis* is a well-known producer of vitamin K2 forms such as MK-7 (Liao et al. 2021). We also quantified the two forms of MKs in the probiotics extract by HPLC and the presence of MKs, mainly

MK-7, could be the reason for the enhanced ALP production seen with *B.subtilis* extract. We could validate the same with immunofluorescent staining where ALP was found to be accumulated in the cytoplasm localized throughout the inner surface of the cellular membrane of the cells treated *B.subtilis* extract, this result was further confirmed by Western blotting analysis where ALP (200 kDa) and BGLAP was significantly higher in the *B.subtilis* extract-treated cells. The presence of ALP activity, which is a phenotypic marker for mature osteoblasts that appears early in the process of differentiation, and the observed mineralized nodules, which occurs later in the process of differentiation, both together indicate that *B.subtilis* extracts accelerated bone formation. Similar enhanced calcium deposition observed in cells treated with *B.subtilis* extract could be again accounted to the *B.subtilis*'s superior menaquinone producing capacity since menaquinones were previously found to in promote the formation of extracellular mineralized nodules (Tang et al. 2021). As a result, we may speculate that the menaquinone concentration in *B.subtilis* extracts may be responsible for the beneficial benefits exerted by this bacterial strain. *Runx2, alpl,* and *tgfb1* expression in hFOB1.19 cells will give insight into the influence of probiotic extract fractions on osteoblast proliferation. *Runx2* is essential for proper skeletal development since it controls chondrocyte and osteoblast differentiation (Komori 2009). Several bone matrix protein genes, such as *spp1*, are upregulated by *runx2* and its promoters are also activated *in vitro* by this transcription factor (Komori 2009). *Alpl* gene expression is a critical marker for osteoblast maturation because of its ability to control the mineralization process by creating free phosphates and its expression is

also known to be regulated by *runx2* (Sun et al. 2009; Yuan et al. 2019). *B.subtilis* extract upregulated the master regulator gene *runx2* in a favorable manner further confirmed by the elevated expression levels of the genes *alpl* and *spp1* both of which are targets of this transcription factor. TGF-1 has been shown to promote ECM deposition in a variety of cells and plays a crucial function in the remodeling of bone (Setzer et al. 2009; Mann et al. 2019). VK2 has been therapeutically used to prevent osteoporosis, and it is thought to exercise its protective effects via increasing osteoblast development and mineralization in the bone matrix (Atkins et al. 2009; Li et al. 2019). In our study, we noticed a uniform up-regulation of *spp1, col3a1, bglap* and *dcn* in all groups during last phases of osteoblast differentiation, which includes the maturation and mineralization of the extracellular matrix. This is indicative towards the differentiation status of the cells at time of sampling and the effect of *B.subtilis* extracts on the ECM maturation and mineralization marker genes as the treatment caused significant upregulation of these genes in the cells. These overall findings, together with vitamin K2's very low toxicity, may be attributable to the exceptional *in vitro* osteogenic performance shown by *B.subtilis* in this study.

The current work establishes for the first time, to our knowledge, that probiotic extracts can increase osteoblast differentiation and ECM mineralization in human embryonic osteoblasts, which may open up new avenues for the investigation and development of functional foods for promoting bone formation in order to prevent osteoporosis. However, the complete molecular mechanisms behind probiotic extract’s

osteogenic action, such as finding out whether these probiotics extracts influence the cellular start of mineralization through the direct activation of promoters and repressors or by some indirect influence, need more exploration. More importantly, separation and characterization of the highly active fractions are required and strongly recommended for further investigation.

Reference

Benderdour M, Bui T, Hess K, et al (2000) Effects of boron derivatives on extracellular matrix formation. J Trace Elem Med Biol Organ Soc Miner Trace Elem GMS 14:168–73. https://doi.org/10.1016/S0946-672X(00)80006-1

Beukhof CM, Medici M, Beld AW van den, et al (2016) Selenium Status Is Positively Associated with Bone Mineral Density in Healthy Aging European Men. PLOS ONE 11:e0152748. https://doi.org/10.1371/journal.pone.0152748

Bozycki L, Komiazyk M, Mebarek S, et al (2018) Analysis of Minerals Produced by hFOB 1.19 and Saos-2 Cells Using Transmission Electron Microscopy with Energy Dispersive X-ray Microanalysis. J Vis Exp JoVE 57423. https://doi.org/10.3791/57423

Dupre JN, Keenan MJ, Hegsted M, Brudevold AM (1994) Effects of dietary boron in rats fed a vitamin D-deficient diet. Environ Health Perspect 102:55–58. https://doi.org/10.1289/ehp.94102s755

Foureaux R de C, Messora MR, de Oliveira LFF, et al (2014) Effects of Probiotic Therapy on Metabolic and Inflammatory Parameters of Rats With Ligature-Induced Periodontitis Associated With Restraint Stress. J Periodontol 85:975–983. https://doi.org/10.1902/jop.2013.130356

Fu Y, Zhao X-H (2013) In vitro responses of hFOB1.19 cells towards chum salmon (Oncorhynchus keta) skin gelatin hydrolysates in cell proliferation, cycle progression and apoptosis. J Funct Foods 5:279–288. https://doi.org/10.1016/j.jff.2012.10.017

Gallardo-Williams MT, Maronpot RR, Turner CH, et al (2003) Effects of boric acid supplementation on bone histomorphometry, metabolism, and biomechanical properties in aged female F-344 rats. Biol Trace Elem Res 93:155–169. https://doi.org/10.1385/BTER:93:1-3:155

Gorustovich AA, Steimetz T, Nielsen FH, Guglielmotti MB (2008) A histomorphometric study of alveolar bone modelling and remodelling in mice fed a boron-deficient diet. Arch Oral Biol 53:677–682. https://doi.org/10.1016/j.archoralbio.2008.01.011

Hakki SS, Bozkurt BS, Hakki EE (2010a) Boron regulates mineralized tissue-associated proteins in osteoblasts (MC3T3-E1). J Trace Elem Med Biol 24:243–250. https://doi.org/10.1016/j.jtemb.2010.03.003

Hakki SS, Bozkurt BS, Hakki EE (2010b) Boron regulates mineralized tissue-associated proteins in osteoblasts (MC3T3-E1). J Trace Elem Med Biol 24:243–250. https://doi.org/10.1016/j.jtemb.2010.03.003

Hunt CD, Nielsen FH (1982) Interaction between boron and cholecalciferol in the chick. Proc Symp Trace Elem Metab Man Anim 597–600

Jakab L (2014) [Bone tissue: rebuilding and inflammation]. Orv Hetil 155:1575–1583. https://doi.org/10.1556/OH.2014.30015

Kanis JA, Norton N, Harvey NC, et al (2021) SCOPE 2021: a new scorecard for osteoporosis in Europe. Arch Osteoporos 16:82. https://doi.org/10.1007/s11657-020-00871-9

Liao C, Ayansola H, Ma Y, et al (2021) Advances in Enhanced Menaquinone-7 Production From Bacillus subtilis. Front Bioeng Biotechnol 9:695526. https://doi.org/10.3389/fbioe.2021.695526

Liu H, Bian W, Liu S, Huang K (2012a) Selenium Protects Bone Marrow Stromal Cells Against Hydrogen Peroxide-Induced Inhibition of Osteoblastic Differentiation by Suppressing Oxidative Stress and ERK Signaling Pathway. Biol Trace Elem Res 150:441–450. https://doi.org/10.1007/s12011-012-9488-4

Liu H, Bian W, Liu S, Huang K (2012b) Selenium Protects Bone Marrow Stromal Cells Against Hydrogen Peroxide-Induced Inhibition of Osteoblastic Differentiation by Suppressing Oxidative Stress and ERK Signaling Pathway. Biol Trace Elem Res 150:441–450. https://doi.org/10.1007/s12011-012-9488-4

Naghii MR, Torkaman G, Mofid M (2006) Effects of boron and calcium supplementation on mechanical properties of bone in rats. BioFactors 28:195–201. https://doi.org/10.1002/biof.5520280306

Narva M, Halleen J, Väänänen K, Korpela R (2004) Effects of Lactobacillus helveticus fermented milk on bone cells in vitro. Life Sci 75:1727–1734. https://doi.org/10.1016/j.lfs.2004.04.011

Nielsen FH (2004) Dietary fat composition modifies the effect of boron on bone characteristics and plasma lipids in rats. BioFactors 20:161–171. https://doi.org/10.1002/biof.5520200305

Nilsson AG, Sundh D, Bäckhed F, Lorentzon M (2018) Lactobacillus reuteri reduces bone loss in older women with low bone mineral density: a randomized, placebo-controlled, double-blind, clinical trial. J Intern Med 284:307–317. https://doi.org/10.1111/joim.12805

Nzietchueng RM, Dousset B, Franck P, et al (2002) Mechanisms implicated in the effects of boron on wound healing. J Trace Elem Med Biol 16:239–244. https://doi.org/10.1016/S0946-672X(02)80051-7

R Core Team (2019) R: A language and environment for statistical computing. Vienna, Austria: R Foundation for Statistical Computing; 2011.

Rizzoli R (2019) Nutritional influence on bone: role of gut microbiota. Aging Clin Exp Res 31:743–751. https://doi.org/10.1007/s40520-019-01131-8

Rizzoli R, Biver E (2020) Are Probiotics the New Calcium and Vitamin D for Bone Health? Curr Osteoporos Rep 18:273–284. https://doi.org/10.1007/s11914-020-00591-6

Ruiz-GaspÃ S, GuaÃ±abens N, Enjuanes A, et al (2010) Lithocholic acid downregulates vitamin D effects in human osteoblasts. Eur J Clin Invest 40:25–34. https://doi.org/10.1111/j.1365-2362.2009.02230.x

Setzer B, Bächle M, Metzger MC, Kohal RJ (2009) The gene-expression and phenotypic response of hFOB 1.19 osteoblasts to surface-modified titanium and zirconia. Biomaterials 30:979–990. https://doi.org/10.1016/j.biomaterials.2008.10.054

Sojan JM, Gundappa MK, Carletti A,Gaspar V, Gavaia P, Maradonna F and Carnevali O (2022) Zebrafish as a Model to Unveil the Pro-Osteogenic Effects of Boron-Vitamin D3 Synergism. Front. Nutr. 9:868805.doi: 10.3389/fnut.2022.868805

ZebrafishStein GS, Lian JB, Wijnen AJ van, et al (2004) Runx2 control of organization, assembly and activity of the regulatory machinery for skeletal gene expression. Oncogene 23:4315–4329. https://doi.org/10.1038/sj.onc.1207676

Sojan JM, Gundappa MK, Carletti A, Gaspar V, Gavaia P, Maradonna F and Carnevali O (2022) Zebrafish as a Model to Unveil the Pro-Osteogenic Effects of Boron-Vitamin D3 Synergism. Front. Nutr. 9:868805. doi: 10.3389/fnut.2022.868805

Strzelecka-Kiliszek A, Bozycki L, Mebarek S, et al (2017) Characteristics of minerals in vesicles produced by human osteoblasts hFOB 1.19 and osteosarcoma Saos-2 cells stimulated for mineralization. J Inorg Biochem 171:100–107. https://doi.org/10.1016/j.jinorgbio.2017.03.006

Subramaniam M, Jalal SM, Rickard DJ, et al (2002) Further characterization of human fetal osteoblastic hFOB 1.19 and hFOB/ER? cells: Bone formation in vivo and karyotype analysis using multicolor fluorescent in situ hybridization. J Cell Biochem 87:9–15. https://doi.org/10.1002/jcb.10259

Takimoto T, Hatanaka M, Hoshino T, et al (2018) Effect of *Bacillus subtilis* C-3102 on bone mineral density in healthy postmenopausal Japanese women: a randomized, placebo-controlled, double-blind clinical trial. Biosci Microbiota Food Health 37:87–96. https://doi.org/10.12938/bmfh.18-006

Tang H, Zhu Z, Zheng Z, et al (2021) A study of hydrophobins-modified menaquinone-7 on osteoblastic cells differentiation. Mol Cell Biochem 476:1939–1948. https://doi.org/10.1007/s11010-021-04062-z

Vescini F, Chiodini I, Palermo A, et al (2021) Selenium: A Trace Element for a Healthy Skeleton - A Narrative Review. Endocr Metab Immune Disord - Drug TargetsFormerly Curr Drug Targets - Immune Endocr Metab Disord 21:577–585. https://doi.org/10.2174/1871530320666200628030913

Wang N, Xie D, Wu J, et al (2020) Selenium and bone health: a protocol for a systematic review and meta-analysis. BMJ Open 10:e036612. https://doi.org/10.1136/bmjopen-2019-036612

Wu W-J, Gao H, Jin J-S, Ahn B-Y (2019) A comparatively study of menaquinone-7 isolated from Cheonggukjang with vitamin K1 and menaquinone-4 on osteoblastic cells differentiation and mineralization. Food Chem Toxicol Int J Publ Br Ind Biol Res Assoc 131:110540. https://doi.org/10.1016/j.fct.2019.05.048

Yen M, Chien C-C, Chiu I, et al (2007) Multilineage Differentiation and Characterization of the Human Fetal Osteoblastic 1.19 Cell Line: A Possible In Vitro Model of Human Mesenchymal Progenitors. STEM CELLS 25:125–131. https://doi.org/10.1634/stemcells.2006-0295

Ying X, Cheng S, Wang W, et al (2011) Effect of Boron on Osteogenic Differentiation of Human Bone Marrow Stromal Cells. Biol Trace Elem Res 144:306–315. https://doi.org/10.1007/s12011-011-9094-x

Zheng C, Wang J, Liu Y, et al (2014) Functional Selenium Nanoparticles Enhanced Stem Cell Osteoblastic Differentiation through BMP Signaling Pathways. Adv Funct Mater 24:6872–6883. https://doi.org/10.1002/adfm.201401263

CONCLUSIONS

Chapter 1- Zebrafish as a model to unveil the pro-osteogenic effects of Boron-Vitamin D3 synergism

1. The two synergistic treatments of B with VD greatly boosted bone development more than VD supplemented alone, as indicated by opercular bone mineralization, RNA-Seq-based differential expression analysis and from the two transgenic osteoblast reporter lines.
2. B at 10 ng/ml combined with VD at 10 pg/ml was found to be having the same opercular bone mineralization as that of the combinatorial group of B at 100 ng/ml combined with VD at 10 pg/ml. Whereas RNA-Seq evidenced more skeletal development related genes modulated by the synergy group with 10 ng/ml of B. The same conclusion was further validated in transgenic reporter lines for *sp7* and *bglap.* Therefore, lower concentration (10 ng/ml) of B supplemented with VD can result in a boosted positive effect on bone.
3. At molecular level, MAPK was the most regulated pathway by the synergy groups in addition to TGF-β signaling, focal adhesion and calcium signaling.
4. This discovery will drive further research into more combinatorial therapies and will open up new avenues for the use of B in healthcare and aquaculture to improve bone health.

Chapter 2- Zebrafish caudal fin as a model to investigate the role of probiotics in bone regeneration

5. Probiotic treatment had a substantial effect on caudal fin regeneration in zebrafish particularly at the midway point of the regeneration process.
6. Apart from speeding up regeneration, the therapy also increased the quantity of well-crystallized hydroxyapatite in the regenerated fins.
7. On the basis of the gene expression data acquired, it can be concluded that probiotics regulate important signaling pathways involved in the regeneration process such as the Wnt/β-catenin and Retinoic Acid signaling pathways.
8. The FTIRI can be proposed as an acceptable tool for measuring the degree of crystallization of hydroxyapatites in regenerated fins, which could be useful for future regeneration studies.
9. The results obtained here could be especially beneficial in bone regenerative medicine research, where probiotics may be a feasible prophylactic approach against bone problems.

Chapter 3- Probiotics enhance bone growth and rescue bmp inhibition: new transgenic zebrafish lines to study bone health

10. The two novel transgenic zebrafish lines created by inserting fluorescent protein-coding cDNA into the promoters of two bone-specific genes*, sp7* and *col10a1a*, allowed us to monitor osteoblast production and bone matrix in real time.
11. The two probiotics studied here, *Bacillus subtilis* and *Lactococcus lactis* had impact on bones; in particular, *Bacillus subtilis* was also able to counteract the detrimental effects of a BMP inhibitor.
12. Probiotics can be used not only as a prophylactic treatment but also as a therapeutic, to counteract the harmful effects of toxic compounds on the bone

Chapter 4- Action of micronutrients and probiotics extracts with vitamin D3 on hFOB1.19 cells differentiation and mineralization

13. B, Se, and probiotics extracts should be considered as modulators of the osteogenic capacity of osteoblasts.
14. In accordance with the *in vivo* findings from chapter 1 in zebrafish, the greatest effects are shown in cases where B is coupled with VD and was confirmed *in vitro* also.
15. In the case of Se, the same combinatorial impact was demonstrated but more studies are required to deeply understand the exact mechanisms in order to make a concrete conclusion.
16. The extract of the probiotic bacteria *Bacillus subtilis* had the greatest impact on osteoblast development and ECM mineralization *in vitro*.
17. In order to investigate the osteogenicity of different probiotics, the use of probiotics extracts in cell culture is introduced as a suitable method.

SUMMARY

Bone health problems such as osteoporosis are a big concern of today's world and the multi-faceted research conducted for this thesis aimed to screen and optimize compounds having effects on bone health and regeneration. The optimal osteogenic concentrations of the selected micronutrients and probiotics were established using both *in vitro* and *in vivo* models. A suitable *in vitro* system was introduced for testing the effects of probiotics in cell cultures by utilizing the extracts of probiotics instead of the whole microbes. The results also highlight the importance of the use of mutant zebrafish models to translate the results to human, in order to contribute towards the development of personalized medicines. We could also show that some micronutrients exert synergistical effect when used with an established pro-osteogenic compound like VD. Future studies are needed to determine whether these micronutrients and probiotics, either alone or in combination with VD, can maintain their enhanced effects on osteogenesis.

PUBLICATIONS

1. **Sojan, J. M.,** Gundappa, M. K., Carletti, A., Gaspar, V., Gavaia, P., Maradonna, F., & Carnevali, O. (2022). Zebrafish as a Model to Unveil the Pro-Osteogenic Effects of Boron-Vitamin D3 Synergism. *Frontiers in Nutrition*, *9*. https://doi.org/10.3389/fnut.2022.868805

2. **Sojan, J. M**., Raman, R., Muller, M., Carnevali, O., & Renn, J. (2022). Probiotics Enhance Bone Growth and Rescue BMP Inhibition: New Transgenic Zebrafish Lines to Study Bone Health. *International Journal of Molecular Sciences*, *23*(9), 4748. https://doi.org/10.3390/ijms23094748

3. **Sojan,J.M.,**Gioacchini,G.,Giorgini,E.,Orlando,P.,Tiano,L.,Maradonna, F., & Carnevali, O. (2022). Zebrafish caudal fin as a model to investigate the role of probiotics in bone regeneration. *Scientific Reports*. https://doi.org/10.1038/s41598-022-12138-z